Mechanisms of ANO1 channel activation in sensory neurons

Shihab Sarwar Shah

Submitted in accordance with the requirements for the degree of
Doctor of Philosophy

University of Leeds
School of Biomedical Sciences

September 2017

The candidate confirms that the work submitted is his own and that appropriate credit has been given where reference has been made to the work of others.

Dedicated to my beloved sister
Tabinda Nisar Shah (1985-2006).
Gone but never forgotten.

Acknowledgements

Foremost, I would like to thank Professor Nikita Gamper for the various opportunities he has provided for me over the years. Without his continued support and belief in me I would not have been able to produce this body of work. Thanks for being a brilliant boss and a great friend.

Past and present members of Gamper lab have all contributed to my development as a research scientist to whom I am extremely grateful. Louisa Pettinger first introduced me to the world of Ca^{2+} imaging and was a great mentor so thanks for putting up with me during your thesis writing (she also acknowledged me in her thesis so I'm repaying the favour). Also a big thank you to Hannah Kirton and Sylvain Gigout for the help during my Masters project and Gabriel Hoppen for his help with this work. Thank you to previous/current Gamper lab members Alex Hogea, Rosmaliza Ramli, Ewa Jarworska, Haixia Gao, Frederick Jones, Stephen Milne and Eleni Kyriakopoulou for all the help with various aspects of my research but more importantly for being great friends throughout these past few years. I look forward to the next adventure in Gamper lab!

A big thank you to the group in Texas- especially Professor Mark Shapiro and Chase Carver for the opportunity to collaborate and assistance throughout. A special thanks to Crystal Archer and Rafael Veraza for making me feel welcome during my visit and helping me settle. I appreciate everything you guys have done for me.

Lots of love and gratitude to my beloved parents and brother Shayaan for supporting me and helping me throughout everything. Without your love and support I wouldn't be in this position today. Thank you to my beautiful wife Affifa for all your love and putting up with me. Finally, to the person who I love the most in this world, my daughter Nurai Fatima Shah, you came into my life and changed my world. Love you always.

Abstract

ANO1 (TMEM16A) is a Ca^{2+} activated Cl^- channel (CaCC) expressed in peripheral somatosensory neurons responding to painful (noxious) stimuli. Previously, our lab has been able to demonstrate specific coupling of ANO1 to inositol 1,4,5-trisphosphate receptor (IP_3R)-mediated Ca^{2+} release from the endoplasmic reticulum (ER) via G-protein coupled receptor (GPCR) activation. This phenomenon underscores excitatory and noxious effects of some mediators of inflammatory pain, such as pro-algesic and vasoactive neuropeptide bradykinin.

To further investigate mechanisms of ANO1 activation in somatosensory neurons, I developed a dual imaging approach, which involved transfecting dorsal root ganglion (DRG) neurons with a halide sensitive EYFP mutant (H148Q/I152L) and simultaneous Ca^{2+} imaging to monitor CaCC activity. This methodology was successfully used to demonstrate robust coupling of CaCC activity to IP_3R activation produced by bradykinin. Blockade of ANO1 using a selective inhibitor (T16A-inhA01) abolished CaCC activity induced by bradykinin application. In contrast to the ER-induced Ca^{2+} release, Ca^{2+} influx produced by depolarisation-induced activation of voltage gated Ca^{2+} channels (VGCCs) was relatively ineffective in activating ANO1, which is in good agreement with previous studies.

TRPV1 activation by capsaicin was able to induce robust CaCC activity. Given the ability of TRPV1 to activate PLC isoforms and produce IP_3, I further tested the mechanism by which ANO1 is activated by TRPV1. Depletion of the ER Ca^{2+} stores severely reduced both, the capsaicin-induced Ca^{2+} signals and the concurrent CaCC activation. Intriguingly, under extracellular Ca^{2+} free conditions capsaicin was still able to induce $[Ca^{2+}]_i$ elevation, further illustrating the ability of TRPV1 to induce intracellular Ca^{2+} release. Finally, monitoring of ER specific-Ca^{2+} dynamics concurrently with CaCC activity unambiguously confirmed the ability of TRPV1 to produce ER-Ca^{2+} mobilisation. Importantly, IP_3R blockade with xestospongin C reduced CaCC activity after TRPV1 activation. Collectively, these experiments suggest that a significant fraction of Ca^{2+} required for activation of ANO1 downstream of TRPV1 is indeed delivered through IP_3R activation.

Using ‘in-situ proteomics’ and super-resolution microscopy I investigated multi-protein complexes in ER-plasma membrane (ER-PM) junctions of DRG neurons involving ANO1, TRPV1 and IP_3R1. I found using proximity ligation assay that all 3

proteins were within 40nm of each other; however there was a greater number of ANO1 and TRPV1 complexes compared to TRPV1/ANO1 and TRPV1/IP_3R1 complexes. Two-colour stochastic optical reconstruction microscopy (STORM) was able to confirm these findings and demonstrate that there is indeed a greater percentage of complexes involving ANO1 and TRPV1. Preliminary triple-colour STORM suggested the presence of ANO1, TRPV1 and IP_3R1-containing protein complexes.

Finally, I used total internal reflection microscopy (TIRF) to monitor the dynamics of the ER-PM junctions following the activation of bradykinin receptors or TRPV1. Application of bradykinin and capsaicin elicited increased intensity proximity of the ER to PM (as evaluated by the TIRF signal of fluorescently-labelled ER), which is suggestive of the ER moving to the PM by internal store mobilisation and highlighting the importance of ER-PM junctions.

In sum, the experiments described in this thesis have discovered and characterised a novel mode of ANO1 activation in pain-sensing neurons: TRPV1-mediated ER Ca^{2+} release in ER-PM junctional signalling complex. These findings describe a hitherto unknown signalling mechanism potentially contributing to inflammatory pain.

Contents

Publications

Papers

Jin X, Shah S, Du X, Zhang H, Gamper N. (2014) **Activation of Ca^{2+} -activated Cl^- channel ANO1 by localized Ca^{2+} signals.** The Journal of physiology.

Jin X, Shah S, Liu Y, Zhang H, Lees M, Fu Z, Lippiat JD, Beech DJ, Sivaprasadarao A, Baldwin SA, Zhang H, Gamper N. (2013) **Activation of the Cl^- channel ANO1 by localized calcium signals in nociceptive sensory neurons requires coupling with the IP_3 receptor.** Science Signaling.

Posters

Shah, S, Carver, C, Shapiro, M and Gamper, N. (2017). **Probing the Composition of TMEM16A-Containing Signaling Complexes in Sensory Neurons.** Biophysical Society Annual Meeting, New Orleans.

Shah, S and Gamper, N. (2016). **Functional Coupling between TRPV1 and ANO1 in Sensory Neurons Requires Ca^{2+}-Release from the Endoplasmic Reticulum.** Biophysical Society Annual Meeting, Los Angeles.

Shah S and Gamper, N. (2015). **Functional Coupling between ANO1 and TRPV1 Channels in Sensory Neurons.** Biophysical Society Annual Meeting, Baltimore.

This thesis builds on the findings of the publications mentioned above. Posters presented were produced from data generated during this study. STORM data was produced at the University of Texas Health Science Center at San Antonio, where I spent 6 weeks to perform experiments with Professor Mark Shapiro and Dr Chase Carver.

List of Figures

List of Tables

Abbreviations

$[Ca^{2+}]_i$	Intracellular Ca^{2+} concentration
$[Cl^-]_i$	Intracellular Cl^- concentration
$[Cl^-]_o$	Extracellular Cl^- concentration
ABC	ATP-binding cassette transporter
AC	Adenylyl Cyclase
AKAP150	A-Kinase-anchoring protein 150
AKT	PI3K-activated protein kinase B pathway
ANK	Ankyrin domain
ANO1	Anoctamin 1
ATP	Adenosine triphosphate
B_1R	Bradykinin receptor 1
B_2R	Bradykinin receptor 2
BAPTA	1,2-bis(*o*-aminophenoxy) ethane-*N*,*N*,*N′*,*N′*-tetra acetic acid
BK_{Ca}	Large conductance Ca^{2+}-activated K^+ channel
CaCC	Ca^{2+} activated Cl^- channel

CALCLR	Calcitonin receptor-like receptor
CaM	Calmodulin
CaMKII	Calmodulin-dependent kinase II
cAMP	cyclic adenosine monophosphate
Ca_v	Voltage gated Ca^{2+} channel
CCL	Chronic constriction injury
cDNA	Complementary deoxyribonucleic acid
CEPIA	Calcium-measuring organelle entrapped protein indicator
CF	Cystic fibrosis
CFA	Complete Freund's adjuvant
CFTR	Cystic fibrosis transmembrane regulator
cGMP	cyclic guanine monophosphate
CGRP	Calcitonin-gene related peptide
CHO	Chinese hamster ovary cells
CICR	Ca^{2+}-induced Ca^{2+}-release
CIP	Congenital insensitivity to pain
CNGC	cyclic nucleotide gated channel
CNS	Central nervous system
CPA	Cyclopiazonic acid
CPECs	Choroid plexus epithelial cells
CRPS	Complex regional pain syndrome
DAG	Diacylglycerol
DIDs	4,4′-diisothio-cyanostilbene-2,2′-disulfonic acid
DMEM	Dulbecco's modified Eagle's medium
DRG	Dorsal root ganglion
DTE	Distal tubular epithelial cells
EC_{50}	Half-maximal (50%) response concentration
E_{cl}	Nernst/equilibrium potential for Cl^-
EGFR	Epidermal growth factor receptor
EGTA	ethylene glycol-bis(β-aminoethyl ether)-N,N,N',N'-tetraacetic acid
E_K	Nernst/equilibrium potential for K^+
ER	Endoplasmic reticulum
ERLIN1	Endoplasmic Reticulum Lipid Raft-Associated Protein 1
ERM	Ezrin-radixin-moesin proteins
E-syts	Extended synaptotagmins
EYFP	Enhanced yellow fluorescent protein
FBS	Fetal bovine serum
FRET	Fluorescence resonance energy transfer
FRT	Fisher rat thyroid cells
GABA	Gamma-Aminobutyric acid

GABARAP	GABA receptor associated protein
GFP	Green fluorescent protein
GPCR	G-protein coupled receptor
H^+	Proton
HCM	Hypertrophic cardiomyopathy
$HCO3^-$	Bicarbonate ion
HEK293	Human embryonic kidney 293 cells
HNSCCs	Head and neck squamous cell carcinomas
HSG	Human salivary gland cells
HVA	High voltage gated Ca^{2+} channel
IBD	Inflammatory bowel disease
IBS	Inflammatory bowel syndrome
ICC	Interstitial calls of Cajal
ICD	Intracellular domain
IL-4	Interleukin-4
IP_3	Inositol 1,4,5-trisphosphate
IP_3R	Inositol 1,4,5-triphosphate receptor
I-V	Current-voltage relationship
KCC2	K^+-Cl^- cotransporter 2
K_d	Dissociation constant
K_v	Voltage gated K^+ channel
LVA	Low voltage gated Ca^{2+} channel
M_1R	Muscarinic 1 receptor
MAPK	Mitogen-activated protein kinase pathway
MOR	μ-opioid receptor
MORN	Membrane occupation and recognition nexus motifs
mRNA	Messenger ribonucleic acid
Na_V	Voltage-gated Na^+ channel
NBD	Nucleotide binding domain
NFA	Niflumic acid
NG	Nodose ganglia
NGF	Nerve growth factor
NIS	Na^+-I^- symporter
NKCC1	Na^+-K^+-Cl^- cotransporter 1
NPPB	5-nitro-2-(3-phenylpropylamino) benzoic acid
PAG	Periaqueducatal gray
PAR-2	Protease-activated receptor 2
PASMC	Pulmonary Artery Smooth Muscle Cells
PB	Parabrachial nucleus
PI3	Phosphoinositide 3 kinase

PIP_2	Phosphatidylinositol 4,5-bisphosphate
PKA	Protein kinase A
PKC	Protein kinase C
PLA	Proximity ligation assay
PLC	Phospholipase C
PM	Plasma membrane
Pma1	Plasma membrane ATPase 1
PSNL	Partial spinal nerve ligation
PTE	Proximal tubular epithelial cells
RHoA	Ras homolog gene family, member A
RNA	Ribonucleic acid
RPE	Retinal pigment epithelial cells
RVM	Rostral ventral medulla
RYR	Ryanodine Receptor
SERCA	Sarcoplasmic/Endoplasmic Reticulum Ca^{2+}-ATPase
siRNA	Small interference ribonucleic acid
Slo1	Large conductance Ca^{2+}-activated K^+ channel
SMP	Synaptotagmin-like, mitochondrial-lipid binding protein domain
SNL	Spinal nerve ligation
SOCE	Store-operated Ca^{2+} entry
SP	Substance P
SR	Sarcoplasmic reticulum
STORM	Stochastic Optical Reconstruction Microscopy
TG	Trigeminal ganglion
TIRF	Total internal reflection fluorescence microscopy
TM	Transmembrane
TrkA	Tyrosine kinase A
TRP	Transient receptor potential channel
TRPA1	Transient receptor potential ankyrin 1
TRPC1	Transient receptor potential canonical 1 channel
TRPV1	Transient receptor potential vallinoid 1 channel
VGAT	Vesicular GABA transporter
VGCC	Voltage gated Ca^{2+} channel
VMSCs	Vascular smooth muscle cells

Chapter 1: Introduction

1.1 What is pain?

What is pain? The answer to this question is quite paradoxical if one was to ponder deeply regarding its existence and physiological nature. The word pain has its origins from the Latin word ‘poena’ which literally translates as punishment. This may well have been the case from ancient civilisations of the past to some parts of present day society, along with a subconscious perception of pain being punishment in nearly every living being to have ever graced the earth. However, if we actually delve deeper into the actual meaning of pain, at least from a biological perspective, then we are able to appreciate the vital aspects of pain rather than the dreadful perceptions that have blemished our minds with the preconceived notions regarding this experience.

Pain is actually an experience emplaced to protect the body from further damage once it has been subjected to injury. This may be hard to acknowledge for the average being that such an unpleasant sensation is indeed providing protection for you and I but this can be contextualised when looking at disorders such as Congenital Insensitivity to Pain (CIP) syndrome. CIP is characterised by patients having an inability to sense any pain that the body endures (Peddareddygari et al., 2014). Patients continually injure themselves and are oblivious to the fact that they are sustaining such injuries, many times to the same part of the body as previously. Children with this disorder require constant attention and education regarding their issues. In some cases this repetitive injury can lead to death (Basbaum et al., 2009; Shorer et al., 2014). A normal person would be able to feel pain and therefore cease the injured body part from sustaining further damage, thus allowing effective and efficient healing to occur. Despite the importance and benefits of pain in physiological terms, abnormal functionality of the nociceptive nervous system can cause unnecessary pain (Wieseler-Frank et al., 2004). In certain physiological or pathophysiological circumstances, pain outlives its usefulness to protect the body and becomes a nuisance for the patient (Linley et al., 2010).

1.1.1 Nociceptors

The transduction of primary sensory signals associated with tissue damage into the sensation of pain is a complex process entailing a constellation of ion channels and

receptors that work in concert to provide the unpleasant experience that we undergo when met with potentially damaging (noxious) stimuli or trauma. The process by which noxious stimuli are detected and realised by the body is referred to as nociception (Dubin and Patapoutian, 2010). Upon the onset of somatic damage (or when prospect of such damage approaches imminence), peripherally located neurons known as nociceptors, are preferentially activated. Nociceptors have unspecialised nerve endings and a high threshold in the noxious range for activation (Dubin and Patapoutian, 2010). Only if the noxious signal is of sufficient intensity will nociceptors be activated. Due to this high threshold, non-noxious (innocuous) stimuli are excluded from activating nociceptors i.e. non-noxious and noxious heat is perceived differently.

Nociceptors can be subdivided into 3 different groups classified as: Aβ (myelinated large fibers), Aδ (thinly myelinated, medium-diameter fibers) and C-fibers (non-myelinated) with the latter 2 groups forming the majority of nociceptors (although a small percentage of Aβ are also implicated in nociception (Djouhri and Lawson, 2004) (Table 1.1). The myelination of these fibers dictates the speed of conduction and the types of pain that are perceived; Aδ fibers are responsible for the initial pain that is felt upon trauma (due to its myelination) whereas the C-fibers provide the secondary slow pain (Basbaum et al., 2009).

Fiber type	Size (diameter)	Myelination	Conduction velocity
Aβ	Large	Myelinated	Fast (>30 m/s)
Aδ	Medium	Thinly myelinated	Medium (5-30 m/s)
C	Small	No myelination	Slow (0.4-1.4 m/s)

Table 1.1: Table demonstrating the different characteristics of nociceptors types.

Nociceptors can also be categorised regarding the modality of response; Aδ fibers are mechanosensitive or mechanothermal whereas C-fibers tend to be polymodal (respond to mechanosensitive, mechanothermal and chemical stimuli). Nociceptors are also characterised on the expression of specific markers; peptidergic C-fibre

nociceptors express and release neuropeptides substance P (SP) and calcitonin-gene related peptide (CGRP) and also express tyrosine kinase A (TrkA) neurotrophin receptor (Snider and McMahon, 1998; Basbaum et al., 2009). Non-peptidergic nociceptors on the other hand bind isolectin IB4 and express c-Ret neurotrophin receptor as well as various G-protein coupled receptors (GPCR) (Dong et al., 2001). Recent next-generation sequencing studies identified further subdivision of nociceptors (Usoskin et al., 2015; Li et al., 2016) however this work is beyond the scope of the present study.

1.1.2 Pain transmission- from the periphery to the brain

As mentioned above, a host of ion channels and receptors are required to process the noxious signals (see below); a complement of channels, specific to the sensory modality of a given neuron is found at unspecialised nerve endings of nociceptors within the innervated tissue (e.g. skin) (Basbaum et al., 2009). Action potential generation at these endings is then propagated through the nociceptive axon (fiber) and passed on to the spinal cord where the first synaptic transmission takes place, and, ultimately to the higher centres of the brain (Fig. 1.1). Afferent projections extend from the periphery and synapse into the superficial laminae of the spinal cord (Basbaum et al., 2009). Cell bodies of nociceptors are located at peripheral ganglia, such as dorsal root ganglia (DRG) and trigeminal ganglia (TG). The smaller C fibers project to more superficial laminae called the ‘substantia gelatinosa’ (I and II) whereas the larger diameter Aδ project deeper into laminae II and V (Basbaum et al., 2009) (Fig. 1.1). Subsequent second order neurons decussate and project via the spinothalamic tract to the thalamus where these neurons terminate. Some second order projections also project to other areas such as the periaqueductal gray, parabrachial nucleus and the rostral ventral medulla regions. Finally third order neurons then project to the cortex and the amygdala where the signals are processed and manifested as the emotional and behavioural aspects of pain (Basbaum et al., 2009; Dubin and Patapoutian, 2010) (Fig. 1.1). Other projections to areas involved in emotional processing include the cingulate and insular cortices (Basbaum et al., 2009). Orofacial pain processing occurs via a different pathway- the trigeminothalamic pathway via the trigeminal nerve (V) and has cell bodies at the TG.

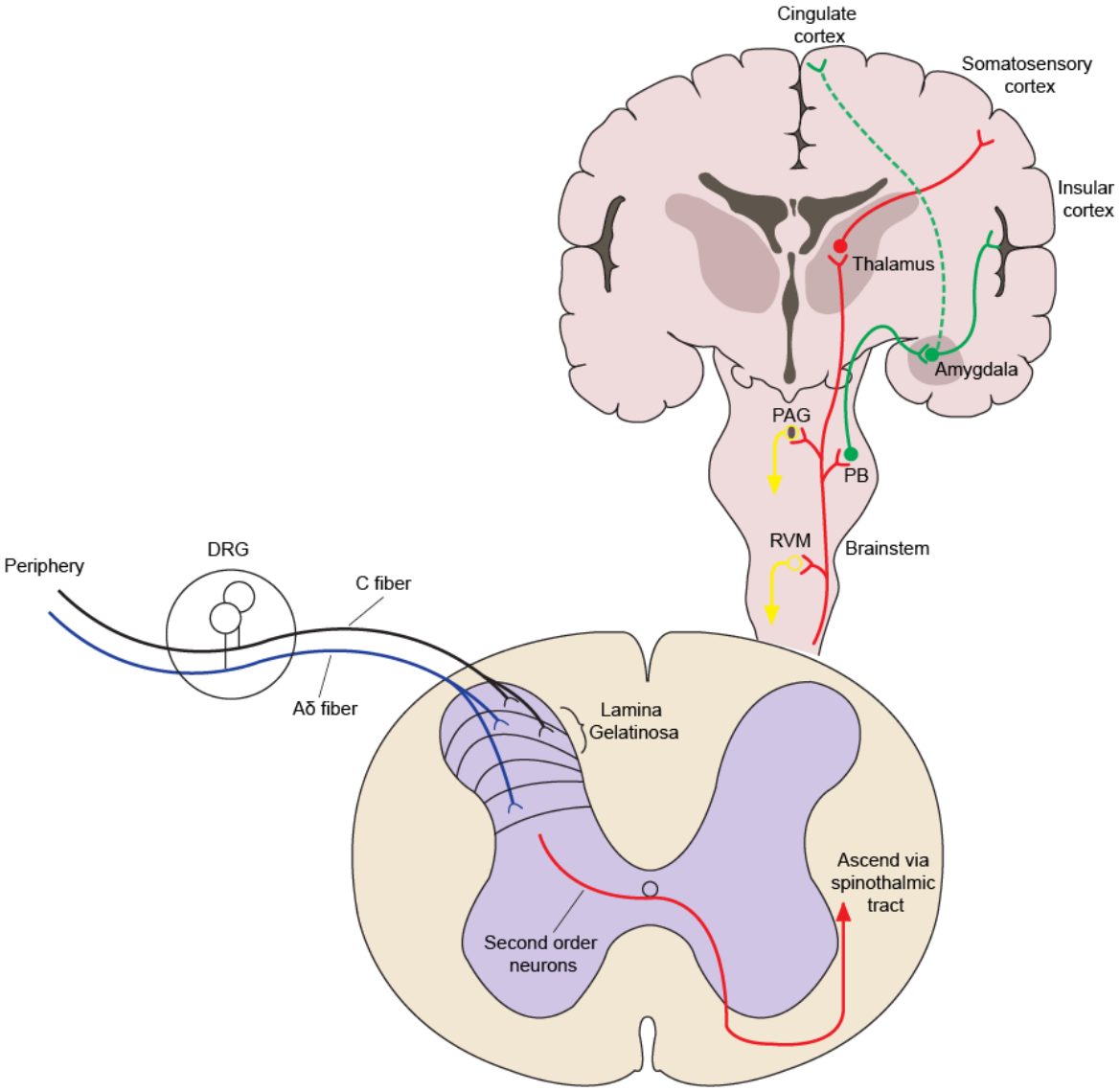

Figure 1.1: Peripheral and central pain pathways. Afferent fibers of nociceptors project from the periphery to the dorsal horn of the spinal cord. Collections of cell bodies of sensory neurons are called DRG (circled). Here C-fibers terminate at the substantia gelatinosa (lamina I and II) whereas Aδ fibers terminate into lamina II and V. Second order neurons then cross the midline of the spinal cord and project to higher centers via the spinothalamic tract. In the CNS, neurons project to the rostral ventral medulla (RVM), periaqueductal gray (PAG) which allow descending modulation. The parabrachial nucleus (PB) projects to the amygdala which in turn sends signals to the insular and cingulate cortices to process the emotional aspect of pain. Projections to the thalamus relay information to the somatosensory cortex regarding localisation and intensity of pain. Figure based on (Basbaum et al., 2009).

1.1.3 Inflammatory pain- sensitisation of nociceptors

Upon injury to body tissue, mechanisms are in place to transduce the signal to the brain. These involve not only the direct transduction of acute pain but also sensitisation of the nociceptive system to make it more receptive to incoming pain signals. There are various mechanisms by which sensitisation can be caused; it can be peripheral (affects peripheral somatosensory fibres) or central (affects central pain pathways, predominantly spinal) (Fischer et al., 2010). One fairly well studied scenario when peripheral sensitisation occurs can be seen in local tissue inflammation. The immune response brought about by an injury or infection often creates a specific local environment referred to as 'inflammatory soup' (Basbaum et al., 2009). It is an amalgamation of various biochemical agents that mediate pro-inflammatory conditions. Bradykinin, prostaglandins, histamine, adenosine triphosphate (ATP) and protons are some of the constituents that are able to activate channels and receptors on the afferent nociceptive fibers innervating the inflamed tissue area and cause action potential generation (Basbaum et al., 2009; Fischer et al., 2010). Immune cells in the vicinity of the injured area are also activated which then release various agents that further sensitise the nociceptive system (Pinho-Ribeiro et al., 2017) (Fig. 1.2).

One outcome of this sensitisation is called 'hyperalgesia' - sensitisation of the nociceptive fibers where there is a heightened sense of pain when painful stimuli occur i.e. a warm shower that begins to burn an injured area of the burnt skin (Fig. 1.3). When tissue is injured, some of the inflammatory mediators are able to modulate the activity of channels implicated in nociception in a way to facilitate the enhancement of nociceptive signals being fired (see below). Central sensitisation is a phenomenon that involves specific changes in the nervous system at the dorsal spinal cord and the brain (Latremoliere and Woolf, 2009). Similarly to peripheral sensitisation, which leads to a heightened sense of pain, central sensitisation also causes a reduction in threshold as well as incorporation of normally innocuous Aβ fibre activation to elicit pain (Woolf, 2010). Ultimately, there is enhancement in the generate action potentials in second order nociceptors before the onset of central sensitisation become sufficient to generate action potentials in the sensitised spinal cord (Latremoliere and Woolf, 2009; Woolf, 2011). Furthermore, molecular changes

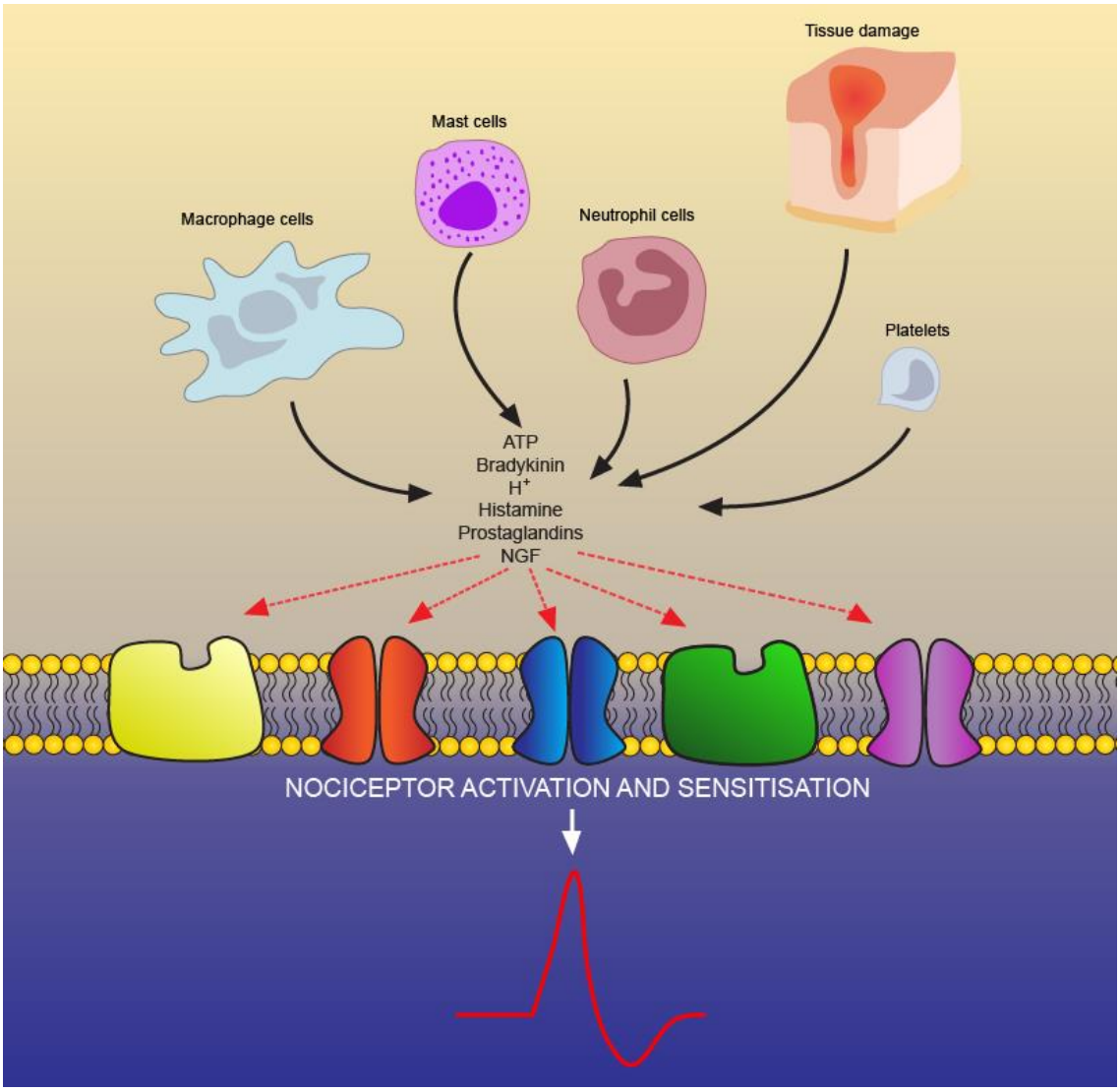

Figure 1.2: Inflammatory response to tissue damage. Immune cells (i.e. mast cells, macrophages, neutrophils) in the vicinity of the injury release the 'inflammatory soup' which encompasses various pro-algesic substances and growth factors. The damages tissue also contributes to the 'inflammatory soup'. These substances activate their corresponding receptors/channels (shown in the membrane), which in turn leads to nociceptor activation and action potential firing as well as nociceptor sensitisation.

excitability of neurons and the nociceptive circuits after increased stimulation of nociceptors (Woolf, 2010). Subthreshold inputs that were previously unable to also facilitate central sensitisation such as abnormally high $Na_v1.3$ channel expression in second order dorsal horn neurons (Hains et al., 2004b). Other effects of central sensitisation include expansion of the primary afferent receptive fields that allows input from uninjured tissue to produce pain (Woolf, 2011). This often results in a phenomenon known as allodynia - a state where innocuous sensations elicit pain; when under normal conditions this wouldn't be the case (Fig. 1.3), as demonstrated in rats (Tal and Bennett, 1994). Upregulation of N-type Ca^{2+} channels in the spinal cord also plays a role in onset of allodynia which is thought to enhance glutamate and SP release at synapses at the dorsal horn (Cizkova et al., 2002; Altier et al., 2007; Lee, 2013). Central sensitisation consists of an element of neural plasticity as the effects of this phenomenon occur for minutes after the stimulation of the afferent fibers (Woolf, 2011). In the brain, sensitisation of the thalamic and somatosensory cortical neurons has been reported in rats that have undergone partial peripheral nerve injury (Guilbaud et al., 1992). Other examples of this phenomenon have been seen in human patients with phantom limb pain and complex regional pain syndrome (CRPS) where imaging studies of the brain have demonstrated changes in cortical representation (Flor et al., 1995; Pleger et al., 2004). Collectively, these sensitisation events allow for increased signal transduction to higher centres to alert the brain regarding the severity of injury but also promote effective healing of the injured tissue. However in some circumstances, this 'protective' mechanism can be altered that leads to spontaneous and unnecessary nociceptive firing which becomes debilitating (Basbaum et al., 2009; Woolf, 2011).

1.1.4 Pharmacology of pain

Various drugs are currently used in the treatment of pain. These 'painkillers' target various aspects of the nociceptive pathway and disrupt the generation of pain, thereby reducing pro-algesic signals sent to higher centres. One class of painkillers are known as non-steroidal anti-inflammatory drugs (NSAIDs). As the name suggests these are anti-inflammatory as they reduce inflammation associated with injury or condition (Day and Graham, 2013). PIP_2 in the lipid membrane is converted into arachidonic acid by phospholipase A 2 (PLA_2) (Day and Graham, 2013). Arachidonic acid (AA) is subsequently converted into prostaglandins, important

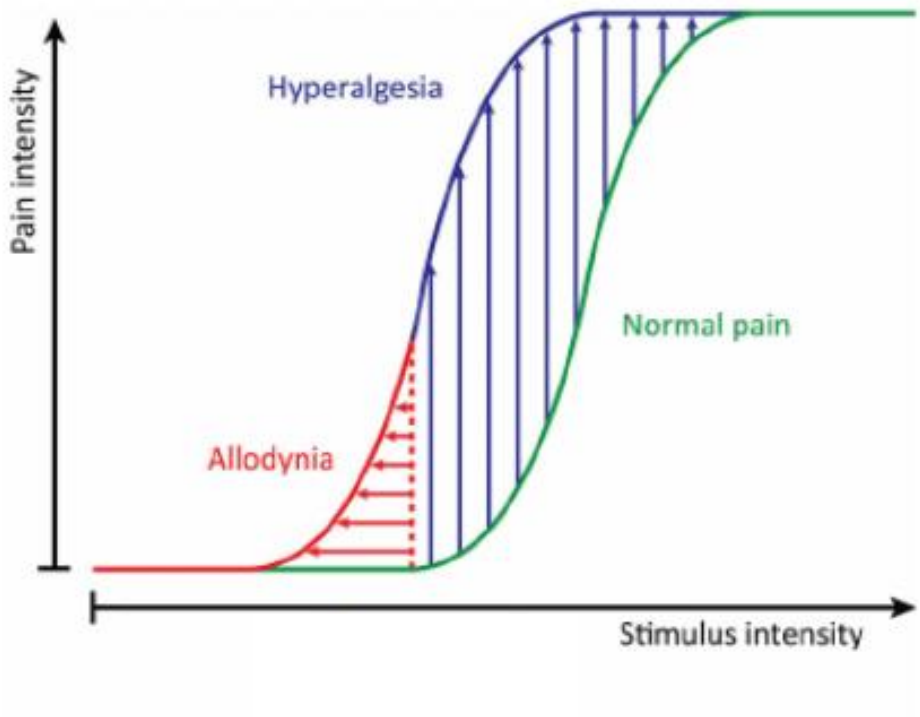

Figure 1.3: Hyperalgesia and Allodynia. Noxious stimuli elicit a response from nociceptors once a threshold is breached, leading to pain sensation (green curve). Hyperalgesia causes a heightened sense of pain to noxious stimuli (represented by the blue curve). A lower stimulus intensity is required to produce the same level of pain as previously. Allodynia results in pain occurring from normally painless stimuli (represented by red section of curve). Previously, these innocuous stimuli did not affect nociception therefore, no pain occurred. Incorporation of Aβ fibres into the nociceptive circuitry results in these stimuli producing pain. Figure adapted from (Lolignier et al., 2015).

mediators of the inflammatory response (see below) by the enzyme cyclooxygenase (COX) I and II. NSAIDS produce their effects by stopping the conversion of AA into prostaglandins by inhibiting COX enzymes (Day and Graham, 2013). Examples of NSAIDs include paracetamol, ibuprofen and aspirin, which have a pain-reducing effect but differing anti-inflammatory effects (Brooks and Day, 1991). Some issues with aspirin and ibuprofen include stomach ulceration and gastrointestinal bleeding (Day and Graham, 2013). Furthermore, Aspirin can't be taken with anticoagulant drugs (such as warfarin) because of their blood thinning properties (Day and Graham, 2013).

Opioids are another set of pain alleviating and are some of the most potent drugs used to combat pain syndromes (Chang et al., 2007). As well as ascending pain signalling, descending signals are also utilised by the brain to modulate pain and reduce the amount of pain felt (Chang et al., 2007). These endogenous signals result from the release of opioids (such as endorphins, enkephalins and dynorphins) which are able to reduce excitability of presynaptic nociceptor nerve terminals (reduce Ca^{2+} influx) (Trescot et al., 2008). Furthermore, opioids also hyperpolarise neurons in the dorsal horn (increase K^{+} currents) (Trescot et al., 2008). Opioid drugs such as morphine, codeine and tramadol are able to activate opioid receptors and mimic the pain-relieving effect of endogenous opioids (Trescot et al., 2008). However, the effects of opioids on the CNS can cause serious side effects including sedation, dizziness, confusion and in some cases respiratory depression (Kosten and George, 2002; Trescot et al., 2008). However, the major issues with opioid drugs is the addiction that is associated with repeated use (Kosten and George, 2002; Chang et al., 2007).

Other drugs include creams or patches consisting of lidocaine or benzocaine which work by numbing specific areas of skin (Brofeldt et al., 1989; Eslamian et al., 2013). Topical creams consisting of capsaicin (see below) are also available which work by 'defunctionalisation' of TRPV1 channels (Anand and Bley, 2011). Another method by which capsaicin creams work is using the phenomenon known as 'depolarisation block', where capsaicin-mediated TRPV1 activation leads to depolarisation of the membrane but this in turn leads to inhibition of voltage gated sodium channels (Anand and Bley, 2011). These are just a few examples of analgesic drugs available and a brief discussion regarding mechanisms by which they produce painkilling

effects. The ultimate goal of research into pain is the development of more analgesic drugs acting on different pathways to maximise the potential for combatting pain syndromes.

1.2 Ion channels involved in pain

All excitable cells such as neurons, muscle cells and cardiac cells, use ion channels to convert stimuli into electrical signals. As mentioned, the nociceptive nervous system uses ion channels in unspecialised nerve endings to process noxious stimuli into action potentials, which are then relayed to the brain allowing perception of pain. Other essential functions of ion channels include generating and shaping action potentials (Jaffe et al., 2011), epithelial transport (Hollenhorst et al., 2011), regulating cell volume (Lang et al., 2007) etc. Ion channels are a diverse family of transmembrane (TM) proteins that allow diffusion of ions down their concentration gradients when activated and their gating mechanism is open (Gadsby, 2009). Furthermore, they can also be categorized depending on the ions they transport- cationic, anionic, non-selective etc and the mode of activation including binding of a ligand or changes in voltage (Gadsby, 2009). The wide variety of channels found in the body is out of the scope of this thesis therefore the following section will focus on ion channels that play a role in nociception.

1.2.1 Sensory channels

1.2.1.1 P2X receptors

The initial phase of nociception is the noxious stimuli, which is sensed by receptors in the free endings of the skin. Ionotropic P2X purinergic receptors are a group of ligand-gated non-selective cation channels that are activated in response to the binding of ATP, allowing the influx of Na^+ and Ca^{2+} into the cell from the extracellular compartment. This group of receptors includes 7 members, P2X1-P2X7, all of which are trimeric complexes (North, 2002). Subunits of these receptors can form homomeric complexes (P2X1-P2X5 and P2X7) or they can form heteromeric complexes (i.e. P2X1/3) (Nicke et al., 1998). On the other hand, it has been discovered that P2X6 receptors are unable to form functional homomeric complexes (Barrera et al., 2005). Each subunit of P2X receptors has a topology consisting of 2 TM domains, a large extracellular domain and internal C- and N-termini (Torres et

al., 1998). The crystal structure of Zebrafish P2X4 binding ATP has been elucidated recently and found to consist of 3 ATP binding sites, which are located at the interfaces between the 3 subunits of the trimer (Hattori and Gouaux, 2012). Expression of these channels have been thought to implicate them in various processes such as modulation of synaptic transmission (Pankratov et al., 1999; Mori et al., 2001; Pankratov et al., 2002, 2003), smooth muscle contraction (Boland et al., 1992; Boland et al., 1993; Gailly et al., 1993; Harhun et al., 2015), the immune response (Burnstock et al., 2014) and nociception (Chizh and Illes, 2001; Waldron and Sawynok, 2004).

P2X2, P2X3 and P2X2/3 have been localised to primary sensory neurons where they play a role in nociception as ATP is one of the factors released by damaged tissue (Chen et al., 1995; Lewis et al., 1995). Studies have shown that knockout (KO) of P2X3 receptors in mice causes reduced afferent nerve activity and nociceptive signalling (Barclay et al., 2002). Furthermore, P2X2 and P2X3 double KO mice also demonstrated attenuated nociceptive responses to intraplantar formalin injection (Cockayne et al., 2005). Development of P2X3-selective antagonists has been able to produce alleviation of neuropathic and inflammatory pain in rat chronic pain models (Jarvis et al., 2002). Antisense oligonucleotide administration against P2X3 receptors has also been successful in reducing mechanical hyperalgesia induced by carrageenan in Wistar rats (Oliveira et al., 2009).

1.2.1.2 Piezo

Piezo proteins have been implicated in mechanotransduction, the physiological process whereby mechanical forces are converted into biological signals to allow organisms to ascertain environmental features (Bagriantsev et al., 2014). Piezo1 and Piezo2 are mechanically activated (MA) non-selective cation channels that allow Na^+ and Ca^{2+} entry into the cell upon activation (Coste et al., 2010; Ranade et al., 2014c).

Piezo1 has been found to be expressed in a wide range of cell types including vascular cells (Ranade et al., 2014a), erythrocytes (Faucherre et al., 2014) and renal tubular epithelial cells (Peyronnet et al., 2013). Piezo2 on the other hand is found in DRG and TG somatosensory neurons (Coste et al., 2010; Bron et al., 2014).

Interestingly, Piezo2 has been implicated in both innocuous and painful mechanoreception (Coste et al., 2010; Bagriantsev et al., 2014), where it is required for mechanotransduction in gentle touch (Ikeda and Gu, 2014; Maksimovic et al., 2014; Woo et al., 2014). Merkel cell-neutrite complexes, which are responsible for gentle touch sensation, express Piezo2 and Merkel cell-specific knockdown of Piezo2 in mice leads to moderately reduced ability to encode gentle touch sensation (Woo et al., 2014). In terms of nociception, Piezo2 is expressed in unmyelinated small-diameter nociceptors (Coste et al., 2010). This channel is also responsible for the rapidly adapting MA current in DRG neurons, which was demonstrated using siRNA against the protein (Coste et al., 2010). Inflammation can also serve to modulate Piezo2 as bradykinin has been shown to enhance these currents suggesting a role for Piezo2 in mechanical hyperalgesia (Dubin et al., 2012). However, Piezo2 KO mice do not display obvious deficits in noxious mechanical sensitivity, therefore the role of this channel in mechanical pain is still requires elucidation (Ranade et al., 2014b).

Structurally, Piezo proteins are very unique proteins owing to their huge size. They have a particularly large number of TM segments, predicted to consist of 30-40 of these structures, which was thought to be produce a homotetrameric structure (Coste et al., 2012). Recently however, the structure of mouse Piezo1 has been solved using cryo-electron microscopy (CryoEM) and has revealed that Piezo1 actually forms as a homotrimer (Ge et al., 2015). Furthermore, each monomer was found to consist of 14 TM segments opposed to the predicted 30-40 (Ge et al., 2015). The homotrimer surrounds a putative ion pore, which is responsible for its ion-conducting properties (Ge et al., 2015).

1.2.1.3 TRP channels

TRP channels are a unique set of proteins that are sensors for a wide spectrum of physical and chemical stimuli (Clapham, 2003; Zheng, 2013). Activation of these diverse channels mediates the flux of Na^{+} and Ca^{2+} into cells, alters the membrane potential and plays an important role in various processes in the body such as sensory transduction (Clapham, 2003), fertilisation (Castellano et al., 2003), vision (Ribelayga, 2010), taste (Ishimaru and Matsunami, 2009), osmoregulation (Arniges et al., 2004) etc. TRP channels are split into various subgroups depending on sequence similarity and are classified as TRPA, TRPC, TRPM, TRPML, TRPN,

TRPP and TRPV. Of these groups, TRPN is the only family to have no mammalian representation (Walker et al., 2000; Sidi et al., 2003).

All TRP channel are presumed to have a similar structure; they have a tetrameric organisation of subunits arranged around a central pore with each subunit consisting of 6TM domains. Unlike voltage-gated ion channels, TRP channels do not have a charged segment 4 domain that provides voltage-sensitivity to these channels. The initially discovered TRP channels were referred to as 'classical' or 'canonical' and categorised as TRPC channel members- TRPC1 being the first mammalian TRP member to be discovered and cloned (Wes et al., 1995). Identification of TRPC1 came from investigations into the process of store operated Ca^{2+} entry (SOCE, see below) (Wes et al., 1995). The TRPC family has 7 members, TRPC1-7 which are split into a further 3 groups depending on functionality and sequence similarity: TRPC1/4/5, TRPC3/6/7 and TRPC2 (Clapham, 2003). However, others have placed TRPC1 on its own suggesting there are in fact 4 groups (Montell, 2005). Despite the many TRP channels present, I will only discuss the TRPV1 channel due to its importance and relevance to my work.

1.3 TRPV1

Transient Receptor Potential Vallinoid 1 (TRPV1) is characterised as a non-selective cationic channel involved with sensing heat as well as being activated by capsaicin (the active compound in chillies) and acidification (H^+) (Rohacs et al., 2008). Nociceptors are known to express TRPV1 and other TRP channel members in order to transduce noxious stimuli into electrical signals for the brain to process. TRPV1 is the most famous of the 'thermoTRP' channels and is able to activate in response to heat above 43°C (Caterina et al., 1997). TRPV1 is found on peptidergic neurons, which also express CGRP and SP, and mainly localise to small diameter C-fibers (Cavanaugh et al., 2011) however some larger diameter neurons also express TRPV1 (Ohsawa et al., 2013). Both pre- and postsynaptic neurons at the dorsal horn of the spinal cord also express TRPV1 (Valtschanoff et al., 2001; Choi et al., 2016). As well as CNS expression, TRPV1 is also expressed in non-neuronal tissues such as liver (Siegmund et al., 2005), mast cells (Stander et al., 2004), keratinocytes (Inoue et al., 2002), hair follicle (Bodo et al., 2005; Biro et al., 2006), bladder

(Szallasi et al., 1993b, a), epithelia (Bodo et al., 2004) and airways (Russell and Lai-Fook, 1979; Lundberg et al., 1983b; Lundberg et al., 1983a).

TRPV1 is strongly implicated in the inflammatory sensitisation of nociceptors; the underlying mechanisms include the sensitisation by inflammatory mediators such as bradykinin (see below) but also increased expression of TRPV1 at the sight of injury (Kim et al., 2008). Furthermore, activation of TRPV1 at the nerve endings also leads to the release of other pro-algesic compounds, such as CGRP and SP, from the nociceptive terminals (Theriault et al., 1979; Wick et al., 2006b). CGRP activates calcitonin receptor-like receptor (CALCLR) which in turn triggers protein kinase A (PKA) and protein kinase C (PKC). CGRP has been known to produce mechanical hyperalgesia and central sensitisation in nociceptors and the dorsal horn of the spinal cord, respectively (Sun et al., 2004a; Sun et al., 2004b).
Two groups generated TRPV1-KO mice and both found that capsaicin and noxious thermal heat were unable to produce currents in cultured DRG neurons (Caterina et al., 2000; Davis et al., 2000). TRPV1-mediated pH changes were also unable to induce currents in TRPV1-KO DRG neurons. Caterina and colleagues showed that there were behavioural deficits in mice during the aversive drinking test. When water (which mice drank for 3 days) was changed to capsaicin containing solution, wild type mice showed nocifensive behaviour whereas TRPV1-KO mice continue to drink water in a similar manner to previous days (Caterina et al., 2000). This suggests that capsaicin produces its effects exclusively through TRPV1 activation. Both groups also showed reduced thermal hyperalgesia induced by carrageenan injection in TRPV1-KO mice (Caterina et al., 2000; Davis et al., 2000). Heat-based behavioural tests (hot-plate and tail immersion tests) showed increased latencies in TRPV1-KO mice compared to wild type littermates, suggesting a role in noxious heat (Caterina et al., 2000). Conversely, Davis and colleagues showed that mice lacking TRPV1 had normal thermoresponsive behaviour. Hot plate tests on TRPV1-KO mice showed normal heat sensitivity; this was paradoxical when considering the same group found DRG from TRPV1-KO mice showed no sensitivity to noxious heat (Davis et al., 2000). The differing responses reported by the 2 independent groups could be explained due to the tests used in these studies. The results from Caterina and colleagues demonstrate that capsaicin requires TRPV1 to produce its activity however Davis and colleagues used noxious heat as the stimulus for TRPV1

activation meaning their results suggest TRPV1 may not be the only channel responsible for noxious heat sensation. Furthermore, a study using skin-nerve preparations reported normal noxious heat sensation in TRPV1-KO mice but showed the importance of TRPV1 in heat sensitisation and hyperalgesia. A sensitiser of TRPV1, 2-aminoethoxydiphenyl borate, was only able to produce hyperalgesia in wild type but not TRPV1-KO mice (Zimmermann et al., 2005). Recently, another group also demonstrated TRPV1-KO DRG neurons still evoked responses to noxious heat however capsaicin produced no effects (Cho et al., 2012). As mentioned above, this suggests the presence of other heat sensors in the range of TRPV1's heat-range (see below).

1.3.1 Structure of TRPV1

Structurally, TRPV1 complexes are composed as a tetramer of subunits, with each subunit consisting of 6TM domains and the pore region found between TM domains 5 and 6 (Moiseenkova-Bell et al., 2008; Liao et al., 2013). Each subunit has a molecular mass of 95kDa (Caterina et al., 1997) and possess intracellular N and C-termini consisting of various areas of interest (Moiseenkova-Bell et al., 2008; Liao et al., 2013). The N-terminus has 6-ankyrin repeat regions where both calmodulin (CaM) and ATP are known to bind whereas the C-terminus has areas for phosphatidylinositol 4,5-bisphosphate (PIP_2) binding as well as further regions for CaM binding (Prescott and Julius, 2003; Lishko et al., 2007) (Fig. 1.4A). Various phosphorylation sites are also scattered around these internal regions of TRPV1. A conserved 25 amino acid region known as the 'TRP box' is located on the C-terminus which is essential for tetramerisation of TRPV1 and is also involved in its allosteric activation (Garcia-Sanz et al., 2004). The channel exists as a homotetramer but can also form chimeric channels with TPRA1 and TRPV3 (Cheng et al., 2007; Cheng et al., 2012; Fischer et al., 2014) (Fig. 1.4A).

The cryoEM structure of mammalian TRPV1 was solved in 2013 and it was discovered that the architecture of TRPV1 closely resembles voltage gated ions channels despite fairly low (~20%) sequence similarity (Liao et al., 2013). The tetrameric structure shows 4-fold symmetry around a central ion conduction pore and the extracellular mouth of the channel is wide with a relatively small selectivity filter (Liao et al., 2013). A 'linker' region on each subunit, which links the Ankyrin repeat

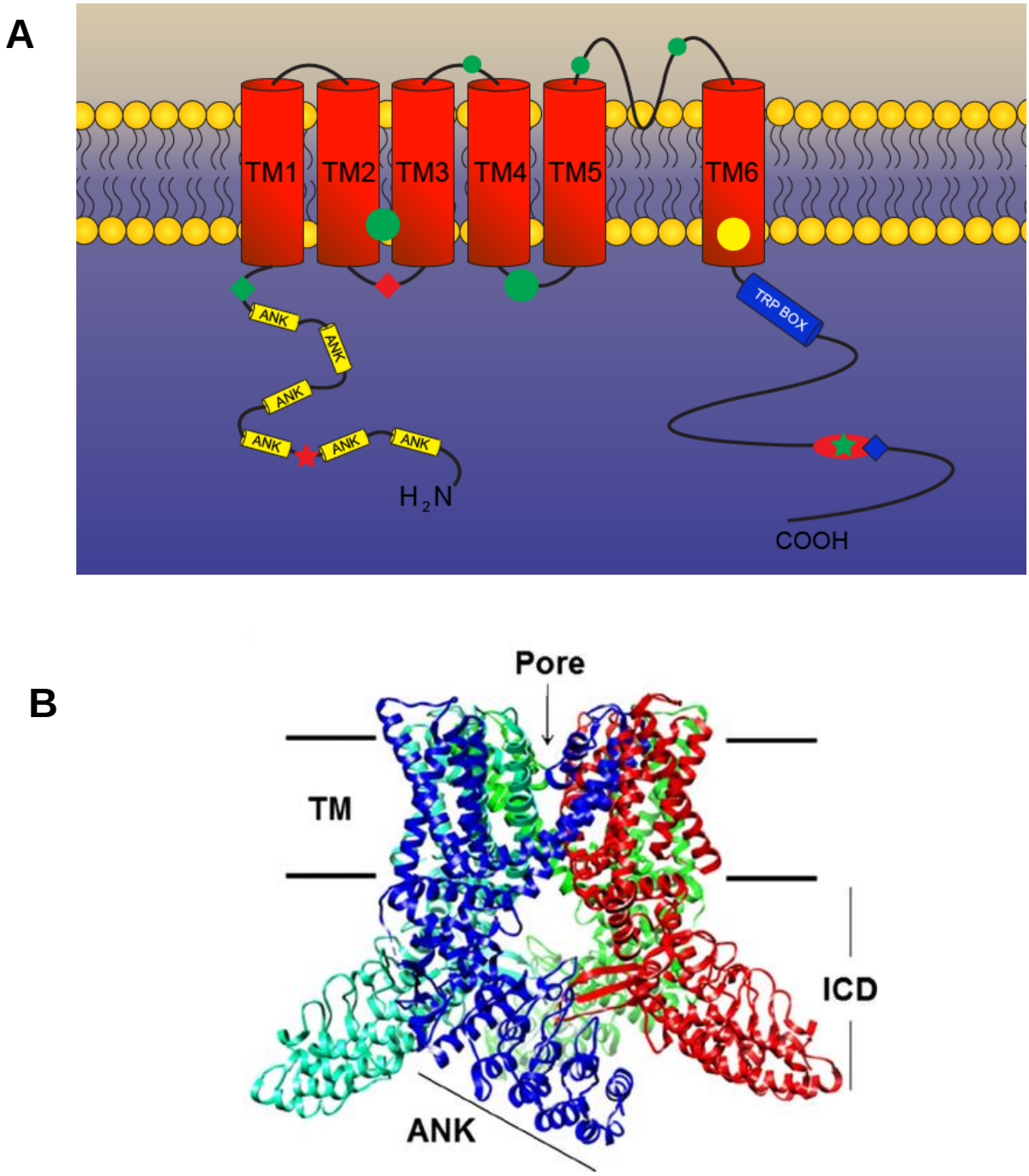

Figure 1.4: TRPV1 Structure. (A) The topology of TRPV1 showing 6 TM domains with a pore loop between TM 5 and 6. Various areas for modulation are indicated as the following: ANK: Ankyrin domains, Large Green Circle: Capsaicin, Small Green Circles: H^+, Green Diamond: PKA, Blue Diamond: PKC Red Diamond: PKA/PKC, Green Star: CaM, Red Star: CaM/ATP, Red Oval. PIP_2, Yellow Circle: Heat. (B) Crystal structure of TRPV1 showing the channel as a tetrameric protein. Ankyrin repeat domains are indicated for a single subunit of TRPV1. ICD: Intracellular domain. Figure adapted from (Liao et al., 2013) and (Morales-Lazaro et al., 2014).

domain section to the TM segments and the C-terminus, interacts with 2 ankyrin repeats of adjacent subunits to assemble the channel (Liao et al., 2013). An interaction between the TRP box domain and the S4-S5 linker also plays a role in stabilising the structure of the channel (Liao et al., 2013) (Fig. 1.4A and B).

1.3.2 Sensitisation

TRPV1 can be influenced by the plethora of pro-algesic mediators that are released under inflammatory conditions (Caterina and Julius, 2001). As mentioned above, sensitisation is an increase in the responsiveness of nociceptors to subthreshold stimuli and this can occur due to effects on the TRPV1 receptor itself, which in essence is 'sensitised' leading to enhanced activity of the channel (Caterina and Julius, 2001; Geppetti and Trevisani, 2004).

1.3.2.1 PKA and PKC

The presence of various kinase-binding sites on the intracellular domains of TRPV1 allows for modulation of its activity (see above) (Touska et al., 2011). Release of pro-algesic agents at the site of injury and as part of the inflammatory response activate their respective receptors and initiate different secondary messenger cascades (Basbaum et al., 2009). Prostaglandins ultimately activate PKA whereas bradykinin and ATP activate PKC, both of which are able to sensitise TRPV1 (Fischer et al., 2010). Bradykinin is one of the inflammatory mediators released during the inflammation process (Golias et al., 2007; Basbaum et al., 2009; Fischer et al., 2010). This polypeptide is made of nine amino acids (Golias et al., 2007) and synthesis of bradykinin occurs through the kinin-kallikrein system where high molecular weight kininogen (found in blood plasma) is converted into bradykinin via the activity of the enzyme kallikrein, a serine protease (Mandle et al., 1976; Blais et al., 2000). Kallikrein is produced by the precursor prekallikrein, which itself is activated by Factor XII and during tissue injury or trauma, Factor XII is released hence accelerating the production of kallikrein (Jukema et al., 2016). Interaction of Factor XII, prekallikrein and kininogen with negatively charge surfaces i.e. endothelial cells, leads to initiation of bradykinin production (Kaplan and Ghebrehiwet, 2010). Further cleavage of bradykinin by carboxypeptidase results in the formation of the active metabolite desArg9-BK (activates B_1 receptor) (Ni et al., 2003). Inactivation of bradykinin is a rapid process, which confines the activity of this

peptide to a small, localised area, making this ideal for mediating inflammatory pain in damaged tissue. This is achieved by kininases such as aminopeptidase P (Golias et al., 2007). Bradykinin is also associated with vasodilation of blood vessels and is broken down by angiotensin-converting enzyme (ACE), hence initiation of the vasoconstrictive Renin-Angiotensin system and leading to a reduction in the levels of bradykinin in the body (Golias et al., 2007). There are 2 principle receptors that are activated by bradykinin- B_1 and B_2 with another speculated B_3 tracheal receptors thought to exist too (Golias et al., 2007). Upon activation of these metabotropic receptors, bradykinin is able to induce a secondary messenger cascade via the G_q pathway which involves the activation of the enzyme phospholipase C (PLC)-β (Mizumura et al., 2009). PLC-β cleaves PIP_2 at the membrane leading to the formation of inositol 1,4,5-trisphosphate (IP_3) and diacylglycerol (DAG). Both products of PIP_2 cleavage have varying effects with IP_3 able to activate IP_3 receptors (IP_3R) in the endoplasmic reticulum (ER) and induce Ca^{2+} release. DAG on the other hand is an activator of PKC which phosphorylates proteins (Rohacs et al., 2008). The latter has implications in inflammation and hyperalgesia as bradykinin-derived PKC phosphorylation of TRPV1 decreases the temperature threshold thus increasing sensitivity to noxious heat (Sugiura et al., 2002) (Fig. 1.5).

Proteases-activated receptor 2 (PAR-2) can also sensitise TRPV1; PAR-2 receptors are activated during the inflammatory process where the release of proteases (i.e. trypsin) occurs. Cleavage of the extracellular N-terminal domain of the receptor allows the newly formed N-terminal to act as a ligand hence activating the receptor (Coughlin, 2000; Arora et al., 2007). This subsequently triggers the G_q pathway and ultimately PKC activation (Arora et al., 2007). Prostaglandin E2 is another inflammatory mediator which is able to initiate the adenylyl cyclase (AC) pathway to increase cyclic adenosine monophosphate (cAMP) production and subsequent PKA activation (Fischer et al., 2010). Activated PKA then proceeds to sensitises TRPV1 (Moriyama et al., 2005). Interestingly, PAR-2 activation has been observed to induce activation of PKA via cAMP/PKA as well as the PKC pathway (Amadesi et al., 2006). This was also coupled to the observation that both of these kinases are involved in the sensitisation of TRPV1 (Amadesi et al., 2006) (Fig. 1.5).

1.3.2.2 TRPV1 upregulation

Another mechanism by which TRPV1 activity is enhanced is through increased expression of the channel in nociceptors (Zhang et al., 2005; Stein et al., 2006). Nerve growth factor (NGF) is known to upregulate TRPV1 expression in nociceptors by activating TrkA receptors and inducing PI3 kinase (Zhuang et al., 2004). Downstream of this, another kinase- Src- is activated which induces the upregulation of TRPV1 into the plasma (Jin et al., 2004; Zhang et al., 2005). Insulin and insulin-like growth factor enhance TRPV1 currents, an effect produced by upregulation of TRPV1 expression (Van Buren et al., 2005).

1.3.2.3 ATP

ATP binds to both N- and C-termini of TRPV1 (Kwak et al., 2000; Lishko et al., 2007). ATP has been shown to enhance TRPV1 activity and also inhibit the desensitisation of the channel when activated by capsaicin (Kwak et al., 2000; Lishko et al., 2007). Interestingly, ATP binds to the N-terminal Ankyrin binding domain where CaM binds and competes with CaM and it has also been suggested that ATP is displaced by CaM from this binding site (Lishko et al., 2007). ATP is a substrate in the production of PIP_2, which is required in the patch pipette to rescue TRPV1 from desensitisation (Liu et al., 2005). Furthermore, blocking kinases involved in the conversion of PI to PIP (precursor of PIP_2) also delayed recovery from desensitisation (Liu et al., 2005).

1.3.3 Desensitisation

Repeated or prolonged stimulation of TRPV1 can lead to the receptor becoming insensitive to further activation. This process of TRPV1 desensitisation seems to require the presence of extracellular Ca^{2+} (Koplas et al., 1997); removal of extracellular Ca^{2+} or buffering of $[Ca^{2+}]_i$ abolishes desensitisation (Koplas et al., 1997). Various theories have been proposed regarding this desensitisation process which I will briefly discuss below.

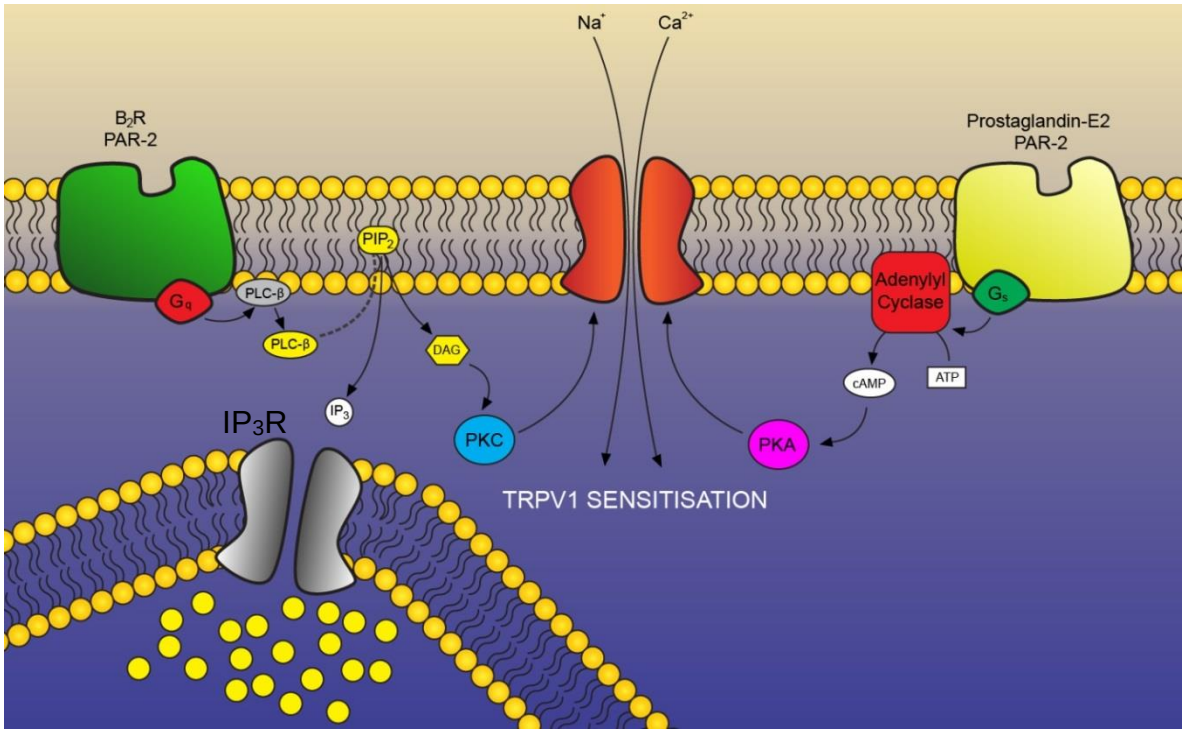

Figure 1.5: Sensitisation of TRPV1 by PKA and PKC. Receptor activation (i.e. Prostaglandin-E2- yellow receptor on right) leads to the initiation of the G_s signalling cascade. Activation of adenylyl cyclase (A) converts ATP to cAMP, which in turn activates PKA. PKA is able to phosphorylate TRPV1 (orange channel) and sensitise its activity. B_2R activation (green receptor on left) leads to initiation of the G_q signalling pathway, activating PLC-β. PLC-β is able to cleave PIP_2 in the plasma membrane and form DAG and IP_3R. DAG activates PKC which can also sensitise TRPV1 activity. IP_3 is able to diffuse to the ER where IP_3R (grey channel) are located and induce ER-Ca^{2+} release into the cytosol. In a pro-algesic model, this Ca^{2+} release would be able to activate other Ca^{2+} dependent proteins/processes (see below). PAR-2 has been known to activate both PKA and PKC pathways (Amadesi et al. 2006).

1.3.3.1 PIP_2

PIP_2 also plays an important role in TRPV1 regulation. Initial studies found that PIP_2 plays an inhibitory role in TRPV1 activity (Chuang et al., 2001). Bradykinin-induced PIP2 cleavage was suggested to release TRPV1 inhibition hence allowing activity of the channel (Chuang et al., 2001). However, contrary to this effect, other TRP channels were found to be activated by PIP_2 (Criddle et al., 2004; Lee et al., 2005; Rohacs et al., 2005; Nilius et al., 2006). Stein and colleagues subsequently found that PIP_2 was able to activate TRPV1 in excised patches (Stein et al., 2006) and this was confirmed by ensuing research by Rohacs' lab but interestingly, this study found that under certain circumstances, PIP_2 also has an inhibitory effect on TRPV1 (Lukacs et al., 2007). PIP_2 depletion was able to potentiate TRPV1 activity at low capsaicin concentrations (1nM) however this was not the case with higher capsaicin concentrations (1μM) (Lukacs et al., 2007). At lower concentrations (1nM), PIP_2 maintains a partial inhibitory effect on TRPV1 which is removed after PIP_2 depletion (Lukacs et al., 2007; Rohacs et al., 2008). The group concluded that higher capsaicin concentrations (1μM) allow increased Ca^{2+} influx which activates PLC and consequently leads to PIP_2 cleavage and channel desensitisation (Lukacs et al., 2007). Furthermore, inhibiting either PLC or PIP_2 depletion (presence of PIP_2 in whole cell patch pipette) caused desensitisation to be abolished in sf21 insect cells and recombinant HEK293 cells (Lishko et al., 2007; Lukacs et al., 2007). In summary, lower capsaicin concentrations lead to low levels of PIP_2 depletion which produces TRPV1 activity however, when greater concentrations of PIP_2 are depleted due to greater capsaicin concentrations, the channel is desensitised- almost acting as a brake to control the effects of TRPV1. Further research is still required to fully elucidate the effects of PIP_2 on TRPV1.

1.3.3.2 CaM

CaM is another proposed desensitiser of TRPV1. There are 2 theories regarding CaM's implications on TRPV1: direct and indirect desensitisation (Rohacs et al., 2008). Direct effects of CaM are controversial despite the presence of CaM-binding domains on the C-terminus of TRPV1 and reported interactions between CaM and this site (Numazaki et al., 2003). Removal of this segment of TRPV1 disrupted the process of desensitisation however an inhibitor of CaM nor the co-expression of a Ca^{2+}-insensitive CaM mutant in HEK293 cells was able to produce similar inhibition

of desensitisation (Numazaki et al., 2003). CaM was found to produce approximately 50% inhibition in excised patches from Xenopus Oocytes heterologous expressing TRPV1 however, this was a slow process which is in stark contrast to the rapid and nearly complete desensitisation seen in native TRPV1 channels (Rosenbaum et al., 2004). CaM was also found to interact with the N-terminus where the repeat Ankyrin domains are located (Rosenbaum et al., 2004; Lishko et al., 2007). In sf21 insect cells, TRPV1 is inhibited by CaM and unlike findings by Numazaki and colleagues, CaM inhibitors abolished capsaicin-induced desensitisation of TRPV1 (Lishko et al., 2007). Indirect mechanisms of CaM desensitisation involve activating calcineurin- a protein phosphatase (Jung et al., 2004). Inhibition of calciuneurin has been shown to reduce TRPV1 desensitisation in both DRG neurons and cell lines (HEK293 and HeLa cells) (Docherty et al., 1996; Mohapatra and Nau, 2005). Ca^{2+} influx into cells is the trigger for desensitisation and seems to be a mechanism by which TRPV1 protects the cell from toxic Ca^{2+} overload (Bhave et al., 2002). Therefore, Ca^{2+} activating CaM to desensitise TRPV1 is a credible theory regarding desensitisation.

1.3.4 TRPV1 in chronic pain

Alterations in the neural circuitry underlying pain transmission can lead to unnecessary pain and long-lasting chronic pain conditions; unsurprisingly, ion channel expression profiles play a significant role in the generation of chronic pain (Linley et al., 2010). Various studies have demonstrated altered TRPV1 expression in chronic pain conditions. Under normal conditions, TRPV1 is expressed in mainly C-fibres and to a lesser extent in Aδ fibres (Guo et al., 1999). However, two weeks after spinal nerve ligation (SNL), TRPV1 expression was decreased in the soma of damaged DRG neurons but was present near the site of injury (Hudson et al., 2001). Furthermore, SNL in lumbar (L) 5 of the spinal cord produced a reduction of TRPV1 in this region but analysis of TRPV1 expression in another, undamaged region L4, showed increased TRPV1 expression (Fukuoka et al., 2002; Rashid et al., 2003; Mitrirattanakul et al., 2006). Interestingly, after partial spinal nerve ligation (PSNL), undamaged neurons showed increased expression of TRPV1 (Hudson et al., 2001). De novo expression of TRPV1 in myelinated A-fibers was also seen after PSNL (Rashid et al., 2003). Despite these findings, other studies have shown increased TRPV1 expression in injured neurons with no new expression of TRPV1 in A-fibers

(Christoph et al., 2007; Vilceanu et al., 2010). Chronic constriction injury (CCI) models of neuropathic pain show not only enhanced expression of TRPV1 in the spinal cord, but also enhanced CGRP release in spinal cord slices (Kanai et al., 2005).

In an animal model of lingual pain injury, overexpression of TRPV1 was demonstrated using imaging techniques (Biggs et al., 2007). Patients suffering from vulvodynia, a painful condition characterised by a burning sensation in the vulva, were showed increased TRPV1 expression in biopsies (Tympanidis et al., 2004). Inflammatory conditions of the bowel such as irritable bowel syndrome (IBS) and chronic inflammatory bowel disease (IBD), characterised by abdominal pain as part of the syndrome, also display enhanced levels TRPV1 in biopses (Yiangou et al., 2001; Geppetti and Trevisani, 2004; Akbar et al., 2008). Accordingly, TRPV1 antagonists are able to reduce experimental colitis (Miranda et al., 2007). Moreover, several studies have provided evidence linking chilli pepper consumption and IBS (Shah et al., 2000; Agarwal et al., 2002; Schmulson et al., 2003). TRPV1 also plays a role in the pathogenesis of pancreatitis, a painful, inflammatory condition of the pancreas (Liddle and Nathan, 2004; Nilius, 2007). An example of pancreatitis induction is through cerulein release (Kim, 2008). Cerulein is a peptide that induces inflammation by producing free radicals in pancreatic acinar cells, which in turn lead to inflammatory cytokine production (Kim, 2008). This pathological activation of nociceptors leads to release of SP and CGRP, hence pain generation related to pancreatitis (Nilius, 2007). These inflammatory mediators act on TRPV1 to generate pancreatitis-related pain sensation (Nathan et al., 2001; Nathan et al., 2002; Nilius, 2007). Capsezipine, a TRPV1 antagonist, reduced cerulein-induced pancreatitis in rats through attenuated SP release and tissue damage (Nathan et al., 2001; Nathan et al., 2002). Interestingly, excessive alcohol consumption is known to be a frequent cause of pancreatitis; this can be explained with respect to TRPV1 as ethanol is able to sensitise TRPV1 activity (Trevisani et al., 2002; Criddle et al., 2004; Nilius, 2007). L-arginine is also able to cause pancreatitis in rats which has been shown to be mediated by TRPV1-induced SP and CGRP release (Wick et al., 2006b; Wick et al., 2006a). Osteoarthritis is a disorder which encompasses joint pain as part of its presentation and chronic pain models of osteoarthritis report both overexpression of TRPV1 and enhanced release of CGRP (Fernihough et al., 2005). TRPV1-KO mice

present with reduced arthritic changes in tibiotarsal joints (Szabo et al., 2005). This effect was also evident in Complete Freund's Adjunct (CFA) -induced knee swelling comparisons with wild type rats (Barton et al., 2006).

1.4 Voltage-gated channels

1.4.1 Voltage-gated sodium channels

Voltage gated ion channels play a vital role in determining the excitability of neurons. Voltage gated sodium channels (Na_v) underlie the sharp rise of the action potential and are critically important for the conduction of signals throughout the nervous system. Closed at resting membrane potentials, Na_v channels open rapidly (within a millisecond) in response to depolarisation and allow Na^+ influx into the cell (Catterall, 2000a). As Na^+ floods into the cells, within milliseconds, the Na_v channels are inactivated due to gating properties of the channel. The inactivation gate moves to occlude the open pore and push the channel into the inactivated state (Capes et al., 2013). As the membrane is repolarised, the occluded pore is unblocked as the inactivation gate recedes back to its initial conformation and closes ready for reactivation.

Structurally, Na_v channels are composed of an α-subunit with 4 homologous domains, each consisting of 6 non-identical TM segments (Beneski and Catterall, 1980; Catterall, 2000a; Mantegazza and Catterall, 2012). This complex has a molecular mass of approximately 260kDa (Beneski and Catterall, 1980). The α-subunit has been found to produce functional Na^+ channels however there are also auxiliary subunits that can also bind to the α subunit. Four β-subunit's exist (β1-4) consisting of an N-terminus extracellular immunoglobulin-like fold with a single TM segment (Catterall, 2012). These auxiliary subunits appear to be involved in modulation of channel gating and cell-cell interactions (Catterall, 2000a). Segments 1-4 in each domain are responsible for the voltage sensitive ability of Na_v channels and are collectively known as the voltage senor domain. It has been proposed that the positively charged residues in segment 4 move outward during depolarisation, which leads to a conformational change and channel opening (Bhave et al., 2002; Namadurai et al., 2015).

There are 9 Na_v channels that have been discovered, $Na_v1.1$-1.9 and an atypical Na^+ channel- Na_x (also referred to as Na_v2). Of these channels, $Na_v1.3$, $Na_v1.7$, $Na_v1.8$ and $Na_v1.9$ are expressed in DRG (Dib-Hajj et al., 2010). $Na_v1.5$ are expressed at very low levels in DRG neurons too (Dib-Hajj et al., 2010). In embryonic neurons, $Na_v1.3$ is the most abundant isoform before receding in neonates and is not detected in adult DRG (Waxman et al., 1994). However, $Na_v1.3$ expression is upregulated in peripheral nerve injury and axotomised rodent DRG (Waxman et al., 1994; Hains et al., 2004b; Lindia et al., 2005). Contactin, a molecule released after axotomy, is known to interact with $Na_v1.3$ in DRG and increase current density (Shah et al., 2004). Phenytoin, a Na_v blocker, has been found to assert a neuroprotective effect on axons and nerves after SCI (Hains et al., 2004a). Despite this increased presence of $Na_v1.3$, other studies have shown a redundancy in its involvement in injury-induced hyperexcitability of neurons. Global or DRG-specific KO of $Na_v1.3$ doesn't disrupt nocifensive behaviour in mice after nerve injury (Nassar et al., 2006). Furthermore, intrathecal antisense oligonucleotides against $Na_v1.3$ did not reduce neuropathic pain in a rat nerve injury model (Lindia et al., 2005).

$Na_v1.7$ is expressed in a wide range of sensory and sympathetic ganglia and in both small and large diameter DRG neurons (Djouhri et al., 2003). In functionally identified nociceptors, expression of $Na_v1.7$ is relatively high (Djouhri et al., 2003; Rush et al., 2006). Its function is thought to involve the amplification of weak stimuli known as 'generator potentials'. Despite activating and inactivating rapidly, the transition from the activated channel to the inactivated configuration is slow when the membrane is depolarised. Ultimately, this allows $Na_v1.7$ to be present and available for further generator potentials (Dib-Hajj et al., 2010). Consistent to its proposed role in nociceptors, $Na_v1.7$ expression has been localised at free nerve endings (Cummins et al., 1998). Inflammation has been shown to increase the expression of $Na_v1.7$ and interestingly, mutations in $Na_v1.7$ have been implicated in CIP (Black et al., 2004).

1.4.2 Voltage-gated calcium channels

One of the vital means by which Ca^{2+} can be increased in cells from outside the cell is through voltage-gated Ca^{2+} channels (VGCCs). Found in excitable cells such as skeletal muscle, cardiac myocytes and neurons, VGCCs, as the name states, are Ca^{2+} channels that activate in response to changes in membrane potential (Zamponi and Snutch, 2013).

These channels are subclassified into 2 groups: low voltage activated (LVA) and high voltage activated (HVA) depending on the membrane potential at which they are activate (Zamponi and Snutch, 2013). The LVAs consist of a single group- T-type Ca^{2+} channels, whereas the HVAs have 4 group members- L, P/Q, N and R-type Ca^{2+} channels (Zamponi and Snutch, 2013). T and L-type VGCCs have more than 1 isoform (Table 1.2). LVAs are unique as they are activated when the membrane potential reaches ~-60mV (Perez-Reyes, 2003) whereas HVAs require greater depolarisation to ~-40mV before they activate (Solinas et al., 2013). Structurally, VGCCs comprise of various subunits that produce the functional channel. This includes an α subunit (~190kDa), which is the primary subunit and forms the Ca^{2+}-selective pore of the channel (Catterall et al., 2005). Furthermore, this α subunit also houses the voltage-sensors and includes sites for drug/toxin binding (Catterall, 2000b). The α1 subunit is made up of a single protein with a tetrameric structure (numbered I-IV) with each of the domains consisting of 6 TM segments (Catterall et al., 2005). The pore loop formed between segments 5 and 6 of each domain contribute to the formation of the actual pore itself (Catterall, 1995; Gurkoff et al., 2013). The pore of the α1 subunit is important in conforming the selectivity of the channel to the divalent Ca^{2+} ion compared to monovalent ions (Cibulsky and Sather, 2003; Sather and McCleskey, 2003). The N and C-termini as well as the intracellular side of the channel (linkers of the 4 domains) are rich in important targets for channel modulators (Catterall et al., 2005). Other subunits are referred to as auxiliary and include the β, α2δ and ɣ- subunits (Dolphin, 2012; Gurkoff et al., 2013). These cytoplasmic proteins are able to modulate the activity of the α1 pore by binding to various parts of the protein along with being involved in trafficking of the channel and modulating the kinetics (Campiglio and Flucher, 2015). In neurons the activity of VGCCs allows robust Ca^{2+} entry in response to depolarisation, e.g. during firing of an action potential.

Type	Isoforms	LVA/HVA	Expression
T	$Ca_v3.1$ $Ca_v3.2$ $Ca_v3.3$	LVA	Heart, pancreas, kidney, DRG, placenta, smooth muscle
L	$Ca_v1.1$ $Ca_v1.2$ $Ca_v1.3$ $Ca_v1.4$	HVA	Cav1.1: skeletal muscle $Ca_v1.2$: CNS, smooth muscle and heart; $Ca_v1.3$: CNS, endocrine cells $Ca_v1.4$: skeletal muscle
P/Q	$Ca_v2.1$	HVA	CNS, heart, pituitary, spinal cord
N	$Ca_v2.2$	HVA	CNS, DRG
R	$Ca_v2.3$	HVA	CNS

Table 1.2: Different types of VGCCs. Isoforms, activation group and expression profile

1.4.2.1 LVA

T-type Ca^{2+} channels are the only group of LVA VGCCs. There are 3 isoforms of the α1 subunit referred to as $Ca_v3.1$, $Ca_v3.2$ and $Ca_v3.3$ (Perez-Reyes, 2003) and are readily expressed in the heart (Ono and Iijima, 2010), smooth muscle (Fry et al., 2006), kidney (Zhou and Greka, 2016), pancreas (Yang and Berggren, 2006) and neurons (Molineux et al., 2006); $Ca_v3.2$ being the most abundant in DRG (Park and Luo, 2010; Rose et al., 2013). Unlike some HVAs, these VGCCs do not require additional auxiliary subunits to function (Lambert et al., 1997). In terms of their nociceptive activity, T-type VGCCs are found in peripheral afferent fibres where they

are involved in modulating the excitability of nociceptors (Bourinet et al., 2005; Todorovic and Jevtovic-Todorovic, 2006; Obradovic et al., 2014). Due to their ability to be activated at lower membrane potentials close to the resting membrane potential, T-type VGCCs allow initial Ca^{2+} entry in response to sub-threshold stimulation leading to slight depolarisation hence priming and enhancing neurons for action potential firing (Huguenard, 1996; Amir et al., 2002; Bodo et al., 2005; Molineux et al., 2006; Park and Luo, 2010). Our lab has also shown how bradykinin application to DRG neurons increases T-type channel abundance, which indicates a possible role in inflammatory pain (Huang et al., 2016). Therefore, T-type VGCCs are a validated target in terms of developing analgesics.

1.4.2.2 HVA

L-type VGCCs are found expressed in a whole host of cell types, including the CNS (Park and Luo, 2010; Morton et al., 2013), cardiac cells (Bodi et al., 2005), VSMCs (Kubo et al., 1998), skeletal muscle (Bannister et al., 2009), retina (Baumann et al., 2004) and the sinoatrial node (Ono and Iijima, 2010). There are 4 different isoforms for L-type VGCCs- $Ca_v1.1$, $Ca_v1.2$, $Ca_v1.3$ and $Ca_v1.4$ (Zamponi and Snutch, 2013); the most plentifully expressed in neurons being $Ca_v1.2$ and $Ca_v1.3$ (Hell et al., 1993; Ludwig et al., 1997). High membrane depolarisation leads to long-lasting activation of L-type VGCCs due to their slow inactivation (Helton et al., 2005). This means that there is a large influx of Ca^{2+} attributed to L-type VGCC activation that makes these channels important for processes such as excitation-transcriptional coupling (Barbado et al., 2009; Lu et al., 2015; Arias-Calderón et al., 2016). $Ca_v1.3$ is different in terms of its biophysical properties as it activates faster and at more negative membrane potentials compared to the other channels possibly leading to spontaneous firing (Koschak et al., 2001; Mangoni et al., 2003; Olson et al., 2005; Perez-Alvarez et al., 2011). In inflammatory pain, L-type current can be enhanced by various proteins such as PKA and CaM, with the latter being able to alter inactivation kinetics of L-type VGCCs (Hell et al., 1993). Neuropathic pain models show increased expression of $Ca_v1.2$ in rats that have undergone SNL (Kim et al., 2001; Fossat et al., 2010; Ohsawa et al., 2013).

P/Q-type VGCCs consist of 1 member- $Ca_v2.1$ which is thought to play a role in neurotransmitter release (Catterall and Few, 2008). The name P/Q suggest the presence of 2 channels however it is actually the product of a single gene with

alternative splicing producing the different variants consisting of additional post translational modifications present in P-type channels (Bourinet et al., 1999; Tsunemi et al., 2002). The P- and Q- type channels differ in their ω-agatoxin IVA (a specific inhibitor of P/Q-type VGCCs) sensitivity as well as their inactivation kinetics (Tottene et al., 1996). In the peripheral somatosensory system these channels are expressed at the pre-synaptic nerve terminal in the spinal cord (Westenbroek et al., 1998). $Ca_v2.1$ channel role in nociception is not fully understood as it was initially thought neurotransmitter release from primary afferent fibers was controlled mainly through P/Q-type VGCCs (Catterall and Few, 2008). However, one study proposed that SP or CGRP release was not affected by ω-agatoxin IVA application to rat sensory neurons (Westenbroek et al., 1998). Aδ and C-fibers inputs were similarly unaffected by application of ω-agatoxin IVA. Instead it was shown that there is high expression in pre-synaptic terminals of the spinal cord of laminae II and VI of the dorsal horn where P/Q-type VGCCs are thought to play a role in the release of neurotransmitters (Westenbroek et al., 1998). Application of ω-agatoxin IVA to the dorsal horn strongly decreased neurotransmitter release suggesting P/Q channels modulating synaptic activity in the dorsal horn (Heinke et al., 2004).

N-type VGCCs ($Ca_v2.2$) are highly expressed in various aspects of the nociceptive neurons such as DRG cell bodies, their processes synapsing onto the dorsal horn and the dorsal horn neurons themselves (Westenbroek et al., 1992). These channels play a definitive role in neurotransmitter release in primary afferent neurons- especially Aδ fibers (Westenbroek et al., 1998). Co-localisation between N-type VGCCs and vesicles carrying neurotransmitters has been demonstrated as well as inhibition of N-type VGCCs being able to stop neurotransmitter release (Santicioli et al., 1992).

1.4.3 Voltage-gated potassium channels

The K^+ channel family is a large family of proteins, subdivided into groups depending on their functioning principle and structure (Gutman et al., 2005; Grizel et al., 2014). These include, inward rectifying K^+ channels (K_{ir}), Ca^{2+} activated K^+ channels (K_{CA}), Two-pore K^+ channels (K_{2P}), ATP-sensitive K^+ (K_{ATP}) and voltage gated K^+ channels (K_v).

K_v channels are the most diverse of the subgroups consisting of 12 member subfamilies (K_v1-K_v12) (Grizel et al., 2014). Whilst various types of K^+ channels are expressed in DRG neurons, this section will briefly focus on K_v and K_{2P} channels. Whilst Na_v and VGCCs play a prominent role in the excitation and depolarisation of cells, to control excitability, K_v channels hyperpolarise cells to bring the membrane potential back to resting levels after depolarisation (Shimomura et al., 1962). Structurally, K_v channels have 4 homo- or heteromeric subunits, each made up of 6 TM domains (segments 1-6) (Du and Gamper, 2013). Segments 1-4 produce the voltage sensor domain which gives the channel its voltage-gating ability and segments 5 and 6 produce the pore through a re-entrant loop (Du and Gamper, 2013). Auxiliary β-subunits are also present which regulate K_v channel activity (Li et al., 2006). In terms of nociception, activation of K_v channels reduces pain signals as membrane hyperpolarisation occurs (Du and Gamper, 2013). Various K_v channels are thought to play a role in nociception; K_v1.1-1.6 mRNA has been found in DRG neurons (Yang et al., 2004) with K_v1.1 and 1.2 being particularly abundant (Rasband et al., 2001). These 2 K_v subtypes were mainly found in large DRG compared to K_v1.4 which was predominantly localised in small-diameter DRG (Rasband et al., 2001). IB4-positive neurons also expressed mainly K_v1.4 (Vydyanathan et al., 2005). K_v7 is another family of K^+ channels that plays strong role in controlling excitability of nociceptors (reviewed in (Du and Gamper, 2013). Detailed discussion of the role of K^+ channels in nociception is outside the scope of this thesis but it can be found in recent reviews (Du and Gamper, 2013; Du et al., 2017a).

Despite not being voltage-gated like K_v channels, K_{2P} channels are are proposed to play a role in nociception and therefore require a mention (O'Connell et al., 2002). Encode by KCNK genes, this family of proteins has 15 members, which are subdivided into 6 subfamilies- TWIK, TREK (including TRAAK), TASK, THIK, TALK and TRESK (Piechotta et al., 2011). What makes these channels distinct to other K^+ channel family members is their structure and activation profile (O'Connell et al., 2002). K_{2P} channels are made up of a ‘dimer of dimers’; each subunit has 4 TM domains and as the name states, 2 pore domains with 2 of these subunits comprising the functional channel (O'Connell et al., 2002; Piechotta et al., 2011). Functionally, K_{2P} channels contribute to the classical background ‘leak’ associated with K^+ channel, hence play a role in setting the membrane potential and controlling

cellular excitability (Du and Gamper, 2013). Due to this vital involvement of K_{2P} channels in excitable cells, their expression is found in a wide range of cells including neurons, epithelial cells and myocytes (O'Connell et al., 2002).

Various K_{2P} channels have been found in DRG neurons including TASK-1-3, TREK-1-2, TRAAK, TWIK-1-2 and TRESK which suggests a role in pain processing (Talley et al., 2001; Marsh et al., 2012; Du and Gamper, 2013; Mathie and Veale, 2015). Despite these findings it is not clear as to which of these channels plays a greater role in nociceptors. Two members which were proposed as candidates underlying the background leak K^+ channels in nociceptors are TREK and TRESK-2 using single cell electrophysiological recordings (Kang and Kim, 2006). However in relation to nociception, perhaps the most interesting aspect of K_{2P} channels is the fact that they respond to various stimuli which can induce pain signals (Plant, 2012; Mathie and Veale, 2015). These channels respond to a combination of different stimuli; an example of this is for TREK-1 (KCNK2.1) which is modulated by temperature, voltage, pH, membrane stretch and ligands (Maingret et al., 1999; Patel et al., 1999; Maingret et al., 2000). Other members respond to thermal (TREK-2; (Kang et al., 2005)), mechanical (TRAAK; (Kang et al., 2005)), acidification (TWIK and TASK-1-3; (Ma et al., 2012)). Interestingly, TASK-1-3 and TRESK have been shown to respond to hydroxyl-α-sanshool, a constituent of Szechuan peppers (Bautista et al., 2008). Ultimately, these channels would be inhibited and hence cause increased excitability and nociceptive firing (Du and Gamper, 2013).

1.5 Chloride channels in pain

A significant amount of research has gone into the various ion channels discussed above and their contributions to pain signalling. One group of ion channels that, until recently, have not received as much attention in terms of nociception are chloride (Cl^-) channels. Our laboratory has found functional data to suggest the presence of Cl^- channels in DRG and their implication in nociceptive processes (see below). Therefore, the rest of this chapter will focus on Cl^- channels as they form the basis of this thesis.

Cl^- channels are a functionally and structurally diverse set of ion channels that are ubiquitously expressed throughout the body. They are involved in various biological

functions such as epithelial transport (Reddy et al., 1999), neuronal excitability (Staley et al., 1996; Huang et al., 2012; Ha and Cheong, 2017), vision (Bader et al., 1982; Feigenspan and Bormann, 1998), olfaction (Reuter et al., 1998; Reisert et al., 2003; Restrepo, 2005; Stephan et al., 2009; Delgado et al., 2016), cell volume regulation (Sardini et al., 2003; Almaca et al., 2009) and cellular contraction (Kitamura and Yamazaki, 2001; Coelho et al., 2004; Leblanc et al., 2005; Sancho et al., 2012; Brozovich et al., 2016) amongst many others.

1.5.1 Inhibitory or excitatory effects of Cl^- channel activation

Upon stimulation or activation, Cl^- channels allow the movement of Cl^- ions depending on the electrochemical gradient present in the type of cell they are expressed in. In the majority of mature CNS neurons Cl^- channels mediate influx of Cl^- and hyperpolarize the membrane thus producing an inhibitory effect (e.g. $GABA_A$ and glycine receptors/channels)(Obata et al., 1978). Neurons generally have a typically low $[Cl^-]_i$ (approximately 5mM) and a much greater $[Cl^-]_o$ (approximately 150mM). From a biophysical perspective with these values, the Nernst potential for Cl^- (E_{Cl}) is more hyperpolarised compared to the resting membrane potential (more negative than -80mV) (Chesnoy-Marchais, 1983). However, this is not to say that Cl^- movement is unable to produce depolarisation in some neurons. Cl^- concentrations inside and outside the cells dictate the movement of ions in a particular direction and therefore whether they produce hyper- or depolarisation. One classical example is the Cl^--induced depolarisation of immature cortical neurons where Cl^- moves out of the cell hence producing an inward current (Ben-Ari et al., 1989; Yamada et al., 2004). These neurons contain elevated $[Cl^-]_i$ and more depolarized E_{Cl} so that opening of a Cl^- channel results in outward flow of Cl^- (inward current) hence a depolarising effect (Obata et al., 1978; Ben-Ari et al., 1989).

The reason for the differing activity of Cl^- channels is due to the presence of various transporters of Cl^- channels in neurons. There are 2 principle transporters of Cl^- - Na^+-K^+-Cl^- - cotransporter 1 (NKCC1) and K^+-Cl^- cotransporter 2 (KCC2) (Delpire, 2000). NKCC1 provides transport of 1 Na^+ and K^+ into the cell along with 2 Cl^- to maintain electroneutrality. KCC2 on the other hand provides an opposite effect, to shuttle out 1 K^+ and Cl^- from the cell (Ben-Ari, 2002). Expression of NKCC1 is abundant in the CNS early in development therefore allowing accumulation of increased levels of Cl^- inside the cells (Fukuda et al., 1998b; Fukuda et al., 1998a;

Ben-Ari, 2002). As development persists, the expression of NKCC1 decreases and KCC2 increases (Rivera et al., 1999; Ganguly et al., 2001) meaning there is less accumulation of Cl^-, shifting the E_{Cl} below the resting membrane potential (Ben-Ari, 2002). It has been postulated that the reason for this developmental Cl^--induced excitability of neurons is due to $GABA_A$- dependent depolarisation which in turn activates VGCCs (Fukuda et al., 1998b). VGCCs allow an influx of Ca^{2+} and subsequently abolish the Mg^{2+} block of NMDA channels (Ben-Ari et al., 1997). Due to the absence of AMPA receptors in early development, this is a necessary mechanism by which activity dependent neural circuits are formed (Ben-Ari et al., 1997). As AMPA receptors are expressed, modulation of depolarisation is turned over to these excitatory receptors, allowing NKCC1 and KCC2 protein expression patterns to change and diverge Cl^- channels towards inhibition (Ben-Ari, 2002).

1.5.2 CLC

CLCs are a well-established member of the Cl^- channels. The first member of this family, CLC-0, was discovered and cloned from the Torpedo marmorata in 1990 (Jentsch et al., 1990). Presently, members of the CLC family are placed into 3 subclasses based upon gene sequences and functional properties of these proteins (Table 1.3).

Subclass 1 (referred to as muscle type CLCs) consists of 4 members which share 50-60% homology. Expression is localised to the plasma membrane to allow the movement of Cl^- in and out of cells (Jentsch et al., 1999; Maduke et al., 2000). Subclass 2 and 3 (non-muscle type CLCs) on the other hand are found in intracellular membranes such as synaptic vesicles and play a role in maintaining the pH of these intracellular compartments (Stobrawa et al., 2001; Gunther et al., 2003; Mohammad-Panah et al., 2003). Subclass 2 CLCs share similar structures with the

Subclass 1	CLC-0, CLC-1 (CLC-N), CLC-2 and CLC-K (Ka and Kb isoforms)
Subclass 2	CLC-3, CLC-4 and CLC-5
Subclass 3	CLC-6 and CLC-7

Table 1.3: Subclasses of CLC proteins

yeast orthologue ScCLC (Borsani et al., 1995; Flis et al., 2005) (Table 1.3).

In terms of the structure of CLC channels, they exist as homodimers with each of the subunits providing a separate ionic pore (Middleton et al., 1996; Dutzler et al., 2002). Each dimer consists of 18 α-helices which are arranged with a fascinating antiparallel architecture (Dutzler et al., 2002). The N-terminus half of the polypeptide is structurally related to the C-terminus which has been proposed to (i) manipulate the polar ends of the helices to stabilise (or destabilise) ions flowing through the selectivity filter, and (ii) to direct the non-polar ends of each helix towards the aqueous environment outside the membrane hence satisfying biophysical energy principles (Dutzler et al., 2003). The structure of bovine CLC-K has very recently been elucidated using cryoEM and was discovered to share an 84% sequence similarity with human CLC-K (Park et al., 2017) (Fig. 1.6). This study revealed the possible differences between muscle-type and non-muscle type CLCs where a difference in ion pore structure (wider ion pore is present for muscle-type CLCs) may allow the fast Cl^- movement whereas vesicular CLCs accommodate Cl^-/H^+ transport in relation to acidification of these organelles (Park et al., 2017).

CLCs also exhibit 2-types of gating; fast gating where independent gates are found for each pore of a homodimer complex and slow (common) gating which gates both pores simultaneously (Miller and White, 1984; Dutzler et al., 2003). In terms of structural changes for these gating mechanisms, slow gating involves conformational changes in the homodimer helices and C-termini whereas fast gating requires minimal rearrangements (Accardi and Pusch, 2003; Basilio et al., 2014).

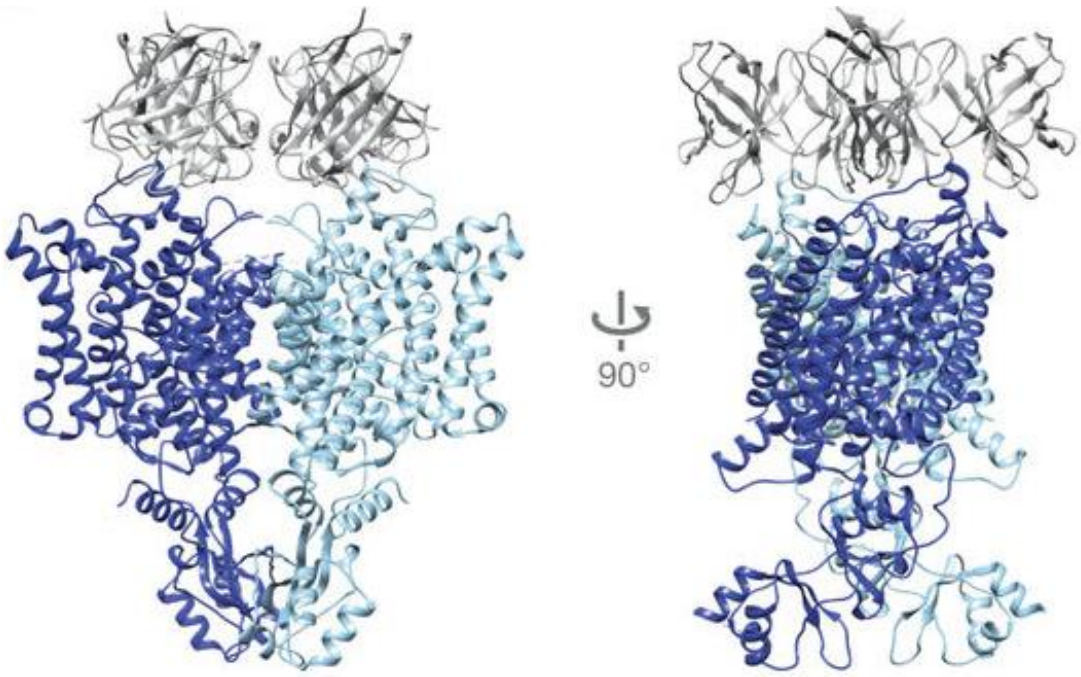

Figure 1.6: CryoEM structure of Bovine CLC-K. Dimer structure of CLC-K (dark blue and light blue) in complex with Fab (grey for each subunit). Compared to non-muscle type CLCs, CLC-K has a narrower pore. Figure adapted from (Park et al., 2017).

1.5.3 GABA receptors

Gamma-Aminobutyric acid (GABA) receptors play a role in inhibition of the mammalian nervous system (Sieghart, 1995). GABA is the ligand that binds to these receptor and allows activation of these channels (Sieghart, 1995). The GABA receptor family consists of 2 members, ionotropic $GABA_A$ channels and metabotropic $GABA_B$ receptors (Sigel and Steinmann, 2012). $GABA_A$ channels are ligand gated ion channels and one of the major players in terms of inhibition of neuronal firing in the CNS (Sigel and Steinmann, 2012). Structurally, $GABA_A$ receptors are arranged in a pentameric structure comprising of different combinations of various subunit subtypes (Barnard et al., 1998) (Table 1.4).

Subunit class	Subtype of subunit
α	1-6
β	1-3
γ	1-3
δ	1
ε	1
π	1
θ	1
ρ	1-3

Table 1.4: Subunit and subtypes of $GABA_A$ receptor.

The general consensus is that the most physiological heteromeric arrangements includes 2 α-, 2 β- and 1 γ-subunits (Sigel and Steinmann, 2012). Each subunit is made up of approximately 450 amino acids and consists a large extracellular N-terminus with 4 TM domains (Sigel and Steinmann, 2012). TM 2 is involved in producing the pore region in each subunit. Interestingly, an intracellular loop is present between TM 3 and 4 which allows for modulation of the channel by phosphorylation and binding of various proteins to specific receptor subtypes (Sigel and Steinmann, 2012). An example of this is the binding of GABA Receptor Associated Protein (GABARAP) which only interacts with $GABA_A$ in the presence of γ1 or γ2 subunits (Wang et al., 1999; Nymann-Andersen et al., 2002). GABARAP is

thought to play a role in anchoring GABA to the cytoskeleton (Wang and Olsen, 2000). Various compounds are thought to modulate $GABA_A$ channel activity such as barbiturates, benzodiazepines, anti-convulsants and neuroactive steroids (Johnston, 2005) and $GABA_A$ antagonists include bicuculline, SR-95531 and picrotoxinin (Kaneda et al., 1995). Recently, GABAergic machinery has been localised in DRG neurons and has been found to play a role in nociceptive transmission, controlling and filtering nociceptive signals at the cell body of neurons (Du et al., 2017b).

1.5.4 Glycine receptors

Along with $GABA_A$, glycine receptors are the other major inhibitory modulators of neurotransmission. Also a ligand gated ion channel, binding of glycine induces activation of this receptor (Lynch, 2004). The fast inhibitory capacity of glycine was first brought to the forefront of scientific research when its distribution was investigated in cat spinal cord (Aprison and Werman, 1965). Application of glycine onto spinal neurons produced strychnine-sensitive hyperpolarisation (Curtis et al., 1967; Werman et al., 1967). This hyperpolarizing activity was subsequently found to be mediated by the glycine receptor (Pfeiffer et al., 1982). Similarly to $GABA_A$, the glycine receptor is composed of 5 subunits surrounding a central pore (Lynch, 2004). Each subunit is made up of 4 TM domains and a large N-terminus domain (Lynch, 2004). Expression of glycine receptors is largely found in the spinal cord, brain stem (Young and Snyder, 1973), cerebellum (Garcia-Alcocer et al., 2008), hippocampus, striatum, cortex (Bristow et al., 1986) and the retina (Haverkamp et al., 2003). Unlike $GABA_A$ channels, there are only 5 subunits identified for glycine receptors, α1-4 and a single β subunit (Grenningloh et al., 1990; Dutertre et al., 2012) and can form homomeric channels with a single α subunit or a heteromeric structures with α and the β subunit (Lynch, 2004). During development, glycine receptors undergo a developmental switch from α2 homomers (fetal) to α1 β heteromers (adults) (Becker et al., 1988). Neonatal rats express mRNA for all 3 subunits (α1, α2 and β) but at postnatal day 20, the adult form takes over (Becker et al., 1988; Watanabe and Akagi, 1995). This is also seen in the mRNA expression profile which falls for the α2 subunit and increases for the α1 subunit (Akagi et al., 1991; Watanabe and Akagi, 1995). However studies have provided evidence for the α2 subunit still being present at significant levels in the retina and brain stem during adulthood (Piechotta et al., 2001). This suggests that the developmental switch is not as complete as previously

believed (Piechotta et al., 2001). Various other cells also express glycine receptors such as adrenomedullary chromaffin cells (Yadid et al., 1990), macrophages, leukocytes (Froh et al., 2002), Kupffer cells (specialised macrophages of the liver) (Ikejima et al., 1997) neural stem progenitor cells (Nguyen et al., 2002) and endocrine pancreatic cells (Weaver et al., 1998). Interestingly in pancreatic cells, activation of glycine receptors produces depolarisation and leads to increased $[Ca^{2+}]_i$ levels (Weaver et al., 1998).

1.5.5 CFTR

The cystic fibrosis transmembrane conductance regulator (CFTR) functions as a Cl^- channel at the apical membrane of epithelial cells (Riordan et al., 1989; Patrick and Thomas, 2012). This protein is a member of the ATP-binding cassette (ABC) transporter superfamily of proteins that confers the ability to hydrolyse nucleotides to transport substances across the membrane. However, unlike ABC transporter function which dictates the movement of substrates against their electrochemical gradients, CFTR has a functionally distinct role as an ion channel (Holland, 2011). CFTR is found in airways (Riordan et al., 1989), liver (Kinnman et al., 2000), digestive tract (Sood et al., 1992; Strong et al., 1994), pancreas (Hyde et al., 1997; Wilschanski and Novak, 2013), salivary glands (Shin et al., 2016) and recently found in exocrine sweat glands (Hanukoglu et al., 2017).

The structure of CFTR consists of a single polypetide consisting of 2 TM domains which are responsible for formation of the pore (Sheppard and Welsh, 1999). These 2 TM domains are connected through a regulatory domain (R). Two nucleotide binding domains (NBD1-2) are also present, which bind ATP to activate and hydrolyse ATP to close CFTR (Duffieux et al., 2000). Interestingly, binding of 2 ATP molecules to the 2 NBD motifs initiates a dimerisation of the 2 segments, inducing a conformational change to the channel (Delpire, 2000; Gadsby et al., 2006; Huang et al., 2009b) (Fig. 1.7). Upon hydrolysis of ATP, this dimerisation is dislocated which causes the channel to close (Csanady et al., 2006) (Fig. 1.7). Phosphorylation of the R-domain with protein kinases (PKA and PKC) has been shown to facilitate channel opening (Bompadre et al., 2005).

Functions of CFTR involve transport of both Cl^- and $HCO3^-$ in the maintenance of electrolyte and fluid transport, which plays an important role in various organs

(Frizzell and Hanrahan, 2012) (Fig. 1.7). Cl^- secretion via CFTR causes paracellular Na^+ secretion providing an osmotic driving force for water and production of an isotonic secretory product (Kunzelmann, 2001; Frizzell and Hanrahan, 2012). For example, airway surface liquid in lungs is essential for the clearance of mucus and in the intestine, the large amount of fluid (~8L per day) produced is vital for digestion (Barrett and Keely, 2000; Kunzelmann, 2001; Frizzell and Hanrahan, 2012). Disruption of this process impairs the production and composition of epithelial fluid and compromises organ functionality (Mehta et al., 2004). CFTR is the channel implicated in the autosomal-recessive disease cystic fibrosis (CF) which is characterised by abnormalities in this ion channel (Mehta et al., 2004). Approximately 70% of CF patients have the F508 deletion mutation in one or both CFTR genes even though over 1600 mutations in the CFTR gene have been reported (Davies et al., 2007). CF patients present mainly in the airways, pancreas and the bowel however the most problematic symptoms are the lungs where mucus clearance is disrupt (Davies et al., 2007).

1.5.6 Bestrophins

Bestrophins are generally regarded in relation to Best disease, a genetic disorder affecting the macula of the eye and disrupting vision (Petrukhin et al., 1998). The light peak of the electrooculogram is thought to be caused by a Cl^- conductance and bestrophins have been put forward as likely candidates mediating this. Furthermore, these channels are found highly expressed at the retinal pigment epithelial (RPE) cells (Marmorstein et al., 2000; Sun et al., 2002). Despite this, their contribution to the development of Best disease has been disputed as RPE cells from mice, with the W93C Best disease mutation, display normal Cl^- conductance (Zhang et al., 2010). The mammalian Bestrophin family consists of 4 members- BEST-1-4. Overexpression of Bestrophin 1 and 2 in HEK293 cells produced robust Cl^- currents when caged Ca^{2+} was applied (Qu et al., 2003; Qu et al., 2004). Bestrophin 1 and 2 are also expressed in mouse trachea and kidney epithelia; these cells also display Ca^{2+} activated Cl^- currents in whole cell patch clamp recordings when extracellular ATP was applied to increase $[Ca^{2+}]_i$ (Barro-Soria et al., 2008; Barro Soria et al., 2009). Knock-down of both Bestrophin 1 and 2 reduced ATP-induced Cl^- currents by 50% in

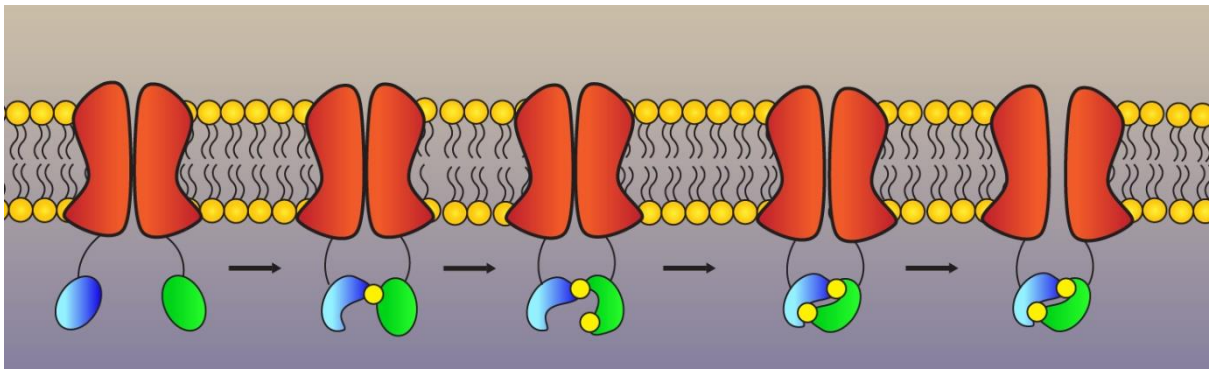

Figure 1.7: Mechanism of CFTR opening. Two NBD domains (Blue and green shapes attached to CFTR) bind ATP (yellow circle) which induces a conformational change through dimerisation. This opens the channel until dissociation of ATP which puts CFTR back into the resting state. Figure based on (Csanady et al., 2006).

mouse trachea (Barro-Soria et al., 2008). These were also reduced with the application of the Cl^- channel blockers DIDS and Niflumic Acid (Barro-Soria et al., 2008). Bestrophin 1 expression has been demonstrated in mouse DRG neurons and spinal cord (Al-Jumaily et al., 2007; García et al., 2014; Pineda-Farias et al., 2015) . Moreover, the expression profile of bestrophin 1 has been shown to be upregulated after nerve injury or axotomisation of sensory neurons (Boudes et al., 2009) but this has been disputed by other groups (García et al., 2014; Pineda-Farias et al., 2015). Despite this, its presence in the dorsal horn of the spinal cord and DRG, and the fact that an anti-bestrophin 1 antibody reduces tactile allodynia after nerve ligation, suggests that bestrophin 1 does play a role in development of neuropathic pain (Pineda-Farias et al., 2015). A role in allodynia makes sense given the fact Boudes and colleagues showed BEST-1 transcripts are greater in large and medium diameter DRG compared to smaller DRG (Boudes et al., 2009).

All isoforms of bestrophins have been found to be expressed in colonic epithelia (Barro-Soria et al., 2008; Ito et al., 2013; Eliasson et al., 2014). Bestrophin 1 has also been implicated in SOCE in the RPE where it has been co-localised with STIM1 (Hidalgo et al., 1986; Barro-Soria et al., 2010; Gomez et al., 2013). Knockdown of bestrophin 1 caused reduced release of Ca^{2+} from the ER (Gomez et al., 2013). It is thought to act as a counterion for Ca^{2+} release and has been shown to affect Ca^{2+} store refilling when BEST-1 was knocked down using siRNA in porcine RPE cells (Neussert et al., 2010; Gomez et al., 2013).

The crystal structure of the homolog of Bestrophin 1 from Klebsiella pneumoniae was resolved showing a stable pentameric organisation of the channel. Each subunit consists of 4 transmembrane domains and a relatively large intracellular portion thought to be important for protein-protein interactions (Yang et al., 2014). The X-ray crystal structure of chicken bestrophin 1-Fab complexes also reported an outer entryway, neck region and an inner cavity which encompasses the pore of the channel (Kane Dickson et al., 2014). The neck region has been implicated in the anionic permeability of the channel ($SCN^- > I^- > Cl^-$) (O'Driscoll et al., 2009). Furthermore, 5 putative Ca^{2+} binding sites around the midsection region of the pentameric structure were revealed; this is contrary to previous reports implicating

the C-terminus of the channels in Ca^{2+} binding (Xiao et al., 2011; Kane Dickson et al., 2014).

Studying the properties of bestrophin channels using electrophysiology has revealed that they are activated by nanomolar $[Ca^{2+}]_i$ whereas under $[Ca^{2+}]_i$ free conditions there were very little currents (Liu et al., 2015). Currents are also largely time and voltage-independent and showed slight outward rectification in various cell types (Qu et al., 2003; Pifferi et al., 2006; O'Driscoll et al., 2008).

1.6 Ca^{2+} activated Cl^- channels

Ca^{2+} activated Cl^- channels (CaCCs) are a distinct group of Cl- channels; CaCCs have been acknowledged since the 1980s in Xenopus Oocytes where Cl^- currents were seen upon depolarisation (Miledi, 1982). Research over the years has yielded various aspects regarding their activity and has allowed CaCCs to be categorised and implicated in various processes.

Epithelial cells express CaCCs where they play a role in the production of mucus from Goblet cells and fluid secretion (Danahay et al., 2002). CaCCs are also found in excitable cells, including neurons and muscle cells (Huang et al., 2009a; Huang et al., 2012). Sensory processing systems are also known to express robust CaCC currents; these include various sensory cells mediating olfaction (Kleene and Gesteland, 1991), vision (Bader et al., 1982; Barnes and Hille, 1989) and taste (Taylor and Roper, 1994).

There has been some ambiguity regarding the classification of CaCCs. The hallmarks of classical CaCCs include:

- Ca^{2+} sensitivity in the range of 0.2 µM– 5µM
- Changes in Ca^{2+} sensitivity depending on membrane potential. For example, at more negative membrane potentials the Ca^{2+} sensitivity is lower compared to more positive membrane potentials
- Outwardly rectifying current-voltage relationships at submaximal Ca^{2+} concentrations which become linear at saturating Ca^{2+} concentrations
- Sensitivity to a broad spectrum of Cl^- channel blockers, including niflumic acid (NFA), 4,4′-diisothio-cyanostilbene-2,2′-disulfonic acid (DIDS) and 5-nitro-2-(3-phenylpropylamino) benzoic acid (NPPB).

- Preference for larger anions in the following order:

$$SCN^- > I^- > Cl^- > F^-$$

However, due to the fact that Cl^- is the most abundant anion in the body, it is the primary charge carrier for CaCC channels.

In addition to this classical CaCC current, a Ca^{2+}-activated Cl^- current with different properties was also described in various cell types. This CaCC was found to be dependent on cyclic guanine monophosphate (cGMP) in rat mesenteric artery smooth muscle cells (Matchkov et al., 2004). In these cells cGMP is an absolute requirement, regardless of Ca^{2+} presence and has been thought to act via cGMP-dependent phosphorylation (Matchkov et al., 2004; Zhuang, 2009).

For decades that followed physiological identification of CaCC, the molecular identity of the underlying ion channel defied identification. Various channels were put forward as candidates for CaCCs but these were ultimately dismissed as bonafide CaCCs due to their channel properties (Hartzell et al., 2005). CLC-3 was proposed as a CaCC because expression in epithelial cells led to CaCC currents being generated however, this was found to be CaM kinase II (CaMKII) dependent (Huang et al., 2001; Robinson et al., 2004), which is not a property of 'classical' CaCCs. Another set of potential candidates were bestrophins but these channels are activated by nanomolar [Ca^{2+}] whereas CaCCs require micromolar levels of [Ca^{2+}]. Furthermore, bestrophins are voltage independent and don't show the same outward rectification seen with classical CaCCs (Tsunenari et al., 2003; Tsunenari et al., 2006). Another family of proteins, the CLCAs, were proposed as CaCC due to their ion selectivity profile however, its activation by voltage without the requirement for Ca^{2+} elevation, linear I-V relationship and pharmacological profile (not blocked by CaCC inhibitors i.e. NFA) led to the dismissal of CLCAs as CaCC candidates (Cunningham et al., 1995). Moreover, it was later discovered that CLCAs are not ion channels but secreted non-integral membrane proteins. It has been proposed that they are catalytic proteins which function in a manner similar to metalloproteases (Pawlowski et al., 2006).

Finally, a novel family of proteins was identified as CaCC correlates in 2008 by 3 independent groups. The next segment of this thesis will focus on the Anoctamin (TMEM16) family of proteins, which have been classified as true CaCCs.

1.7 Discovery of ANO1

The first of the true CaCCs to be identified was ANO1 (TMEM16A) in 2008. Three different laboratories were able to clone and physiologically express this channel in heterologous systems (Caputo et al., 2008; Schroeder et al., 2008; Yang et al., 2008). Co-expression of ANO1 and various Ca^{2+} mobilising receptors (i.e. endothelin, angiotensin etc.) in HEK293 cells produced robust Ca^{2+} activated Cl^- currents (Yang et al., 2008). Xenopus oocytes endogenously block polyspermy-fertilisation of the egg with more than one sperm- due to CaCC currents they possess (Runft et al., 1999). Therefore, to find a novel expression system for CaCC currents, Axolotl Salamander oocytes were identified as physiologically polyspermic and showed no endogenous CaCC currents (Schroeder et al., 2008). When mRNA for Xenopus oocytes was injected into Axolotl oocytes, robust CaCC currents appeared in response to photo-releasable IP_3, which was responsible for $[Ca^{2+}]_i$ elevation (Schroeder et al., 2008). Size-fractionated Xenopus oocyte RNA segments expressed in Axolotl oocytes showed CaCC currents were only present in the specific ~5-7kb fraction. Further analysis revealed a single 5191 base pair cDNA clone was responsible for producing CaCC currents (Schroeder et al., 2008). Databases showed that this was the Xenopus orthologue of human and mouse ANO1. Another interesting approach involved analysing upregulation of genes after treatment of human bronchial cells by interleukin (IL)-4 and 13, which are known to increase Ca^{2+} activated Cl^- currents. ANO1 was identified to be gene responsible for this as knockdown of ANO1 reduced CaCC activity (Caputo et al., 2008). Thus, these 3 studies set the ball rolling and peaked interest in ANO1 research.

1.7.1 Heterologously expressed ANO1 reproduces properties of a classical CaCC

Properties of ANO1 closely match those specified in general for classical CaCCs. When Ca^{2+} is not present, no CaCC currents are seen in HEK293 cells transfected with ANO1 (Yang et al., 2008). However, when submicromolar Ca^{2+} is present, ANO1 shows the typical outward rectification expected from CaCCs (Caputo et al., 2008; Schroeder et al., 2008; Yang et al., 2008). When Ca^{2+} is increased to higher concentrations, the outwardly rectifying current-voltage relationship becomes linear (Yang et al., 2008; Romanenko et al., 2010; Xiao et al., 2011; Crutzen et al., 2016). Another characteristic of CaCCs is their interrelated sensitivity to Ca^{2+} and voltage

(Fig. 1.8). Ca^{2+} and voltage-dependence show a synergistic relationship with regards to ANO1 activation. In conditions where the membrane potential is depolarised, Ca^{2+} sensitivity for ANO1 increases (Yang et al., 2008; Xiao et al., 2011; Cho et al., 2012). Consequently, the EC_{50} for ANO1 was found to be 2.6μM at -60mV and 0.4μM at +60mV (Yang et al., 2008; Ferrera et al., 2009). One interesting property on ANO1 is its ability to be activated under Ca^{2+} free conditions by strong depolarisations. Depolarising the membrane to +200mV or above is able to induce ANO1 activity (Xiao et al., 2011; Vocke et al., 2013).

Single channel conductance of ANO1 has been found to be 3.5pS which is in line with that reported for native CaCCs (Piper and Large, 2003; Adomaviciene et al., 2013). ANO1 also exhibits time dependence when activated by Ca^{2+} (Sheridan et al., 2011; Xiao et al., 2011). When activated, there is an instantaneous current followed by the time-dependent current which increases (Fig. 1.8). The instantaneous current is miniscule which reflects channels open at the holding potential whereas the second component is due to time-dependent opening induced by depolarisation (Xiao et al., 2011). This activation period is shortened when intracellular Ca^{2+} increases (Xiao et al., 2011; Yu et al., 2012). The time course for ANO1 to reach half maximal current at 274nM Ca^{2+} concentration was approximately 120ms at +100mV in HEK293 cells expressing ANO1 (Adomaviciene et al., 2013). Rat pulmonary artery smooth muscle cells (PASMCs) showed a time constant for full activation of 491ms at +90mV with 600nM Ca^{2+}. (Manoury et al., 2010) Depolarising the cells causes slowing of the activation kinetics and deactivation of ANO1 requires Ca^{2+} unbinding from its binding site which is a voltage-dependent process (Xiao et al., 2011; Yu et al., 2012). At more depolarised voltages, the time constant for deactivation is longer compared to negative voltages. It was proposed that this may be due to the actual binding site for Ca^{2+} being close to the voltage-sensitive areas of the channel, however the voltage-sensitive domain was found to be at the intracellular loop between TM 3 and 4 whereas the proposed binding site is found in the pore region (see below) (Yu et al., 2012; Brunner et al., 2014; Yu et al., 2014; Paulino et al., 2017).

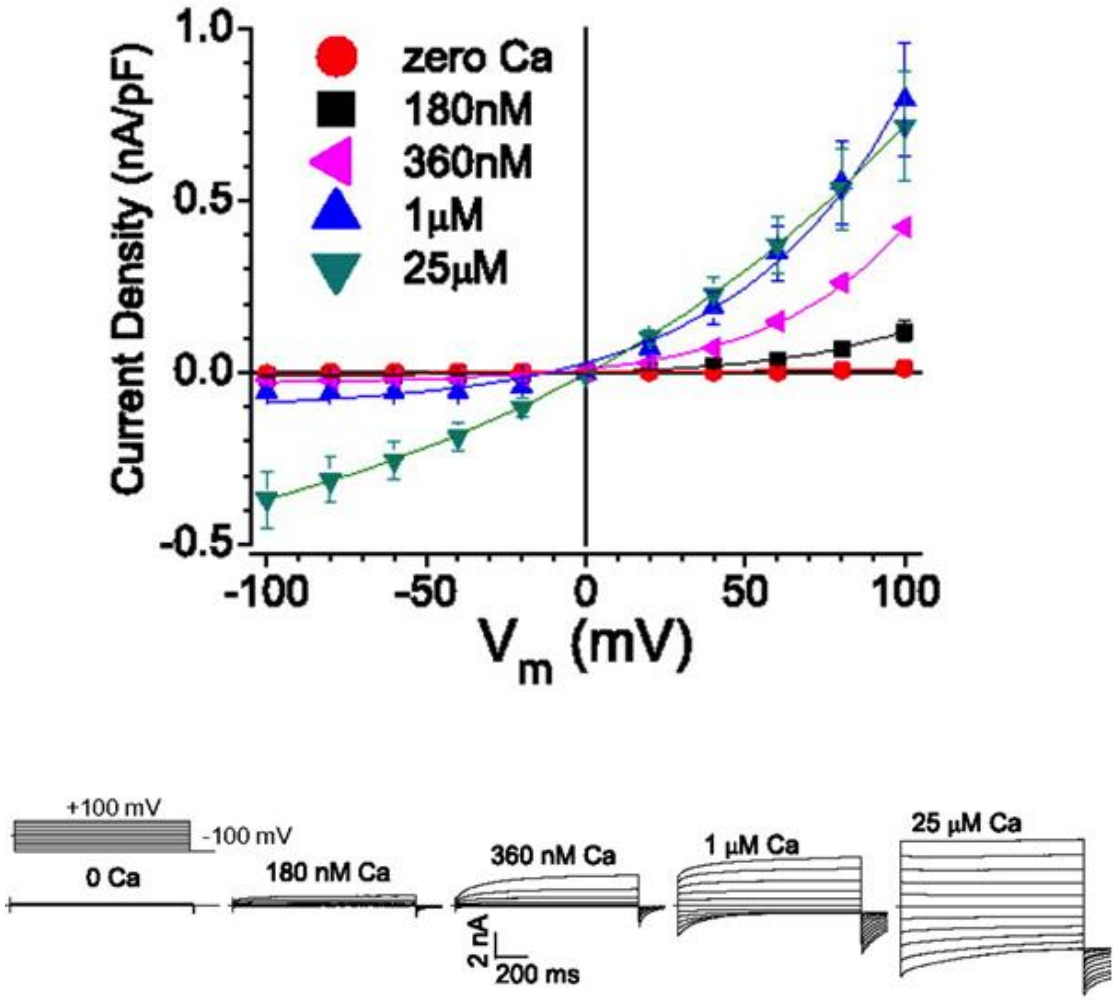

Figure 1.8: Electrophysiological properties of ANO1 in HEK293 cells transfected with ANO1. Increasing Ca^{2+} produces a linear I-V relationship. Figure adapted from (Xiao et al., 2011)

1.7.2 Structure of ANO1

Based on hydrophobicity studies, the structure of ANO1 was first predicted to consist of 8 transmembrane domains with intracellular N and C-termini (Yang et al., 2008) (Fig. 1.9A). A re-entrant loop was predicted to occur between TM 5 and 6 however after a study using HA-tag epitopes and subsequent accessibility experiments to various areas of the channel, it was proposed that the re-entrant loop was in fact an intracellular commodity between TM 6 and 7 (Yu et al., 2012). The crystal structure of an Anoctamin family member, ANO6, in the fungus *Nectria haematococca* (nhTMEM16) was ben solved in 2014, revealing insights into the structure and topology of Anoctamins (Brunner et al., 2014) (Fig. 1.10A). Despite being a lipid scramblase in function, it shares ~40% sequence homology with mammalian ANO1 in the TM region. One important discovery elucidated by the crystal structure of nhTMEM16 is the presence of 10 TM domains and not the 8 previously presumed. The protein is found in a homo-dimeric complex with internal C and N-termini (Sheridan et al., 2011; Tien et al., 2013; Brunner et al., 2014).

A small peptide region (residues 161-179) in the N-terminus has been implicated in being responsible for the ability of ANO1 to dimerise and is perceived as the critical region for channel assembly (Tien et al., 2013). This peptide stretch seems to be involved in the production of an α-helix involved in the dimer, hence mutagenic alterations to this region result in non-assembly of ANO1 in HEK293 cells (Tien et al., 2013). However, this dimerisation region was not identified in the crystal structure of nhTMEM16 despite it also being found in a homo-dimeric complex (Brunner et al., 2014). The crystal structure of nhTMEM16 also revealed N-terminus interactions with the C-terminus of the opposing ANO1 subunit, such that the C-terminus actually wraps around the N-terminus leaving 2 dimer cavities (Brunner et al., 2014). Another more interesting feature of the nhTMEM16 structure is the presence of a small subunit cavity or ‘open furrow’ which has been presumed to be the ion conduction path (Fig. 1.10B). It also harbours various regions involved in ion selectivity and conduction in ANO1 (Yang et al., 2008; Yu et al., 2012). Recently, the structure of mouse ANO1 has been solved using cryoEM (Paulino et al., 2017) (Fig. 1.10A). Structurally, it was confirmed that ANO1 has a homo-dimeric structure and is relatively similar to nhTMEM16, with 10 transmembrane domains and internal C and N-termini (Paulino et al., 2017). ANO1 consists of a slightly larger extracellular

domain compared to nhTMEM16; this compact domain is where 6 cysteines residues critical for channel activity are found (Yu et al., 2012). Unlike findings by Tien and colleagues, there is no N-terminus interaction between adjacent subunits, which was proposed to be essential for homo-dimerisation (Tien et al., 2013). The C-terminus domain interactions found in nhTMEM16 are also not present in ANO1 meaning dimerisation is produced by other interactions than those proposed in nhTMEM16 (Brunner et al., 2014; Paulino et al., 2017). Instead, interactions between the extracellular section of TM 10 of each subunit produce the likely homo-dimerisation interactions (Paulino et al., 2017). Interestingly, TM 10 of each subunit protrudes and extends further than in nhTMEM16, possibly to allow these interactions (Paulino et al., 2017).

The pore region of ANO1 is composed of TM 3-7 and unlike the lipid scramblase nhTMEM16; the pore of ANO1 is also slightly rearranged in that TM 3, 4 and 6 shield the pore from the lipid membrane. Along with TM 5 and 7, this provides an aqueous pore for ion conduction (Paulino et al., 2017) (Fig. 1.10B). The two Ca^{2+} binding sites are found between TM 6, and 8- coinciding with the binding sites of Ca^{2+} in nhTMEM16 (Paulino et al., 2017). The pore is narrow but widens at the intracellular side of the channel.

1.7.3 Mechanisms of ANO1 activation

The mechanisms behind Ca^{2+} dependency of ANO1 activation have been the subject of intense speculation and this is still considered a controversial topic. One hallmark of CaCC activity is the ability to be activated by free Ca^{2+} in the micromolar range (Zhuang, 2009). There is a split in opinion regarding ANO1 activation; some groups maintain that free Ca^{2+} is necessary and sufficient to activate ANO1 but others believe activation requires CaM.

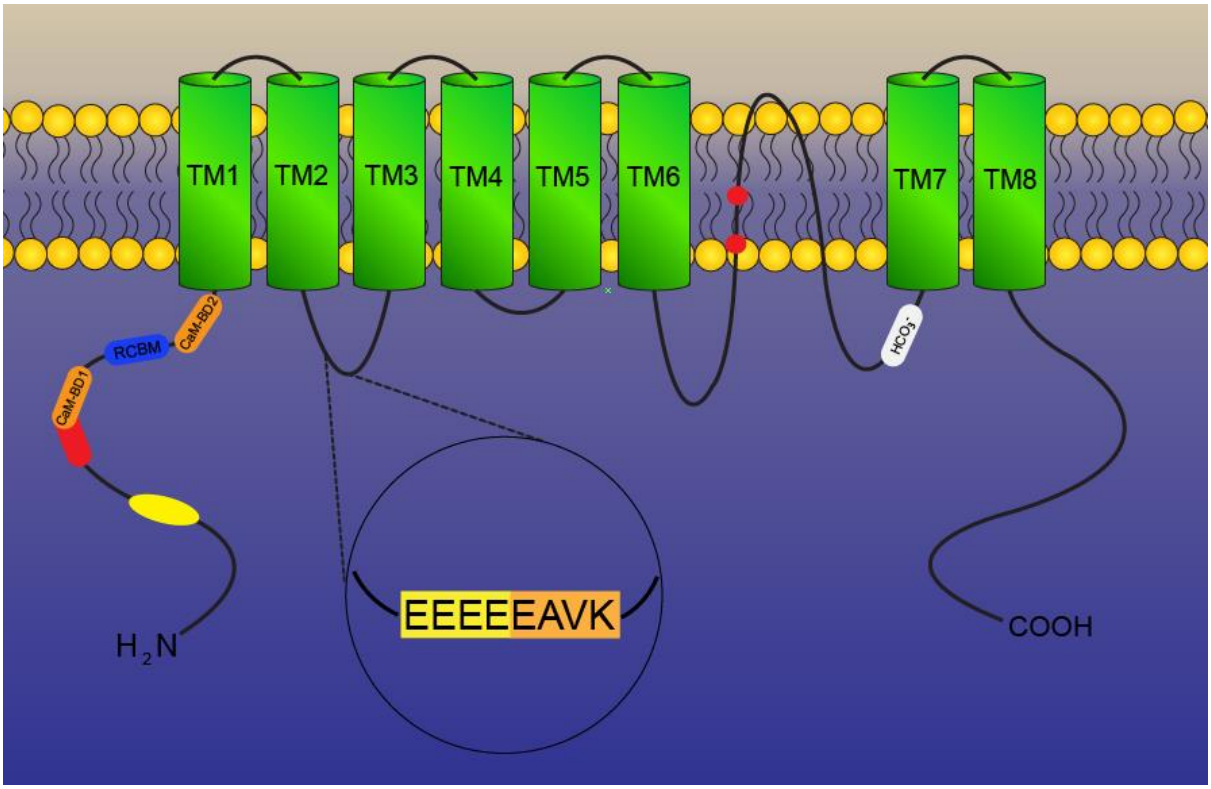

Figure 1.9: Originally proposed topology of ANO1. ANO1 was thought to consist of 8 TM domains. A change in the topology of ANO1 was proposed which placed the pore-loop between TM 6 and 7. N-terminus houses a potential dimerisation domain (yellow oval) and various CaM-binding domains. Another CaM domain has been identified before TM 7 (white segment) which increases the HCO_3^- permeability. Red segment of N-terminus indicates segment *b* (splice variant exon proposed for CaM binding). Red circles show the location of 2 glutamate residues (E702 and E705) important for Ca^{2+} binding. Also shown is the EEEEEAVK segment at the intracellular loop between TM 2 and 3. EEEE has been shown to play a role in voltage dependence (highlighted yellow) of ANO1 and EAVK in Ca^{2+} sensitivity (highlighted orange). Figure based on (Pedemonte and Galietta, 2014; Leblanc et al., 2015)

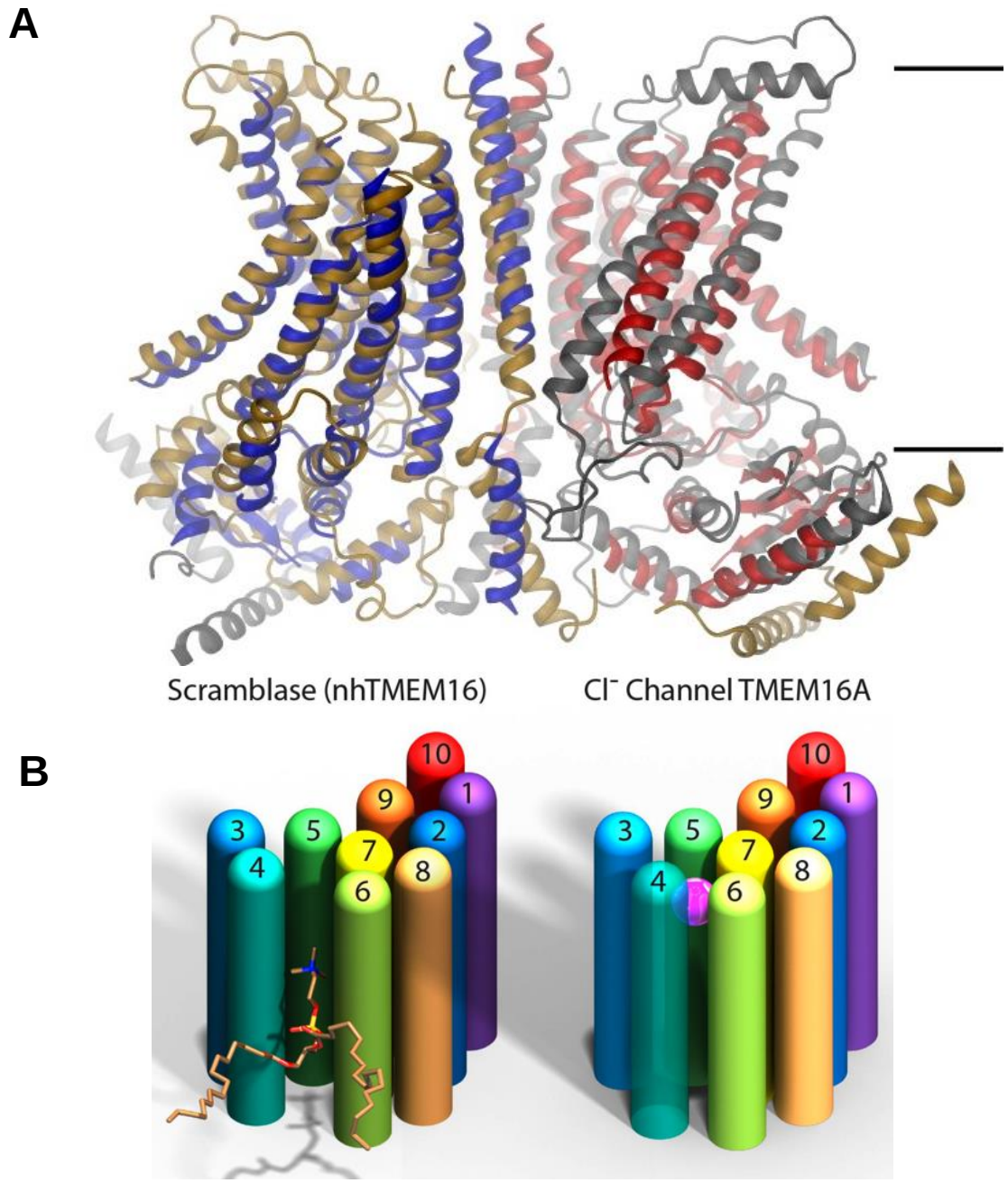

Figure 1.10: Structures of nhTMEM16 and mANO1. (A) Crystal structures of nhTMEM16 (beige and grey) and mANO1 (red and blue) superimposed over each other. (B) Schematic representation of the differences between the pores of nhTMEM16 and mANO1. TM 4 and 6 are further apart allowing for the formation of an 'open furrow' where the hydrophilic heads of lipids such as phosphatidylcholine (shown) are able use to move from layer to layer. This allows the tails to remain in the hydrophilic core of the membrane. Rearrangements of TM 4 and 6 in mANO1 allow the formation of an aqueous conduit for ion permeation. Figures adapted from (Fisher and Hartzell, 2017; Paulino et al., 2017)

1.7.3.1 CaM activation theory

CaM seems essential for ANO1 Ca^{2+}-dependent activation in various experiments carried out by different groups. Before the discovery of ANO1 in 2008, CaM was found to be an important regulator of CaCC currents in olfactory epithelial cells (Kaneko et al., 2006). CaM mutants were shown to reduce the Ca^{2+} sensitivity of CaCC in these cells (Kaneko et al., 2006). Kunzelmann's group identified 2 putative CaM binding domains (CaM-BD1 and CaM-BD2) which were proposed to bind CaM and control channel activity (Tian et al., 2011). Similar to Ca^{2+} activated K^+ channels (SK_{Ca}), which require CaM for activation (Fanger et al., 1999), it was demonstrated that molecules such as 1-DBIO, DCEBIO and riluzole (known activators of SK_{Ca}) were able to activate ANO1 currents in recombinant expression systems and in native cells (Tian et al., 2011). Moreover, inhibitors of CaM such as trifluoperazine and J8 caused a large reduction of ANO1 current in HEK293 cells (Tian et al., 2011). CaM was also found to bind to splice variants of ANO1 containing segment b (segment b overlaps with CaM-BD1) through co-immunoprecipitation studies, however the ac segment-containing splice variant of ANO1 was activated without this CaM-BD present which suggests CaM may play a role in other areas of ANO1 activation (Tian et al., 2011). Mutations of these binding sites also caused a reduction in ANO1 activation by Ca^{2+}. Interestingly, another CaM binding domain was found in the ac splice variant of ANO1 in another study (Jung et al., 2013). As well as potential implications in ANO1 activation, CaM is thought to also play a role in ANO1 permeability changes from Cl^- to $HCO3^-$ under high Ca^{2+} conditions (see above). In support to this idea, experiments demonstrated that inhibitors and siRNA against CaM inhibit this phenomenon from occurring as well as application of exogenous CaM being able to recapitulate this property of ANO1 (Jung et al., 2013). As with CaM-dependent activation of ANO1, this permeability-altering ability of CaM has also been challenged as Yu and colleagues were unable to reproduce permeability changes when using mouse ANO1 expressed in HEK293 cells (Yu et al., 2014). Another regulatory CaM binding motif (RCBM) was identified in ANO1 and ANO2 (Vocke et al., 2013). CaM was found to interact with small peptides containing the sequence for the RCBM. Mutagenesis studies revealed this domain was important for Ca^{2+}-dependent activation of ANO1 and the binding of CaM (Vocke et al., 2013).

1.7.3.2 Direct activation by Ca^{2+} theory

Other groups have been able to generate data which opposes this notion of CaM-required activation. A strategy utilising liposomes expressing ANO1 to study ANO1-mediated Cl^- efflux required only Ca^{2+} and voltage to induce activation- not CaM (Terashima et al., 2013). The addition of CaM in the liposomes had no effect on Cl^- efflux. This group also found no interaction between ANO1 and CaM in pull down assays (Terashima et al., 2013). Again in opposition to findings of the 'pro-CaM camp', the Hartzell laboratory found no differences in current when exogenous CaM was applied to cytosolic portions of ANO1-expressing membranes in inside-out patches (Yu et al., 2014). Ca^{2+} insensitive mutants of CaM had no effect on ANO1 currents in this study either, whereas they were shown to abolish SK_{Ca} currents (Yu et al., 2014). No interactions were seen between ANO1 and CaM in co-immunoprecipitation assays either. In Xenopus oocytes, Ca^{2+} insensitive CaM mutants did not affect ANO1 current nor were anti-CaM antibodies and W7 (a potent CaM antagonist) able to affect ANO1 current (Tien et al., 2014).

ANO1 has no canonical Ca^{2+} binding domains i.e. EF-hands seen in STIM1 (Huang et al., 2009a) and aequorin (Tricoire et al., 2006). Yet, negatively charged amino acid residues (EEEEEAVK) in the internal regions of ANO1 (also found in Ca^{2+} activated K^+ channels and bestrophins) have been proposed to play a part in voltage and Ca^{2+} sensitivity (Xiao et al., 2011). Mutating these residues showed that the EAVK segment caused reduced Ca^{2+} sensitivity of ANO1 whereas removal of the initial EEEE segment eliminated the intrinsic voltage dependence without influencing ANO1 sensitivity (Xiao et al., 2011). Two highly conserved glutamate residues (E702 and E705) have also been implicated in the actual binding of Ca^{2+} to ANO1. Mutating these residues to cysteine and applying cysteine-modifying reagents showed decreased sensitivity to Ca^{2+} (Yang et al., 2008; Yu et al., 2014). The most direct evidence for direct gating of ANO1 by Ca^{2+} came from structural studies as Ca^{2+} ions were present in the channel structure (Brunner et al., 2014). The binding site for Ca^{2+} in nhTMEM16 consists of residues from TM 6, 7 and 8, including 3 glutamates, 2 aspartates and an asparagine (Brunner et al., 2014). Mutating these residues reduced the activity of nhTMEM16 in the presence of Ca^{2+}.

1.8 Anoctamin family

1.8.1 ANO2

The ANO1 family consists of 10 members with ANO1 being the first to be characterised. ANO1 and ANO2 are the only 2 members of the family that have undisputed CaCC activity, which can be attributed to a 62% sequence similarity between the channels (Yang et al., 2008). ANO2 has different properties compared to ANO1. The activation and deactivation kinetics are faster than ANO1 however the Ca^{2+} sensitivity is 10 times lower (Pifferi et al., 2012). Chimeric ANO1/ANO2 channels where the 3rd intracellular loop of ANO2 was incorporated into ANO1, containing the glutamate residues at positions 702 and 705 demonstrated that these residues are critical to lower Ca^{2+} sensitivity of ANO1 (Scudieri et al., 2013). Single channel conductance of ANO2 is also smaller than that of ANO1 (1pS compared to 3.5pS, respectively) (Stephan et al., 2009). ANO2 is expressed in various tissues of the body with olfactory neurons showing abundant expression of ANO2 (Stephan et al., 2009; Rasche et al., 2010). Upon stimulation of receptors on olfactory sensory neurons, an increase in cAMP leads to activation of cyclic nucleotide-gated channels (CNGSs) which are non-selective to cations (Kaupp, 2010). Depolarisation occurs and Ca^{2+} entry through CNGCs is able to activate ANO2 which essentially amplifies the excitable effects of the odorant (Rasche et al., 2010). ANO2-expression in HEK293 cells also produced CaCC currents similar to those seen in native olfactory cilia.

1.8.1.1 ANO2 in Olfaction

As mentioned previously, neurons can accumulate Cl^- which allows Cl^- efflux upon stimulation of ANO2. Vomeronasal sensory neurons (VSNs), involved in the detection of pheromones, also express ANO2 (Dibattista et al., 2012). Odorant receptors are able to activate the G_q pathway and induce DAG, which activates TRPC2 channels (Dibattista et al., 2012). These channels induce Ca^{2+} influx hence activating ANO2 (Dibattista et al., 2012). KO of ANO2 causes no CaCC currents to be generated in olfactory neurons, showing that ANO2 is the main CaCC-forming channel in this cell type (Billig et al., 2011). However, contrary to the general consensus that CaCCs have a core role in olfactory transduction, KO of ANO2 did not massively impair odorant-sensing ability of these neurons (Billig et al., 2011). However, recently it was reported that ANO2-KO in mice produced deficiencies in

the odor-related food finding ability (Pietra et al., 2016). Furthermore, the rate of action potential firing is greater and prolonged in ANO2-KO olfactory neurons which suggests that ANO2 plays a role in controlling the action potential firing rate in these neurons (Pietra et al., 2016). Nevertheless, due to this ongoing controversy, the exact role of ANO2 in olfactory signalling remains to be elucidated.

1.8.1.2 ANO2 in Vision

Photoreceptors also express ANO2 which has been localised to the retina, where these channels play a dual role in a photoreceptor's response to light. Generally, Na^+ influx via cGMP-gated cation channels is an incessant process in the dark causing depolarisation of the membrane (Cia et al., 2005; Pedemonte and Galietta, 2014). Accordingly, Ca^{2+} also enters the cells through VGCCs at the synaptic terminals, which is accompanied by a constant release of glutamate. This arrangement sets the resting membrane potential higher than normal (~between -40mV and -50mV) (Thoreson et al., 2004; Dauner et al., 2013). In cones the E_{cl} is close to the resting membrane potential (~-46mV) therefore, activation of ANO2 tends to have a less pronounced effect (Stohr et al., 2009). In rods on the other hand, the E_{cl} is approximately -20mV compared to the dark resting membrane potential (Thoreson et al., 2002). Here Cl^- efflux occurs, adding to the depolarisation of the cells. This makes sense when we look at the function of rod cells, which are highly sensitive to light therefore contain greater mechanisms to distinguish light from dark.

1.8.1.3 ANO2 in the hippocampus

ANO2 has been proposed to play a role in hippocampal neurons, where it is expressed in CA1 and CA3 pyramidal neurons (Huang et al., 2012). In contrast, ANO1 was not expressed in these neurons and whereas ANO2-KO inhibited the CaCC current, ANO1-KO had no such effect (Huang et al., 2012). Unlike ANO1, VGCC and NMDA receptor activation activated ANO2 in these neurons; furthermore, experiments using Ca^{2+} chelators indicated that the ANO2 is found close to the source of Ca^{2+} (Huang et al., 2012). Recording at CA1 neurons after CA3 stimulation, it was also discovered that ANO2 produces its effect in the somatodendritic region where it acts as an inhibitory entity (low Cl^- in pyramidal neurons; see above) and raises the excitability threshold. Overall, this acts as a brake on neuronal excitability.

1.8.1.4 Other Anoctamins

Functionally anoctamins can be subdivided into two groups: (1) CaCCs (ANO1 and ANO2) and (2) lipid scramblases (ANO3-10). Lipid scramblases are proteins that are involved with the distribution of phospholipids across the lipid bilayer (Bevers and Williamson, 2010). Scramblases move phosphatidylserine from the internal leaflet of the lipid bilayer to the external layer (Bevers and Williamson, 2010). The importance of this activity lies in processes such as coagulation where platelet cells expose phosphatidylserine which, in turn, triggers phagocytosis of dying cells (Malvezzi et al., 2013). However, in relation to the other anoctamins, different opinions exist between different groups regarding their activity. Thus, Kunzelmann's group found that expression of ANO6, 7 and 10 produced CaCC currents; however, in ATP-induced I^- flux assays, these channels only produced activity that was approximately 10% of ANO1 activity (Schreiber et al., 2010). Conversely, another group found that there are no robust CaCC currents for ANO3-7, probably due to little or no plasma membrane expression of these proteins (Tsutsumi et al., 2004; Mizuta et al., 2007; Duran et al., 2012).

ANO3 has been implicated in playing a role in nociception with high expression in DRG neurons with ANO3-KO mice displaying hypersensitivity to temperatures over 50°C (Huang et al., 2013). Furthermore, it was discovered that ANO3 plays a role in regulating Na^+ activated K^+ activity in DRG (Huang et al., 2013). Mutations in ANO5 have been linked to musculoskeletal disorders such as gnathodiphyseal dysplasia (GDD). This leads to bone fragility due to abnormal bone mineralisation (Tsutsumi et al., 2004; Mizuta et al., 2007; Duran et al., 2012). Other disorders linked to ANO5 include recessive muscular dystrophies (Bolduc et al., 2010; Hicks et al., 2011). ANO6, has been found to play a role in lipid scrambling (Suzuki et al., 2010). Mutations in ANO6 lead to Scott syndrome, a rare congenital disorder characterised by defective blood coagulation (Suzuki et al., 2010; Castoldi et al., 2011). Underlying this disorder is abnormal lipid scrambling which causes an altered phospholipid composition of the external layer of the membrane (Suzuki et al., 2010; Malvezzi et al., 2013). ANO6 has also been proposed to function as both an ion channel and a scramblase however, its ion conducting ability was only present under micromolar Ca^{2+} concentrations and at positive membranes (Scudieri et al., 2015). ANO7 is found expressed in the prostate and has been suggested to play a role in cell-cell

adhesion (Das et al., 2007). Moreover, ANO7 has been implicated in prostate cancer due to its high expression profile however its role in the development of this type of cancer is unknown (Cereda et al., 2010). ANO10 mutations have been linked to an autosomal recessive called cerebellar ataxias (Vermeer et al., 2010; Duran et al., 2012).

1.9 Expression and functions of ANO1

1.9.1 Airways

ANO1 is widely expressed in the body. Various cell types that were known to produce CaCC currents express ANO1. ANO1 is present in the airways where it is involved with secretion of Cl^- and hydration (Yang et al., 2008; Rock et al., 2009; Gallos et al., 2013; Caputo et al., 2015). Caputo and colleagues, one of the initial three independent groups to identify ANO1, found that IL-4 treatment caused a near sevenfold upregulation of ANO1 mRNA in bronchial cells (Caputo et al., 2008). Transfecting this mRNA into CFPAC-1 (pancreatic) or CFBE41o (human bronchial epithelial) cell lines and using a halide-sensitive YFP assay or performing whole-cell patch clamp experiments, produced CaCC activity. This was reduced by 60-70% when siRNA was used to silence ANO1 (Caputo et al., 2008). ANO1 also plays a role in the release of mucus from goblet cells (Costa and Catterall, 1984; Zhuang, 2009; Scudieri et al., 2012). Under normal conditions there is minute presence of ANO1 but in patients with asthma or mouse models mimicking asthma, there is increased ANO1 expression in mucus-producing goblet cells (Caputo et al., 2008; Zhuang, 2009; Kondo et al., 2017). Another interesting point to mention is the importance of $HCO3^-$ secretion for mucus release. Altering $HCO3^-$ secretion has been shown to change the consistency of mucus in sheep, pigs and human trachea (Joo et al., 2001). In small intestine of mice, absence of $HCO3^-$ led to a 50% reduction in agonist-stimulated mucus release (Garcia et al., 2009). In relation to this, an interesting property of ANO1 is its ability to transport $HCO3^-$, especially at high Ca^{2+} concentration where the permeability changes from preferring Cl^- to $HCO3^-$ (Jung et al., 2013). It was hypothesized that this property of ANO1 relies on the presence of CaM (see above).

Overall, this strengthens the notion that ANO1 is a vital component of mucus release where it can accommodate the movement of fluid through Cl^- transport and $HCO3^-$.

1.9.2 Vasculature

It has long been known that vasculature expresses functional CaCC (Criddle et al., 1996; Zhuang, 2009). Accordingly, vascular smooth muscle cells (VSMCs) in various regions of the body have been shown to express ANO1, including the thoracic aorta and cerebral arteries (Bulley et al., 2012; Davis et al., 2013; Wang et al., 2016). Due to an accumulation of Cl^- inside VSMCs, ANO1 activation leads to a depolarising effect and vasoconstriction indicating a role for ANO1 in hypertension. (Vaughan-Jones, 1979; Baumgarten and Fozzard, 1981; Bulley et al., 2012). Consequently, siRNA against ANO1 was able to reduce pressure-induced vasoconstriction indicating that ANO1 channels contribute this process (Bulley et al., 2012). Following on from these findings, spontaneous hypertensive rats were shown to have overexpression of ANO1 and accordingly, pharmacological blockade or knockdown of ANO1 resulted in reduction in blood pressure (Heinze et al., 2014; Wang et al., 2016). Interestingly, Angiotensin II, a vasoactive peptide that increases blood pressure, has been shown to increase the expression on ANO1 (El Chemaly et al., 2014). Other effects of ANO1 in VMSCs are thought to include the progression of vascular remodelling by inducing VMSC proliferation (Wang et al., 2015; Qu et al., 2016). ANO1 overexpression in these cells could therefore serve as a trigger to the development of hypertension (Wang et al., 2015). PASMCs were known to possess CaCC currents and siRNAs against ANO1 in PASMCs caused an almost total loss of whole cell CaCC current (Manoury et al., 2010). There is also evidence to suggest that PASMCs increase ANO1 expression in response to chronic hypoxia, leading to increased vasoreactivity, which in turn produces pulmonary hypertension (Sun et al., 2012). Both conditions highlight the importance of ANO1 and how its regulation is necessary in the vasculature.

1.9.3 Gastrointestinal tract

The Gastrointestinal tract also expresses ANO1. Interstitial Cells of Cajal (ICC) are a specialized set of pacemaker cells responsible for the generation of ‘slow waves’- phasic contractions that occur in an autonomous nature in the gastrointestinal tract (Takaki, 2003). The slow waves are driven by Ca^{2+} oscillations; ANO1 is present in

these cells and activated due to IP_3R-induced Ca^{2+} release. ANO1 seems to be vital for slow waves of electrical activity, as knockdown of ANO1 severely disrupts both the electrical activity and the contraction involved with this process (Gomez-Pinilla et al., 2009; Hwang et al., 2009; Singh et al., 2014). Recently it was discovered that ANO1 also plays a role in the tone of the internal anal sphincter (Zhang et al., 2016a; Cobine et al., 2017). Accordingly, tone is reduced when ANO1 antagonists are applied and genetically encoded deletions of ANO1 also lead to a loss of ICC slow waves and spontaneous contractions in mice (Cobine et al., 2017). Further analysis demonstrated that the anal sphincter tone requires VGCC-induced activation of ryanodine receptors (RYR). The elevation of $[Ca^{2+}]_i$ in turn activates ANO1 and induces contraction (Zhang et al., 2016a).

1.9.4 Kidney

ANO1 is expressed at the proximal renal tubules of the kidney. *Uhtaek* Oh's group, pioneers of ANO1 discovery, showed the presence of ANO1 in kidney cells (Yang et al., 2008). ANO1 was immunohistochemically localised to the proximal and distal tubular epithelial (PTE, DTE) cells and also to podocytes in humans and rat (Faria et al., 2014). ANO1 knockdown in mice led to development of proteinuria, which indicates a significant role for ANO1 in glomerular function (Faria et al., 2014). However, this was attributed to loss of PTE ANO1, not podocyte ANO1 loss (Faria et al., 2014). ATP application has also been shown to induce CaCC currents in inner medullary collecting duct cells of kidneys causing Cl^- secretion through a mechanism reliant on PLC and Ca^{2+} (Cuffe et al., 2000; Rajagopal et al., 2012). ANO1 is expressed in these cells with minimal bestrophin-1 expression. It has been proposed that this Cl^- secretion provides an adaptive mechanism for NaCl removal when there is high dietary salt intake (Rajagopal et al., 2011). In disease states of the kidney, ANO1 has also been implicated in the formation of renal cysts (Buchholz et al., 2014; Tanaka and Nangaku, 2014).

1.9.5 ANO1 in nociception

Sensory neurons have been known to express CaCCs since 1987 when Bader and colleagues discovered CaCC current activation in quail sensory neurons when $[Ca^{2+}]_i$ was elevated (Bader et al., 1987). Subsequent buffering of Ca^{2+} was able to supress this current (Bader et al., 1987). Interestingly, nerve injury induced through axotomy

of the sciatic nerve in rats produced increased CaCC currents in injured DRG neurons (Andre et al., 2003). This increased CaCC current was only present in a subset of axotomised neurons that showed ‘regenerating’ axon growth typical after nerve injury but was only to medium and large neurons (Andre et al., 2003). Furthermore, CaCC candidates such as bestrophin 1 and Tweety2 were also upregulated after SNL in mice (Al-Jumaily et al., 2007). Another study involving nerve injury proposed that the increased CaCC current was mediated by bestrophin 1 and bestrophin 3 in large and medium-diameter DRG neurons (Boudes et al., 2009). As mentioned earlier, this indicates the involvement of CaCCs in nociception and related conditions such as nerve injury, inflammation, chronic pain etc.

After ANO1 discovery, Yang and colleagues demonstrated its expression in DRG neurons- particularly small-diameter (Yang et al., 2008). ANO1 was recently suggested to also play a role as a heat sensor, similar to TRPV1 (Cho et al., 2012). Temperatures above 44°C were able to activate ANO1 regardless of Ca^{2+} presence, however Ca^{2+} was able to lower the heat threshold of ANO1 in a similar manner to the synergistic relationship between voltage and Ca^{2+} that ANO1 displays (Cho et al., 2012). Mice lacking TRPV1 still displayed behavioural responses to heat and DRG from TRPV1-KO mice produced inward Cl^- currents in response to heat (Cho et al., 2012). Conditional KO of ANO1 in sensory neurons reduced temperature-induced Cl^- currents and siRNA against ANO1 also had a similar effect (Cho et al., 2012). Furthermore, blockers of both TRPV1 and ANO1 were found to completely abolish heat responses. Independent verification of these finding is yet to be obtained. Other implications of ANO1 in nociception will be discussed below.

The inflammatory mediator, bradykinin was found to induce a depolarising CaCC current along with inhibiting the K_v7 current in DRG neurons with both effects attributed to bradykinin activating the G_q pathway (see above) (Liu et al., 2010). Again, the relatively high expression of the NKCC1 cotransporter in DRG neurons means there is a build-up of Cl^- in these cells (Rocha-Gonzalez et al., 2008; Mao et al., 2012). Consequently, CaCC activation is excitatory (Cl^- efflux) meaning the net effect of the inhibition of hyperpolarizing K_v7 channels and the excitatory Cl^- channels would be summated in strong depolarisation and action potential firing (Liu et al., 2010). Knockdown of ANO1 using siRNA or pharmacological inhibition produced a reduction in CaCC current in DRG neurons and reduced inflammatory

pain and itch (Liu et al., 2010; Lee et al., 2014; Ru et al., 2017). Ultimately, in DRG it was found to be local Ca^{2+} elevation from the ER through IP_3R which activated ANO1 (see chapter 4). As Ca^{2+} sensitivity of ANO1 is fairly low, especially at resting membrane potentials, it was proposed that these channels are arranged in a local Ca^{2+} microdomains at the ER-PM junctions (Jin et al., 2013).

1.10 Local Ca^{2+} Microdomains

Ca^{2+} is one of the most important intracellular second messengers. These ions are important mediators of various cell-signalling processes where they can; (i) alter the membrane potential, and (ii) function as intracellular signalling messengers for a wide spectrum of processes such as gene transcription, cell proliferation, apoptosis, and neurotransmitter release (Bootman et al., 2001). $[Ca^{2+}]_i$ is kept low (~100-500nM) to allow steep gradients for Ca^{2+} entry, thereby priming cells for this event (Berridge, 2006).

Importantly however, not every rise in $[Ca^{2+}]_i$ will lead to every Ca^{2+}-dependent process occurring in a cell. The ability of Ca^{2+} to function as a secondary messenger depends on both its temporal and spatial properties (Berridge, 2006). This means that activation of Ca^{2+}-sensitive channels/proteins by Ca^{2+} will require the relevant concentration to exist in the immediate environment before any effect occurs along with maintaining specificity of Ca^{2+} signalling (Rizzuto and Pozzan, 2006).

To facilitate this in various instances, components of the Ca^{2+} signalling cascade are often organized into functional Ca^{2+} microdomains (Berridge, 2006). These Ca^{2+} microdomains are sites within cells (~10-100nm) where there is a high, localised Ca^{2+} concentration which serves to enhance signalling fidelity and strengthen the response to a stimulus in an efficient, selective manner (Berridge, 2006). Ca^{2+} release into microdomains is adjudged to be local due to its transient and spatial restriction within a cell (Bootman et al., 2001). For example, Ca^{2+} entering the cell from the extracellular space or Ca^{2+} release into the cytosol from the ER may lead to the production of highly specific and concentrated Ca^{2+} levels (reported to be up to ~50μM) around the mouth of the channel and in the local vicinity (Neher, 1998; Bauer, 2001; Bootman et al., 2001). However, the presence of proteins and membranes stops the spread of Ca^{2+} to the rest of the cell (Fig. 1.11). Alternatively,

these signals can be summated in a cell to lead to the elevation of this 'global' Ca^{2+} (Berridge, 1993; Bootman et al., 2001; Rizzuto and Pozzan, 2006). Below I will discuss some examples of microdomains and the roles they play in cellular processes.

1.10.1 SOCE

SOCE is the process whereby the internal Ca^{2+} stores in the ER are refilled after depletion (Parekh and Putney, 2005). Activation of GPCRs activate PLC and generate IP_3, which subsequently activates IP_3Rs. Activation of this receptor causes Ca^{2+} to rapidly exit the ER and into the cytosol (Berridge, 1993). Upon depletion of the ER Ca^{2+} content, two proteins, STIM1 and Orai1, found in the ER and the PM, respectively, are able to interact and initiate the refilling process (Smyth et al., 2006). The close apposition between the ER and PM facilitates this process (Carrasco and Meyer, 2011). STIM1 is a Ca^{2+} sensor protein, which relays the depletion signal to Orai1 through a physical interaction (Smyth et al., 2006). Orai1 forms a pore to allow Ca^{2+} entry into the cell and back into the ER through the SERCA pumps (Smyth et al., 2006). Microdomains involving SOCE are important in various cell types and allow a restricted area for Ca^{2+} entry to refill the ER as well as playing a role in other functions. In skeletal muscle, SOCE microdomains are vital in the rapid repletion of the sarcoplasmic reticulum (SR) (Launikonis and Rios, 2007; Stiber et al., 2008). STIM1 is localised close to the T-tubule PM in skeletal muscle and subsequent depletion of SR Ca^{2+} allows rapid SOCE- within 1 second compared to in T-lymphocytes which require of approximately 1 min before SOCE occurs; this has been attributed to the pre-existence of microdomains in T-tubule structures (Launikonis and Rios, 2007).

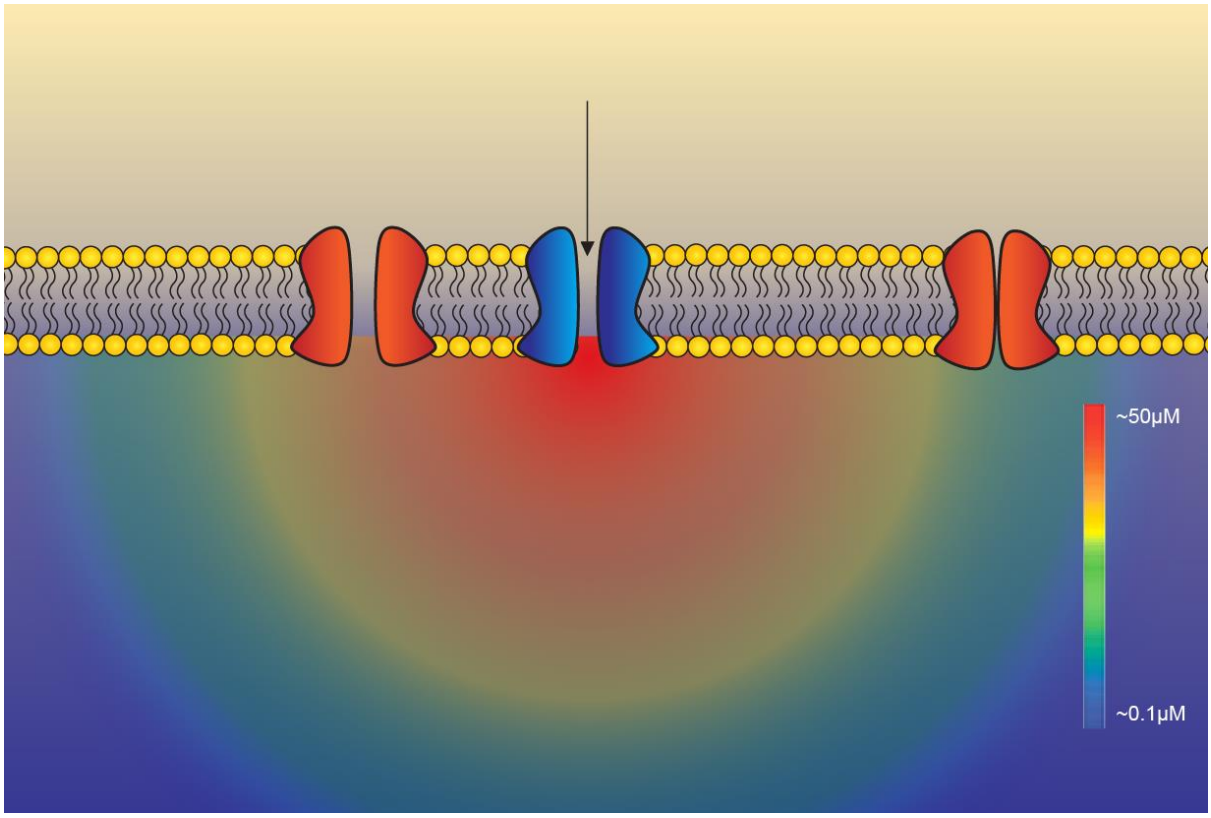

Figure 1.11: High Ca^{2+} in a microdomain close to the mouth of a Ca^{2+} channel.
Ca^{2+} concentration reaches ~50μM around the channel however, as we move away by a few hundred nanometers (Naraghi and Neher, 1997; Neher, 1998; Bauer, 2001; Rizzuto and Pozzan, 2006), the concentration of Ca^{2+} rapidly decreases to ~100nM. A Ca^{2+} sensitive channel close to the high concentration of Ca^{2+} can be activated whereas channels further away are not activated. Based on figure from (Rizzuto and Pozzan, 2006).

1.10.2 Regulation of AC

Another function of SOCE Ca^{2+} microdomains is in the activation of AC. Some isoforms of AC (1 and 8), the enzyme required in the production of cAMP and subsequent activation of PKA, require Ca^{2+} for activation (Willoughby and Cooper, 2007). In non-excitable cells, Ca^{2+} entry through Orai1 channels is able to activate AC however, other means of $[Ca^{2+}]_i$ elevation have been found to be incapable of activating this enzyme (Martin et al., 2009). Agonist-, thapsigargin- and ionomycin-induced $[Ca^{2+}]_i$ elevations were unable to induce AC in C6-2B glioma cells (Chiono et al., 1995; Fagan et al., 1996). Interestingly, the global Ca^{2+} rise seen through SOCE was less than that caused by mechanisms mentioned above but was still able to activate AC activity, demonstrating the importance of specific Ca^{2+} signals (Fagan et al., 1996; Fagan et al., 1998). AC 8 was also found in lipid rafts with Orai1 in MIN6 cells which suggests they may be in close proximity (Martin et al., 2009). Furthermore, BAPTA was able to inhibit AC activity but EGTA was unable to produce this effect further supporting that this is due to local Ca^{2+} (Fagan et al., 1998). Taken together, this data suggests that AC is located in close proximity to Orai1 and STIM1 proteins and Ca^{2+} via Orai1 in the local vicinity is able to modulate AC activity (Parekh, 2008).

1.10.3 Excitation-contraction coupling

Excitation-contraction coupling is another process where microdomains play a vital role. The process of excitation-contraction coupling links membrane depolarisation with contraction in cardiomyocytes (Aronsen et al., 2013). L-type VGCCs are localised to the sarcolemma of myocytes where activation of these channels leads to Ca^{2+} influx (Aronsen et al., 2013). The close proximity of RYR in the SR to the sarcolemma (Scriven et al., 2010), means L-type VGCCs influx activates RYR receptors, a process known as Ca^{2+}-induced Ca^{2+} release (CICR) (Mackenzie et al., 2001). In ventricular cells, activation of a single L-type VGCCs activates 10-15 RYRs (Wang et al., 2001) therefore, a small number of L-type VGCCs in the T-tubules can activate a great number of RYR; the summation of this effect is a large rise in $[Ca^{2+}]_i$ sufficient to trigger contraction (Berridge, 2006). The importance of L-type VGCCs and RYR coupling in microdomains has been demonstrated in heart failure where there is a loss of coupling between these proteins therefore insufficient cardiac contraction (Benitah et al., 2002; Bito et al., 2008; Sanchez-Alonso et al., 2016).

In cerebral arterial smooth muscle, T-type Ca^{2+} channels have been found to assemble into microdomains with RYR to activate CICR-like events (Abd El-Rahman et al., 2013). Ultimately, CICR induces large conductance Ca^{2+} activated K^+ channel (BK_{Ca}) activity to reduce arterial constriction (Harraz et al., 2014). KO of T-type Ca^{2+} channels causes reduced BK_{Ca} activity and enhanced myogenic tone of arterial smooth muscle due to loss of RYR activation (Harraz et al., 2014; Harraz et al., 2015).

1.10.4 Coupling of ANO1 to different Ca^{2+} sources

Extracellular Ca^{2+} entry can activate ANO1 in many situations, particularly in expression systems. Thus, ionomycin is able to activate ANO1 in HEK293 cells where it is able to induce the linear I-V relationship seen for ANO1 in the presence of high Ca^{2+} (Zhuang, 2009; Tian et al., 2011; Jung et al., 2013). This was also seen in ICC pacemaker cells (Kim et al., 2014) and thyroid follicular cells (Iosco et al., 2014). Ionomycin application to Fisher rat thyroid (FRT) cells transfected with ANO1 are also able to induce ANO1 activity in I^- based quenching assays, which was not possible in Ca^{2+}-free conditions (Schreiber et al., 2010). Photoreceptors expressing ANO1 have been shown to interact with VGCCs where the *Cacna2d4* mutation in the $\alpha_2\delta_4$ subunit of the VGCC disrupts both this interaction and the activation of ANO1 (Caputo et al., 2015). In canine ventricular myocytes, sarcolemmal L-type VGCCs are essential for ANO1 activity and have also been shown to co-localise with these Ca^{2+} channels (Horvath et al., 2016). Furthermore, in Xenopus oocytes, expression and stimulation of G_q-gated $P2Y_2$ receptors generates ANO1 currents however these are almost abolished when extracellular Ca^{2+} was removed suggesting a prominent role for extracellular Ca^{2+} in ANO1 activation in these cells (Kunzelmann et al., 2011).

CaCCs were found to be activated through the ER after IP_3 application and also through SOCE where they showed different I-V profiles- outwardly rectifying and linear for the Ca^{2+} source, respectively (Hartzell, 1996; Kuruma and Hartzell, 1999). However this SOCE-activation was later suggested to be a secondary effect of Ca^{2+} channelled via IP_3R after the SOCE-mediated store refill (Courjaret and Machaca, 2014). Yang and colleagues also demonstrated the importance of ER Ca^{2+} when they transfected HEK293T cells with ANO1 and various GPCRs which induced Ca^{2+}

release from the ER. These receptors (i.e. $P2Y_2$ receptors activated by ATP) induced CaCC currents when stimulated with the corresponding agonist (Yang et al., 2008). Furthermore, depleting the ER of Ca^{2+} stopped ANO1 activation (Yang et al., 2008). $P2Y_1$ and $P2Y_2$ receptors are known to be expressed endogenously in HEK293T cells (Schachter et al., 1997). When no additional $P2Y_2$ receptors were overexpressed in HEK293T cells, there was activation of ANO1 currents however, upon overexpression of $P2Y_2$ receptors, the ANO1 current was greatly enhanced (Kunzelmann et al., 2011). Thus, it was proposed that there must be close proximity between ANO1 and the Ca^{2+} source for activation to take place and more receptors leads to more interactions between the ANO1 and IP_3R (Kunzelmann et al., 2011). The above examples highlight several features of ANO1 coupling to a Ca^{2+} source: (i) ANO1 channels can be activated by various Ca^{2+} signals in different cell types or expression systems but the common theme is it's close coupling to the ER Ca^{2+} release; (ii) due to low Ca^{2+} sensitivity, ANO1 channels need to be positioned closely to the Ca^{2+} source to be reliably activated. Further examples regarding the proximity of the Ca^{2+} source to ANO1 will be discussed in subsequent chapters.

1.11 Aims of this study

The aim of this study is to investigate activation of ANO1 channels in nociceptive sensory neurons by localised Ca^{2+} signals and to investigate whether different types of nociceptive Ca^{2+}-signalling pathways are able to activate ANO1. Specific focus will be given to three independent Ca^{2+} signalling pathways: (i) pro-inflammatory GPCR; (ii) VGCC and (iii) TRPV1. To investigate this I will develop a new imaging technique combining Ca^{2+} imaging and a halide sensitive quenching to monitor intracellular Ca^{2+} dynamics and CaCC activity simultaneously. Furthermore, I will also look at the relationships between proximity of ANO1 to potential Ca^{2+} sources using biochemical and super-resolution imaging approaches to provide insight into underlying mechanisms regarding ANO1 activation. If the Ca^{2+} source is found in close proximity to ANO1, then in theory it should be able to activate ANO1.

Chapter 2: Materials and Methods

2.1 DRG culture and transfection

Handling of rats throughout this whole process was done in accordance with Home Office regulations. Wistar rats (7 day old) were culled by over-exposure to Isoflurane followed by cervical dislocation to confirm death. Decapitation and removal of the spine allowed DRG to be extracted and isolated. The spine was sliced in half along the sagittal plane to expose the spinal cord; gentle removal of the spinal cord revealed small spherical DRGs in small grooves within the spine. Extraction of DRG was made with fine forceps and stored in ice-cold Hanks Balanced Salt Saline (HBSS) during the extraction process. Once all DRG were isolated, they were transferred to a dissociation solution consisting of pre-warmed (37°C) HBSS, dispase (10mg/ml) (Invitrogen) and collagenase type 1A (1mg/ml) (Sigma). The dissociation solution containing isolated DRG was incubated at 37°C for approximately 13 minutes to allow dissociation of cells until the mixture became cloudy. Gentle trituration (~5 times) of the mixture helped the dissociation process after which cells were replaced at 37°C for a further 2 minutes. Further trituration was done (~10-20 times) to ensure maximal DRG dissociation. Termination of the dissociation process was achieved by supplementing the incubated mixture with ice cold growth media (DMEM and GlutaMAX) (Invitrogen), containing penicillin (50U/ml), streptomycin (50ug/ml) and 10% Fetal Calf Serum (FCS). DRG were centrifuged twice for 5 minutes at 800rpm (4°C), to wash the solution and collect the cells. Fresh media was used to resuspend the pellet prior to the second spin. Resuspended cells were transferred onto coverslips pre-coated with poly-D-lysine and laminin in 24-well culture plates. Plates were incubated in a humidified incubator (5% CO2) at 37°C for 4 hours after which cells were supplemented with fresh warm growth media. Cells were cultured at 37°C for a further 2-4 days.

When transfection was necessary, cells collected after the final wash (see above) were resuspended in a rat neuron transfection buffer (Lonza) and mixed with 5µg of mutant EYFP DNA constructs (pcDNA6 vectors) with mutations at H148Q and I152L positions. The solution was quickly loaded into a Lonza-certified cuvette and transferred into the Lonza Nucleofector I console and transfected on setting O-03. Transfected cells were then resuspended in 500-550µl warm DMEM media before

plating onto coverslips (~90µl per 13mm coverslip). Coverslips were pre-coated with poly-D-lysine and laminin in 24-well culture plates. Plates were incubated in a humidified incubator (5% CO2) at 37°C for 4 hours after which cells were supplemented with fresh warm growth media. Cells were cultured at 37°C for a further 2-4 days.
EYFP (H148Q/I152L) DNA was kindly provided by Dr Jonathan Lippiat.

2.2 Triple-wavelength Imaging

Extracellular solution was produced to bathe cells (mM): NaCl (160); KCl (2.5); $MgCl_2$ (1); $CaCl_2$ (2); HEPES (10) and Glucose (10). The pH was buffered to 7.4 using NaOH (1M) (All from Sigma). Each coverslip was broken into 3-4 pieces (or chips) with a diamond pencil and a single piece was incubated with 2µM fura-2 AM (Life Technologies) and pluronic F-127 (0.01%) (Sigma) at 37°C for 45 minutes. Loading was done with no light in the microflow safety cabinet. After loading with fura-2 AM, the chip was washed with extracellular solution before imaging. Foil was used to shield cells from light during transferral of cells from the incubator to the imaging rig. Chips containing fura-2 loaded cells was placed on the camera chamber for imaging. Extracellular solution was used to perfuse the cells through a gravity driven perfusion system. Imaging was performed with a Nikon TE-2000 microscope (inverted) with the 40x objective. The imaging setup was equipped with T.I.L.L Phototonics fluorescent imaging system (Polychrome V monochromator, IMAGO CCD camera and TILLVison 4.5.56 software/Live Acquisition 2.2.0). Live images of cells were used to locate neurons that had been successfully transfected with the EYFP mutant using 488nm excitation at 40ms exposure fluorescent light to avoid photobleaching. Glial cells (bipolar processes) were excluded from the search and only successfully transfected DRG with a diameter of ~20µm were selected. Ca^{2+} loading was identified using the same process as for the mutant EYFP identification but with a 380nm excitation wavelength. Filter cubes allowing EYFP and fura-2 imaging was used for emission (GFP-B and UV-2A, respectively (Nikon MicroscopyU)). UV-2A was used for dual imaging. Only cells successfully transfected and loaded with the EYFP mutant and fura-2, respectively, were imaged. Exposure for all 3 wavelengths (340, 380 and 488) was adjusted during imaging to provide optimal signal-to-noise parameters (ranging from 50ms-500ms maximum).

Regions of interest (ROI) were marked on a snapshot taken from which live recordings were made for all 3 wavelengths.

Extracellular solutions containing various concentrations of I^- instead of Cl^- were made by equimolar substitution of the NaCl with NaI (30mM, 10mM and 5mM). Drugs were added to the NaI containing solution whilst imaging (GABA 100μM, capsaicin 1μM, bradykinin 250nM). The 50mM K^+ solution was produced by subtracting the 47.5mM increase in KCl (50mM) from the NaCl content (160mM to 112.5mM) to maintain a balance in the ion content of the solution. Ca^{2+} free solutions were produced with increased NaCl (165mM) to compensate for Cl^- lost with the removal of $CaCl_2$; 1mM EGTA was also added. Pre-incubation with thapsigarigin (LKT Laboratories) (1μM) was done during the fura-2 loading process and thapsigarigin was kept in solutions during imaging to maintain its effects.

Protocols for imaging involved perfusion of standard extracellular solution for 50 seconds, before switching to NaI containing extracellular solution for 50 seconds. NaI containing NaI + drug/agonist/condition was then applied for 100 seconds to visualise the effects produced. Fluorescent images were taken every 2 seconds (1 step) sequentially at 488nm, 340 and 380 nm. Fluorescence intensity at 488 nm was used as a reporter of I^- influx; ratio of fluorescence intensities at 340 and 380 was used as a reporter of intracellular Ca^{2+} concentration.

2.2.1 Imaging analysis

Once imaged, ratios between 340nm and 380nm were produced and transferred to Microsoft Excel for analysis along with data for fluorescence intensity at 488nm. Fura-2 ratios were normalised to the change in the ratio to t=0 ($\Delta R/R_0$) and EYFP (H148Q/I152L) mutant fluorescence data were normalised to the change in fluorescence recorded at t=0 ($\Delta F/F_0$), for each cell. Cells where either of the recording channels gave unstable baseline or oscillations during recording were discounted form analysis. All cells included in the analysis were temporarily aligned to the point of Ca^{2+} increase by 3 times the standard deviation of the baseline. Agonist-dependent EYFP (H148Q/I152L) mutant fluorescence quenching was also monitored from this point until the end of agonist application. Statistical analysis was then carried out between the end of the agonist-independent quenching period to the completion of the agonist-dependent quenching period.

2.2.2 Standard Ca^{2+} imaging

Standard Ca^{2+} imaging involved no transfection. After the second wash, cells were resuspended in warm DMEM media and plated onto pre-coated coverslips and grown for 2 days. Cells were loaded with fura-2 and imaging was done in the same manner as above but using only 340nm and 380nm excitation wavelengths.

2.2.3 Four-wavelength imaging

Chinese hamster ovary (CHO) cells were grown in tissue culture plates at 37°C (5% CO2) and passaged when confluent (~70%). DMEM:F12 (1:1) media with Glutamax (supplemented with penicillin (50U/ml), streptomycin (50ug/ml) and 10% Fetal Calf Serum (FCS)) (Thermofisher) was used to grow CHO cells. Transfection was done using Fugene HD (Promega) according to manufacturer's instructions. cDNA plasmids coding for EYFP (H148Q/I152L), TRPV1, ANO1 and red CEPIA (400ng each) were used to overexpress the corresponding proteins CHO cells. Cells were plated onto 13mm glass coverslips and loaded with fura-2 before imaging. Triple imaging (including Red CEPIA imaging) was done by adding a fourth channel, 560nm for excitation. A special dichroic filter (Chroma) was used to allow all 4 channels to be imaged simultaneously (combining DC/59022bs-XR-360-UF1 and DC/59022m). During IP_3R-blocking experiments, xestospongin C (Abcam) (1μM) was pre-incubated with cells during the fura-2 loading process and kept in solutions during imaging to maintain its effects.

2.2.4 Statistical analysis

All cells imaged for a certain condition were collated and averaged before being plotted as a graph. Students T-test (paired) was used to compare pre-agonist and post-agonist values for both fura-2 Ca^{2+} signals and EYFP (H148Q/I152L) quenching. Comparison of maximal quenching/Ca^{2+} elevation between 2 conditions were compared using students T-test (unpaired). ANOVA was used when comparing more than 2 conditions (with Tukey test for comparison between groups). If results were not normally distributed (tested for all datasets using Origin normality test setting), then comparisons for data sets were made using Wilcoxon-Signed (paired comparison), Mann-Whitney (unpaired comparison) and Kruskal-Wallis ANOVA to compare more than 2 datasets (in conjunction with Mann-Whitney to compare

individual datasets). If a result is deemed to be significantly different, the p value must be below 0.05 ($p \leq 0.05$). All results are provided as mean ± S.E.M.

The *n* number is equal to the number of cells used for each experiment. Each dataset consists of cells taken from at least 3 DRG preparations from rats. If transfection in cell lines was used, a minimum of 3 transfections was made for each dataset.

2.3 Immunocytochemistry

DRG cultures were prepared on coverslips in the same manner as mentioned above (without transfection). Neurons were fixed using 1:1 ice-cold acetone/methanol solution before being washed three times with 1X PBS. Blocking solution made up of 0.05% Tween 20, 0.25%Triton™ X-100 and 5% donkey serum in 1X PBS was used to block the culture for 1 hour at room temperature before cells were incubated with either 1:100 ANO1 primary antibody (Santa Cruz) or TRPV1 primary antibody (diluted in 1X PBS/10mg/ml BSA) or both overnight at 4°C on a rocking table. Cultures were then washed again with 1X PBS three times and incubated with 1:1000 Alexa Fluor ® 488 (Life Technologies) (donkey anti goat) or Alexa Fluor ® 555 (Life Technologies) (goat anti guinea pig) diluted in antibody dilution buffer for 2 hours. Finally coverslips were washed and mounted on glass coverslips with VECTASHIELD mounting medium supplemented with 4,6 diamidino-2-phenylindole (DAPI). Imaging was performed with a Carl Zeiss LSM510 inverted confocal microscope and Zeiss ZEN imaging software. See table 1 for all antibodies and concentrations used. Acetone/methanol was used as a fixative for all antibodies to maintain consistency.

Antibody	Species	Species raised in (secondary only)	Dilutions	Company
ANO1	goat rabbit		1:200 1:500	Santa Cruz Abcam
TRPV1	guinea pig		1:500	Neuromics
IP_3R1	rabbit		1:500	Cell Signaling Technology
MOR	rabbit		1:500	Abcam
Alexa Fluor ® 488	Anti-goat Anti-rabbit Anti-guinea pig	Donkey Goat	1:1000	Thermofisher
Alexa Fluor ® 555	Anti-goat Anti-rabbit Anti-guinea pig	Donkey Goat	1:1000	Thermofisher
Alexa Fluor ® 633	Anti-rabbit	Goat	1:1000	Thermofisher

Table 2.1: Antibodies used for immunohistochemistry. Table shows primary (white) and secondary (grey) antibodies used, species, dilutions used and company.

2.4 Proximity Ligation Assay

Proximity ligation assay (PLA) uses the principle of 2 oligonucleotide labelled antibodies (primary or secondary) being able to bind and fluoresce, only when they are in close proximity to one another (30-40nm). This technique was first developed in 2002 by Fredriksson and colleagues who showed its ability to detect platelet-derived growth factor in situ (Fredriksson et al., 2002). Primary antibodies (different species) against two proteins presumed to be less than 40nm apart from each other are used to bind the proteins of interest (Fig. 2.1). A pair of secondary antibodies, which are conjugated to oligonucleotides (referred to as PLUS and MINUS probes), are used to bind the primary antibodies. If the proteins of interest are indeed less than 40nm apart, complimentary connector oligonucleotides can allow formation of a single-stranded DNA circle between the 2 secondary oligonucleotide-conjugated probes (Fig. 2.1). One of the conjugated probes in the DNA circle can then act as a primer for rolling circle amplification (RCA), with the DNA-circle acting as a template. Addition of DNA polymerase allows formation of a long DNA product which contains repeated sequences that can be targeted for detection using fluorescently labelled oligonucleotides (Fig. 2.1). Hybridisation of these fluorescent tags can then be visualised to indicate the presence of 2 proteins in close proximity (Fig. 2.1).

PLA kits (Sigma) were purchased and the assay was completed in accordance with the manufacturer's instructions. For the protocol, DRG cultures (untransfected) were plated and grown directly on to glass microscope slides coated with poly-D-lysine and laminin. Fixation was again done using 1:1 acetone/methanol and cells were washed 3 times with 1X PBS. Prior to blocking, an ImmEdge hydrophobic barrier pen (Vector laboratories) was used to delimit the reaction to an approximate area of $1cm^2$. Blocking solution provided in the PLA kit was used to block the cells for 30 minutes at 37°C. Subsequently, cells were treated with primary antibodies (combination of 2 from ANO1, TRPV1 or IP_3R1, same dilutions as immunocytochemistry) in an antibody dilution buffer provided in the kit. Cells were put on a rocker at 4°C overnight. PLA buffer A was used to wash the cells twice (5 minutes) before PLA probes (secondary antibodies conjugated with oligonucleotides) were added. No commercial kit for anti-guinea pig probes is available so an anti-guinea pig secondary antibody was conjugated to a MINUS oligonucleotide using a PLA conjugation kit (Sigma). Both anti-guinea pig MINUS and anti-goat PLUS antibodies were diluted in the antibody dilution buffer (see Table 2.2 for dilutions of each probe) and incubated with the cells for 60 minutes at 37°C. Further washes were then carried out (5 minutes again) using PLA wash buffer A. For ligation, a solution consisting of ligation stock solution in high purity water (1:5) was made and ligase was added to produce a final ligase dilution of 1:40. This was incubated with cells for 30 minutes at 37°C. PLA buffer A was used to wash the cells again (2 minutes) twice before the amplification solution was produced. Amplification stock was diluted in high purity water (1:5) before polymerase was added to give a final polymerase dilution of 1:80. Cells were incubated with the amplification solution for 100 minutes at 37°C. Final washes using PLA buffer B were done twice for 10 minutes before a final wash using 1:100 buffer B solution. Cells were then sealed using DAPI-containing mounting medium. Imaging was performed with a Carl Zeiss LSM510 inverted confocal microscope and Zeiss ZEN imaging software. PLA puncta were counted for each condition and quantified. PLA conditions for testing interactions between proteins is shown in Table 2.2.

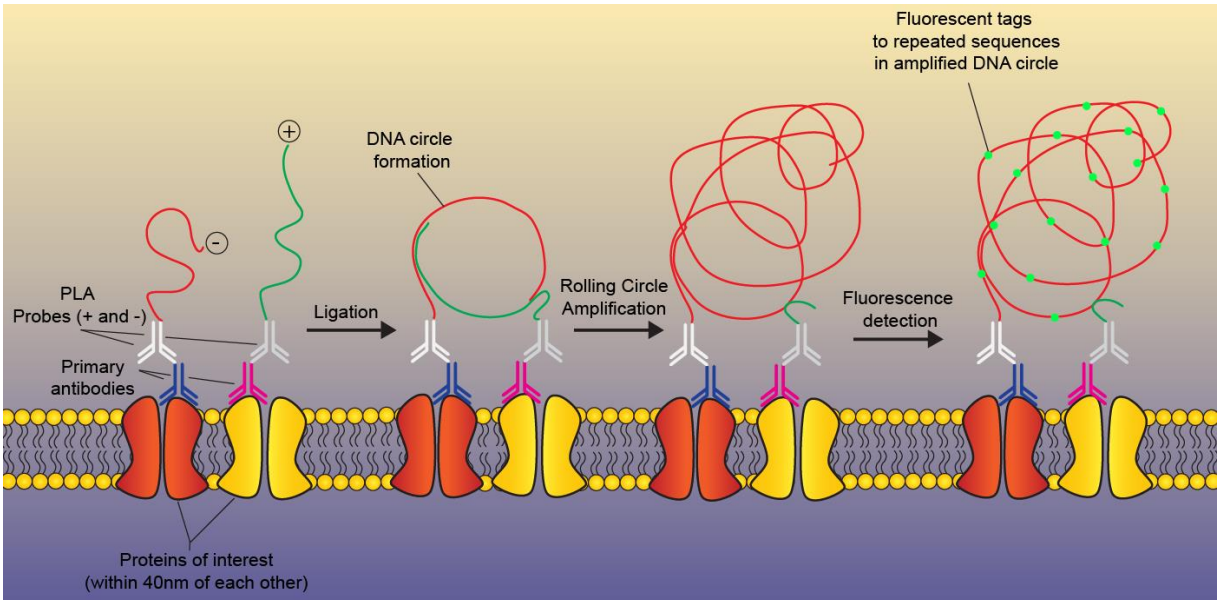

Figure 2.1: Schematic illustration of the PLA principle. Primary antibodies against 2 proteins of interest are detected by PLA probes (+ and -). If these are within 40nm of each other, a DNA circle is able to for through ligation. One of the ligated ends acts as a primer for RCA to occur. The resulting DNA product has repeat sequences that can be tagged with fluorescent molecules for detection.

Antibody 1	Species	PLA Probe /dilution	Antibody 2	Species	PLA Probe /dilution
ANO1	Goat	Anti-Goat PLUS (1:5)	TRPV1	Guinea Pig	Conjugated-MINUS (1:200)
ANO1	Goat	Anti-Goat PLUS (1:5	IP_3R1	Rabbit	Anti-Rabbit MINUS (1:5)
IP_3R1	Rabbit	Anti-Rabbit PLUS (1:5)	TRPV1	Guinea Pig	Conjugated-MINUS (1:200)
ANO1	Goat	Anti-Goat PLUS (1:5)	ANO1	Rabbit	Anti-Rabbit MINUS (1:5)
ANO1	Goat	Anti-Goat PLUS (1:5)	-	-	Conjugated-MINUS (1:200)

Table 2.2: PLA combinations. Table showing PLA probe combinations for different primary antibodies and dilutions used. Second to bottom row shows ANO1-ANO1 positive control and bottom row shows negative control with only 1 primary antibody.

For negative and positive controls PLA was also repeated with just ANO1 primary antibody and no second primary antibody present (negative control) and with 2 ANO1 primary antibodies (positive control).

2.5 STORM

A number of methods that allow to resolve objects at distances closer than the diffraction barrier have become available within the last decade; these are collectively called ‘super-resolution’ imaging techniques. The development of super-resolution imaging is potentially a game-changer in life sciences, a fact that was recognised in the award of the 2015 Nobel Prize in Chemistry (to Eric Betzig, Stefan Hell and William Moerner). One of these techniques is called Stochastic Optical Reconstruction Microscopy (STORM) which was first reported back in 2006 (Rust et al., 2006). STORM exploits the principles of photo-switchable fluorophores targeted against proteins of interest. During each imaging cycle, only a small subset of fluorophores are turned on which subsequently allows nanometer localisation accuracy for each fluorophore to be determined (Rust et al., 2006). This process is repeated for many iterations and finally the individual localisations can be reconstructed to provide a full image of the target (Rust et al., 2006). This ingenious approach allows the diffraction limited resolution to be broken and high resolution to be achieved which initially was approximately 20nm, however recent studies have been able to further increase this to 2nm laterally and 41nm axially (Dudok et al., 2015). In the version of the technique used in this study, the methodology requires so called ‘dye-pairs’ where two photo-switchable fluorophores are attached to an antibody, one of these is referred to as the activator and the other a reporter i.e. Cy3 (activator) and Cy5 (reporter) (Zhang et al., 2016b). The Cy3 activator is stimulated with green light which in turn allows energy transfer to the Cy5 reporter molecule (Fig. 2.2). The energy transfer allows Cy5 to fluoresce and the subsequent point spread function (psf) of the activated reporter can be derived. The reporter fluorescence is recorded whereas the activator fluorescence is not- it is only part of the technique itself. In each cycle that is done, reporter dyes are first driven in non-emitting ‘dark state’, then a small subset of fluorophores is activated by stimulation of the activators and the process is repeated until an overall image can be generated (Rust et al., 2006; Zhang et al., 2016b). Using different activators can allow multi-colour STORM experiments to be done (see chapter 6).

DRG cultures were prepared and grown in glass-bottomed dishes. The same protocol for immunocytochemistry was carried out until the secondary antibody stage. Secondary antibodies consisted of in-house conjugated dye-pairs (activator-reporter) (Zhuang, 2009; Zhang et al., 2016b). The ratio of activator: antibody: reporter required was 2-3:1:0.6-1 for optimum results (Nikon N-STORM protocol). Before imaging, a buffer containing Tris (50mM, pH8), NaCl (10mM), Glucose (10% w/v) and GLOX solution consisting of glucose oxidase (0.5mg/ml), catalase (40µg/ml) and cysteamine MEA (10mM) was used to submerge cells in.

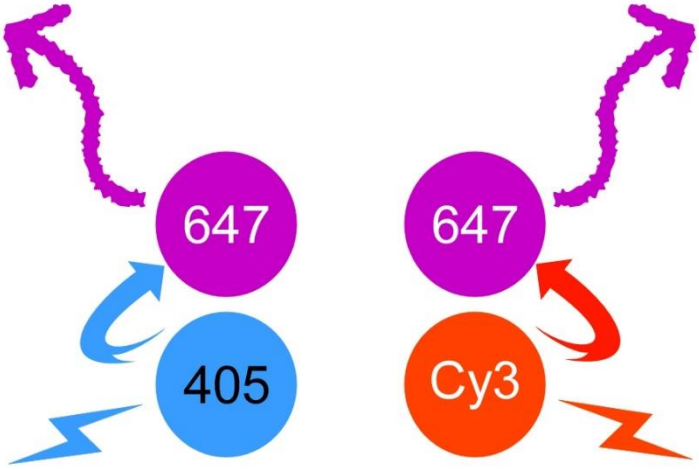

Figure 2.2: Schematic illustration of STORM principles. Schematic representation of multicolour STORM using photo-switchable dye-pair activation. Activator molecules (405 and Cy3 in this example) are stimulated with their respective laser lines causing them to fluoresce. Subsequent energy transfer from the activator to the reporter (647 for both molecules) leads to fluorescence of this molecule which is then recorded. Therefore, reporter activity is only generated when the corresponding laser line of the reporter is used, allowing multicolour STORM.

For image acquisition, a Nikon Ti inverted microscope with an EMCCD camera (Andor iXon3) was utilised with Nikon N-STORM super-resolution imaging setup (Nikon Elements software) (Nikon Instruments). A CFI 100X/NA 1.49 oil immersion objective was used for imaging. Activators used were Alexa 405, 488 and Cy3 whereas the reporter was always Alexa 647. These were stimulated with 405nm, 488nm, 561nm and 647nm laser lines, respectively. Strong laser stimulation of the reporter molecules (647nm) cause photoswitching of the molecules into a temporary dark state. Weak stimulation of reporter molecules (405, 488 or 561nm) allowed activation of a subset of reporter molecules through energy transfer. Only the reporter molecules were imaged for several frames (1 frame= 16ms), before being switched back into the dark state and the whole process repeated for over 30 minutes (~10,000 cycles), with each time a different subset of reporters being imaged (Zhang et al., 2016b). This allows a super-resolution image to be built up. Cluster analysis was done using an in-house developed software based on density based spatial clustering algorithm with noise (DBSCAN) (Ester et al., 1996; Zhang et al., 2016b). The localisation precision is based on 2 parameters, the size of the cluster (larger diameter, the less precision) and intensity of localisations (more intense localisation, the more precise the signal is deemed to be). Filtering of images was done to remove background noise. Dense regions of localisations or ‘clusters’ were identified within a directly-reachable radius proximity (between 20 and 80nm) with a minimum number of localisations surrounding a single core point of the cluster. Localisations not within the radius size were considered to be noise. Clusters were characterised using the activator dye used to detect a certain protein. Using this data, the percentage of clusters belonging to a protein was calculated from total clusters and presented as histograms.

2.6 ER TIRF

Total Internal Reflection Fluorescence (TIRF) imaging is an imaging technique that allows events occurring near or at the plasma membrane to be visualised (Fish, 2009). As light travels through two different (transparent) media, each with differing refractive indices, light is partially diffracted and partially reflected. TIRF only occurs if light passes through the medium with a higher refractive index (i.e. glass dish, n=1.512) to a medium with a lower refractive index (i.e. sample specimen, n=1.33). As the angle of incidence is increased, so does the level of diffraction. Once the

angle of incidence is increased beyond the critical angle, light is no longer diffracted but fully reflected back into the medium thus allowing formation of an evanescent wave to at the glass-cell interface as some of the light energy is converted into this electromagnetic field. The evanescent wave decays exponentially when moving away from the interface (i.e. moving deeper into the sample). It has been estimated that the evanescent field can excite fluorophores that are not farther than 100-200nm away from the glass-cell interface, therefore providing a very good signal-to-noise ratio with low background fluorescence from out of focus planes (Fish, 2009) (Fig. 2.3). The critical angle (θ_C) can be calculated using Snell's Law which determines the angle at which total internal reflection occurs. This uses the refractive indices of the two media used in individual set ups:

A

$$\theta_c = \sin^{-1}\left(\frac{n_1}{n_2}\right)$$

B

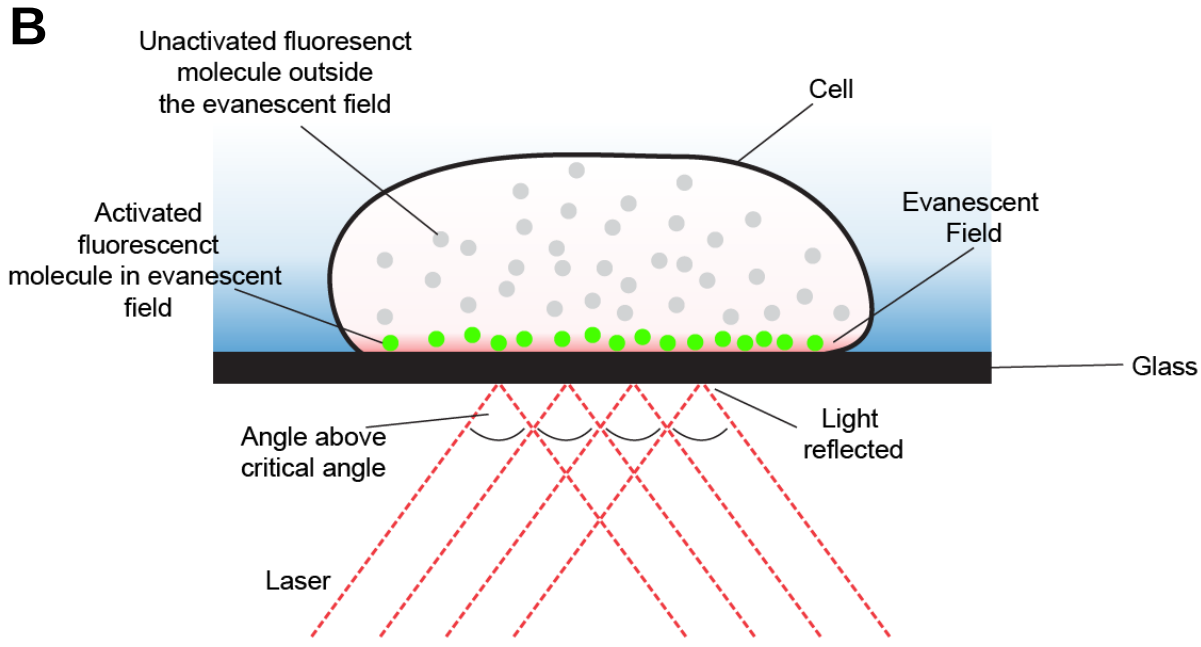

Figure 2.3: Principle of TIRF. (A) Snell's Law equation to determine critical angle, θ_c. (B) Laser light excitation when over the critical angle produces an evanescent wave which decays exponentially. Fluorescently labelled molecules to be seen only in this wave and not further into the cytoplasm meaning events close to the plasma membrane can be monitored.

2.6.1 DRG TIRF

For TIRF imaging, DRG cultures were grown onto 25mm glass coverslips. Cells were loaded with the 1µM ER-tracker Green (Thermo-fisher) for 30 minutes at 37°C before imaging. Coverslips were inserted into a perfusion chamber to allow direct placement onto a 60X oil immersion lens (Apo TIRF 60X, Nikon) and perfused with standard extracellular solution. An imaging system comprising of a Nikon TE-2000 E microscope with a CCD camera was utilised for TIRF imaging. Cells were located using brightfield and epi-fluorescence (488nm excitation) before being imaged for TIRF. The angle of the 488nm laser line was changed to produce TIRF at the plasma membrane. Drugs (bradykinin 250nM and capsaicin 1µM) were produced in standard extracellular solution before being perfused onto cells. Images were taken and analysed using Nikon Elements software.

2.6.2 HEK293 cell TIRF

HEK293 cells were grown in tissue culture dishes with DMEM and Glutamax containing penicillin (50U/ml), streptomycin (50ug/ml) and 10% Fetal Calf Serum (FCS). HEK293 cells were transfected with B_2R or TRPV1 with mCherry (identification) cDNA using Fugene HD (Promega). Before plating onto 25mM coverslips, 10µl CellLight ER-GFP (BacMam 2.0) was added to the pellet to induce ER-GFP expression. After 24 hours, cells were imaged in the same manner as with DRG cultures.

2.6.3 Analysis of TIRF data

Cells imaged were divided into grids to monitor all areas of the cell. Averages of single cell grids and multiple cells in a condition were calculated and plotted as histograms. Paired T-tests were used to compare pre-drug and post-drug average responses in multiple cell calculations. ANOVA was used to test the comparisons between peak responses between cells in a single condition.

Chapter 3: Optimisation of the EYFP (H148Q/I152L) mutant fluorescence quenching methodology

3.1 Introduction

Electrophysiology is the primary technique used by researchers to yield the vast majority of information regarding ANO1. This includes data ranging from activation and deactivation kinetics to single channel conductance for ANO1 activity (Adomaviciene et al., 2013; Pedemonte and Galietta, 2014). There is no doubt that electrophysiology is a powerful method when it comes to ion channel study however, other techniques must continually be developed to provide well-rounded analysis and cover as much ion channel properties as possible. Some drawbacks of electrophysiology include relatively low throughput as only one cell can be recorded at a time and, particularly pertinent to the aims of this study, is in a situation when a CaCC channel is activated by Ca^{2+} influx through a non-selective cation channel (e.g. TRPV1) in the same cell. This means that it is very difficult to electrophysiologically separate the simultaneous activities of these two types of channel, as ionic current is a readout for both. Fluorescence imaging is an alternative technique which can potentially solve this problem as different optical probes for Ca^{2+} and Cl^- can be utilised. In addition, live fluorescence imaging can offer higher throughput as compared to single-cell electrophysiology recordings.

3.1.1 Green Fluorescent Protein

Green fluorescent protein (GFP) was first discovered by Osuma Shimomura in 1962 from Aequorea Victoria in which the protein aqeuorin is able to emit a blue glow in the presence of Ca^{2+} (Shimomura et al., 1962). This blue light is able to excite neighbouring GFP through an energy transfer process and therefore emit green fluorescence (Shimomura et al., 1962; Shimomura, 2005). The discovery of GFP provided the backbone for a whole host of fluorescent protein labels and sensors to be developed which has revolutionised cellular biology, leading to this ground breaking discovery winning a Nobel Prize in 2008. These proteins have quickly became an important tool in a researchers repertoire and used in a wide range of experimental techniques not limited to visualising gene expression (Chalfie et al., 1994), protein targeting (Snapp, 2005), live imaging (Ettinger and Wittmann, 2014) as well as being used in optogenetics (Tantama et al., 2012).

3.1.2 Structure

The most important factor regarding the fluorescent protein is the general β-barrel structure. This rigid structure is comprised of 11 β-pleated sheets which encases a central α-helix and it is this central portion of the protein where the light-emitting chromophore is located (Ormo et al., 1996; Yang et al., 1996) (Fig. 3.1A). To allow the formation of the chromophore, 4 processes must occur; (1) folding, (2) cyclisation, (3) oxidation and (4) dehydration (Craggs, 2009). Folding of the protein into its tertiary structure is an important and prerequisite step in chromophore formation (Fig. 3.1B). This can be demonstrated by denaturing the tertiary structure of GFP and seeing a loss of fluorescence (Reddy et al., 2012). In GFP, 3 amino acids are thought to be critical for the fluorescent property; S65, Y66 and G67. This tripeptide is able to undergo an autocatalytic event and produce the fluorescent species, however only G67 is indispensable to GFP as changing the other amino acids can result in altered properties of GFP (Heim et al., 1994). Cyclisation involves nucleophilic attack of the G67 amide nitrogen on the carbonyl carbon to form an imidazoline ring, thus highlighting the importance of the G67 amino acid (Pakhomov and Martynov, 2008). Subsequent oxidation and dehydration are able to 'trap' the fluorophore in the mature state, providing fluorescence, in this reversible reaction. (Barondeau et al., 2003; Craggs, 2009).

3.1.3 Variants of GFP

Introducing various mutations into GFP enabled researchers to alter its properties in terms of stability of the protein itself or the fluorescent activity (Remington, 2006; Pakhomov and Martynov, 2008). One of the Nobel prize winning pioneers of GFP studies, Rodger Tsien, and his group engineered a single point mutation at the tripeptide member S65 to threonine (S65T) which shifted the bimodal excitation-emission spectra of GFP from 395nm and 475nm with emission at 508nm and 503nm, respectively to just 488nm and with emission at 509nm (Heim et al., 1995). This also resulted in 5 times better fluorescence and stability of the protein compared to wild type GFP. One important mutation includes F64L which results in greater folding efficiency at 37°C and greater fluorescence and therefore aptly named enhanced GFP (EGFP) (Craggs, 2009). Other mutations have been found to shift the excitation-emission spectra to allow different coloured fluorescent proteins to be engineered (Remington, 2006). These include cyan fluorescent protein (CFP), yellow

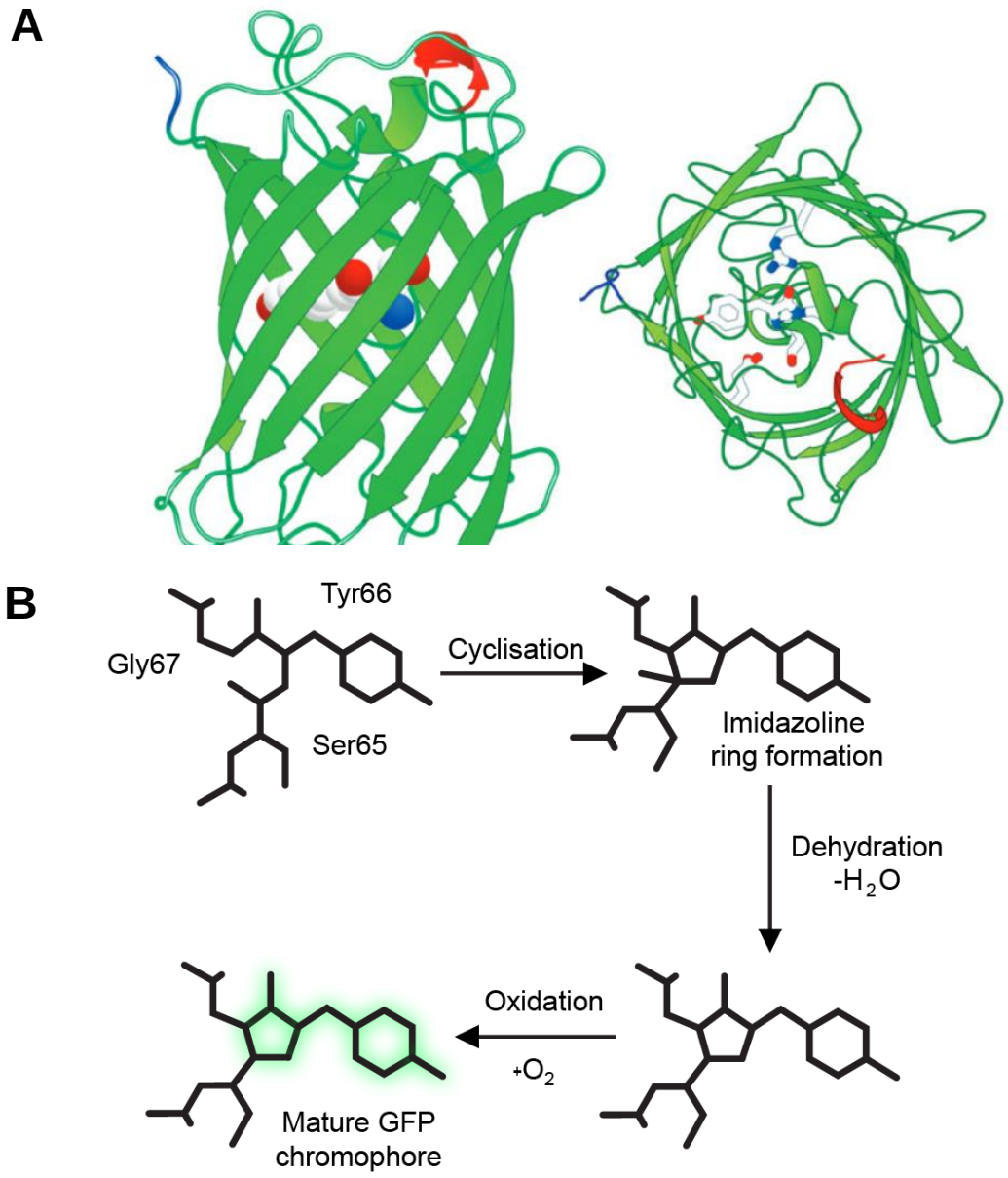

Figure 3.1: Structure of GFP. (A) Left panel shows the structure of GFP from a side on view which highlights the β-pleated sheet structure. N-terminus domain depicted in red and C-terminus shown in blue. Right panel shows the structure from the top highlighting the chromophore in the middle of the 'barrel' structure. (B) Steps required for the formation of chromophore (see text). Figures adapted from (Craggs, 2009).

fluorescent protein (YFP) and red fluorescent protein (RFP), which has in turn led to offshoots of these various species being developed with different properties (Shaner et al., 2007; Day and Davidson, 2009).

3.1.4 Fluorescent proteins as Cl^- channel activity sensors

Some of the mutations incorporated into GFPs were able to confer new and useful properties to the fluorescent proteins. For instance, enhanced YFP (EYFP) contains 4 mutations, S65G; V68L; S72A and T203Y causing red-shifted excitation-emission spectra (514nm excitation and 528nm emission) and provides intense fluorescence (Elsliger et al., 1999). Interestingly, two further mutations engineered in EYFP were H148Q and I152L, which have been found to allow enhanced halide sensitivity to this protein whereby the fluorescence is quenched upon binding of a halide ion (Jayaraman and Verkman, 2000; Galietta et al., 2001a). This mutant has a K_d of 3mM for I^- and 88mM for Cl^- (1.9mM and 85mM for purified proteins at pH7.4, respectively) (Galietta et al., 2001a), making it possible to use this mutant to detect fairly small changes of I^- concentration on the background of physiological concentrations of Cl^- (Galietta et al., 2001b).

As mentioned earlier, one interesting property of ANO1 (and most other Cl^- channels) is its ability to transport other anions apart from Cl^- (Yang et al., 2008). In general, halide ions such as I^- are able to permeate Cl^- channels better than Cl^- itself however because Cl^- is the main anionic charge carrier in the body, these channels are known as 'Cl^- channels' (Verkman and Galietta, 2009). There are some instances where I^- plays a physiological role and its movement is required, an example being in thyroid glands where the sodium-iodide symporter (NIS) transports 2 Na^+ and 1 I^- into follicular cells for the production of thyroid hormone (Dohan et al., 2003). Deficiencies in iodine in the diet lead to disorders such as hypothyroidism, thyroid goiters (enlargement of the thyroid gland) and mental retardation in children where the mother has had iodine-deficiency during pregnancy (Zimmermann et al., 2008). Interestingly, ANO1 has also been implicated in the production of thryroid hormones (Iosco et al., 2014). Thyroid follicular cells uptake I^- before a protein known as pendrin pumps I^- into the follicle colloid where production of the hormones occurs (Fugazzola et al., 2001; Bizhanova and Kopp, 2009). These cells have long been known to display CaCC currents (Martin, 1992; Viitanen et al., 2013) and radioiodide efflux was found to occur after GPCR-agonist activation (Weiss et al., 1984; Corda et

al., 1985; Iosco et al., 2014). Therefore, ANO1 was suggested to play a role in I^- transport where it acts as a Ca^{2+}-activated I^- channel (Iosco et al., 2014; Twyffels et al., 2014).

The permeability of Cl^- channels to I^- provides an opportunity for us to develop a method whereby we can utilize fluorescent proteins in order to study Cl^- channel activity, more specifically ANO1.

3.1.5 Protocol development

The basis of a protocol allowing us to visualise Cl^- channel activity would require: (i) expression of the halide sensitive fluorescent protein in cells (ultimately – the DRG neurons); (ii) presence of a Cl^- channel in the cells (endogenous or transfected) and (iii) presence of I^- in the bath solution to be able to induce quenching. Figure 3.2 shows the protocol in schematic form. Activation of the Cl^- channel would open the anion-conducting pore and use the concentration gradient for I^- to drive it into the cells. Upon interaction of I^- with the halide sensor, the fluorescence would quench to provide an indirect measurement of Cl^- channel activity. This halide sensitive fluorescence approach has been used in previous studies but hitherto not in single-cell imaging of neurons. A YFP (H148Q/I152L) mutant was utilised by Johansson and colleagues in CHO-K1 cells in the search for high throughput assays to develop $GABA_A$ channel modulators (Johansson et al., 2013). This study used different concentrations of NaI (5mM, 10mM, 20mM and 40mM) and measured both agoinst-independent and dependent quenching. Overall, they came to the conclusion that 10mM was the optimal NaI concentration to use for assays using CHO-K1 cells (Johansson et al., 2013). In the context of ANO1 studies, this approach has been used in the development of a novel ANO1 blocker Ani9 as part of a high throughput assay in fisher rat thyroid (FRT) cells (Seo et al., 2016). Ani9 was found to be more selective for ANO1 over ANO2 in its inhibitory activity (Seo et al., 2016). Other studies looking at ANO1 activators and inhibitors also used the YFP mutant biosensor to assay compounds in HEK293 and FRT cells, respectively, due to the high throughput screening it allows (Namkung et al., 2011; Huang et al., 2012). Moreover, this technique has also been used to look at the effects of various

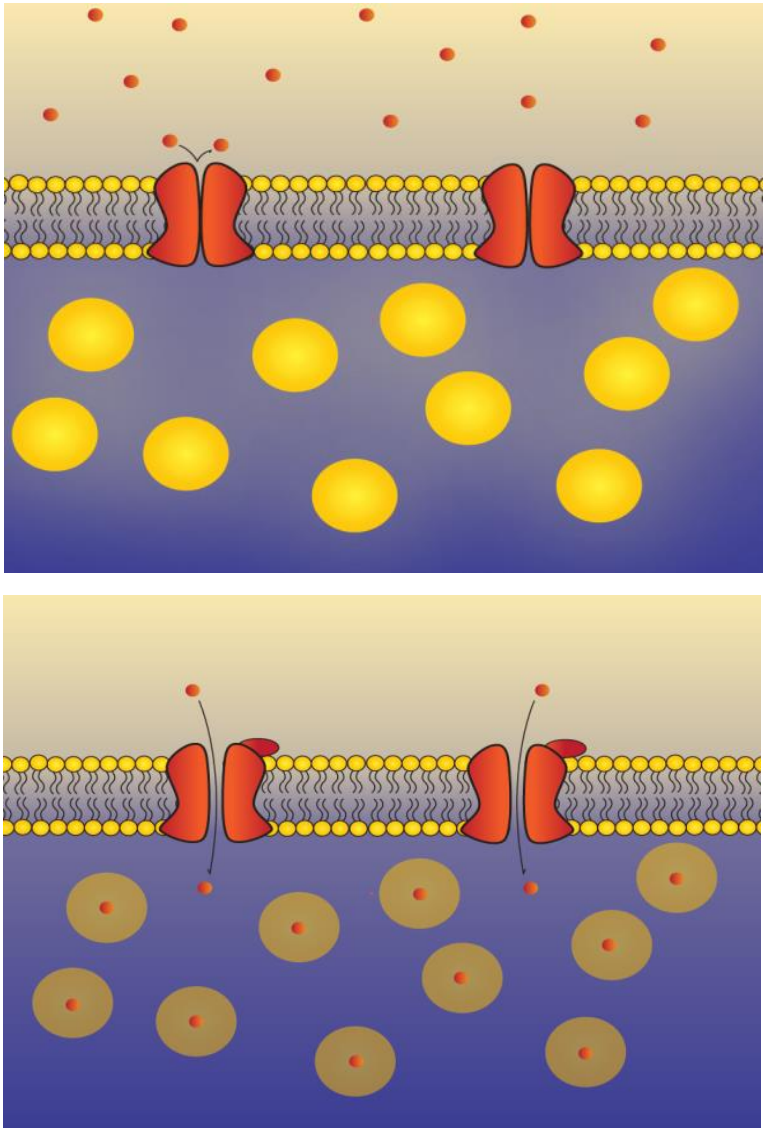

Figure 3.2: Schematic outlining the principle of I^- imaging experiments. DRG neurons are transfected with the halide-sensitive HI48Q/I152L EYFP mutant (yellow circles). DRG neurons are known to express Cl^- channels (red shapes in membrane) and at rest mutant EYFP is able to fluoresce and I^- (red circles) is unable to enter the cells (Upper panel). Activation of Cl^- channels allows I^- to flow into the cells and induce quenching of the mutant EYFP fluorescence hence allowing Cl^- channel activity to be monitored (Lower panel).

mutations in ANO1 and how they affect channel activity (Bill et al., 2015). The protocol involved applying carbachol to activate ANO1 channels with various mutations and measuring the responses. Interestingly, the most significant mutation they reported was S741T in the pore loop which enhanced Ca^{2+} sensitivity of ANO1 and rendered the Ca^{2+} gating of the channel insensitive to voltage (Bill et al., 2015). In all of these studies, expression systems in combination with fluorescence plate readers were used.

In our previous study we used primary DRG neurons transfected with EYFP (H148Q/I152L) and individually imaged these cells in the presence of standard bath solution consisting of 30mM NaI to test activation of endogenous CaCC in DRG neurons by Ca^{2+} release from the ER or by the activity-dependent Ca^{2+} influx through the VGCC (Jin et al., 2013). However, this method displayed significant agonist-independent YFP quenching (Fig. 3.3A), so it was impossible to apply more than one agonist during a single experiment.

We have therefore decided to optimise this technique to minimise agonist-independent quenching and allow efficient agonist-dependent response in a single protocol (Fig. 3.3B). For this optimisation stage it was more beneficial to use a direct agonist-activated channel such as $GABA_A$, which is abundantly expressed in DRG (Maddox et al., 2004; Du et al., 2017b) instead of CaCC, which requires intracellular Ca^{2+} to activate and displays more heterogeneous responses in DRG. Recently, Gamper's group demonstrated that rat sensory ganglia contain the 'machinery' for GABA synthesis such as the vesicular GABA transporter (VGAT) and electron micrographs revealed the presence of GABA packaged inside vesicles ready for release (Du et al., 2017b). Release of GABA after depolarisation of DRG neurons shows that it plays a vital role in the control of nociceptive signals that are thought to allow DRG neurons to filter and gate signals for nociceptive transmission (Du et al., 2017b). Using $GABA_A$ as part of the optimisation process, we can quickly visualise a response and titrate the extracellular I^- in order to determine optimal concentration that provides a good dynamic range for the agonist-dependent quenching while keeping the agonist-independent 'rundown' of fluorescence to the minimum. Similarly to ANO1, $GABA_A$ channels have a halide permeability sequence as $I^- > Br^- > Cl^- > F^-$, where larger anions are able to permeate through these channels better than smaller ones.

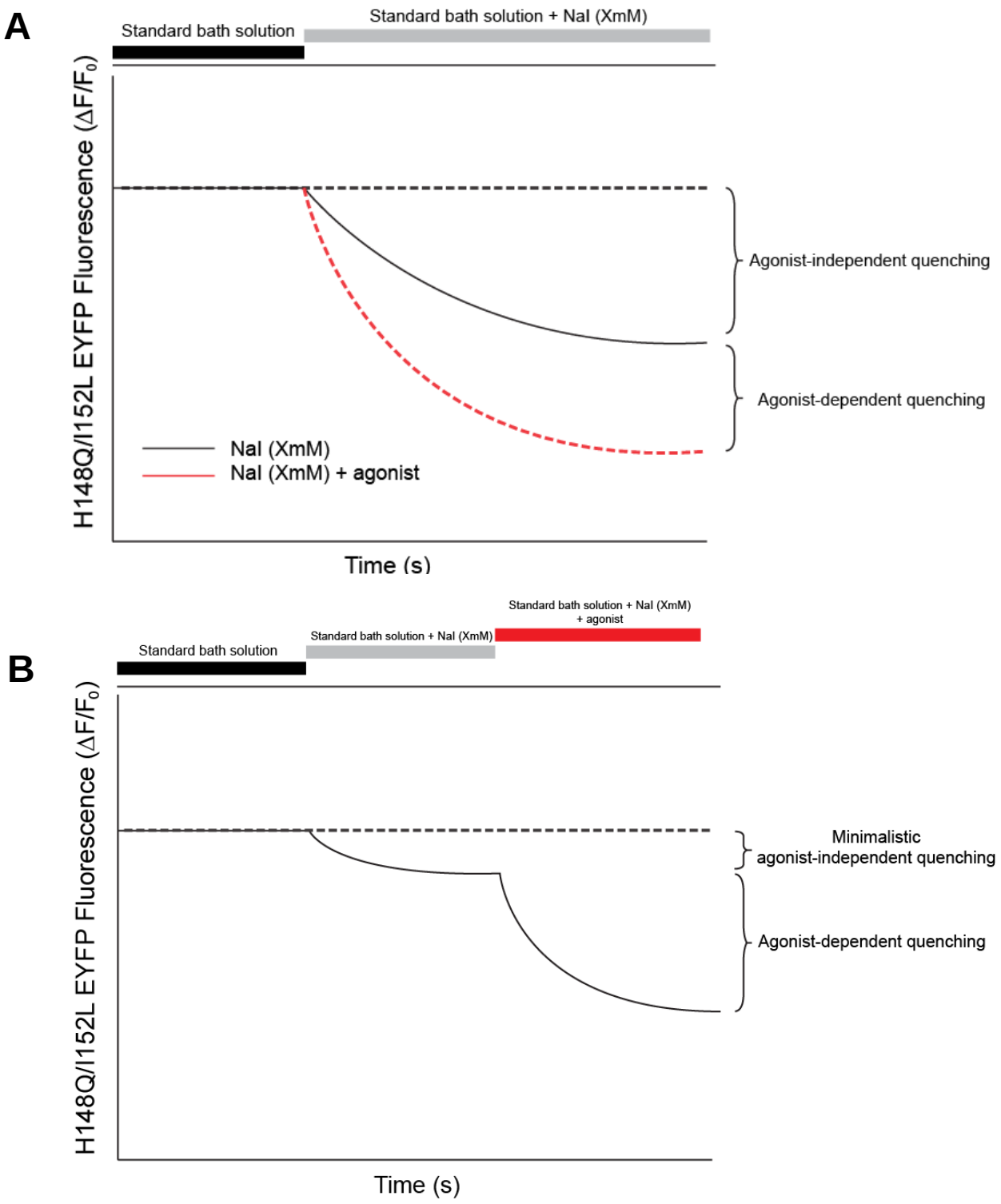

Figure 3.3: Protocols used for recording Cl^- channel activity using mutant EYFP (H148Q/I152L). (A) Previous protocol required application of NaI made to a separate set of cells with and without agonist to provide a measure of agonist-independent quenching. (B) Newly devised protocol will require titration of I^- concentration to produce minimal agonist-independent quenching to allow application of agonist during a single experiment.

3.2 Results

To optimise this halide-sensitive quenching approach, DRG neurons were dissociated and before plating out, cells were transfected with EYFP (H148Q/I152L) mutant cDNA using Lonza's nucleofector. As DRG neurons are postmitotic, heterologous expression of genes in these cells is difficult and common transfection reagents are unable to transfect cells, yet previous studies from our lab have shown that DRG neurons can stably express proteins after transfection using the 'nucleoporation' method (Kirton et al., 2013). Furthermore, we have previously used this approach in DRG neurons using the same mutant EYFP to carry out ANO1 studies (Jin et al., 2013). After culturing cells for 48 hours, the cells were imaged using TillPhotonics fluorescence imaging system. A simple protocol was carried out which involved perfusing cells with standard bath solution for 50 seconds before applying the same bath solution with a fraction of NaCl substituted with NaI (for 50 seconds) to provide a source of I^- to induce quenching of the fluorescence. NaI perfusion produced agonist-independent quenching which we have previously encountered therefore our main objective was to reduce this to a minimal level as possible. Finally, the NaI containing bath solution with GABA (100μM) added was applied (for 50 seconds) to induce agonist-dependent quenching. Optimisation of the agonist-dependent quenching was required to provide a distinctive, visible response while maintaining minimal agonist-independent quenching.

We prepared 30, 10 and 5mM NaI containing bath solutions to apply to DRG cultures that were transfected with EYFP (H148Q/I152L) (Fig. 3.4A and B). Perfusion of 30mM NaI led to fluorescence being quenched almost immediately by 0.26 ± 0.068 ($n=7$, $p<0.05$, ANOVA with Tukey). When subsequent GABA (100μM) was applied, only relatively small further quenching was observed (from 0.26 ± 0.068 to 0.37 ± 0.073) however this was not significantly different to the agonist-independent quenching. Thus, at the 30mM concentration of NaI in extracellular solution, the rate of agonist-independent quenching exceeds the rate of agonist-dependent quenching (Fig. 3.4A and B), which is not ideal. Therefore, lower NaI concentrations (10 and 5mM) were tested. Using 10mM NaI gave a significantly smaller agonist-independent quenching (by 0.038 ± 0.0059), as compared to 30mM NaI ($p<0.05$, unpaired T-test) however this was not significantly different to quenching caused by standard bath

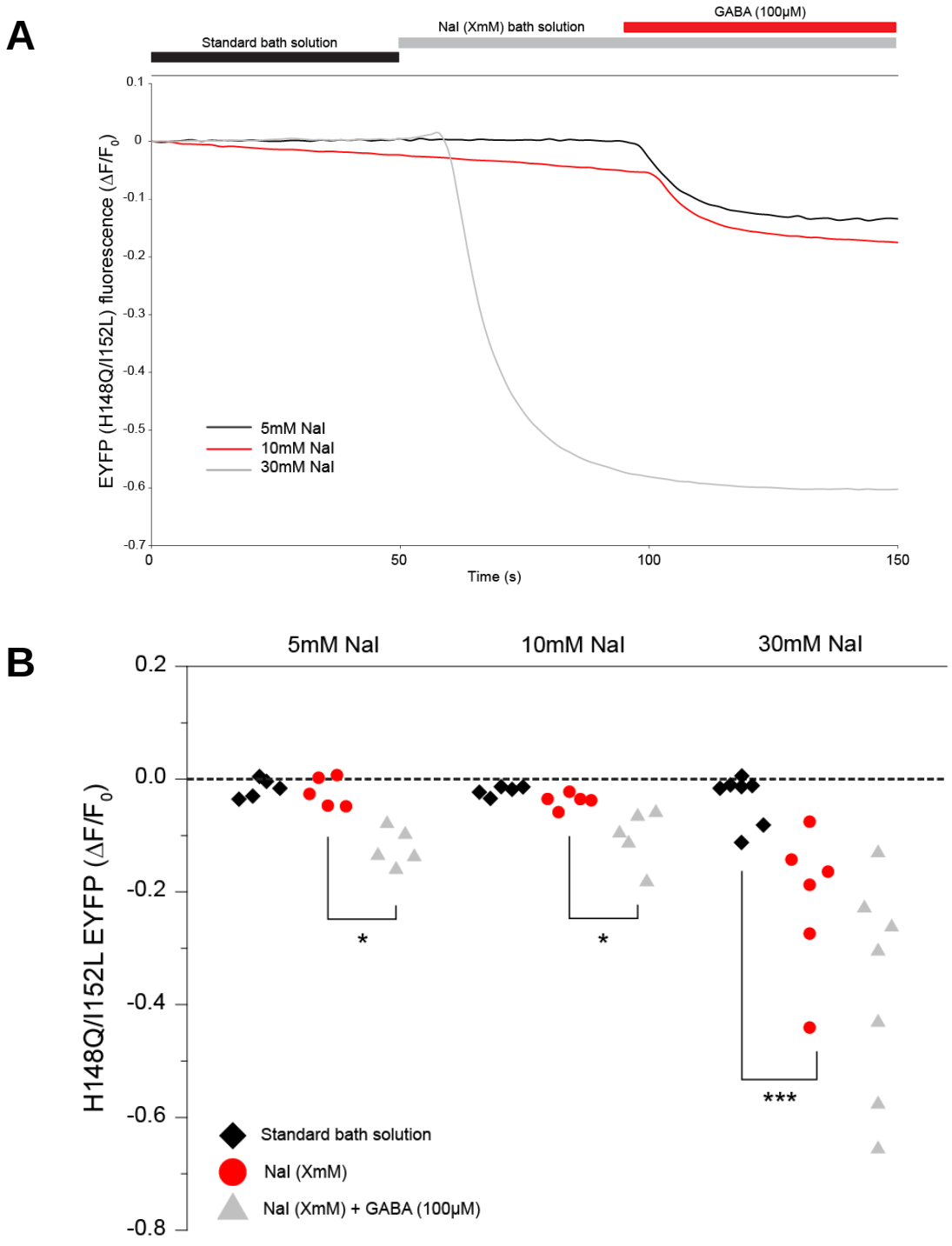

Figure 3.4: Optimisation of EYFP (H148Q/I152L) fluorescence quenching technique. (A) Representative traces for 5, 10 and 30mM NaI application. (B) Average data for 5 (n=5), 10 (n=5) and 30mM (n=7) NaI solutions. (◆) denotes end of standard bath solution application, (●) denotes end of the NaI extracellular solution application and (▲) denotes end of NaI extracellular solution + GABA (100µM) application.

solution. Furthermore, application of 100µM GABA produced an obvious decrease in the EYFP fluorescence by 0.102 ± 0.02 ($p<0.001$, ANOVA with Tukey). Finally, 5 mM NaI was also tested; it produced very small agonist-independent quenching by 0.02 ± 0.01 (not significant). GABA (100µM) application produced quenching in a similar manner to that of 10mM NaI; quenching occurred by 0.12 ± 0.014 ($n=5$, $p<0.01$, ANOVA with Tukey). In the experiments with 10 and 5mM NaI there was minimal rundown of fluorescence in the standard bath solution (0.01 ± 0.007, $n=7$ and 0.02 ± 0.003, $n=5$, respectively). There was no significant difference between agonist-independent or dependent quenching between 5mM and 10mM NaI (Fig. 3.4B). We have therefore chosen 5mM NaI for subsequent experiments to minimize possible non-specific effects of iodide in DRG.

To confirm that this technique is not affected by our bath solution, we decided to perform some imaging of neurons transfected with the EYFP (H148Q/I152L) mutant and perfuse normal bath solution. Application of normal bath solution gave no significant quenching which validated our protocol to be used for monitoring anion channel activity (0.004 ± 0.0089, $n=5$) (Fig. 3.5).

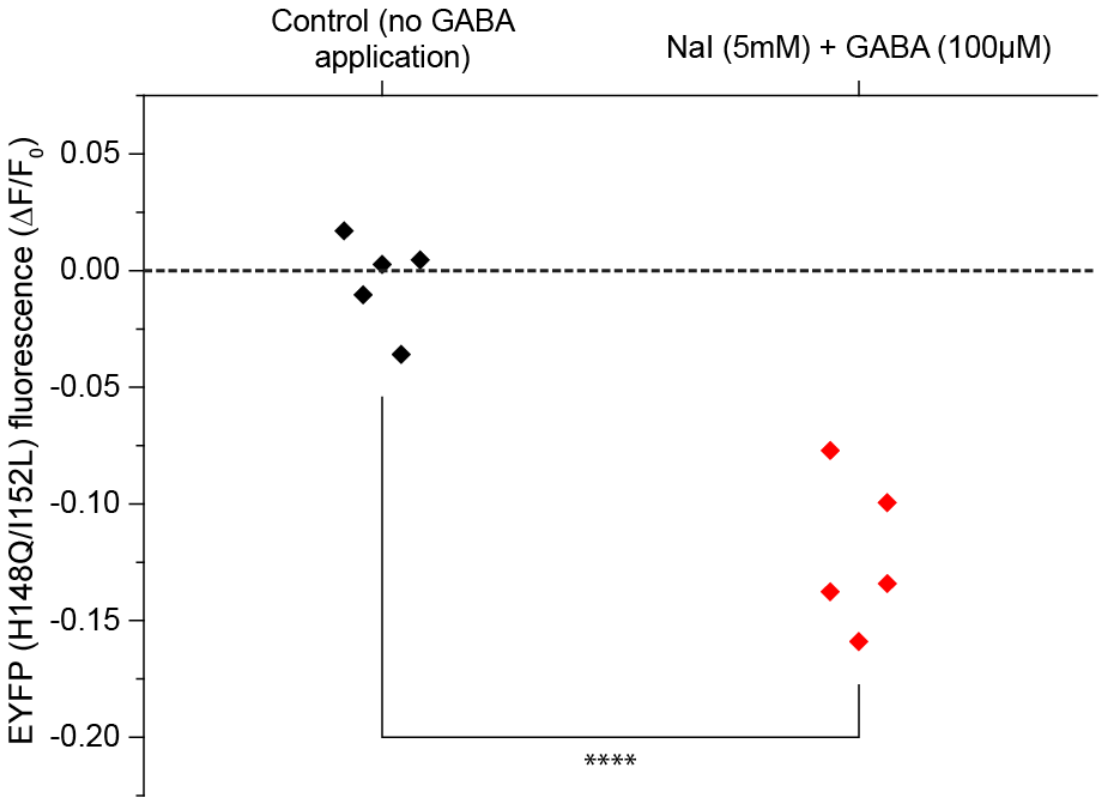

Figure 3.5: Effects of standard extracellular bath solution on EYFP (H148Q/I152L) quenching. Quenching induced by standard extracellular solution (containing no NaI or GABA application, n=5) after 150 seconds. Effects of 5mM NaI solution and quenching caused by GABA are also shown for comparison.

The agonist-independent quenching can also be analysed by looking at the equilibrium potentials for $GABA_A$ channels in DRG which have an intracellular concentration of 40mM (Rocha-Gonzalez et al., 2008). When using standard bath solutions, the equilibrium potential for Cl^- (and hence $GABA_A$ channels) is calculated as ~-35mV using the Nernst Potential equation (extracellular 165.5mM; intracellular 40mM). Due to the fact that our methodology incorporates I^- and Cl^- channels are permeable to I^-, the effects of both ions on the equilibrium potential must be taken into account. This is done using the Goldman-Hodgkin-Katz (GHK) voltage equation (Fig. 3.6):

$$E_{Cl} = 58 \log \frac{P_{Cl}[Cl^-]_i + P_I[I^-]_i}{P_{Cl}[Cl^-]_o + P_I[I^-]_o}$$

Figure 3.6: Goldman-Hodgkin-Katz voltage equation used to calculate the equilibrium potential for Cl^- channels.

When 5mM NaI (substituted for equimolar NaCl) is included in the solutions, the equilibrium potential for $GABA_A$ channels is set to -36.4mV using a published permeability ratio of 1.88 (P_I/P_{Cl}) for $GABA_A$ in DRG (Robertson, 1989). When the NaI concentration is raised to 10mM, the equilibrium potential for $GABA_A$ is changed to -37.1mV and when the concentration of NaI is increased to 30mM, it is -39.5mV. This is even more significant for ANO1 given the fact that I^- permeability is greater for ANO1 compared to $GABA_A$ channels (Peters et al., 2015). If we calculate the equilibrium potentials for ANO1 using 5mM, 10mM and 30mM concentrations of NaI in DRG with a P_I/P_{Cl} of 5 at resting Ca^{2+} levels (Peters et al., 2015), we get values of -38.6mV, -41.2mV and -49.5mV, respectively. For ANO1, the equilibrium potentials are closer to the resting membrane potential for DRG (~-55mV; Rocha-Gonzalez et al., 2008), especially for 30mM NaI. Therefore, when the membrane potential is greater than these calculated equilibrium potentials, I^- will move into the cells- the higher the NaI concentration, the greater the danger of this happening. Additionally, the greater concentration gradient for I^- also means a large driving force at higher NaI concentrations and spontaneously open channels will allow I^- to be driven into the DRG, therefore causing greater agonist-independent quenching (Fig. 3.4). To summarise, the electrochemical gradient at higher NaI concentrations results in greater agonist-independent quenching, which supports the decision to use 5mM NaI for my experiments.

4.3 Discussion

Our results, along with previous work, have demonstrated that a halide sensitive mutant YFP can be used to monitor Cl^- channel activity in DRG neurons. It is a well-known fact that DRG neurons express $GABA_A$ (Du et al., 2017b), which makes them an attractive channel for us to utilise as a means to optimise our halide-sensitive approach as $GABA_A$ is a bona fide Cl^- channel. In our previous studies we started with a full exchange of the NaCl content (160mM) to NaI to enable EYFP quenching however, apart from a solitary response, there was almost total quenching in every experiment that we performed. This was not the case in thyroid follicular cells where 100mM exchange of NaCl to KI caused only a 20% quenching response (Iosco et al., 2014). The potential reasons for agonist-independent quenching may include activity of the NKCC1 cotransporter or Cl^- channels that are spontaneously open. NKCC1 cotransporter is found in DRG neurons where it is known to accumulate Cl^- and despite I^- being a poor substitute for Cl^- in terms of NKCC1 activity, it has nonetheless been shown to allow I^- movement (Markadieu and Delpire, 2014). Therefore in the presence of I^-, NKCC1 may be able to transport I^- into neurons and cause quenching. In terms of channel activity, there are various Cl^- channels expressed in DRG and if some are open in a spontaneous manner, then this will allow I^- influx and quenching will occur. Furthermore, the larger NaI concentration provides a greater driving force for I^- entry which will also result in more I^- entering cells. For this reason, the concentration of NaI was reduced to 30mM in order to stop this quenching (Jin et al., 2013). This manoeuvre reduced quenching somewhat so it become possible to compare the degree of quenching after exposure of different sets of DRG neurons to NaI with or without agonist. Yet, the agonist-independent quenching with 30mM NaI was still significant (Fig. 3.4) so it was not possible to apply compounds in succession and perform paired measurements on the same neuron. Therefore further steps were taken in order to improve this imaging protocol, minimize the agonist-independent quenching and enable successive application of multiple compounds during a single recording.

Lower NaI (10mM and 5 mM) gave significantly less agonist-independent quenching while still providing clear response to agonist-induced Cl^- channel activation. Our data are in very good agreement with theses reported earlier; thus, Johansson and colleagues reported very small agonist-independent quenching in CHO-K1 cells was

for 5mM and 10mM NaI and approximately 30% for 40mM (Johansson et al., 2013). On the other hand, the responses obtained in CHO-K1 cells were greater when GABA was applied compared to what we have found in DRG. The agonist-dependent quenching was approximately 15% and 25% for 5 and 10mM NaI, respectively in CHO-K1 cells. Differences between our results and those seen in CHO-K1 cells could be due to overexpression of GABA receptors allowing more channels to be activated, hence more activity of GABA on the quenching. Application of GABA in 40mM NaI only gave a 15% quenching response which could be due to the larger agonist-independent quenching masking the response achieved. Even though 40mM NaI gave the largest response overall, the majority of this was due to agonist-independent quenching. Therefore, we concluded that all further experiments will utilise 5mM NaI despite the fact 10mM also gave similar responses. Using the lower of the 2 concentrations would safeguard cells from potential side effects of the higher NaI concentration.

After optimising and confirming the ability of this halide sensitive mutant EYFP technique in observing Cl^- channel activity, the next chapter will focus on modification and application of this method to monitor CaCC activity in DRG neurons in response to pro-algesic compounds.

Chapter 4: Simultaneous EYFP (H148Q/I152L) and Ca^{2+} imaging to monitor activation of CaCC in DRG neurons

4.1 Introduction

There are various routes by which cytosolic Ca^{2+} signals can be produced in neurons, including influx via ligand-gated ion channels, SOCE, VGCCs as well as through the release from the internal Ca^{2+} stores found in the ER. The latter 2 examples are significant pathways engaged in sensory neurons as Ca^{2+} entry through VGCC occurs during action potential firing while Ca^{2+} release from the ER is used in multiple GPCR signalling cascades, including these triggered by pro-algesic inflammatory mediators such as bradykinin (Golias et al., 2007). VGCCs have been discussed in the general introduction therefore I will briefly discuss ER Ca^{2+} release mechanisms.

4.1.1 Ca^{2+} release from the ER

The ER hosts a vast concentration of Ca^{2+}, approximately 1-2mM (de la Fuente et al., 2013), which can be released upon stimulation of a receptor producing a secondary messenger or through Ca^{2+} itself ultimately leading to an increase in cytosolic Ca^{2+} (Marks, 1997). There are 2 types of receptors found in the ER that mediate Ca^{2+} release- IP_3R (Taylor and Tovey, 2010) and RYR (Lanner et al., 2010). The IP_3R has 3 isoforms: IP_3R1, IP_3R2 and IP_3R3, with IP_3R1 being the most abundantly expressed isoform throughout the body and also the one that predominates in DRG (Dent et al., 1996; Taylor and Tovey, 2010). IP_3Rs are essentially tetrameric ion channels- each subunit consisting of 6 TM domains and have a molecular mass of approximately 1100kDa (Taylor and Tovey, 2010). Interestingly, IP_3Rs can be activated by 2 secondary messengers- IP_3 and Ca^{2+} itself (Finch et al., 1991; Marchant et al., 1997). GPCRs that couple to G_q- and G_{11} type of Gα activate PLC, which subsequently cleaves PIP_2 giving rise to IP_3 and DAG (Tuteja, 2009). IP_3 is able to diffuse through the cytosol and bind to the IP_3R channels and induce robust Ca^{2+} release into the cytosol (Tuteja, 2009). Ca^{2+} on the other hand has a biphasic effect on IP_3R where concentrations of ~500nM work in tandem with IP_3 to provide efficient channel activity however greater Ca^{2+} concentrations inhibit channel activity (Iino, 1990; Marshall and Taylor, 1993; Taylor and Tovey, 2010). This is a vital inhibitory mechanism by which Ca^{2+} release into the cytosol is regulated to avoid toxic Ca^{2+} overload (Taylor and Tovey, 2010). RYR

channels are extremely important in the process of excitation-contraction coupling in muscle cells (Santulli and Marks, 2015). There are 3 isoforms- RYR1, 2 and 3; the former 2 are found predominantly in skeletal muscle (Takeshima et al., 1989) and myocardium (Nakai et al., 1990; Otsu et al., 1990) respectively, whereas the latter is widely expressed and also found in the brain (Hakamata et al., 1992; Lanner et al., 2010). Structurally RYRs form as homotetramers- each monomer consists of approximately 5000 amino acids (Lanner et al., 2010). RYRs are unique in their ability to activate CICR. CICR involves Ca^{2+} entry (i.e. L-type Ca^{2+} channels), which is able to bind and activate RYR. Subsequent opening of RYRs allows Ca^{2+} release from the ER/SR (Endo, 2009). However due to their critical involvement in inflammatory signalling and ANO1 activation in DRG neurons (Jin et al., 2013), this chapter will focus on IP_3R.

4.1.2 ANO1 coupling to IP_3R in DRG neurons

It is a well-known fact that ANO1 is expressed in DRG neurons (Yang et al., 2008; Liu et al., 2010; Jin et al., 2013; Lee et al., 2014; Takayama et al., 2015). ANO1 and IP_3R form ER-PM junctional microdomains which allow preferential activation of ANO1 in DRG neurons (Jin et al., 2013). Conversely, there is poor coupling of ANO1 and VGCCs in DRG due to the lack of proximity as demonstrated using proteomics and biochemical approaches (Jin et al., 2013). G_q- protein coupled receptor activation was able to induce ANO1 currents. Disrupting ANO1 or ER activity using NFA (block ANO1) or thapsigargin (deplete ER Ca^{2+}) abolished currents from occurring (Jin et al., 2013). Furthermore, ANO1 and GPCRs (activation of which lead to IP_3 production) are found in lipid rafts- areas rich in lipids (cholesterol, sphingolipids and sphingomyelin) (Korade and Kenworthy, 2008), which serve to compartmentalize cellular processes by acting as organizing hubs for signalling complexes (Korade and Kenworthy, 2008). In DRG neurons, lipid rafts allow these proteins to form closely positioned domains, at ER-PM junctions which allows the activation of ANO1 (Jin et al., 2014). VGCCs are not part of this lipid raft microdomain hence the poor coupling with ANO1. To this end PAR-2, another GPCR, was also able to activate ANO1. Removal of Ca^{2+} from the bath solution had no effect on ANO1 activity; robust CaCC currents were seen after bradykinin application (Jin et al., 2013). Recently, Cabrita and colleagues have also demonstrated coupling of ANO1 activity to IP_3R in cell lines (Cabrita et al., 2017).

Taken together this demonstrates the importance of microdomains in various aspects of cell signalling and also shows how vital junctional ER-PM microdomains are for ANO1 activation.

In this chapter, I will focus on these ANO1-activation properties and investigate them using a novel dual-imaging approach which allows us to monitor CaCC activity and Ca^{2+} signalling concurrently in a single cell approach.

4.2 Results

We used our improved imaging protocol which (i) minimized agonist-independent quenching of the halide sensor and (ii) combined I^- influx-based monitoring of Cl^- channel activity with Ca^{2+} imaging using fura-2. In contrast to previous experiments, this method allowed interrogation of CaCC properties and simultaneous monitoring of cytosolic Ca^{2+} levels in the same live neuron. Using this method we revisited coupling of ANO1 to bradykinin-activated B_2R and VGCCs in cultured small DRG neurons. EYFP (H148Q/I152L) was stably transfected in DRG neurons using the Lonza Nucleofector kit and cultured for 48 hours. Prior to our experiments, fura-2 AM was loaded into cells to enable us to visualize the Ca^{2+} dynamics. At the beginning of each experiment standard bath solution was perfused for 50s before switching to NaI (5mM) extracellular solution (for 50s). Bradykinin (250nM) was then perfused into the chamber in the presence of NaI solution (for 100s; see Fig. 4.1A). Application of bradykinin led to a significant increase in Ca^{2+} and a concurrent reduction in fluorescence (n=12) (Fig. 4.1A and B). The Ca^{2+} rose sharply and rapidly and peaked at 12 seconds before falling. This was followed quickly by initiation of quenching of the EYFP (H148Q/I152L) mutant fluorescence. The EYFP quenching was recorded in all cells in which there was a bradykinin-induced Ca^{2+} transient. Of the 12 cells that were imaged, the average Ca^{2+} signal ($\Delta F/F_0$) amounted to 1.96 ± 0.18 fold over the baseline (Fig. 4.1B). The EYFP fluorescence decreased by 0.11 ± 0.018 (n=12, $p<0.0001$, paired T-test) showing that bradykinin-application is indeed able to induce I^- influx into cells to quench the fluorescence (Fig. 4.1B). Overcoming the shortcomings of the previous study (Jin et al., 2013) we can confirm that the EYFP quenching was closely correlated with the rise in intracellular Ca^{2+} due to the effects of bradykinin (Fig. 4.1).

A

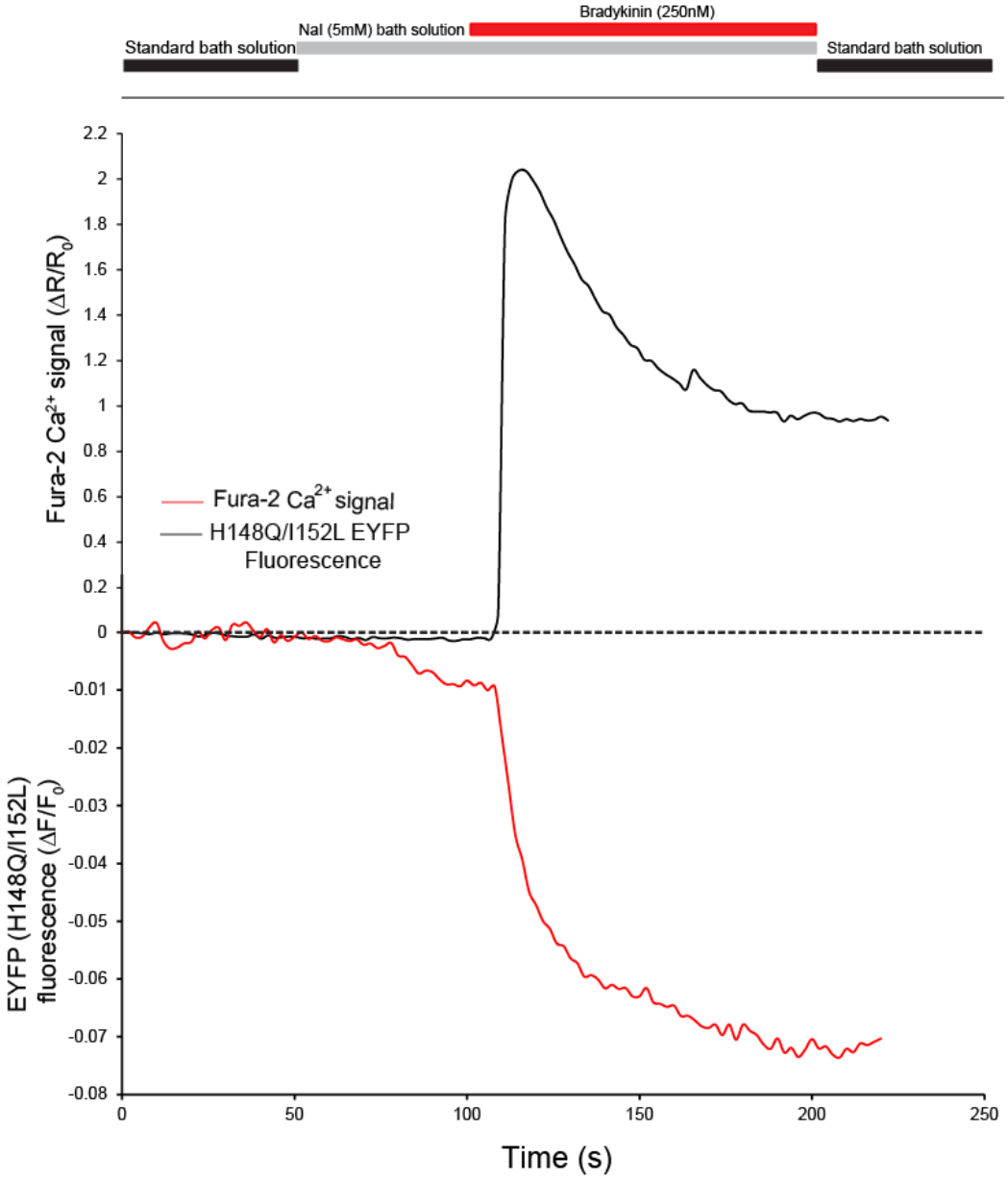
Bradykinin (250nM)
NaI (5mM) bath solution
Standard bath solution
Standard bath solution
Fura-2 Ca2+ signal (ΔR/R0)
EYFP (H148Q/I152L) fluorescence (ΔF/F0)
Fura-2 Ca2+ signal
H148Q/I152L EYFP Fluorescence
Time (s)

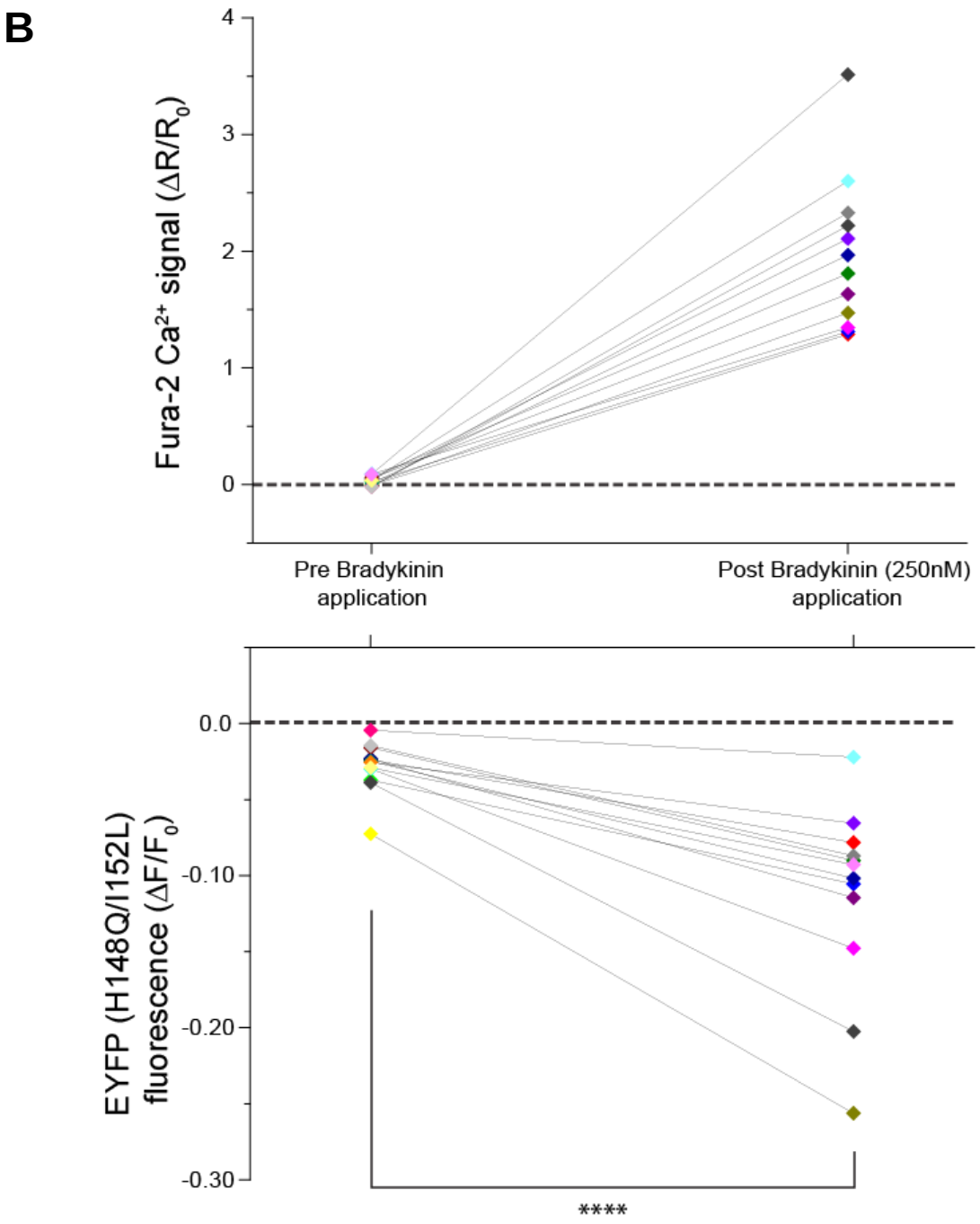

Figure 4.1: Bradykinin application induces fura-2 measured Ca^{2+} increase and concurrent EYFP (H148Q/I152L) mutant fluorescence quenching upon application of bradykinin (250nM) to small DRG neurons. (A) Representative trace of one DRG in response to bradykinin. (B) Individual cell responses for fura-2 (upper) and EYFP (H148Q/I152L) fluorescence quenching (lower) for bradykinin application (n=12). ****p<0.0001

To validate our experiments and prove that this effect was due to ANO1 and not another anionic conductance, the selective ANO1 inhibitor T16Ainh-A01 (50µM) was used to block ANO1 to see if there was any EYFP fluorescence quenching when bradykinin was applied in this instance. Transfected cells were incubated with the inhibitor during the fura-2 loading process and T16Ainh-A01 was also included in the solutions during the imaging protocol. Satisfyingly, T16Ainh-A01 completely Inhibited the bradykinin induced quenching seen in the previous experiment- there was significantly less quenching compared to bradykinin application (0.0017 ± 0.001, n=6 vs. 0.11 ± 0.018, n=12, p<0.001, unpaired T-test) (Fig. 4.2). However, whilst bradykinin was still able to cause an increase in Ca^{2+}; the BK-induced Ca^{2+} transients in the presence of T16Ainh-A01 were significantly lower than in control conditions (0.70 ± 0.23, n=6 *vs.* 1.96 ± 0.18, n=12; p<0.001, unpaired T-test). Interestingly, T16Ainh-A01 also reduced the agonist-independent quenching. When comparing the agonist-independent quenching for control (bradykinin application dataset) and T16Ainh-A01, there is a significant difference in the agonist-independent quenching (0.028 ± 0.0049, n=12 *vs*. 0.00052 ± 0.00082, n=6; p<0.01, unpaired T-test). Therefore, it seems as though ANO1 could be at least in part responsible for this phenomenon. Resting levels of Ca^{2+} present in cells being imaged could influence results due to the Ca^{2+} sensitive nature of ANO1. If there is greater Ca^{2+} present, this could depolarise the resting membrane potential of the cell and induce sensitisation of ANO1 channels- this may lead to open cells before agonist application. To see if this was the case, the agonist-independent EYFP quenching was compared between 2 cells with identical resting Ca^{2+} ratios (182.02 and 182.16). Before application of bradykinin, the EYFP quenched by 0.02 and 0.04 for each cell. This suggests that agonist-independent quenching is not influenced by resting Ca^{2+} ratio. Furthermore, the cell with the greatest resting Ca^{2+} ratio (202.04) showed 0.03 agonist-independent quenching, again showing that this doesn't necessarily affect quenching. This may be due to photobleaching of the sensor or condition of the cell (damaged cell membranes may allow more I^- entry).

These data sets demonstrate that: (i) our imaging protocol allows simultaneous measurement of CaCC and Ca^{2+} dynamics in live individual neurons; (ii) B_2R activation is able to induce EYFP (H148Q/I152L) mutant quenching which closely

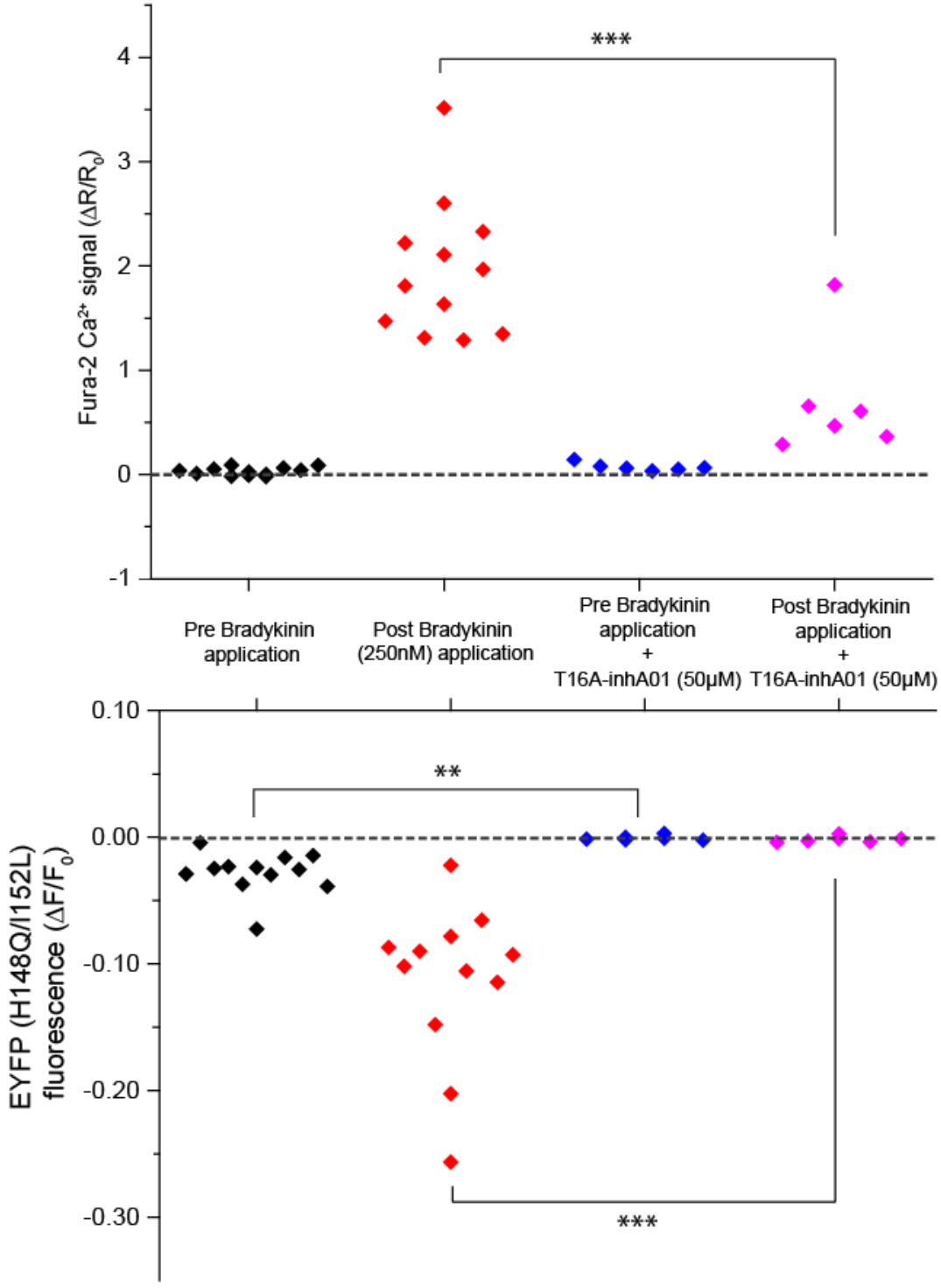

Figure 4.2: T16A-inhA01 abolishes EYFP (H148Q/I152L) mutant fluorescence quenching when bradykinin is applied but still evokes a Ca^{2+} rise in small-diameter DRG neurons. Individual cell data showing the effects of T16A-inhA01 on both Ca^{2+} and EYFP quenching. **p<0.01, *** p<0.001

follows Ca^{2+} release evoked by bradykinin application and (iii) this bradykinin-dependent quenching of EYFP (H148Q/I152L) is dependent on CaCC.

Previously, it has been demonstrated that activation of ANO1 is closely coupled to IP_3R activation and poorly coupled to VGCC activation in small diameter DRG neurons (Jin et al., 2013). This was confirmed through both whole-cell patch clamp recordings and EYFP (H148Q/I152L) mutant fluorescence quenching however again there was no simultaneous Ca^{2+} imaging in these earlier experiments so the Ca^{2+} entry through the VGCC could not be directly correlated with the ANO1 activity (Jin et al., 2013). Our optimised imaging protocol was therefore used to re-evaluate coupling of ANO1 to VGCC activation in DRG neurons. To activate VGCCs, 50mM of extracellular NaCl was replaced with KCl to induce depolarisation (E_K = -25.9 mV) hence allowing Ca^{2+} entry from outside the cell. Remarkably, there were 2 types of responses from VGCC activation in neurons recorded from (Fig. 4.3A and B). The majority of neurons (15/23; 65%) showed no response which was what was expected and correlates to the results obtained by Jin and colleagues (quenching of 0.018 ± 0.004). This was regardless of an increase in Ca^{2+} being present in every single neuron recorded from (Fig. 4.3C). However, the remaining 8/23 (35%) neurons actually showed varying degrees of EYFP quenching which we considered a response (quenching of 0.16 ± 0.028). We divided the neurons into ‘responders and ‘non-responders’ based on the degree of EYFP quenching induced by the high-K^+ depolarisation: if quenching did not exceed the rate of agonist-independent quenching (i.e. 4% over 100s), the neuron was considered a non-responder, all other neurons were classified as responders (Fig. 4.3C). On average for the full population of neurons that were tested (including responders and non-responders to VGCC activation), there was significant quenching when VGCCs were activated (Fig. 4.3C). The proportion of responding neurons was somewhat higher than in our previous experiments (5-20%) (Liu et al., 2010; Jin et al., 2013).

However, in our previous study (Jin et al., 2013) some depolarisation-induced inward currents were observed in the presence of VGCC blocker, cadmium, suggesting that there may be other, non-CaCC currents involved. We decided to investigate this by removing the extracellular Ca^{2+} during VGCC activation with 50mM KCl solution. In cells we tested, there was no Ca^{2+} signal in any cell (Fig. 4.4A and B), however, there was still some quenching of the EYFP (H148Q/I152L) mutant fluorescence

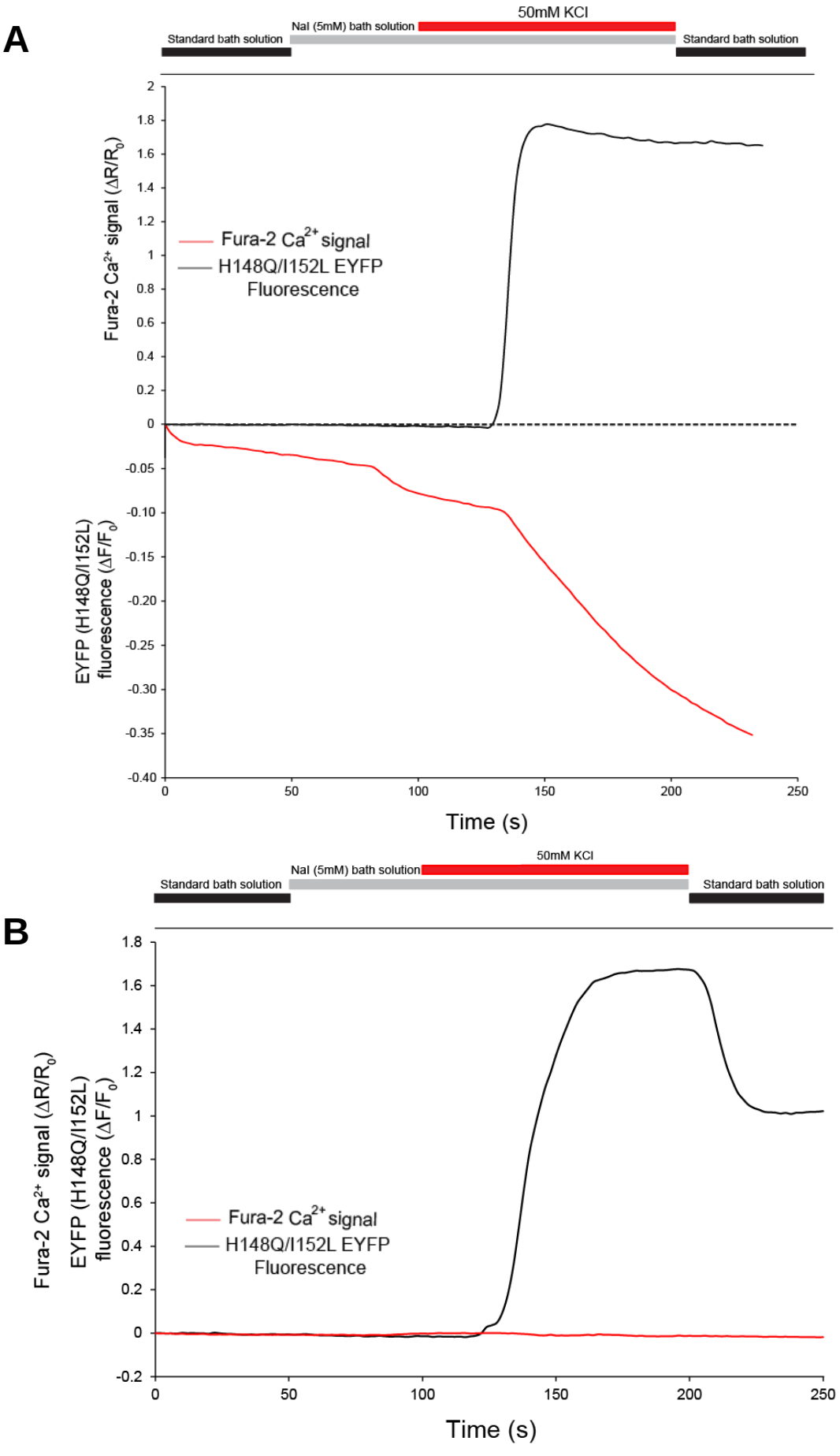
A
50mM KCl
NaI (5mM) bath solution
Standard bath solution
Standard bath solution
Fura-2 Ca2+ signal (ΔR/R0)
EYFP (H148Q/I152L) fluorescence (ΔF/F0)
Fura-2 Ca2+ signal
H148Q/I152L EYFP Fluorescence
Time (s)
B
50mM KCl
NaI (5mM) bath solution
Standard bath solution
Standard bath solution
Fura-2 Ca2+ signal (ΔR/R0)
EYFP (H148Q/I152L) fluorescence (ΔF/F0)
Fura-2 Ca2+ signal
H148Q/I152L EYFP Fluorescence
Time (s)

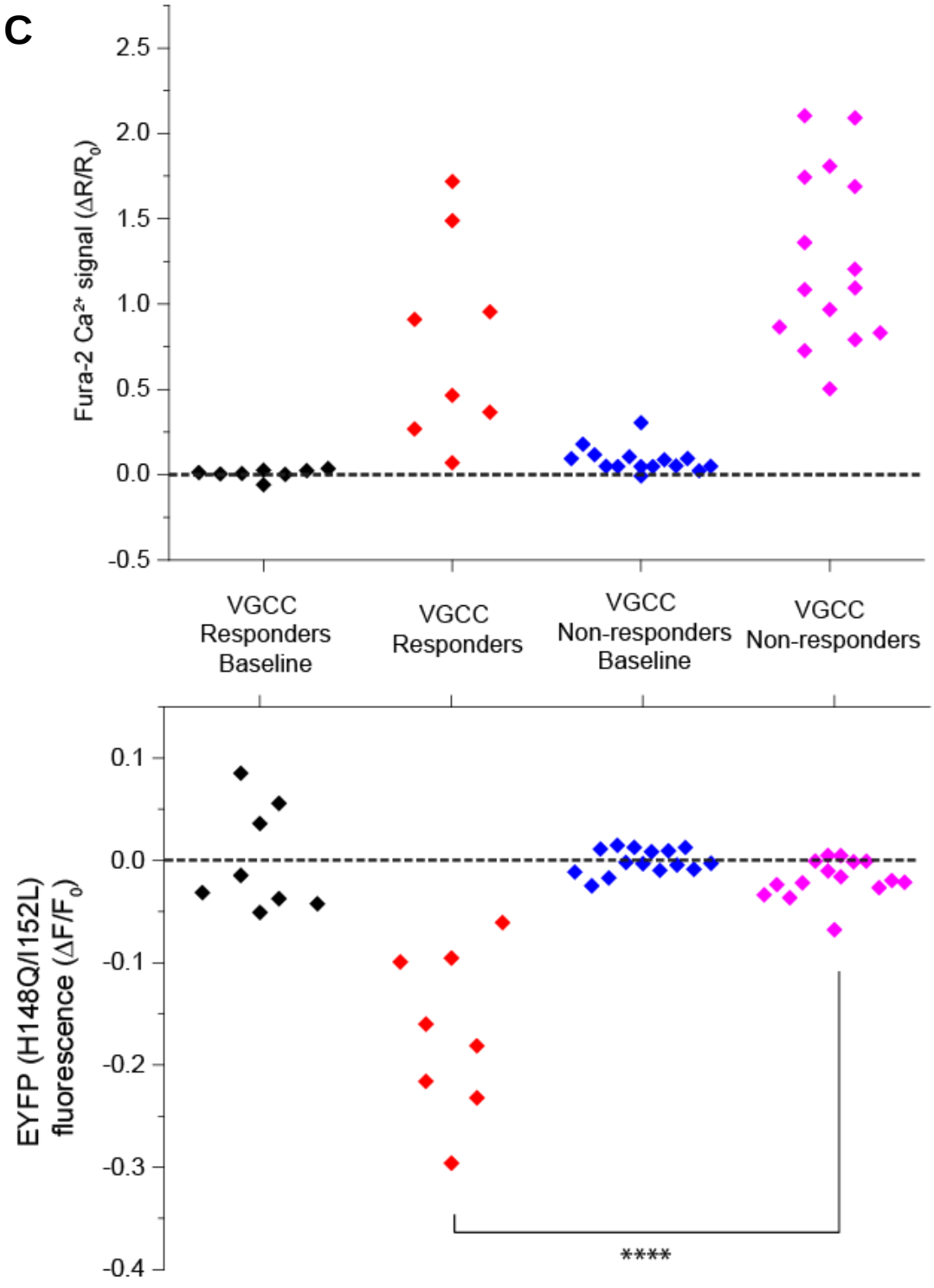

Figure 4.3: VGCC activation (50mM KCl application) produces 2 different responses in small-diameter DRG neurons. (A) Representative traces of one DRG 'responder' and (B) one DRG 'non-responder' after VGCC activation. (C) Individual cell data showing fura-2 and EYFP (H148Q/I152L) mutant fluorescence quenching for VGCC activation showing subsets of responders (n=8) and non-responders (n=15; total n=23) ****p< 0.0001.

(n=7). This confirms that there is a portion of the quenching that is not due to CaCC during depolarisation with the high-K^+ solution. When Ca^{2+}-free responses to 50mM KCl are compared to the responsive-subset neurons, there is no significant difference between the quenching achieved by both conditions, however both conditions elicited significantly greater quenching compared to VGCC non-responsive neurons (Ca^{2+}-free: 0.104 ± 0.022, *vs*. non-responsive neurons, $p<0.0001$, unpaired T-test).

In sum, our data are broadly in agreement with our previously published conclusions that VGCC are poorly coupled to ANO1 in small-diameter DRG neurons: (i) 65% of such DRG neurons did not show CaCC-dependent EYFP quenching in response to depolarisation (even though there were large Ca^{2+} transients in these cells); (ii) the majority of quenching in 'responding' neurons was Ca^{2+}-independent and, thus involves mechanisms other than CaCC.

Finally, to definitively conclude that bradykinin-induced quenching of EYFP (H148Q/I152L) fluorescence depends on ER Ca^{2+} release, rather than on any Ca^{2+} influx mechanisms, we repeated bradykinin application in Ca^{2+} free conditions. There was a 1.07 ± 0.30 increase in Ca^{2+} ($p<0.05$, n=5) when bradykinin was applied in the absence of Ca^{2+} in the extracellular solutions (Fig. 4.5A and B). This was somewhat smaller than the Ca^{2+} rise seen with bradykinin application in the presence of Ca^{2+} ($p<0.0001$, unpaired T-test) (Fig. 4.5B). The time taken to reach the maximal response was also longer (22 seconds). More importantly, EYFP (H148Q/I152L) mutant fluorescence was still significantly quenched when bradykinin was applied in Ca^{2+} free conditions (0.15 ± 0.03, n=5, $p<0.01$). Satisfyingly, the levels of quenching were almost identical, regardless of Ca^{2+} levels reached in the cells (Fig. 4.5B). Therefore, this result confirms the importance of IP_3R Ca^{2+} release in the bradykinin-induced ANO1 activation.

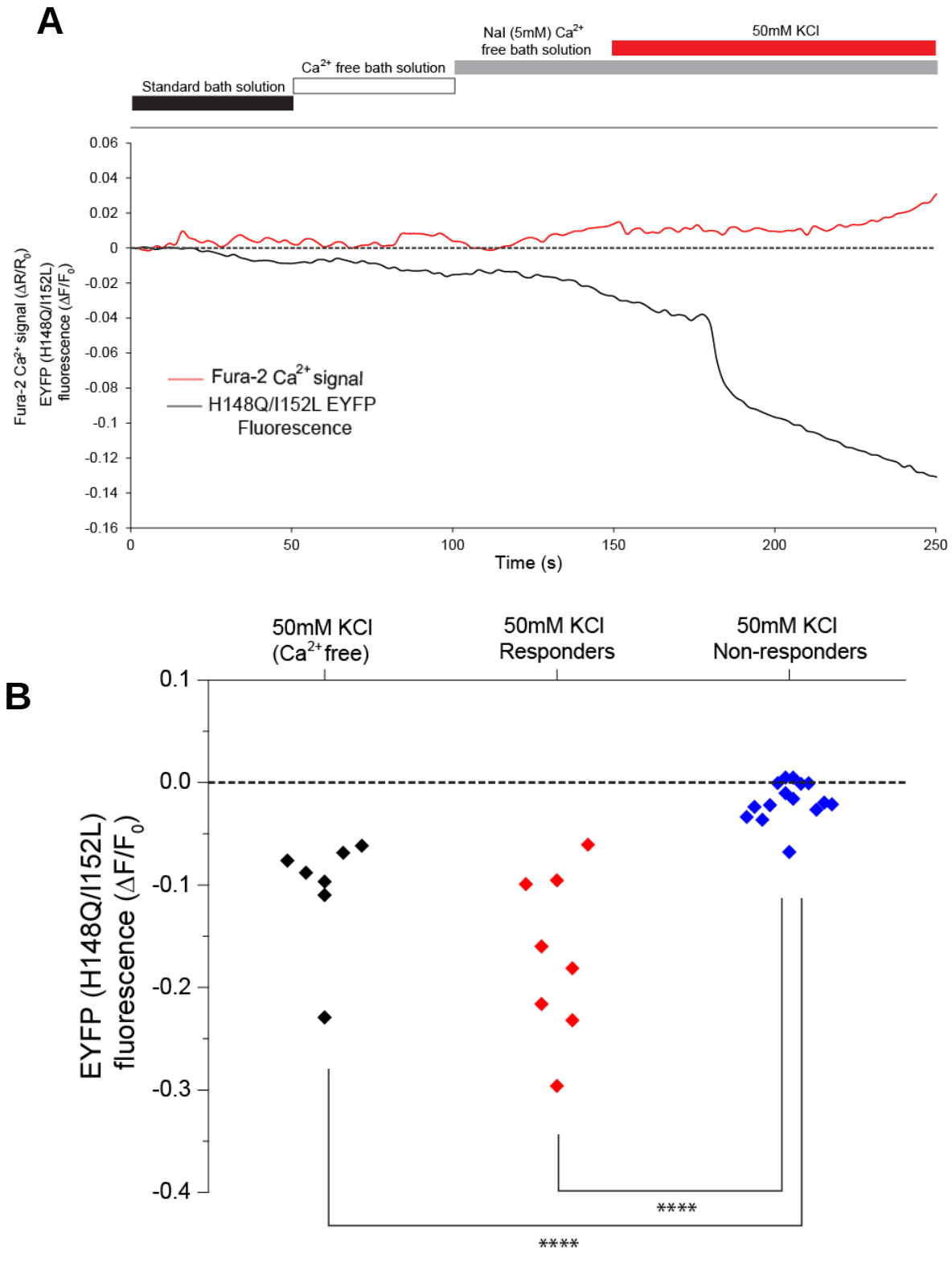

Figure 4.4: Removing extracellular Ca^{2+} and activating VGCCs still induces EYFP (H148Q/I152L) quenching. (A) Representative trace for one DRG response to 50mM KCl application to small-diameter DRG neurons, (B) Individual cell data for EYFP (H148Q/I152L) mutant fluorescence quenching showing pre and post responses to 50mM KCl application in different conditions (n=7). ****p<0.0001

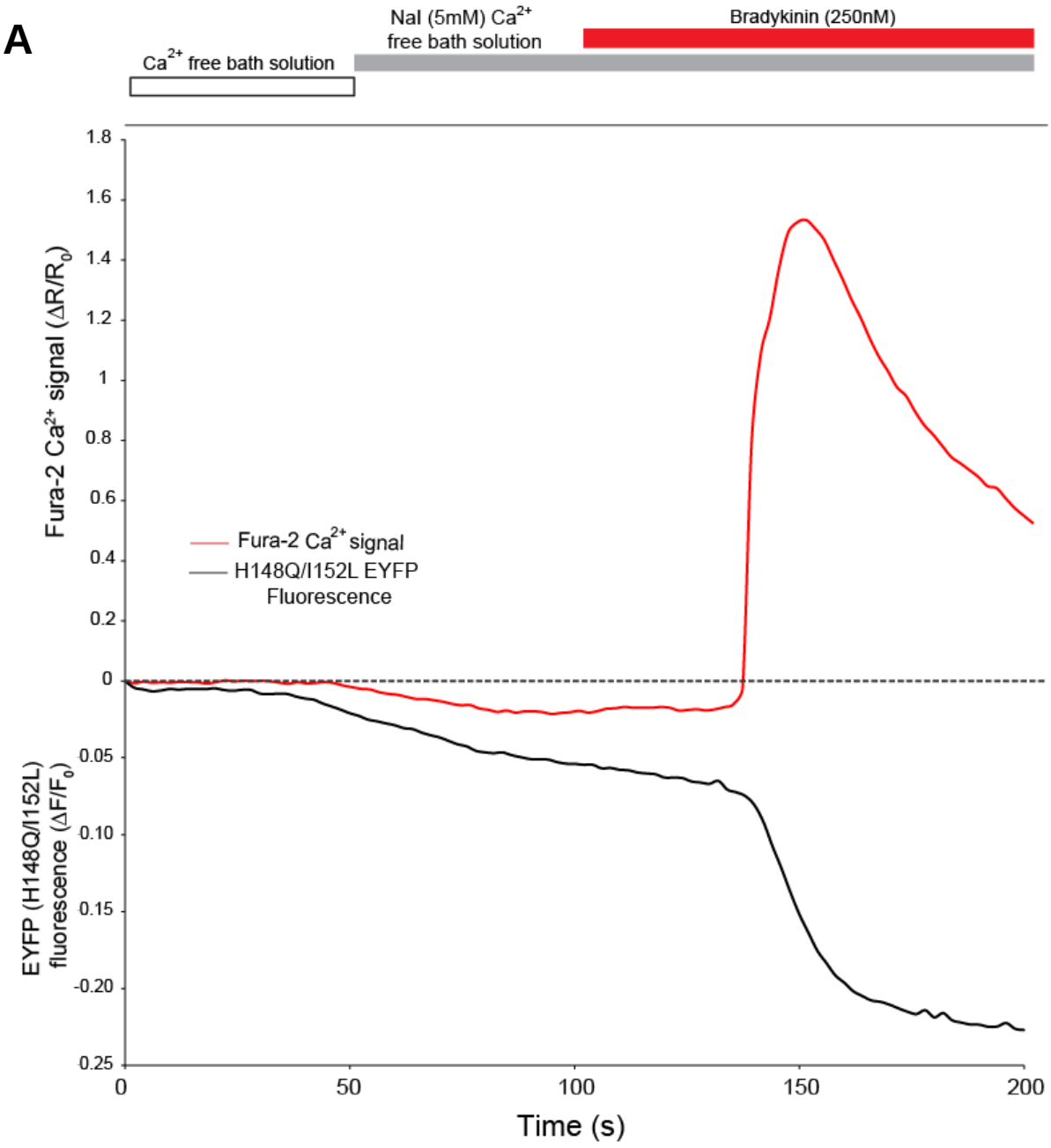
A
Ca2+ free bath solution
NaI (5mM) Ca2+ free bath solution
Bradykinin (250nM)
Fura-2 Ca2+ signal (ΔR/R0)
EYFP (H148Q/I152L) fluorescence (ΔF/F0)
Fura-2 Ca2+ signal
H148Q/I152L EYFP Fluorescence
1.8
1.6
1.4
1.2
1
0.8
0.6
0.4
0.2
0
0.05
0.10
0.15
-0.20
0.25
0
50
100
150
200
Time (s)

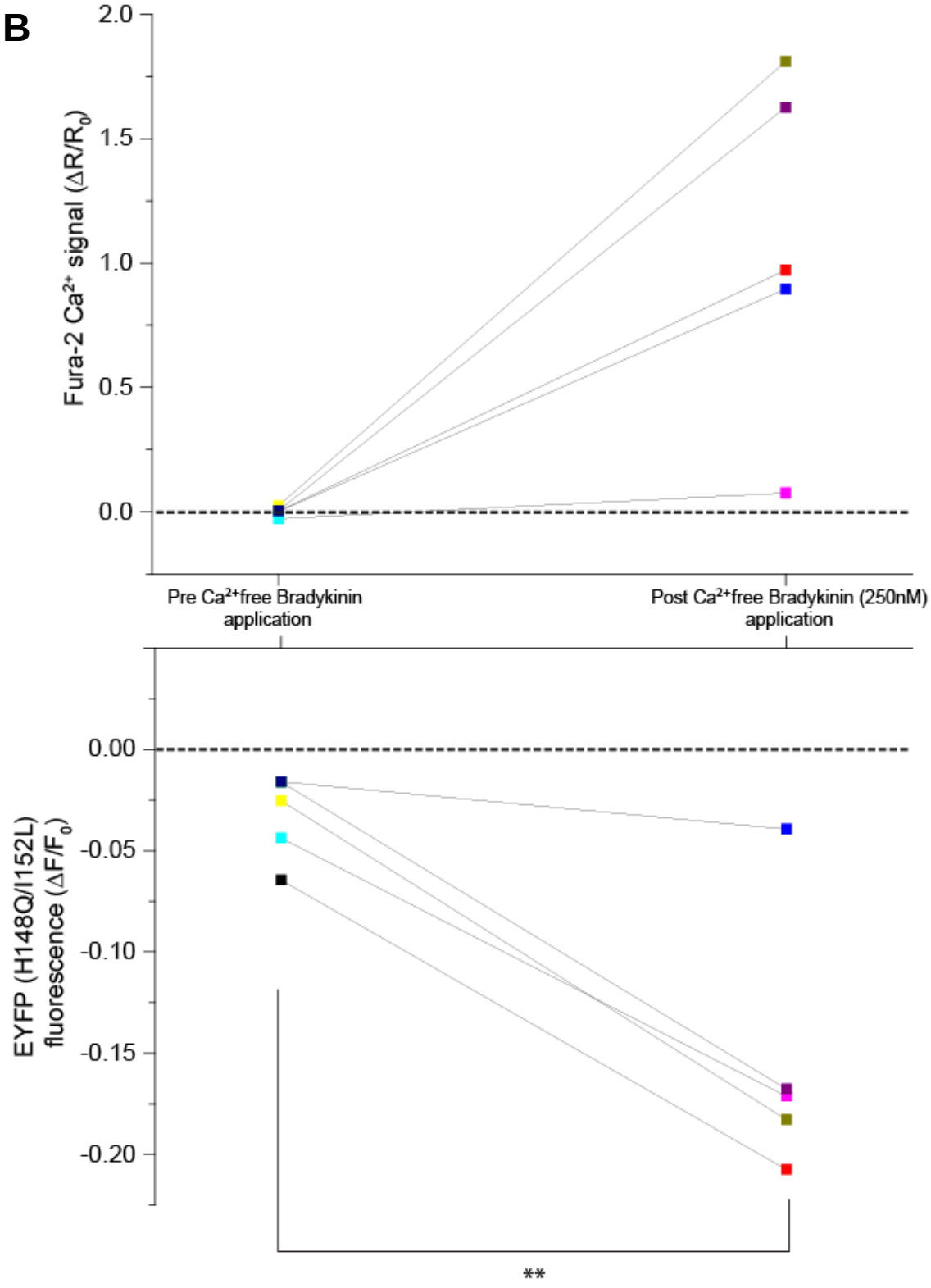
B
2.0
1.5
1.0
0.5
0.0
Fura-2 Ca2+ signal (ΔR/R0)
Pre Ca2+free Bradykinin application
Post Ca2+free Bradykinin (250nM) application
0.00
-0.05
-0.10
-0.15
-0.20
EYFP (H148Q/I152L) fluorescence (ΔF/F0)
**

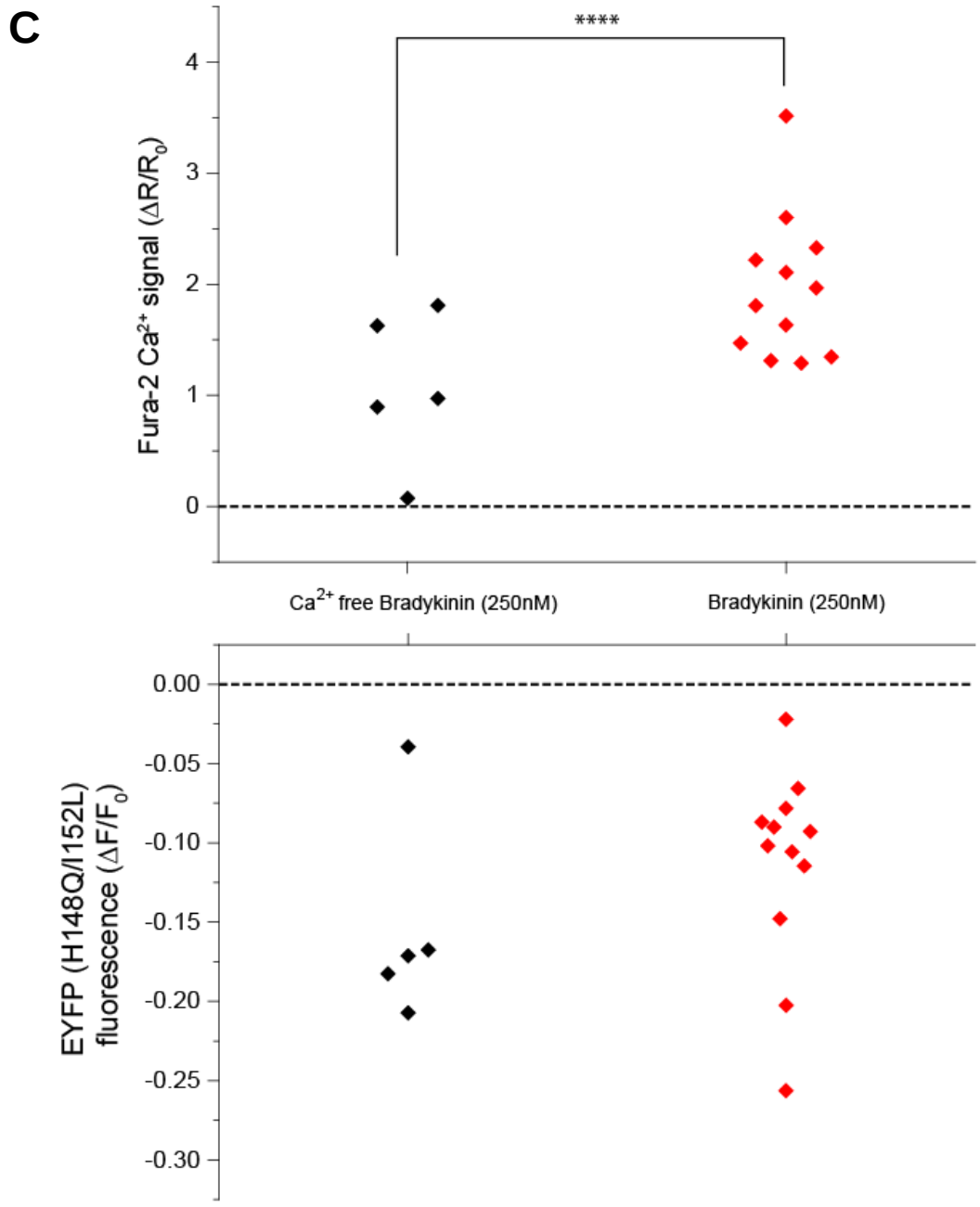

Figure 4.5: Bradykinin application induces fura-2 measured Ca^{2+} increase and concurrent EYFP (H148Q/I152L) mutant fluorescence quenching upon application of bradykinin (250nM) in small DRG neurons. (A) Representative trace of one DRG in response to bradykinin in Ca^{2+} free conditions. (B) Individual cell responses for fura-2 data for bradykinin application and represents EYFP (H148Q/I152L) fluorescence quenching for bradykinin application before and after application of bradykinin in Ca^{2+} free conditions (n=5) and (C) comparison between responses to bradykinin application in control or Ca^{2+} free conditions (n=5). ****p<0.0001

4.3 Discussion

This chapter demonstrates that our halide sensitive quenching technique can be used to monitor CaCC activation in DRG cultures and allows us to apply a sequence of solutions in a single protocol- something we were unable to do previously. Furthermore, coupling this with fura-2 imaging enables alignment of reported CaCC activity with Ca^{2+} dynamics in native cells to demonstrate that this is a Ca^{2+}-coupled event. We have shown that application of bradykinin is able to induce quenching of EYFP (H148Q/I152L) fluorescence in all neurons where there was a rise in $[Ca^{2+}]_i$. On the other hand, activation of VGCCs using 50mM KCl solution to depolarize neurons was unable to activate CaCC in 65% of DRG. The remaining 35% of neurons did respond to VGCC activation, however the majority of the EYFP quenching seen in these neurons was unlikely CaCC-dependent as removing Ca^{2+} from the bath solution did not abolish quenching. These findings are in good agreement with previous observations that ANO1 activity in DRG neurons is functionally coupled to IP_3R-induced Ca^{2+} release (Liu et al., 2010; Jin et al., 2013).

4.3.1 Halide sensor and fura-2 imaging provide an effective means to study CaCC activity

This EYFP (H148Q/I152L) quenching methodology using I^- ions was previously used to demonstrate bradykinin-induced ANO1 activity however there were 2 issues with this; the first being the experiment had to be done in 2 steps with 30mM NaI application on a set of cells followed by 30mM NaI in the presence of bradykinin on another set of cells, which required comparing responses in different populations of neurons, and the second being the inability to monitor Ca^{2+} levels. The first of these issues was resolved when we optimised our methodology to be able to image the EYFP (H148Q/I152L) mutant fluorescence in a single protocol with 5mM NaI extracellular solution (see previous chapter). Previous studies have utilized halide sensitive YFP quenching to study CFTR and glycine receptors in the search for channel modulators in high throughput screening assays (Galietta et al., 2001b; Sui et al., 2010) as well as in the development of ANO1 inhibitors (Seo et al., 2016). However, no one has previously coupled Ca^{2+} imaging with this method to visualise activation of a channel such as ANO1 in a single-cell setting. Satisfyingly, the increase in Ca^{2+} is closely followed by quenching in all responses measured. Despite this, both Ca^{2+} but mainly EYFP quenching does not recover. The fura-2 signal can

be explained by overload of the Ca^{2+} extrusion mechanisms but even when Ca^{2+} recovers back to baseline level, EYFP quenching shows no recovery. This may well be due to a slow unbinding process of the I^- (high K_d) from EYFP as well as the potential mechanisms for I^- extrusion being inefficient compared to physiological processes such as Cl^- extrusion. Further research is required to fully elucidate the reasons for this phenomenon.

4.3.2 CaCC coupling to IP_3R in DRG neurons using dual imaging approach

It has been proven that GPCR activation i.e. through bradykinin or PAR-2 application, in DRG neurons and cell lines leads to the activation of ANO1 (Jin et al., 2013; Cabrita et al., 2017). To test our optimized methodology, we used an established phenomenon- the ability of bradykinin to activate CaCC (ANO1) in DRG neurons and the poor coupling of VGCCs to CaCC (Jin et al., 2013). The results confirmed that CaCC can indeed be activated by bradykinin application via Ca^{2+} release from the ER. This conclusion is based on the facts that (i) ANO1 inhibitor T16inh-A01 completely abolished the bradykinin-induced anion influx, but not Ca^{2+} transients (Fig. 4.2) and (ii) removal of extracellular Ca^{2+} did not prevent neither the Ca^{2+} transients nor the anion influx (Fig. 4.5). This exemplifies CaCC coupling to IP_3R due to the fact that even though VGCC activation induced a similar $[Ca^{2+}]_i$ elevation to bradykinin in Ca^{2+} free conditions, only bradykinin was able to induce quenching (Fig. 4.3 and 4.5). Furthermore, VGCC quenching has been demonstrated to be Ca^{2+} independent and consists of 'responding' and 'non-responding cells'. Activation of B_2R activates the G_q-signalling cascade, ultimately producing IP_3 which in turn releases Ca^{2+} from the ER through IP_3R (Fig. 4.6). This IP_3-induced Ca^{2+} release seems to be the defining step for ANO1 activation; so why is this Ca^{2+} release from the ER so vital for ANO1 activation? As suggested earlier, close juxtaposition of the ER and the PM allows the formation of a local Ca^{2+} microdomain enabling ANO1 activity. ER-PM junctions are important aspects of intracellular signalling in various types of cells and are vital for processes such as STIM-ORAI-mediated SOCE and excitation-contraction coupling in muscle cells (see introduction). Looking at our functional microdomain consisting of ANO1 and B_2R as the plasmallemal components and IP_3R as the reticular component, B_2R activation leads to IP_3 formation which in turn activates ANO1 through IP_3R (Fig. 4.6). Furthermore, ANO1 and B_2R have been known to localise to lipid rafts of the

membrane, areas of the PM rich in cholesterol and glycosphingolipids (Jin et al., 2013). Similarly, ANO1 is present at lipid raft domains in VSMCs (Sones et al., 2010) as well as B_2R being found at lipid rafts in sensory neurons (Jeske et al., 2006). The presence of these proteins in lipid rafts of DRG neurons has further strengthened the notion that they are located in similar areas and work in a localised system.

4.3.3 Why does ANO1 display preference over the Ca^{2+} source for activation?

ANO1 seems to selectively discriminate over the source of Ca^{2+} present to activate it. Both VGCCs and IP_3R channels induced relatively high 'global' Ca^{2+} transients (as measured with cytosolically loaded fura-2) upon activation but IP_3R Ca^{2+} release is much more efficient to activate ANO1. What are the potential reasons for this? As mentioned, ANO1 has reportedly low Ca^{2+} sensitivity (-60mV; EC_{50}= 2.6µM) (Yang et al., 2008), therefore the presence of a local microdomain is logical to allow facilitation of its activation (Fig. 4.6). The crystal structure of the fungal orthologue of ANO6 nhTMEM16 has revealed the Ca^{2+} binding site to be enclosed deep in the hydrophobic transmembrane area of the protein which would necessitate the requirement of high Ca^{2+} to be able to reach this site (Brunner et al., 2014). Additionally, Ca^{2+} release at the mouth of IP_3R has been reported to reach 100µM which dissipates rapidly just microns away from the channel (Naraghi and Neher, 1997; Foskett et al., 2007). Thus, close proximity or, as we suggested earlier, even a physical coupling of ANO1 and IP_3R within a junctional microdomain would further assist Ca^{2+} reaching the binding site (Jin et al., 2013). Taken together, the ER-PM junctions, proximity of ANO1 and IP_3R, presence of B_2R receptors in the local microdomain along with other factors such as the presence of the cytoskeleton serve to allow the formation of a potent Ca^{2+} microdomain able to activate the relatively insensitive ANO1 channel (Fig. 4.6).

In terms of VGCCs, Ca^{2+} entering cells from this source seems to couple poorly to ANO1. Again, this may come down to the aspect of spatial arrangement where the VGCCs are not a component of the ANO1-activating functional microdomain (Fig. 4.6). PLA, a biophysical technique where probes can only produce a positive signal if there is proximity under 40nm of 2 target protein, has revealed no close proximity between ANO1 and VGCCs in small DRG neurons (Jin et al., 2013). As mentioned earlier, it would make sense for VGCCs not to activate ANO1 in the context of nociception as Ca^{2+} influx and depolarisation would lead to further VGCC activation

and induce a positive-feedback loop. Ultimately this over-excitability in nociceptors could lead to chronic pain conditions. This is an interesting scenario to probe as VGCC activity can induce ANO1 activity when lipid rafts are destroyed in DRG (Jin et al., 2013). It may well be that the loss of the lipid rafts causes VGCCs to come closer to ANO1 which was seen in VSMCs of rats where there was a redistribution of ANO1 in the membrane upon raft disruption and in DRG after lipid raft destruction (Sones et al., 2010; Jin et al., 2013). As well as this, there was an augmentation of ANO1 activity which could be due to Ca^{2+} from VGCCs now being able to activate the channel without reaching such a high Ca^{2+} concentration as previously required (Sones et al., 2010; Jin et al., 2013). One potential source for this augmentation could be the loss of PIP_2 upon membrane alterations caused by destroying lipid rafts. PIP_2 reportedly has an inhibitory effect on ANO1 in rat pulmonary arteries where it binds to the channel (Al-Jumaily et al., 2007; Pritchard et al., 2014). Removing this inhibition was found to increase ANO1 activity, which may be another significant reason for the ability of G_q-coupled GPCRs to be able to activate ANO1. However, conflicting data presented by Ta and colleagues suggests that there is no inhibitory effect of PIP_2 on ANO1 but rather it induces ANO1 activity (Ta et al., 2017). However, at this current stage, more research is required to make a conclusive judgement regarding this topic. This is not to suggest VGCCs are unable to play a role in ANO1 activation in the context of nociception; VGCC activation during action potential firing may serve to sensitise the environment through global Ca^{2+} elevation and depolarisation (both factors influence ANO1 activity), hence making it easier for other potential proteins to activate ANO1. During inflammation, this may become significant where the pro-algesic modulators of ANO1 (i.e. bradykinin and PAR-2) are released. Furthermore, in inflammatory conditions, three times the normal $[Cl^-]_i$ is accumulated in DRG due to NKCC1 (Funk et al., 2008) meaning that ANO1 activity will produce greater pro-nociceptive effects.

4.3.4 Ca^{2+} independent quenching in DRG neurons

In the small percentage of neurons where we observed some EYFP quenching in response to high-K^+ depolarisation, we concluded that this anionic influx seemed to be largely independent of Ca^{2+} (as quenching was still present when experiments were repeated in Ca^{2+}-free extracellular bath solutions). Thus, it doesn't necessarily mean that this anion influx was due to CaCC activation; other sources for this

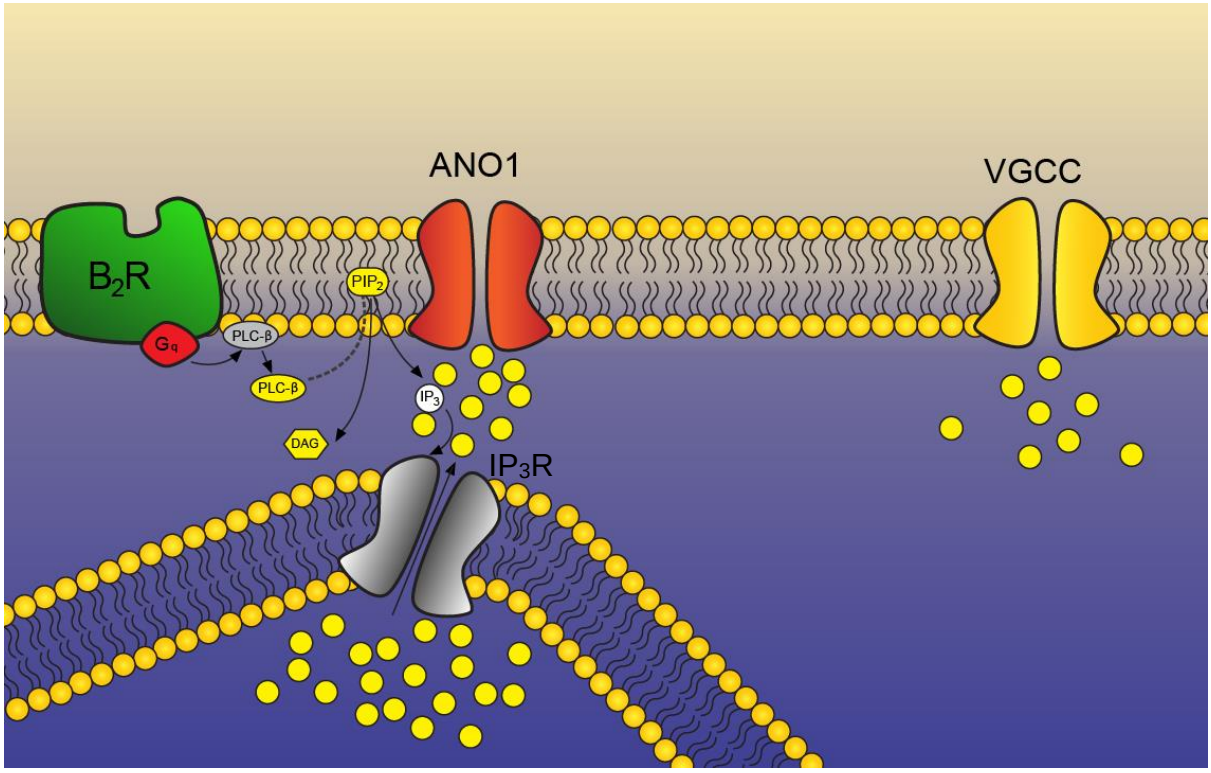

Figure 4.6: Activation of ANO1 in DRG. Activation of G_q-coupled receptors produces IP_3R activation by generation of IP_3. Arrangement of ANO1 and IP_3R in an ER-PM, functional microdomain means Ca^{2+} release from IP_3R is sufficient and able to activate ANO1. VGCCs on the other hand are not in this arrangement so are unable effectively activate ANO1.

quenching could well be the activity of the NKCC1 cotransporter. Further to this point, depolarisation of the membrane may lead to action potential firing, which in neurons has been found to increase Cl^- levels (Amir et al., 2002; Woodin et al., 2003; Fiumelli et al., 2005). Furthermore, this has also been found to enhance and increase activity of the Na^+-K^+ ATPase leading to reduced $[Na^+]_i$ (Morita et al., 1993; Parker et al., 1996). Subsequently, Brumback and Staley, demonstrated that action potential firing causes NKCC1 to re-establish $[Na^+]_i$ and as part of this process, to maintain electroneutrality, also allows Cl^- influx into cells (Brumback and Staley, 2008). Therefore, during action potential firing, there is an increase in $[Cl^-]_i$ which can be blocked by Na^+-K^+ ATPase blockers (Brumback and Staley, 2008). This could be occurring in DRG neurons as after potential action potential firing caused by VGCCs, accumulation of $[Cl^-]_i$ may result due to NKCC1 activity. Therefore, in the presence of I^-, this may be transported and cause quenching of the fluorescence which is not attributed to ANO1 activity.

Having confirmed the ability of our methodology in studying CaCC activity, I will test the ability of TRPV1 to activate ANO1 in our newly developed system.

Chapter 5: Studying TRPV1 activation of CaCC in DRG neurons using dual imaging

5.1 Introduction

Non-selective cation channels (i.e. P2X, Piezo, TRP) allow Na^+ and Ca^{2+} influx into cells upon activation, therefore providing a means by which Ca^{2+} can potentially activate ANO1. Even though several lines of research indicate functional coupling between ANO1 and IP_3R, recent studies have shown ANO1 can be activated by non-selective cations channels too. I will therefore discuss some examples of this in the following section.

5.1.1 P2X7 in oocytes

ATP is able to evoke anionic conductance's when applied in various cell types such as Schwann cells (Amedee and Despeyroux, 1995; Colomar and Amedee, 2001) and parotid acinar cells (Arreola and Melvin, 2003). P2X7 has been shown to functionally couple to ANO1 in Xenopus and Axolotl oocytes heterologously expressing ANO1 and P2X7 (Stolz et al., 2015). Application of ATP to these oocytes exhibited robust ANO1 currents when extracellular Ca^{2+} was available, which were 10 times greater than when no extracellular Ca^{2+} was present (Stolz et al., 2015). These currents were sharply reduced upon Ca^{2+} removal from the perfusion or by BAPTA (the Ca^{2+} chelator that inhibits fast rises in Ca^{2+}) pre-injection (Stolz et al., 2015). Interestingly, however no physical interaction between these proteins was detected. This functional coupling was also evident in AsPC-1 cells (Stolz et al., 2015). Even though P2X7 is expressed in astrocytes and microglia and not in DRG neurons, it shows how there is scope for potential coupling with other P2X receptors.

5.1.2 TRPV6 in epididymal cells

Recently, ANO1 has been shown to couple to TRPV6 in epithelial principal cells in rat epididymis (Gao et al., 2016). Removal of extracellular Ca^{2+} leads to loss of both TRPV6 and CaCC current in these cells. Using biochemical and pharmacological approaches, the authors were able to show that these proteins were co-expressed in epididymal principle cells at the apical membrane (Gao et al., 2016). Furthermore, blockade of TRPV6 with lanthanum (non-specific cation channel blocker) and ANO1 with tannic acid, led to loss of the respective currents (Gao et al., 2016). It has been postulated that the functional role for coupling between ANO1 and TRPV6 is

involved in regulating membrane excitability in these cells. Constitutively open TRPV6 channels allow a local Ca^{2+} elevation in epididymal principle cells producing a depolarising effect. This 'local' Ca^{2+} is then able to activate nearby ANO1 channels, which produces hyperpolarisation of the cells to bring the membrane potential back to resting levels (Gao et al., 2016).

5.1.3 TRPC6 in smooth muscle

TRPC6 is also coupled to ANO1 in smooth muscle cells (Wang et al., 2016). Co-expression of both proteins has been found in resistance-size cerebral arteries and using a co-immunoprecipitation approach, Wang and colleagues were able to pull down ANO1 and TRPC6 together from these cells (Wang et al., 2016). Hyp9, a selective activator of TRPC6 was found to stimulate CaCC currents in arterial myocytes which were also reduced using T16Ainh-A01. Furthermore, this was dependent on a local Ca^{2+} elevation as BAPTA and not EGTA, was able to abolish CaCC currents (Wang et al., 2016). Physiologically, functional coupling between TRPC6 and ANO1 plays a role in pressurized cerebral arteries with ANO1 mediating vasoconstriction through TRPC6-induced activation. To emphasise the importance of ANO1 activation requiring specific and local Ca^{2+} signals for activation in these cells, VGCC activation using 60mM KCl produced no ANO1 currents, suggesting that VGCCs are not spatially positioned to allow activation of ANO1 (Wang et al., 2016).

5.1.4 TRPV4 in choroid plexus epithelial cells

ANO1 has been found to functionally interact with TRPV4 in choroid plexus epithelial cells (CPECs). TRPV4 and ANO1 are expressed in CPECs and play a role in the modulation of water efflux from these cells (Takayama et al., 2014). In CPECs and HEK293T heterologously expressing ANO1 and TRPV4, stimulation of TRPV4 by GSK1016790A (GSK) produced robust CaCC currents whereas T16inh-A01 abolished these TRPV4-evoked Cl^- currents (Takayama et al., 2014). Moreover, there was a physical interaction between these proteins as discovered using co-immunoprecipitation studies (Takayama et al., 2014). Due to the fact that water movement follows Cl^- flux in cells, ANO1-induced Cl^- efflux caused a reduction in cell volume of CPECs. This was also seen in HEK293T cells transfected with ANO1 and TRPV4 as GSK was able induce cell size reduction through ANO1 activation. It has been proposed that hyposmotic conditions activate TRPV4 which in turn triggers

ANO1 through the Ca^{2+} influx hence producing water efflux (possibly by aquaporins) (Takayama et al., 2014).

5.1.5 TRPV1 in DRG

Several recent studies have correlated the activity of ANO1 and TRPV1 in nociceptors. Oh's lab produced evidence to suggest ANO1 can be activated by heat (Cho et al., 2012). Heat ramps in HEK293T cells transfected with ANO1 produced robust activation of a Cl^- conductance when temperatures were increased above 44ºC. This was also seen with ANO2 (albeit a smaller current compared to ANO1) however not with ANO4 or ANO5 (Cho et al., 2012). DRG expressing endogenous ANO1 also behaved in an analogous manner. Similarly to ANO1's synergistic relationship between Ca^{2+}- and voltage-dependence, the presence of Ca^{2+} enhanced the temperature sensitivity of ANO1 by lowering the temperature threshold (Cho et al., 2012). Additionally, increased temperatures also produced greater currents when the membrane was depolarized. This shows that temperature is also an important determinant of ANO1 activity, especially in the field of nociception. DRG and TG neurons also show a very high level of co-expression between ANO1 and TRPV1 (Kanazawa and Matsumoto, 2014; Lee et al., 2014; Takayama et al., 2015). Intriguingly, pharmacological blockade or genetic deletion of TRPV1 in mice resulted in DRG neurons still being able to respond to heat with depolarizing currents which were only abolished when a CaCC blocker was introduced (Lee et al., 2014). Similarly, siRNA against ANO1 was also able to reduce nocifensive behaviours thermal hyperalgesia in rats (Lee et al., 2014).

5.1.6 Functional coupling between ANO1 and TRPV1

Functional data regarding ANO1 activation induced by TRPV1 is also available. HEK293 cells expressing ANO1 and TRPV1 show CaCC currents after application of capsaicin (Takayama et al., 2015). Furthermore, TRPV1 and ANO1 have been shown to physically interact in co-immunoprecipitation experiments. It has therefore been suggested that ANO1 and TRPV1 are found very close to each other, possibly physically coupled which allows Ca^{2+} influx through TRPV1 to activate ANO1 (Takayama et al., 2015). Activation of TRPV1 allows Ca^{2+} and Na^+ to enter cells leading to depolarisation; this would have 2 effects on ANO1: (i) the depolarisation would cause ANO1 to become more sensitive to Ca^{2+} and (ii) Ca^{2+} entering the cells

may be able to activate ANO1 directly (Takayama et al., 2015). As mentioned in the introduction, due to the high Cl^- concentration activation of DRG neurons, ANO1 would also produce depolarisation, with the effects summating with TRPV1-induced depolarisation providing a stronger response (Takayama et al., 2015). In nociceptive neurons, this would lead to increased excitability and more pain transmission.

Another touted role for ANO1 and TRPV1 is in the process of synaptic transmission at synapses of the primary afferent fibers in the spinal cord. Proteins produced in cell bodies are transported to nerve endings in sensory neurons and into the presynaptic terminals of the spinal cord (Takayama et al., 2015). Recordings in the substantia gelatinosa showed spontaneous excitatory post synaptic potentials (sEPSP) which were facilitated upon capsaicin application. However, when ANO1 was blocked using T16A-inhA01, this facilitation was abolished (Takayama et al., 2015). It has been hypothesized that upon ANO1 activation through TRPV1 at the presynaptic terminal, the depolarisation caused (see above) activates VGCCs that then allow release of glutamatergic vesicles (Takayama et al., 2015).

In TG neurons, ANO1 expression is decreased with the injection of CFA in the tongue, which was linked to an increase in TRPV1 expression (Suzuki et al., 2016). Furthermore, T16A-inhA01 was also able to reduce AP firing in DRG neurons generated by TRPV1 activation by capsaicin application (Suzuki et al., 2016). This further adds to the speculation that there is possibly some intricate coupling between ANO1 and TRPV1.

The close relationships between TRPV1 and ANO1 are somewhat difficult to elucidate unambiguously due to the following issues: (i) activation of both channels results in inward currents of similar kinetics under physiological conditions (i.e. resting membrane potential ~-60 mV, native $[Cl^-]_i$) (Liu et al., 2010), (ii) both channels are sensitive to heat within roughly similar range and (iii) some pharmacological modulators of these channels suffer from cross-reactivity. Thus, the small-molecule ANO1 activator E_{act} has been demonstrated to also activate TRPV1 (Liu et al., 2016). In another study E_{act} was reported to induce CaCC currents in DRG neurons (Deba and Bessac, 2015) however, in this study there was no mentioning of the cross-reactivity reported by Liu and colleagues. E_{act} also induced nocifensive behaviors in mice, which were reduced in the presence of T16A-inhA01 (Deba and Bessac, 2015). This effect was also seen when capsaicin was used to replace E_{act} in

mice. Yet, due to the supposed cross-reactivity, these studies lack clarity as to what the relative contribution of ANO1 and TRPV1 is regarding the excitatory effects of E_{act} and, to lesser extent, of capsaicin as well. Therefore, this chapter will focus on the activation of TRPV1 by ANO1, again using our newly developed dual imaging approach to dissect the mechanisms of ANO1 activation by TRPV1. The advantage of our imaging approach is in that TRPV1 and ANO1 are recorded with different fluorophores (fura-2 and EYFP H148Q/I152L, respectively), which circumvents the difficulty of patch-clamp recording, where both channels generate similar currents.

5.2 Results

We firstly decided to demonstrate the activation of ANO1 through TRPV1 using our dual imaging protocol. Similarly to the previous chapter, EYFP (H148Q/I152L) was expressed in DRG neurons and cultured for 48 hours; one hour before analysis cultures were loaded with fura-2 AM. No NGF was utilized in our cell preparations.

Application of capsaicin (1μM) to DRG neurons expressing the halide-sensor induced significant Ca^{2+} transients and a concurrent EYFP quenching (Fig. 5.1A and B). On average, capsaicin caused the fluorescence to decrease by 0.12 ± 0.026 (n=9, p<0.001). This was also coupled to an increase in Ca^{2+} ($\Delta R/R_0$ = 1.8 ± 0.26, n=9, p<0.001) (Fig. 5.1B). Comparing the effects produced by TRPV1 activation and conditions tested in the previous chapter, Ca^{2+} signals produced by capsaicin and bradykinin were similar however, VGCC activation produced a smaller Ca^{2+} response compared to these Ca^{2+} sources (VGCC vs capsaicin, p<0.05; VGCC vs bradykinin, p<0.01, both ANOVA with Tukey) (Fig. 5.2). Bradykinin application induced significantly greater EYFP (H148Q/I152L) fluorescence quenching to that produced VGCC activation (VGCC vs bradykinin, p<0.05, Mann Whitney) (Fig. 5.2). However, capsaicin application showed no significant difference with VGCC application despite producing a marginally smaller response compared to bradykinin application. However, as mentioned above, the non-responsive population of neurons to 50mM KCl is the 'true' effect expected and comparing this to capsaicin indeed shows a significantly greater response induced by capsaicin application (p<0.01, Mann Whitney). Therefore, this demonstrates that TRPV1 application can activate CaCC in DRG neurons.

TRPV1 activation has been known to induce PLC activation, PIP_2 cleavage and subsequent IP_3 generation (Lukacs et al., 2007). This means that there may be two distinct processes underlying a capsaicin-induced Ca^{2+} transient: (i) primary Ca^{2+} influx through the TRPV1 channel pore and (ii) ER store release stimulated by Ca^{2+}-sensitive PLCδ (Lukacs et al., 2007; Rohacs et al., 2008) or other mechanisms. Given the tight coupling between ANO1 and IP_3R established in previous studies, this may well be an interesting mode by which ANO1 is coupled to TRPV1 in DRG neurons. To test if Ca^{2+} released from the ER contributes to capsaicin-induced activation of ANO1, we applied thapsigargin (1μM) in an acute manner to deplete the Ca^{2+} in the ER. However, this produced a large Ca^{2+} elevation on its own, as the

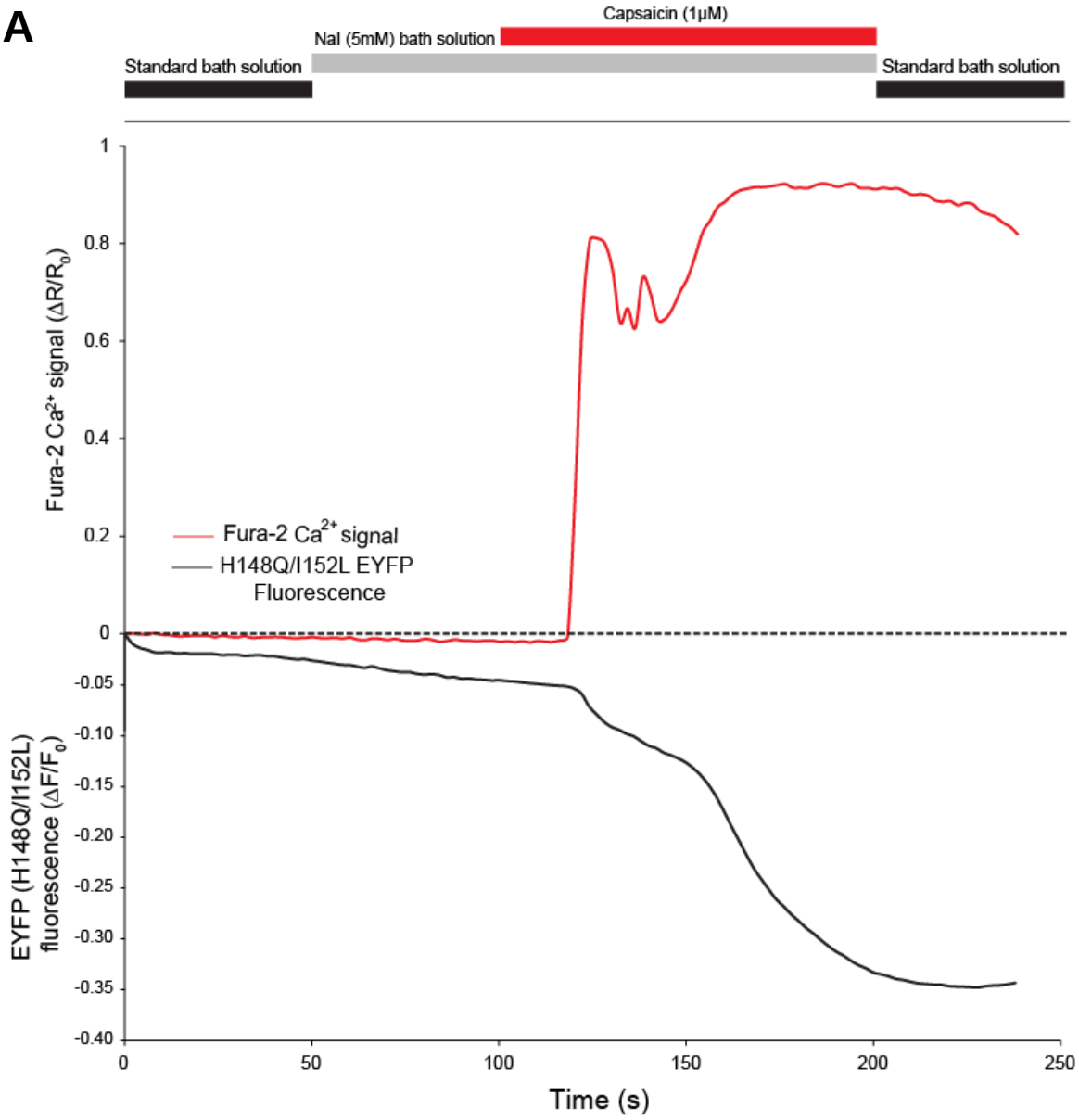
A
Capsaicin (1μM)
NaI (5mM) bath solution
Standard bath solution
Standard bath solution
Fura-2 Ca2+ signal (ΔR/R0)
Fura-2 Ca2+ signal
H148Q/I152L EYFP Fluorescence
EYFP (H148Q/I152L) fluorescence (ΔF/F0)
Time (s)
1
0.8
0.6
0.4
0.2
0
-0.05
-0.10
-0.15
-0.20
-0.25
-0.30
-0.35
-0.40
0
50
100
150
200
250

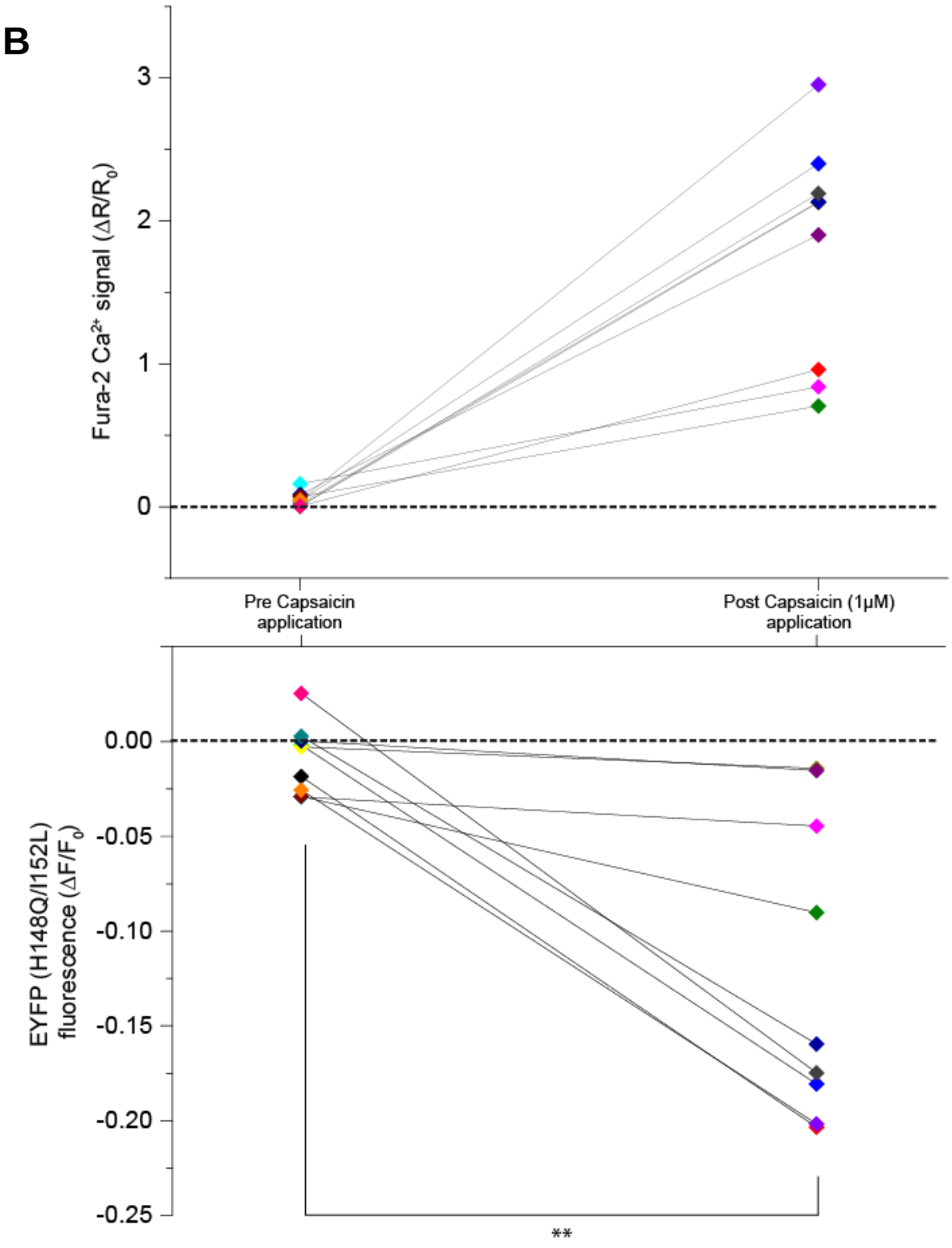

Figure 5.1: Capsaicin application induces fura-2 measured Ca^{2+} increase and concurrent EYFP (H148Q/I152L) mutant fluorescence quenching upon application of capsaicin (1μM) to small DRG neurons. (A) Representative trace of one DRG in response to capsaicin. (B) Individual cell responses for fura-2 (upper) and EYFP (H148Q/I152L) fluorescence quenching (lower) for capsaicin application (n=9). **p<0.01

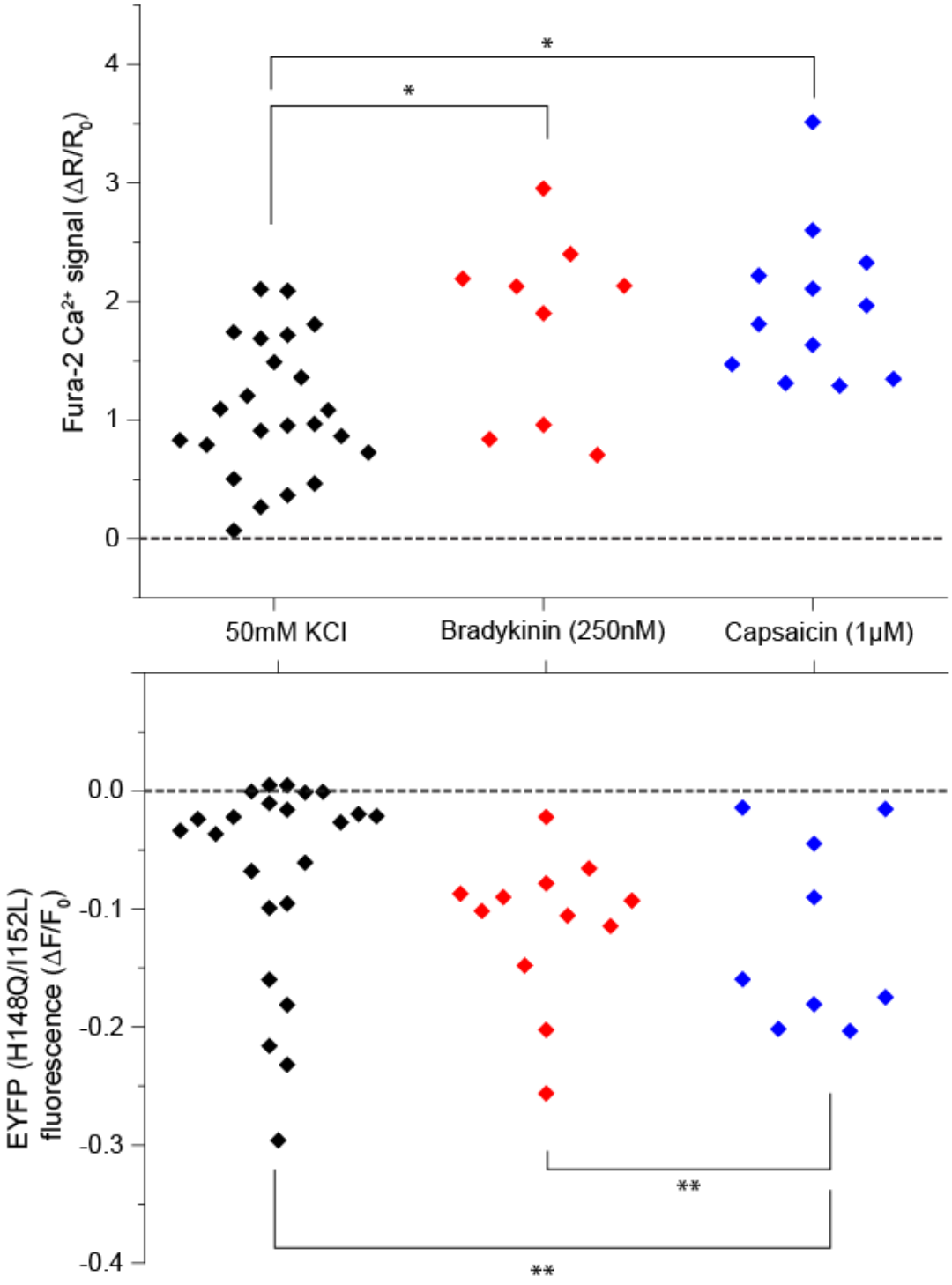

Figure 5.2: Comparison of Ca^{2+} signals and EYFP quenching between different agonist/conditions applications in DRG neurons. Peak individual cell data for fura-2 signals (upper) and EYFP (H148Q/I152L) fluorescence quenching (lower) evoked after 50mM KCl (n=23), capsaicin (n=9), and bradykinin (n=12) application. *p<0.05, **p<0.01

Ca^{2+} leaves the ER and into the cytosol where fura-2 is present (data not shown). Therefore, in the next set of experiments we pre-incubated DRG cultures with 1µM thapsigargin (1 hour at 37^{o}C) and included thapsigargin in the solutions during the perfusion to maintain depletion of the Ca^{2+} stores. The results showed that the capsaicin-induced fura-2 Ca^{2+} signal was severely reduced by thapsigargin application in the majority of the cells we tested (Thapsigargin pre-treatment: 0.34 ± 0.13, n=6 Vs Control: 1.8 ± 0.26, n=9, $p<0.0001$), which in most cells rendered TRPV1 unable to activate ANO1 (Fig. 5.3). This was also seen in the EYFP (H148Q/I152L) mutant fluorescence quenching (Thapsigargin pre-treatment: 0.007 ± 0.017, n=6 Vs Control: 0.12 ± 0.026, n=9, $p<0.01$) (Fig. 5.3). These data indicate that a significant portion of Ca^{2+} attributed to TRPV1 activation in fact originates from the ER and when this is removed from the 'total' Ca^{2+} signal produced by TRPV1 activation, ANO1 cannot be activated in a manner previously demonstrated.

To test this further, we performed standard fura-2 Ca^{2+} imaging (no transfection with EYFP (H148Q/I152L)) and measured capsaicin-induced Ca^{2+} transients in DRG neurons using Ca^{2+}-free bath solution. This would be able to demonstrate if $[Ca^{2+}]_i$ can be elevated without the extracellular Ca^{2+} component of TRPV1 activation. The results showed that removal of extracellular Ca^{2+} reduced but not completely abolished Ca^{2+} rises in our cells (0.71± 0.11, n=9) (Fig. 5.4). The global Ca^{2+} signal measured in Ca^{2+}-free medium was of a similar level to the Ca^{2+} rise seen in cells pre-incubated with thapsigargin or cyclopiazonic acid (CPA, 1µM), another inhibitor of the SERCA Ca^{2+}-ATPase pump used to deplete ER Ca^{2+} stores also produced a reduction of Ca^{2+} in DRG neurons (Thapsigargin pre-treatment: 0.49 ± 0.11, n=12, CPA pre-treatment 0.67 ± 0.14, n=16) (Fig. 5.4). There was no significant difference between these conditions however, all three of these conditions evoked significantly lower Ca^{2+} transients compared to capsaicin (1µM) application in control conditions (1.33 ± 0.15, n=19, $p<0.05$, ANOVA with Tukey).

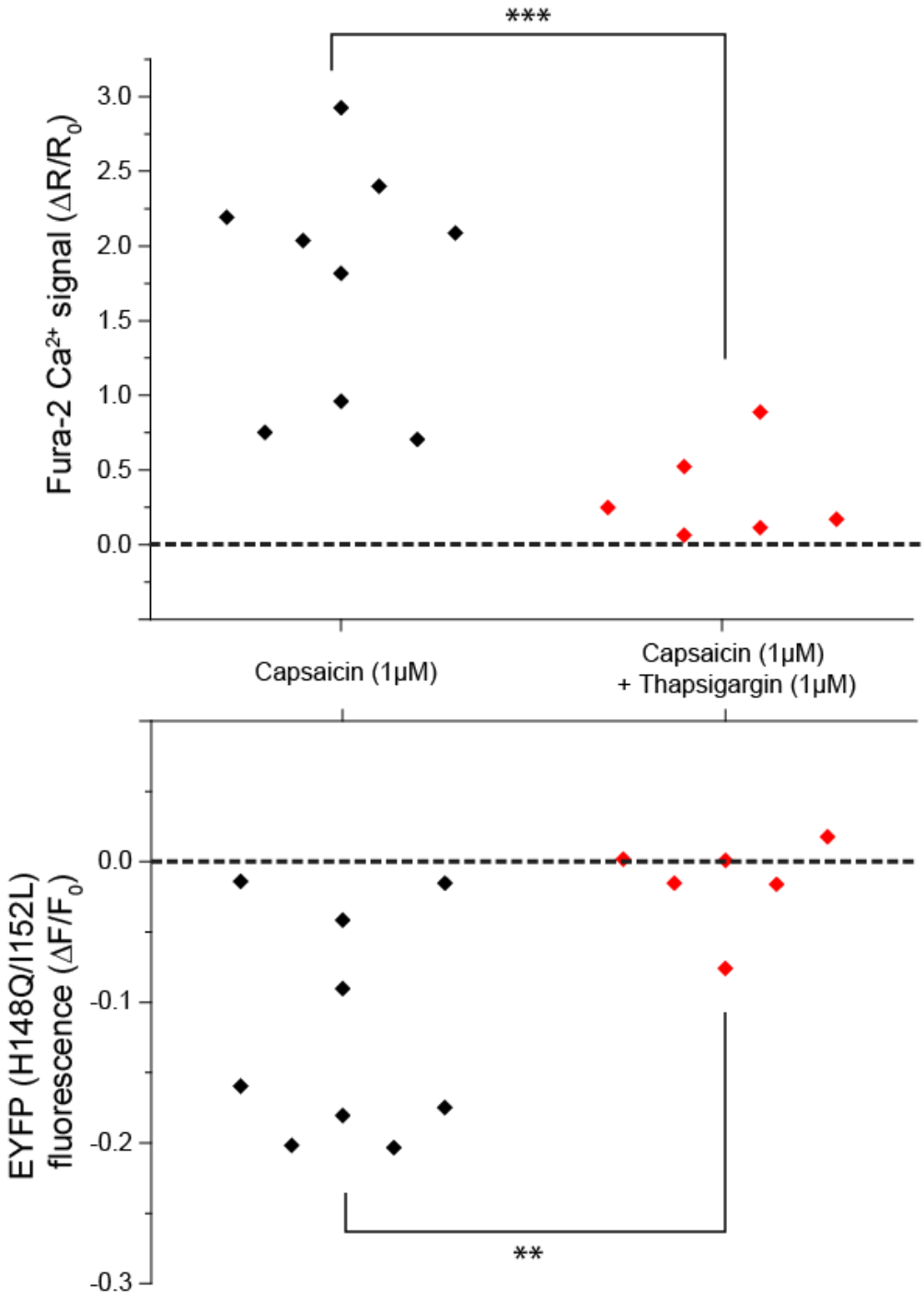

Figure 5.3: Effects of thapsigargin (1μM) pretreatment on DRG neurons and capsaicin (1μM) application. Comparison between individual cell data for fura-2 signals (upper) and EYFP (H148Q/I152L) fluorescence quenching (lower) in response to control (capsaicin only) and after pretreatment with thapsigarign. **p<0.01, ***p<0.001.

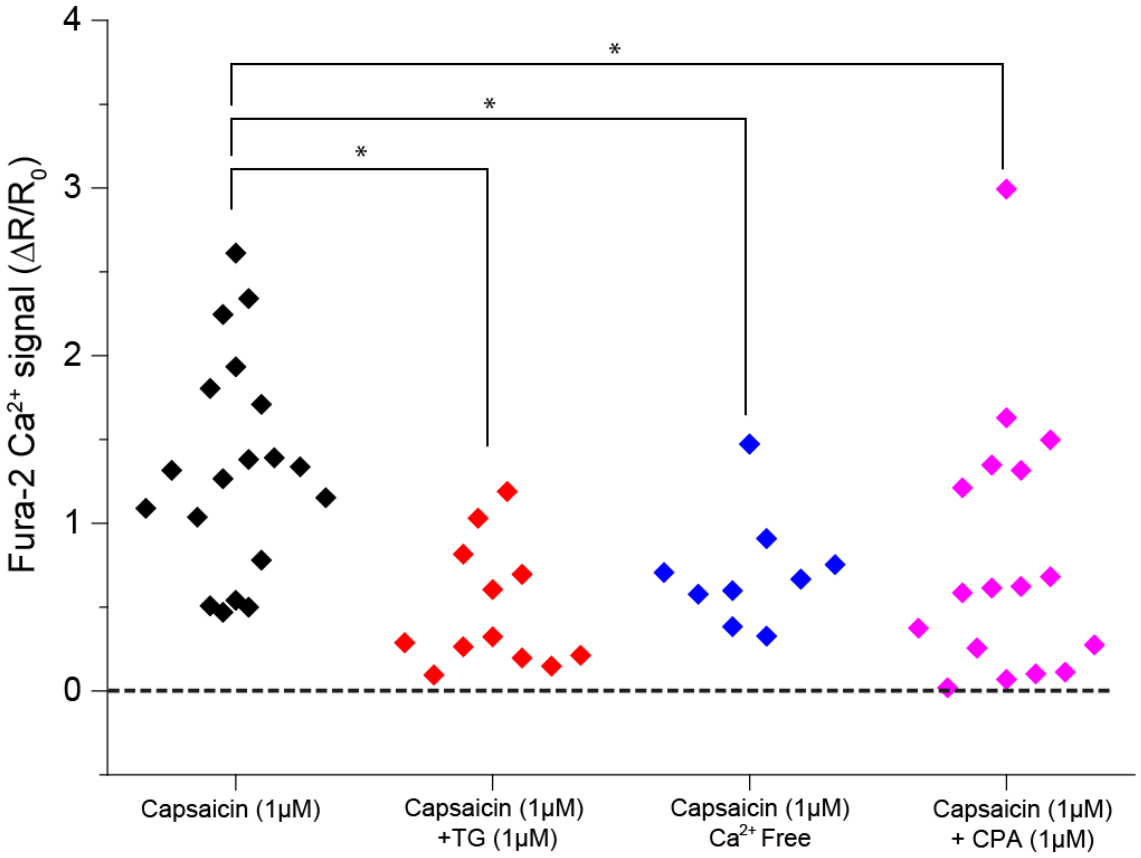

Figure 5.4: Ca^{2+} imaging in cells loaded with fura-2 in response capsaicin (1μM) in various conditions. Graph shows Ca^{2+} signal in response to capsaicin application in control conditions (n=19), after pre-incubation with thapsigargin (n=12), in the Ca^{2+} free extracellular bath solution (n=9) and after pre-incubation with CPA (n=16). Data presented as mean ± SEM Statistics performed using ANOVA with Tukey. * representing significance at $p<0.05$.

DRG neurons are particularly difficult to transfect (Kirton et al., 2013) and while the 'nucleofection' technique that we utilised does allow transfection of some neurons, the difficulty with the technique is in its tendency to destroy the majority of DRG neurons during the electroporation stage of the transfection. This means that transfection efficiency is low (~5%) and cells that do express the mutant EYFP protein are sometimes damaged. This makes it difficult to perform complex imaging experiments on DRG neurons co-transfected with several proteins. Alternatively, cell lines can be used to stably express fluorescent proteins in a relatively efficient manner with common transfection reagents. Moreover, researchers have successfully employed EYFP (H148Q/I152L) quenching assays in cell lines. Another advantage of using cell lines is that they allow more reliable transfection of multiple proteins. Thus, to confirm that ER Ca^{2+} is being mobilized due to TRPV1 activation, CHO cells were transfected with TRPV1, ANO1, EYFP (H148Q/I152L) and an ER-specific Ca^{2+} indicator known as Red-Calcium-measuring organelle-Entrapped Protein IndicAtor (Red-CEPIA) (Suzuki et al., 2014) as well as being loaded with fura-2. Similarly to the EYFP halide sensor, CEPIA decreases in fluorescence upon Ca^{2+} exiting the ER. Therefore, if ER Ca^{2+} is involved in the process of ANO1 activation through TRPV1, along with EYFP quenching and a Ca^{2+} increase, there will also be a concurrent decrease in CEPIA fluorescence. Fascinatingly, our experiments showed that there was indeed a significant quenching of both EYFP mutant fluorescence and Red-CEPIA, as well as a significant Ca^{2+} rise as measured by fura-2 (Fig. 5.5A and B). Fura-2 signal rose to 0.66 ± 0.11, EYFP (H148Q/I152L) fluorescence showed quenching by 0.089 ± 0.044 ($n=5$, $p<0.05$, Wilcoxon Signed) and Red-CEPIA quenched by 0.061 ± 0.019 ($n=5$, $p<0.05$, paired T-test). This confirms our previous findings in DRG that TRPV1 mobilizes the ER and this is perhaps the major Ca^{2+} source for ANO1 activation (Fig. 5.5B).

TRPV1 can also generate IP_3 through PLC activation (Lukacs et al., 2007). Alternatively, the ER is also known to consist of functional TRPV1 proteins (Gallego-Sandin et al., 2009), which could be producing a large Ca^{2+} release to activate ANO1. To investigate potential mechanisms by which ANO1 activation occurs, we repeated these triple imaging experiments in the presence of xestospongin C (1μM), a blocker of IP_3R. Cells were pre-incubated with xestospongin C during the fura-2

loading and was also included in perfusion solutions to maintain inhibition of IP_3R. Results demonstrated that there was a reduction in all 3 parameters being investigated (Fig. 5.6). Fura-2 Ca^{2+} signal was reduced from 0.66 ± 0.11 (n=5) in control conditions to 0.18 ± 0.051 (n=5, $p<0.01$, unpaired T-test), EYFP quenching was reduced from 0.089 ± 0.044 (n=5) in control conditions to 0.026 ± 0.013 (n=5, $p<0.05$, not significant with Mann Whitney) and Red-CEPIA levels went from 0.061 ± 0.019 (n=5) in control conditions to 0.018 ± 0.0016 (n=6, $p<0.05$, unpaired T-test) (Fig. 5.6). Even though EYFP (H148Q/I152L) mutant quenching isn't significantly reduced when xestospongin C is applied, it is still considerably lower compared to the control conditions. Overall, this suggests that TRPV1 can activate ANO1 through IP_3R activation.

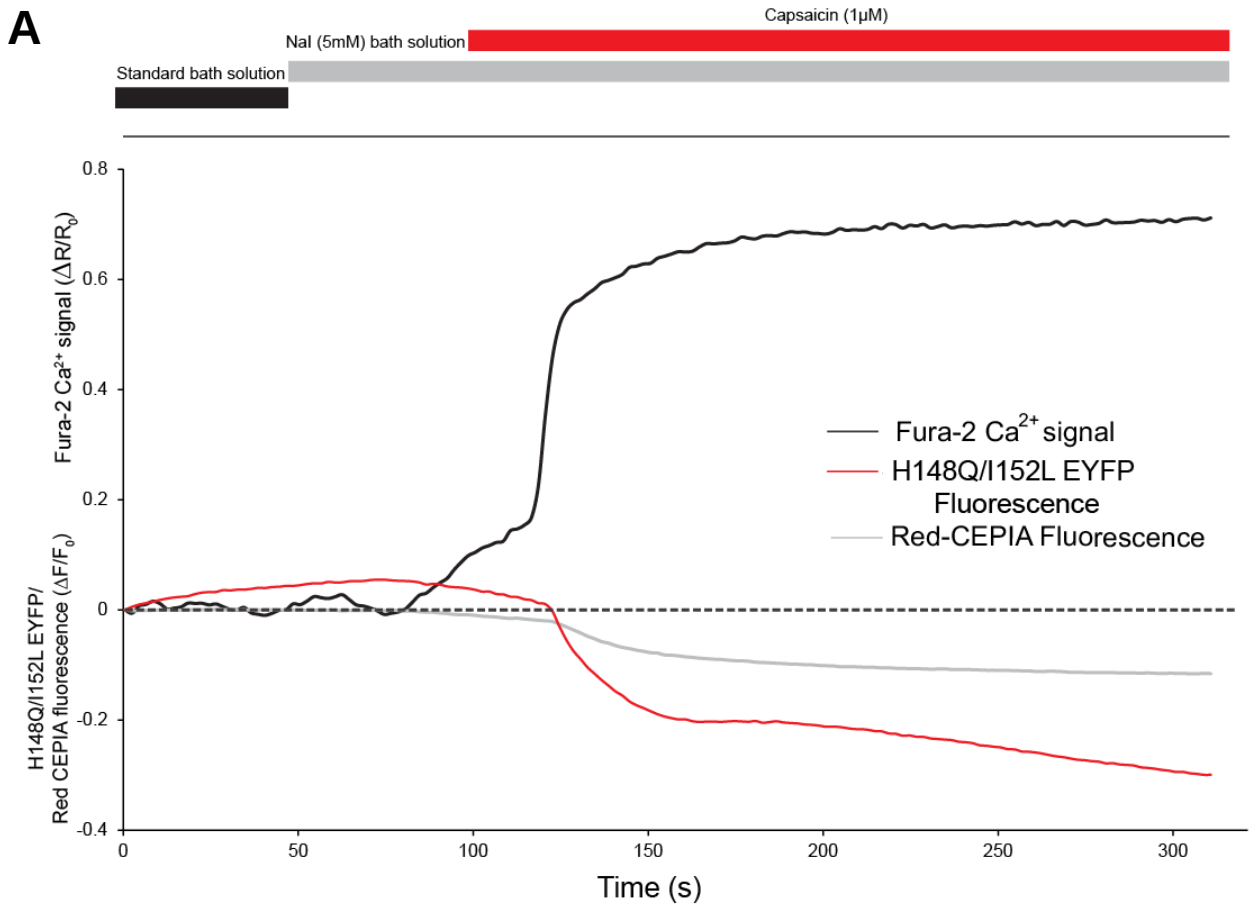
A
Capsaicin (1μM)
NaI (5mM) bath solution
Standard bath solution
Fura-2 Ca2+ signal (ΔR/R0)
H148Q/I152L EYFP/
Red CEPIA fluorescence (ΔF/F0)
0.8
0.6
0.4
0.2
0
-0.2
-0.4
0
50
100
150
200
250
300
Time (s)
Fura-2 Ca2+ signal
H148Q/I152L EYFP
Fluorescence
Red-CEPIA Fluorescence

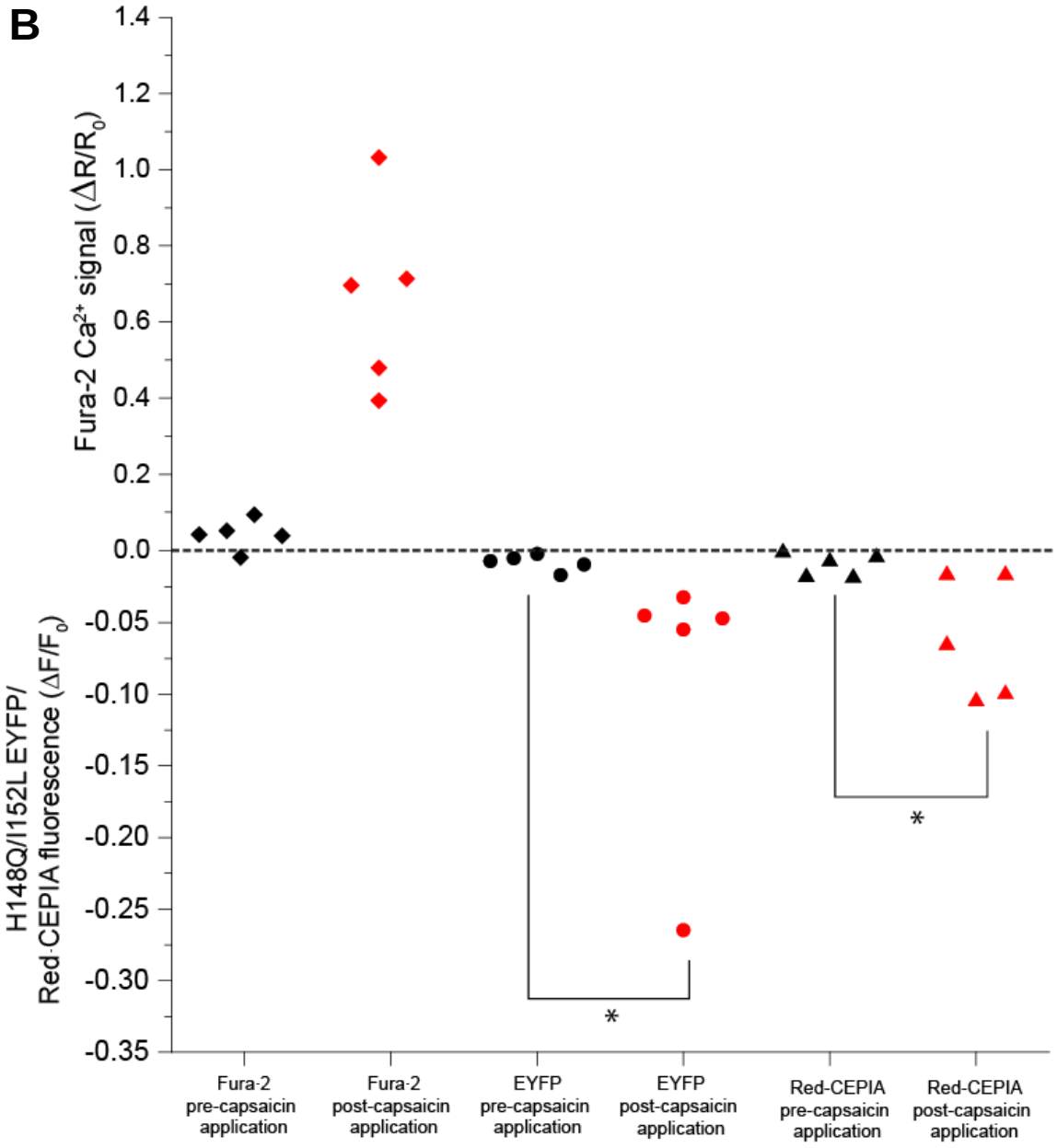

Figure 5.5: Triple imaging in CHO cells transfected with ANO1, TRPV1, EYFP (H148Q/I152L), Red-CEPIA and loaded with fura-2. (A) Representative traces from a single cell showing fura-2 signals, EYFP (H148Q/I152L) and Red-CEPIA quenching. (B) Individual cell data showing pre and post- capsaicin (1µM) application signals for fura-2, EYFP (H148Q/I152L) and red-CEPIA (n=5).* $p<0.05$

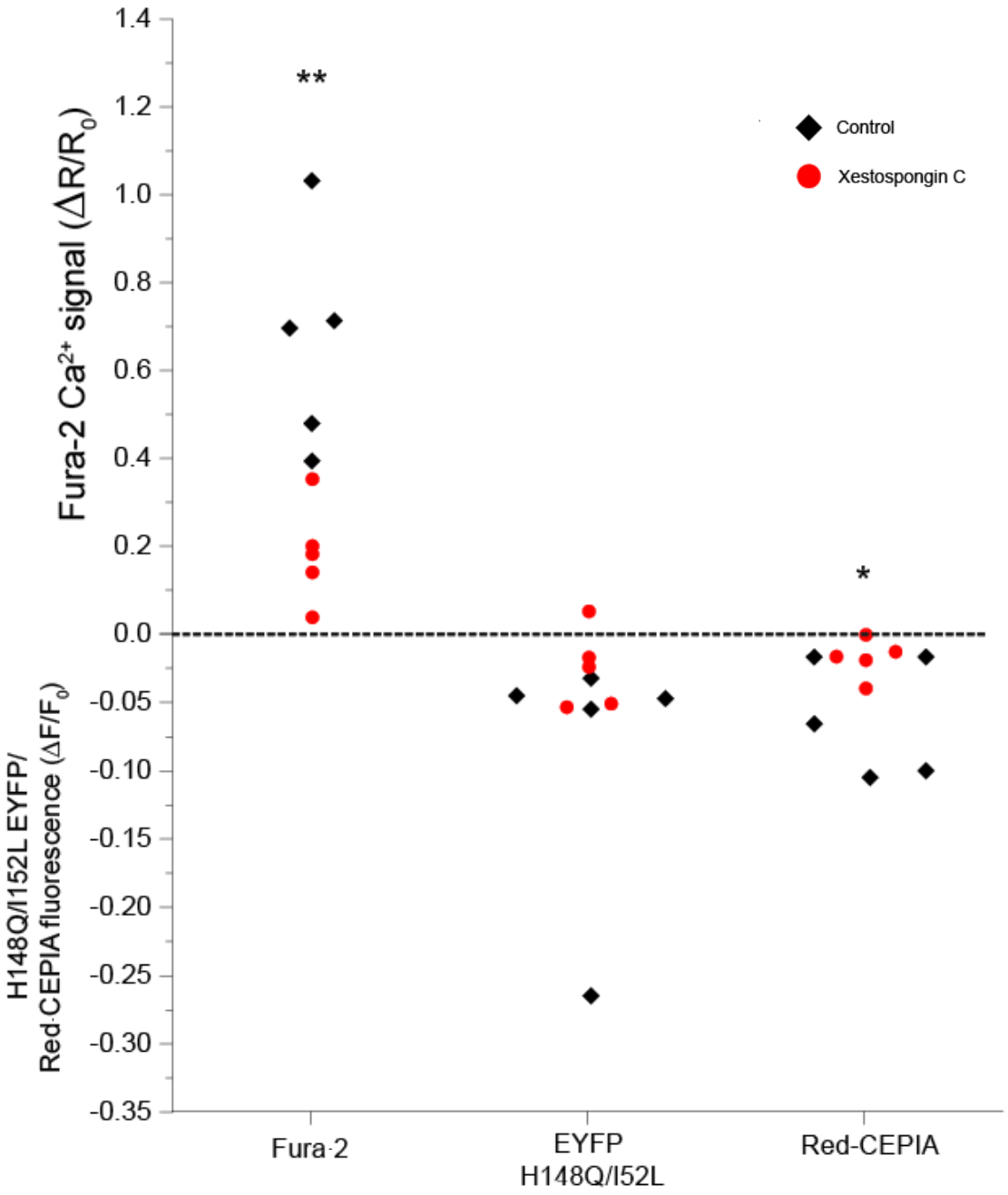

Figure 5.6: Comparison between capsaicin application (1µM) in control and xestospongin C pretreatment (1µM) triple imaging using CHO cells transfected with ANO1, TRPV1, EYFP (H148Q/I152L), Red-CEPIA and loaded with fura-2. Comparison between individual cell data showing responses for fura-2, EYFP (H148Q/I152L), Red-CEPIA after capsaicin (1µM) application for control (n=5) and xestospongin C pretreatment (n=5). * p<0.05, **p<0.01

5.3 Discussion

This chapter focuses on the activation of ANO1 by TRPV1 using our dual and triple imaging approaches. Our findings are in agreement with the work of other groups as TRPV1 is able to induce ANO1 activity which is seen as EYFP (H148Q/I152L) fluorescence quenching, in both DRG neurons and CHO cells. Another point that is important for the methodology being utilized is that there is generally a good correlation between the kinetics of Ca^{2+} signal and EYFP (H148Q/I152L) quenching. Fig. 5.1A depicts an experiment with a biphasic Ca^{2+} transient which dips before rising again; these dynamics are also visualized in the EYFP (H148Q/I152L) fluorescence quenching. The quenching re-engages after the brief cessation and follows the Ca^{2+} transient fairly closely. This effect demonstrates that this technique is suitable for studies of CaCC activation by Ca^{2+}.

5.3.1 TRPV1 is able to activate CaCC in DRG neurons

Considering the basis for ANO1 activation by TRPV1, it appears that such coupling would make sense physiologically as: (i) both channels are heat sensors with similar temperature thresholds; (ii) ANO1 is activated by Ca^{2+} while TRPV1 delivers Ca^{2+} to the cytosol; and (iii) activation of both channels will lead to pain signals. Therefore, functional coupling of these two channels may increase the dynamic range of heat sensitivity and the output signal of individual DRG neurons. The activation of ANO1 by TRPV1 can be superficially compared to the coupling of the K^+ channel Slo1 to VGCCs whereby Ca^{2+} influx through the latter channels is able to activate the former (Lu et al., 2007). Slo1 channels require close proximity or co-localisation with the Ca^{2+} source for activation to occur. The analogy is further supported by the fact that Slo1 channels also have relatively low Ca^{2+} sensitivity (hence the requirement for close proximity to the Ca^{2+} source, as is the case of ANO1). Importantly, physical association between ANO1 and TRPV1 has been suggested in the literature (Takayama et al., 2015), which supports the fact that some form of direct activation of ANO1 through TRPV1 Ca^{2+} is occurring.

5.3.2 TRPV1 engages the ER in order to activate CaCC

Interesting as this data may be, where does this fit in with the context of localised Ca^{2+} signalling in DRG neurons? As discussed and demonstrated in the previous chapter, ANO1 activation is coupled to IP_3R which facilitates the activation of this

poorly Ca^{2+}-sensitive channel. Ca^{2+} sources such as VGCCs that provide Ca^{2+} entry by other means are seemingly ineffective in activating ANO1, an effect possibly due to the spatial arrangements of the channels. The simplest explanation for TRPV1-induced EYFP (H148Q/I152L) fluorescence quenching would be that direct activation of ANO1 occurs via TRPV1 Ca^{2+} influx (Takayama et al., 2015). Somewhat counter-intuitively, the ability of TRPV1 to activate PLC-isoforms could provide another link between ANO1 activation by TRPV1 and this may involve the ANO1-IP_3R functional complex. This concept that a sizeable fraction of the Ca^{2+} generated by TRPV1 application is due to the internal Ca^{2+} store release will be quite startling to many but it becomes more understandable given the fact Ca^{2+} entry through TRPV1 under physiological conditions is relatively low as the majority of the TRPV1 current is carried by Na^{+} ions (Samways et al., 2008). This has been demonstrated in studies where the fraction of Ca^{2+} entering the cell through the channel itself has been found to be approximately 10%, even though the permeability of Ca^{2+} is greater than that of Na^{+} (Samways et al., 2008; Samways and Egan, 2011). This raises the question of whether Ca^{2+} influx through TRPV1 alone is sufficient for ANO1 activation observed in experiments. In any likelihood that this be the case, the only way that this could be achieved is through the proposed physical coupling between ANO1. Yet, the fact that capsaicin-induced EYFP quenching was almost abolished by thapsigargin strongly suggests that even if TRPV1 and ANO1 are in close proximity in DRG neurons, Ca^{2+} influx through TRPV1 alone is not sufficient to strongly activate ANO1 (Fig. 5.3). Nonetheless, TRPV1's ability in engaging ER Ca^{2+} stores fits nicely into the accepted notions of ANO1-IP_3R coupling in DRG.

To confirm that ER Ca^{2+} was involved in the ANO1-dependent EYFP quenching induced by capsaicin, we pioneered a quadruple-wavelength imaging approach using CHO cells transfected with the ANO1, TRPV1, EYFP (H148Q/I152L), Red-CEPIA and loaded with fura-2 (Fig. 5.5). The benefit of this approach is in that it allows measurement of ANO1 activity along with corresponding cytosolic Ca^{2+} levels and, simultaneously, to directly visualize Ca^{2+} dynamics of the ER. When Ca^{2+} is released from the ER, Red-CEPIA fluorescence intensity decreases, which is manifested by the downward deflection on the measurement trace. This ER-specific indicator was developed from cfGCaMP2, a genetically encoded Ca^{2+} indicator and includes ER localisation and retention sequences (Suzuki et al., 2014). The K_d of

CEPIA is 565μM in vitro making it suitable to measure the high Ca^{2+} concentrations found in the ER (Suzuki et al., 2014). CEPIA has been used in studies to visualize processes such as SOCE, thus upon stimulation of ER Ca^{2+} release with histamine in HeLa cells (Ca^{2+} free conditions), there was a strong reduction in the CEPIA signal which went back to baseline levels once Ca^{2+} was reintroduced (Suzuki et al., 2014). One study also used CEPIA when looking at EB3, a microtubule-associated protein and its involvement in IP_3R regulation. CEPIA imaging revealed that loss of EB3 leads to attenuation of IP_3R-dependent Ca^{2+} release in endothelial cells (Geyer et al., 2015). In our approach, we used CEPIA to test whether the ER is complicit in the quenching of EYFP (H148Q/I152L) mutant fluorescence when capsaicin is applied. The results confirmed this fact and definitively showed that ER Ca^{2+} is depleted by capsaicin application and this, together with the inhibition of capsaicin-induced anionic permeability by thapsigargin, strongly suggests that ER Ca^{2+} release is a major factor in TRPV1 activation of ANO1. Again this makes sense as there is already thought to be coupling between ANO1 and IP_3R, so in theory, anything that can drive this functional complex will be able to activate ANO1.

5.3.3 ANO1 activation via TRPV1 is mediated by IP_3R

It has been suggested that TRPV1 channels are present in the ER (Gallego-Sandin et al., 2009; Imler and Zinsmaier, 2014). This is thought to be part of a reserve pool of TRPV1 channels that are rapidly inserted into the membrane in response to various signals including NGF-induced phosphorylation and PKC activation (Zhang et al., 2005). These processes occur during inflammation where TRPV1 is known to be upregulated (Zhang et al., 2005; Stein et al., 2006). Apart from this reserve pool, functional TRPV1 channels are also present in the ER, however activation of these is thought to lead to cell death in some cases as seen in human lung cells (Thomas et al., 2007). Gallego-Sandin and colleagues showed expression of TRPV1 in the ER of DRG neurons and also demonstrated that capsaicin-induced Ca^{2+} release could be evoked without the need for extracellular Ca^{2+} in HEK293T cells (Gallego-Sandin et al., 2009). They also utilised an ER-targeted Ca^{2+}-indicator to show this and attributed this effect to the presence of TRPV1 in the ER however there was no attention paid to the PLC-mobilising ability of TRPV1, nor was this potential mechanism tested in this study. Our experiments using xestospongin C to block IP_3R show reduced levels of cytoplasmic Ca^{2+}, reduced levels of ER Ca^{2+} release and

also a reduction in EYFP (H148Q/I152L) mutant quenching in transfected CHO cells (despite not being significant), implicating IP_3R activity in the effects of TRPV1 activation (Fig. 5.6). The general hypothesis behind TRPV1-mediated ER Ca^{2+} release is that Ca^{2+}-dependent PLCδ activation is induced by the initial Ca^{2+} influx through TRPV1 (as well as TRPM8) (Rohacs et al., 2005; Lukacs et al., 2007; Yudin et al., 2011). Researchers have utilised PIP_2 binding domains of proteins (i.e. Tubby) to visualize the effects of PIP_2 translocation from the plasma membrane to the cytoplasm upon TRPV1 activation hence confirming activation of PLC (Lukacs et al., 2007; Rohacs et al., 2008). Ca^{2+}-independent PLC isoforms may also exist which could possibly be the reason for Ca^{2+} elevation seen in our Ca^{2+}-imaging experiments under extracellular Ca^{2+} free conditions.

Therefore, our results suggest that, whilst not completely ruling out ER-TRPV1 Ca^{2+} release, IP_3R-mediated Ca^{2+} release is most likely playing an important role, at least in the context of TRPV1-dependent ANO1 activation. Further research is required to elucidate whether ER-TRPV1 play any role in ANO1 activation.

To summarize, in this chapter a functional relationship between ANO1, TRPV1 and IP_3R has been demonstrated. Therefore, the next logical step to take is to study possible proximity between these proteins in DRG neurons to provide further insight into the mechanisms underlying ANO1 activation.

Chapter 6: Investigating arrangements of ANO1, TRPV1 and IP_3R1 in DRG neurons using biochemical and super-resolution imaging approaches

6.1 Introduction

Ion channels function to control the excitability of neurons within the nervous system however it is not always a case of single ion channels working alone to achieve this. In various instances, ion channels may form into multi-protein complexes comprising of different ion channels and other important molecules to work together and operate in a myriad of pathways to alter neuronal functionality (Marsh and Teichmann, 2015). This results in synergistic interplay between channels that results in either activation of adjoining protein channels or the initiation of signalling cascades which may lead to changes in cellular activity (Marsh and Teichmann, 2015). However, it must be pointed out that in many instances it is unknown as to how the interplay may result in the effect seen. Below I will discuss some examples of such complexes involving our proteins of interest, ANO1 and TRPV1.

6.1.1 TRPV1-TRPA1

TRPA1 is the sole member of the TRP Ankyrin (TRPA) subfamily of proteins. The denotation of the A comes from the 14 ankyrin repeats that are found in this channel. TRPA1 is expressed in primary afferent fibers of sensory ganglia (DRG, TG and Nodose ganglia- NG). Functionality of TRPA1 involves a role in the sensing of cold stimuli (Kwan et al., 2006). Heterologous TRPA1 expression in CHO cells showed channel activation at temperatures below 15°C as well as by compounds such as mustard oil, methysalicylate and gingerol (Kwan et al., 2006). Furthermore, KO of TRPA1 in mice was found to severely impair temperature sensitivity to cold stimuli and reduce cold hyperalgesia (Story et al., 2003; Obata et al., 2005; Kwan et al., 2006). It has been established that TRPA1 and TRPV1 can reciprocally affect the activity of the other channel through secondary messenger cascades (Weng et al., 2015). Moreover, TRPA1 and TRPV1 are found in heteromeric complexes in various cells including sensory ganglia (Akopian, 2011) and cardiac myocytes (Andrei et al., 2016). This is somewhat perplexing, especially in sensory afferents with these proteins being on opposite ends of the temperature-sensitivity scale. Using various techniques, Staruschenko and colleagues demonstrated the interaction between TRPV1 and TRPA1 using co-immunoprecipitation studies in CHO cells transfected with the proteins and in TG neurons from both rats and mice (Staruschenko et al.,

2010). A Förster resonance energy transfer (FRET) based TIRF microscopy approach was also employed by this group to visualise the interaction between TRPV1 and TRPA1 at the plasma membrane. It was revealed that the FRET efficiency between TRPV1 and TRPA1 is similar to that seen between TRPV1 and TRPV1 (labelled with the different fluorescent proteins). This interaction seems to provide TRPA1 with the outward-rectification property which is reduced when TRPV1 is lacking which suggests that the activity of TRPA1 is reigned in due to the presence of TRPV1 (Staruschenko et al., 2010). Recently, evidence emerged to suggest that the interaction between TRPV1 and TRPA1 is regulated by an adapter protein TMEM100, which prevents an interaction between these 2 proteins (Weng et al., 2015). KO of this TMEM100 'adapter' protein causes a tight interaction between TRPV1 and TRPA1, which in turn inhibits TRPA1. Interestingly, KO of TMEM100 in mouse models only affects TRPA1-related pain behaviours, not TRPV1 (Weng et al., 2015). Furthermore, TMEM100 expression in CHO cells with TRPV1 and TRPA1 enhances TRPA1 activity. One critical finding of this study was the requirement of a specific site (3 amino acids) within TMEM100 that prevents the interaction between TRPV1 and TRPA1. Administration of a TMEM100 cell-permeable peptide incorporating the triple mutation attenuated TRPA1 activity whilst alleviate pain in an animal model (Weng et al., 2015).

6.1.2 ANO1-ERM

Amongst the interactions of ANO1 with different proteins, there is also scope for potential interactions between ANO1 and various aspects of the cytoskeleton. The so called 'ERM' proteins (ezrin, radixin, moesin) along with Ras homolog gene family, member A (RhoA) are involved in coordination of the cortical cytoskeleton by linking actin filaments to plasma membrane proteins (Perez-Cornejo et al., 2012; Solinet et al., 2013). ERM proteins play important roles in producing specialised and distinct cortical domains i.e. apical brush border of the small intestine (McClatchey and Fehon, 2009; McClatchey, 2012) and also modulate dynamic cellular events such as mitosis, migration and junctional remodelling (McClatchey and Fehon, 2009; Fehon et al., 2010; McClatchey, 2012). Binding of ANO1 to ERM proteins may signify a role for these proteins in ANO1 activity, expression and trafficking. For example, moesin knockdown in HEK293 cells co-transfected with ANO1 and moesin leads to reduced ANO1 current amplitude (Perez-Cornejo et al., 2012). This also ties

in well with other research, which shows reduced ANO1 activity when actin is disrupted with cytochalasin-D A (Tian et al., 2011). The cytoskeleton may well play a significant role in ANO1 activity. Moesin expression at the membrane is increased when ANO1 is co-expressed which suggests that ANO1 may play a role in organising the cytoskeleton (Perez-Cornejo et al., 2012). Interestingly, oocyte microvilli length is also increased in the presence of ANO1 which is independent of its activity (Courjaret et al., 2016). It has been proposed that ANO1 may well be a means to further strengthen the PM-cytoskeleton link by reinforcing the scaffold between these aspects of the cell (Courjaret et al., 2016).

6.1.3 ANO1-EGFR

In diseases states such as cancer, ANO1 has been implicated in playing a role in development of tumours by inducing cell signalling cascades to promote tumour growth (Britschgi et al., 2013; Qu et al., 2014; Jia et al., 2015). Epidermal growth factor receptor (EGFR) is a known instigator of cell proliferation, tumour growth and metastasis in head and neck squamous cell carcinomas (HNSCCs) (Cassell and Grandis, 2010; Bill et al., 2015). EGFR produces its effects through phosphorylation of tyrosine residues of the receptor, which in turn activates the mitogen-activated protein kinase (MAPK) or PI3K-activated protein kinase B (AKT) pathways. These cascades then cause the cell to undergo oncogenic changes (Bill et al., 2015). In 90% of HNSCCs, EGFR is found to be upregulated (Yarden, 2001). ANO1 is also overexpressed in various cancers including HNSCCs and breast cancers and has been found to enhance EGFR activity (Britschgi et al., 2013; Bill et al., 2015). In breast cancer, ANO1 activity is essential for cell viability as well as enabling EGFR activity as KO of ANO1 resulted in reduced tumour growth and maintenance in vivo (Britschgi et al., 2013). It has been proposed that ANO1 is able to regulate EGFR activity through an imbalance of intracellular ion homeostasis (Horiuchi et al., 2007; Bill et al., 2015). However it seems as if the presence of ANO1 is sufficient for stimulation of proliferation, independent of its anion channel activity, as amongst several CaCC inhibitors tested, only CaCCinh-A01, which promotes ANO1 degradation, was able to reduce proliferation (Bill et al., 2014). Interestingly, it has recently been discovered that ANO1 and EGFR form complexes in HNSCCs and in heterologous expression systems which was revealed using an unbiased proteomics screen and co-immunoprecipitation experiments (Bill et al., 2015).

6.1.4 Orai1-STIM1-TRPC1-$Ca_v1.2$

There are plenty of other examples of ion channels apart from ANO1 and TRPV1 that can co-assemble. SOCE is a mechanism which involves numerous protein interactions between protein components. Ca^{2+} removal from the internal Ca^{2+} stores after stimulation of cells causes STIM1 and Orai proteins to interact and induce replenishment of the stores (Prakriya and Lewis, 2015). Another protein often implicated in this process is TRPC1 (Liu et al., 2003; Ambudkar, 2007; Liu et al., 2007). Orai1-dependent Ca^{2+} entry after STIM1 activation leads to insertion of TRPC1 into the PM (Cheng et al., 2011). TRPC1 is then able to partake in Ca^{2+} entry in a manner similar to Orai1 (Liu et al., 2003; Ambudkar, 2007; Liu et al., 2007). However, TRPC1 is dependent on Orai1 activity; demonstrated using Orai1 knockdown which led to inhibition of TRPC1-induced Ca^{2+} entry in a human salivary gland (HSG) cell line (Cheng et al., 2011). Orai1 and TRPC1 have been shown to interact and form puncta upon store-depletion in TIRF experiments and immunoprecipitation studies (Ong et al., 2007; Cheng et al., 2011). Furthermore, both of these distinct processes require STIM1 mediation (Ong et al., 2007), as demonstrated through co-expression of a mutant form of STIM1, which caused loss of SOCE and abolishment of the Orai1-TRPC1 interaction (Cheng et al., 2011).

In VSMCs, vasoreactive agonists such as serotonin are able to generate an increase in Ca^{2+} leading to vessel contraction (Avila-Medina et al., 2016). There are 2 stages to this, one involving SR Ca^{2+} release and the second involving $Ca_v1.2$ activation and Ca^{2+} influx (Catterall, 2012; Arias-Calderón et al., 2016; Brozovich et al., 2016). Interestingly, L-type VGCCs also interact with Orai1 and TRPC1 in VSMCs and aortic ring preparations (Avila-Medina et al., 2016). It has been demonstrated that agonist stimulation (i.e. serotonin) causes Ca^{2+} release from the SR, which in turn causes SOCE (Brozovich et al., 2016). This Ca^{2+} depolarises the cells further causing activation of L-type VGCCs in both VSMCs and rat myometrium (Bolotina, 2012; Noble et al., 2014).

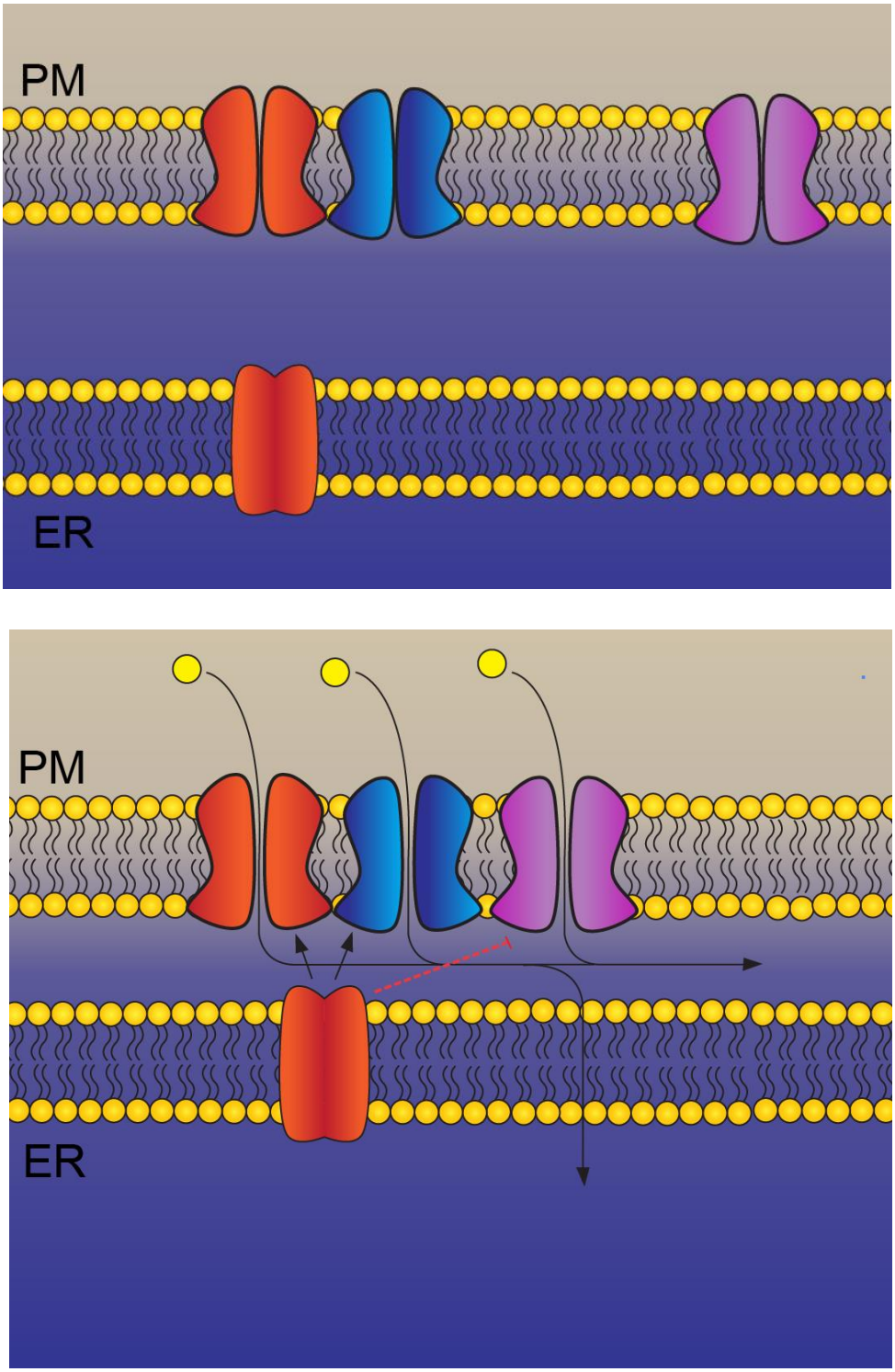

Figure 6.1: Orai1-TPRC1-STIM1-Ca_v1.2 macromolecular complexes in VSMCs. Upper panel: Resting state of channels. Lower panel: Agonist stimulation leads to depletion of ER Ca^{2+}, inducing SOCE. Orai1 (orange channel in PM) and TRPC1 (blue channel) activation is mediated by STIM1 (orange protein in ER), leading to ER Ca^{2+} store repletion. The impending Ca^{2+} entry (yellow circles) causes a slight depolarisation which activates Ca_v1.2 to cause vessel contraction. STIM1 also modulates Ca_v1.2 to avoid Ca^{2+} overload. Figure based on (Dionisio et al., 2015).

Additionally, both Orai1 and TRPC1 are in close proximity to L-type VGCCs in unstimulated cells as demonstrated through PLA and upon agonist application, more PLA puncta are seen (Avila-Medina et al., 2016). Overall, a macromolecular signalling complex is formed which incorporates STIM1, Orai1, TRPC1 and L-type VGCCs. SOCE occurs through Orai1 and TRPC1, which cluster together upon depletion. Interaction of these proteins is mediated by STIM1. Furthermore, STIM1 has also been known to inhibit L-type VGCCs which suggests involvement of STIM1 prevents issues such as Ca^{2+} overload and regulates cellular excitability (Dionisio et al., 2015) (Fig. 6.1).

6.1.5 Studying protein-protein interactions

I have explained some different scenarios where proteins interact with each other to provide various functions. The majority of techniques used to identify these interactions is through molecular biology (i.e. immunoprecipitation studies, Western blots, PLA etc). Other ways to study protein-protein interactions include fluorescent microscopy techniques, for example FRET and TIRF microscopy (Staruschenko et al., 2010). Fluorescence microscopy is an extensively utilized technique in research to date allowing vast advantages such as the non-invasive nature and ability to use molecular labelling with high specificity (Henriques et al., 2011). Despite this there are some restrictions which limit the ability to obtain certain data. One issue is the inability of fluorescent microscopy to deliver high enough optical resolution to allow visualisation of individual molecules in the nanometer range or protein-protein interactions. Light disseminates as a wave and focussing this on a small area will only allow a finite sized image to be resolved, which is approximately half of the wavelength propagated from the microscope (Henriques et al., 2011). The maximal resolution that fluorescent microscopy can provide is approximately 200nm transversely and 500nm longitudinally due to the size of the wave. In terms of protein-protein interactions, or looking at proteins with close proximity, fluorescent microscopy is unable to resolve the location of the target molecules if they are closer to each other than these limits. This phenomenon is referred to as diffraction limited resolution and therefore to be able to obtain higher/finer resolution, sub-diffraction limit imaging must be developed. Super-resolution imaging techniques such as STORM provide the opportunity to study protein-protein interactions in the nanometer range (see chapter 2 for details regarding STORM).

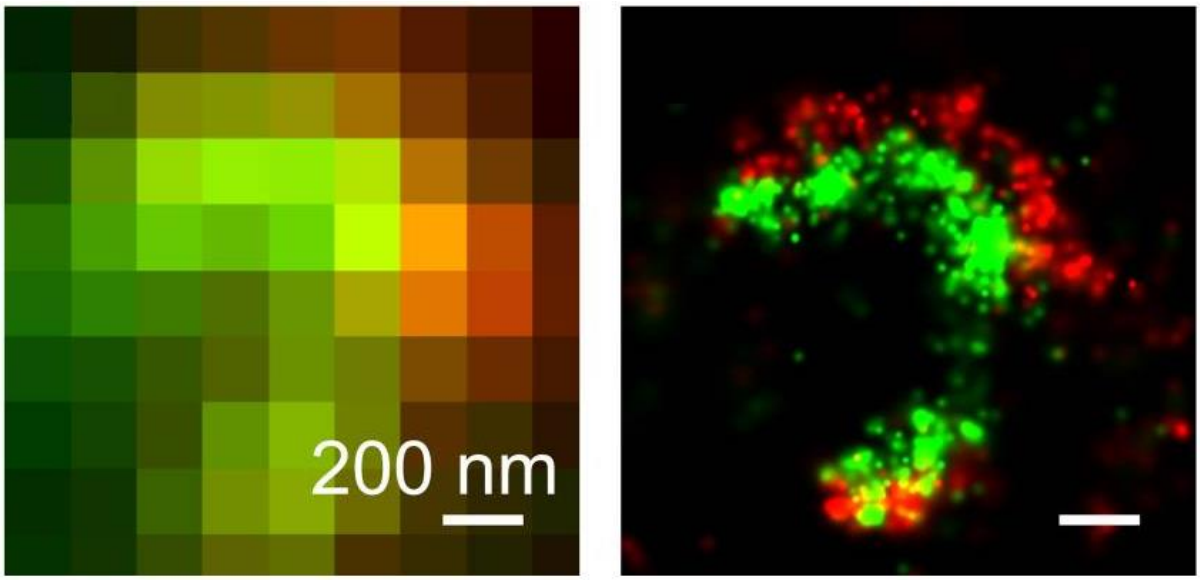

Figure 6.2: Use of STORM in the localisation of proteins. Use of STORM in resolving Bassoon (red) and Homer1 (green) at pre- and post-synaptic nerve terminals, respectively in main olfactory bulb glomeruli in mice. Left panel demonstrates conventional microscopy image and right panel demonstrates STORM-resolved image. Figure adapted from (Dani et al., 2010).

6.1.6 Use of STORM in localisation of proteins

STORM has been able to successfully label and resolve individual actin filaments in COS-7 fibroblast and BSC-1 epithelial cells as well as allowing the visualisation in 3D (Xu et al., 2012). It was also shown that the actin filaments are separated in 2 layers which are denser in the dorsal region of the cells compared to the ventral portion. Fascinatingly, the effects of actomyosin perturbing drugs cytochalasin D and latrunculin A can be clearly visualised in the STORM image which reveal the presence of much less dense regions of actin and aggregate formation (Xu et al., 2012). Voids were also formed in the dorsal region of the cells and were clearly detected using STORM (Xu et al., 2012). Chemical synapses of neurons have also been resolved using STORM (Dani et al., 2010). Two scaffold proteins Bassoon and Homer1 found on presynaptic and postsynaptic membranes, respectively, were successfully resolved by STORM providing clear and distinct sections surrounding the synaptic cleft in mouse olfactory bulb slice preparations (Fig. 6.2). The size of the synaptic cleft is approximately 20nm (Zuber et al., 2005) and under conventional fluorescent microscopy, the resulting image would be a pixelated amalgamation of colours; the results therefore demonstrate the high resolution that STORM is able to ascertain (Dani et al., 2010). More than 2 probes can also be used to target proteins in STORM. Three-colour STORM was used to visualise the location of other scaffold proteins relative to Bassoon and Homer1 such as a scaffold protein structurally related to Bassoon called Piccolo (Dani et al., 2010). This was found at a similar distance from the presynaptic terminal as Bassoon whereas RIM1, which plays a role in synaptic release was found close to the membrane itself (Dani et al., 2010; Kaeser et al., 2011). This is evidence that small differences in protein localisation can be detected with the high accuracy of STORM.

Recently STORM has been utilised to look at the interactions between different proteins with protein A-kinase-anchoring protein (AKAP) 150 in neurons (Zhang et al., 2016b). This chaperone protein is able to assemble and organise various proteins into intimately associated multi-channel complexes. Homomeric $K_v7.2$ and 3 and 2/3 multimer channels form tight complexes with AKAP150 whereas $K_v7.1$ channels do not associate with AKAP150 when co-transfected in CHO cells (Zhang et al., 2016b). It was also demonstrated in superior cervical ganglia neurons that not all GPCRs interact with AKAP150 as there was association between AKAP150 and

muscarinic M_1 receptors (M_1R) but not with B_2R (Zhang et al., 2016b). This array of interactions revealed by STORM make sense as it has been established that M_1R activation leads to 'M-current' (combination of K_v7 channel currents) inhibition through AKAP150 signalling (Hoshi et al., 2003; Zhang et al., 2011a). However, the most interesting discovery was the fact that AKAP150 prefers $K_v7.2/3$ multimers over other K_v7 subtypes. This data was supplemented with this groups own intricate clustering analysis that allows the proportion of genuine 'clusters' that are formed between 2 or more proteins using stringent parameters to assess what contributes an actual cluster (Zhang et al., 2016b). Interestingly, TRPV1 and $K_v7.2/3$ were shown to interact physically in DRG neurons and it has been established that TRPV1 activation is also able to inhibit the M-current (Zhang et al., 2011b). Zhang and colleagues also looked at this interaction and found clustering between these proteins only occurred when AKAP150 was present. It was also demonstrated in NG neurons that TRPV1 and L-type VGCCs are able to form complexes with AKAP150 (Zhang et al., 2016b). Taken together these various interactions between these proteins prove how effective STORM can be in visualising not only structural data but also provide information regarding protein-protein interactions for more than 2 proteins.

6.2 Results

After demonstrating the various functional aspects of ANO1 and TRPV1 in the previous chapter, we decided to change our approach and focus on the localisation of these proteins in DRG neurons to elucidate potential mechanisms by which these proteins may be functionally coupled. In previous studies looking at the relationship between ANO1 and TRPV1, it has been proposed through biomolecular studies that at least some ANO1 and TRPV1 molecules are in physical association with each other when expressed in DRG (Takayama et al., 2015). We decided to look at this potential association in DRG neurons using two alternative localisation techniques: an *in situ* proteomics approach known as PLA and the super resolution microscopy technique discussed above, STORM.

As both, PLA and STORM are antibody-based techniques, we first performed immunostaining in combination with confocal microscopy to confirm the validity of the antibodies to be used in the experiments. All antibodies were previously validated by our lab (ANO1 and IP_3R1) and Zhang and colleagues (TRPV1) (Jin et al., 2013; Zhang et al., 2016b). ANO1 and TRPV1 were shown to co-stain with each other in DRG cultures (Cho et al., 2012; Takayama et al., 2015) and provided clear signal in our immunostainings, whereas secondary antibodies only (no primary antibodies) provided no signal (Fig. 6.3A and B). We also checked the IP_3R1 antibody and it also showed positive staining (not shown). Next, we attempted triple staining with all 3 antibodies however, this was unsuccessful due to poor signal with our third-secondary antibody (Alexa-633). Therefore we decided to perform IP_3R1 staining with ANO1 and found both conditions provided positive staining as well as no staining when primary antibodies were not included (Fig. 6.4A and B). Despite this positive staining, we were unable to confirm whether there was close proximity between ANO1 and IP_3R1 using confocal microscopy due to insufficient resolution (see above). Similarly, despite signals from ANO1 and TRPV1 forming overlapping puncta, there was no conclusive answer as to whether there is association of these proteins in these puncta, again, due to the insufficient resolution of confocal microscopy.

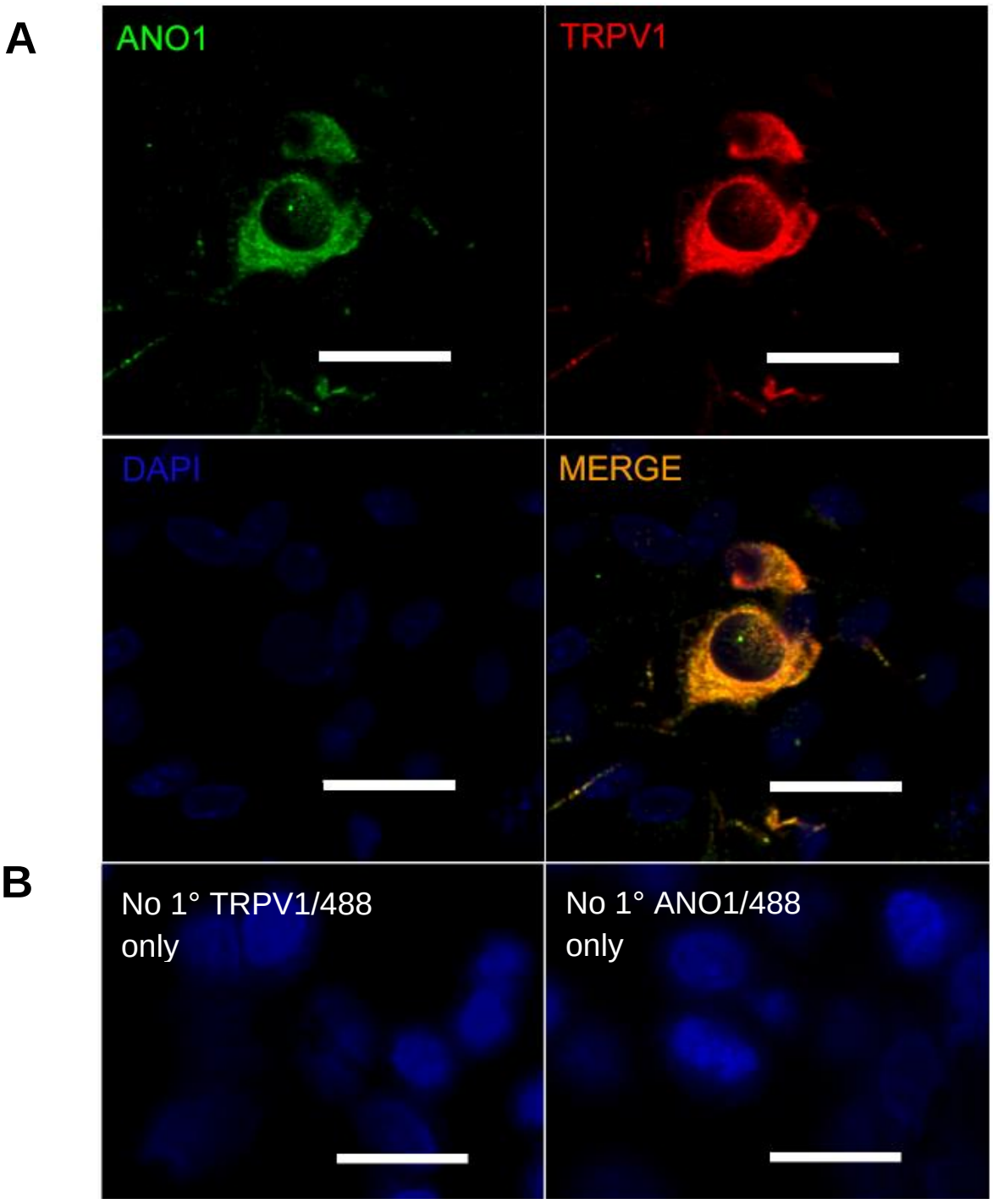

Figure 6.3: Immunostaining of DRG neurons with ANO1 and TRPV1 antibodies in small-diameter DRG neurons. (A) ANO1 and TRPV1 co-immunostaining. Top left panel; Positive ANO1 staining in a DRG neuron with Alexa 488 secondary antibody. Top right; Positive TRPV1 staining in a DRG neuron with Alexa 555 secondary antibody. Bottom left; DAPI staining showing the presence of glial cells. Bottom right; Merged staining consisting of ANO1, TRPV1 and DAPI (B) Negative control experiments with no primary antibody present (secondary only). Left; No primary TRPV1 antibody. Right; no primary ANO1 antibody (Alexa 488 secondary only). Scale= 20μm for all images

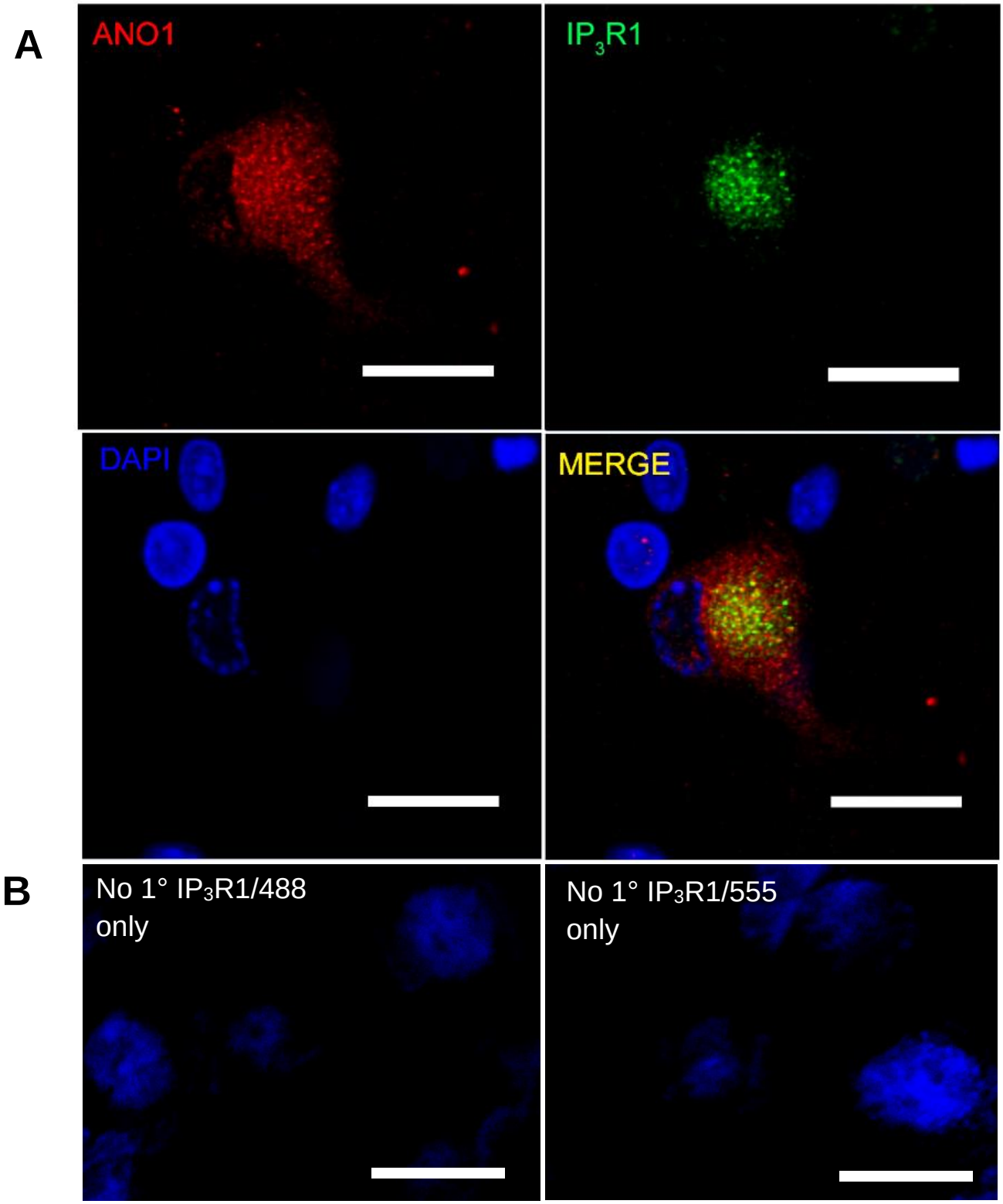

Figure 6.4: Immunostaining of DRG neurons with ANO1 and IP₃R1 antibodies in small-diameter DRG neurons. (A) Top left panel; Positive ANO1 staining in a DRG neuron with Alexa 555 secondary antibody. Top right; Positive TRPV1 staining in a DRG neuron with Alexa 488 secondary antibody. Bottom left; DAPI staining. Bottom right; Merged staining consisting of ANO1, IP_3R1 and DAPI (B) Negative control experiments with no primary IP_3R1 antibody present (Left panel Alexa 488 secondary only; Right panel Alexa 555 secondary only). Scale= 20μm for all images.

The next step was to perform PLA between the various pairs of proteins. To validate the PLA approach we performed positive and negative controls utilising our protein of interests. For the negative control we performed PLA between TRPV1 and the μ-opioid receptor (MOR). Both proteins are present at the plasma membrane of many nociceptors (Fields et al., 1980; Endres-Becker et al., 2007) but, to the best of our knowledge, were never shown (or suggested) to physically interact. Yet, MOR has been shown to modulate the activity of TRPV1 in CFA-induced paw inflammation of mice through an intracellular signalling cascade (Breese et al., 2005; Endres-Becker et al., 2007). There was also an upregulation of both proteins in inflammatory pain models (Endres-Becker et al., 2007). Initially, immunostaining was performed for both MOR and TRPV1, which revealed the presence of both MOR and TRPV1 in many DRG neurons (Fig. 6.5A). PLA was then carried out between MOR and TRPV1; analysis of the PLA-treated samples showed no positive signals which suggested that despite the presence of both proteins in DRG neurons, they are further than 40nm from each other and therefore there is not any physical association (Fig. 6.5B).

As a positive control for the PLA investigations, we also decided to visualise a single protein with two antibodies raised in different species. Due to it being the focal point of our studies, ANO1 was used for this control. ANO1 antibodies used were Santa Cruz anti-goat and Abcam anti-rabbit detected by the ‘plus’ and ‘minus’ PLA probes, respectively (Fig. 6.6). In this approach both probes are expected to bind to the same protein and, thus, a positive ‘proximity’ signal is expected. The results indeed showed robust puncta for ANO1-ANO1, demonstrating that the assay reliably recognises the proximity between two probes attached to their target protein(s).

We then used PLA to test the proximity of ANO1 and TRPV1 in small-diameter DRG neurons. PLA analysis showed that there was positive signal for this pair in 40 cells that we imaged meaning that the proteins are within 40nm of each other in these cells (Fig. 6.7A and E). Due to our findings in the previous chapter, which indicated the ability of TRPV1 to activate IP_3R as part of its response and in the literature which states the presence of TRPV1 in lipid rafts (Szoke et al., 2010) where GPCRs and ANO1 are also found, we next tested possible proximity between TRPV1 and IP_3R1 (Fig. 6.7B and E). PLA analysis again showed positive results however it must

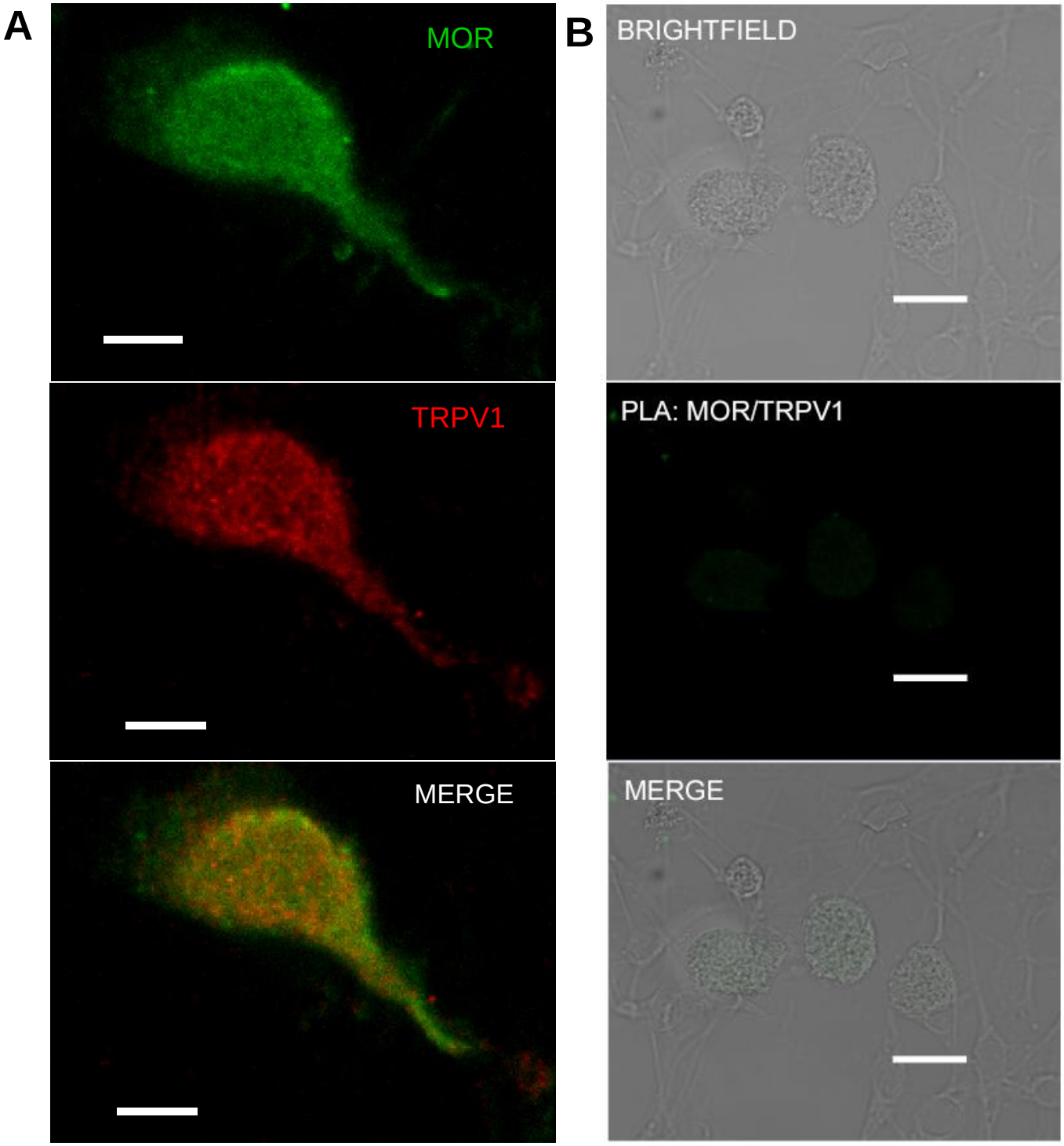

Figure 6.5: Co-localisation of MOR and TRPV1 in small-diameter DRG neurons. (A) MOR and TRPV1 co-immunostaining. Top left panel; Positive MOR staining in a DRG neuron with Alexa 488 secondary antibody. Middle left panel; Positive TRPV1 staining in a DRG neuron with Alexa 555 secondary antibody. Bottom left panel; Merged staining consisting of MOR and TRPV1. Scale= 10µm (B) MOR-TRPV1 PLA. Top right panel; brightfield image. Middle right panel; PLA (green) between MOR and TRPV1 showing no puncta. Bottom right panel; Merge between brightfield and PLA (green) channels. Scale= 20µm for all images.

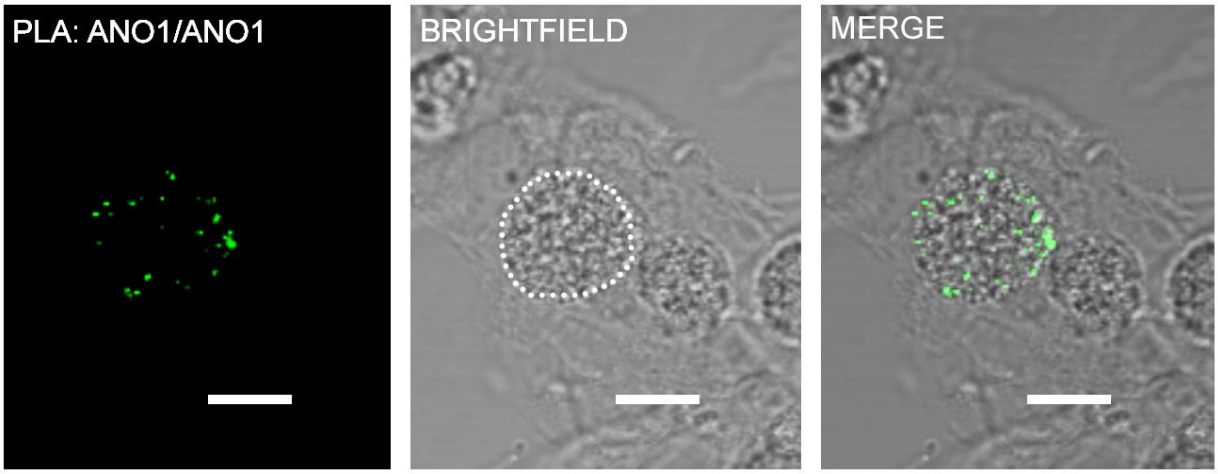

Figure 6.6: Positive PLA control. ANO1-ANO1 PLA. Left panel; Brightfield image. Middle panel; PLA (green) between 2 anti-ANO1 (goat and rabbit) primary antibodies. Right panel; Merge between brightfield and PLA channels. These experiments were performed by Gabriel Hoppen. Scale= 10µm for all images.

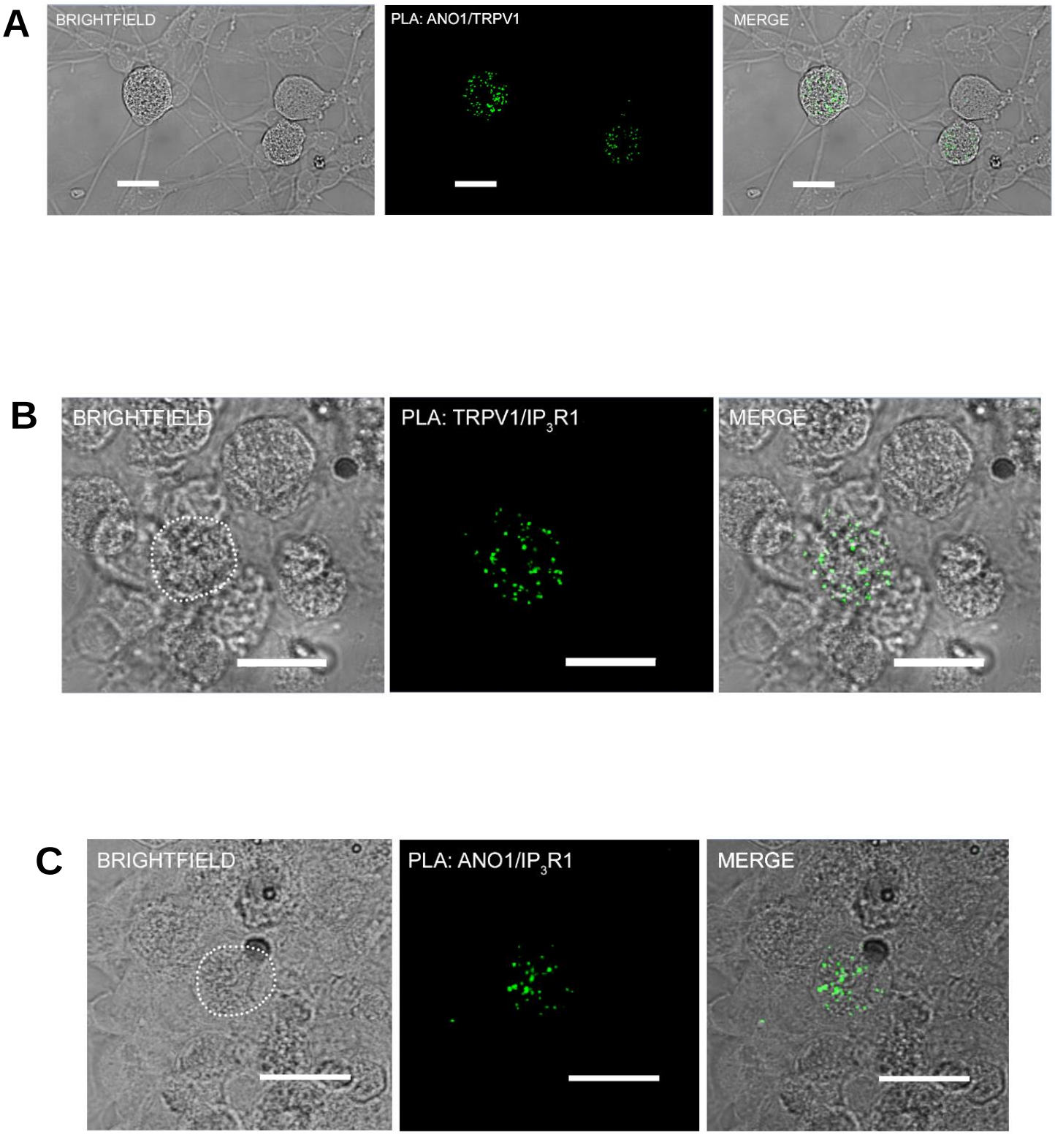
A
BRIGHTFIELD
PLA: ANO1/TRPV1
MERGE
B
BRIGHTFIELD
PLA: TRPV1/IP3R1
MERGE
C
BRIGHTFIELD
PLA: ANO1/IP3R1
MERGE

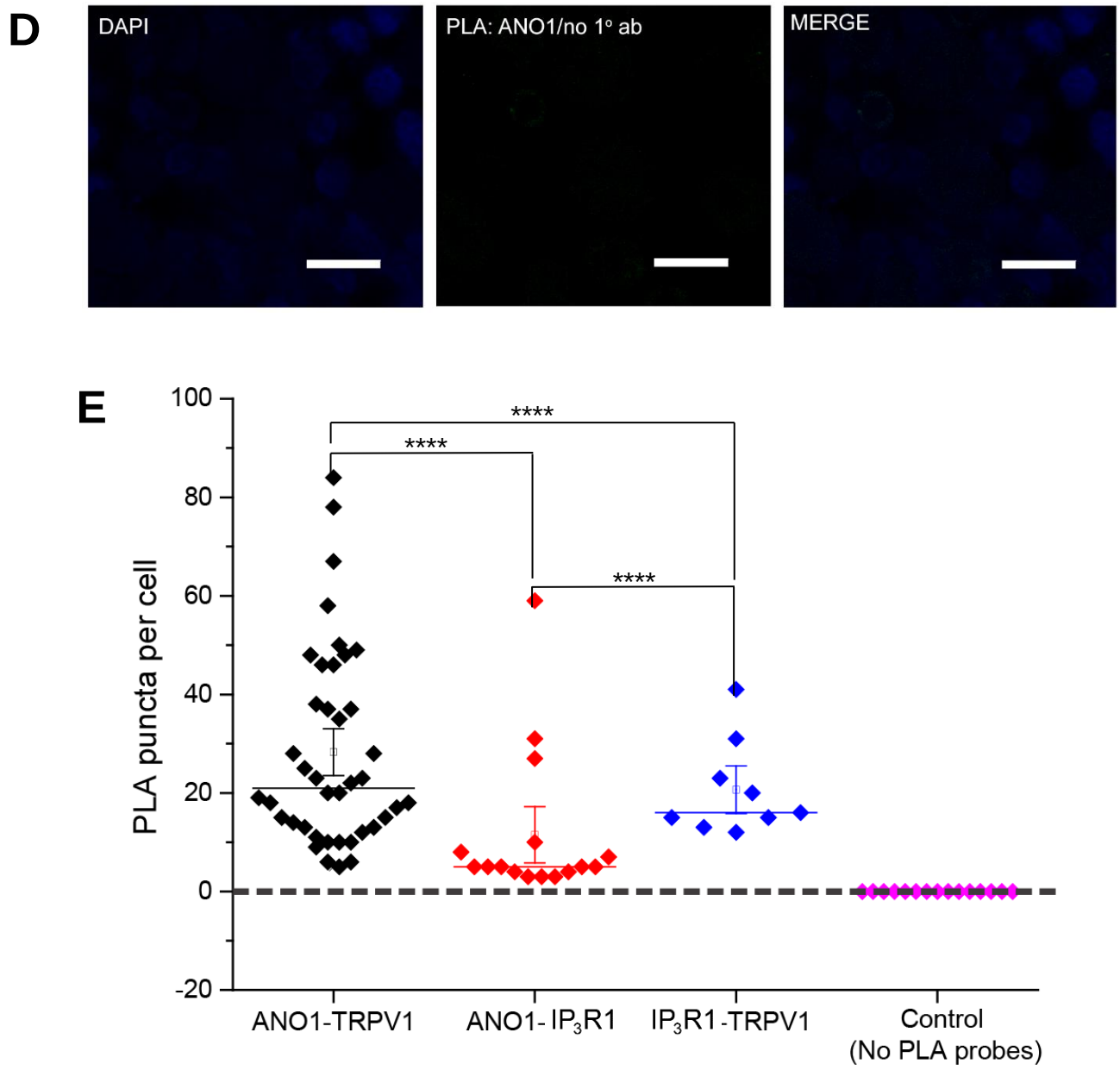

Figure 6.7: PLA between ANO1, TRPV1 and IP$_3$R1. (A) PLA between ANO1 and TRPV1 in small diameter DRG neurons. Left panel; brightfield image. Middle panel; PLA between ANO1 and TRPV1 (green). Right panel; merge between brightfield and PLA channel. (B) PLA between TRPV1 and IP$_3$R1 in small diameter DRG neurons. Left panel; brightfield image. Middle panel; PLA between TRPV1 and IP$_3$R1 (green). Right panel; merge between brightfield and PLA channel. (C) PLA between ANO1 and IP$_3$R1 in small diameter DRG neurons. Left panel; brightfield image. Middle panel; PLA between ANO1 and IP$_3$R1 (green). Right panel; merge between brightfield and PLA channel. (D) Single primary antibody PLA. Left panel; DAPI staining. Middle panel; PLA with single primary ANO1 only (no pair of primary antibodies) showing no signal. Right panel; Merge between DAPI and PLA channels. (E) PLA pair puncta per cell analysis. Plot showing the number of puncta detected per cell for different protein pairs. Scale= 20µm for all images. ****p<0.0001

be noted that there were less puncta in these cells as compared to that between ANO1 and TRPV1 (only 9 cells showed puncta compared to 40 for TRPV1 and ANO1). Furthermore, the average puncta per cell that we identified were greater for ANO1 and TRPV1 (28.23) compared to TRPV1 and IP_3R (20.6) ($p<0.0001$, Mann Whitney). This confirmed that TRPV1 and IP_3R1 are indeed in close proximity to each other in some cells. We also tested the proximity of ANO1 and IP_3R1 (Fig. 6.7C and E). Even though we have already shown close association of these proteins in our previous study (Jin et al., 2013), we have repeated these experiments to demonstrate reproducibility. As previously, there was positive signal between this pair of proteins, however, this was significantly less than that found in ANO1-TRPV1 PLA (16 cells, average 11.5 puncta per cell, $p<0.0001$, Mann Whitney). Even though, there were more PLA-positive cells for ANO1 and IP_3R1 compared to TRPV1 and IP_3R1, the number of puncta per cell are lower ($p<0.0001$, Mann Whitney). Overall, this indicates that this trio of proteins may form complexes. ANO1 and TRPV1 appear to display more robust association, as compared to that between plasmallemal and ER proteins (Fig. 6.7E).

As an additional negative control, we omitted the TRPV1 primary antibody (leaving only the ANO1 primary antibody) and visualised no signal, demonstrating that 'by chance' proximity of the PLA probes is negligible (Fig. 6.7D).

To confirm our results, we decided to analyse these protein pairs using two-colour STORM technique. We have shown that TRPV1 and MOR show no positive signals for PLA, which suggests that they are not in close proximity despite the presence of both proteins in DRG neurons. To test the STORM methodology and visualise potential protein-protein interactions, these 2 proteins were also used as negative controls for initial investigations. Immunostaining was performed as previously discussed but the secondary probe was changed to include the photo-switchable activator-reporter dye-pairs (Cy3 and Alexa 647, respectively). Running the samples under STORM microscopy yield images which showed the presence of individual clusters of proteins (Fig. 6.8A). TRPV1 and MOR STORM analysis showed that the majority of the clusters identified were either TRPV1 (1304 clusters, 38.7 ± 3.4% n=5) or MOR (1556 clusters, 52.7 ± 4.2%, n=5) only (Fig 6.8B). Interestingly, the remaining 8.6% of clusters consisted of a combination of TRPV1 and MOR which

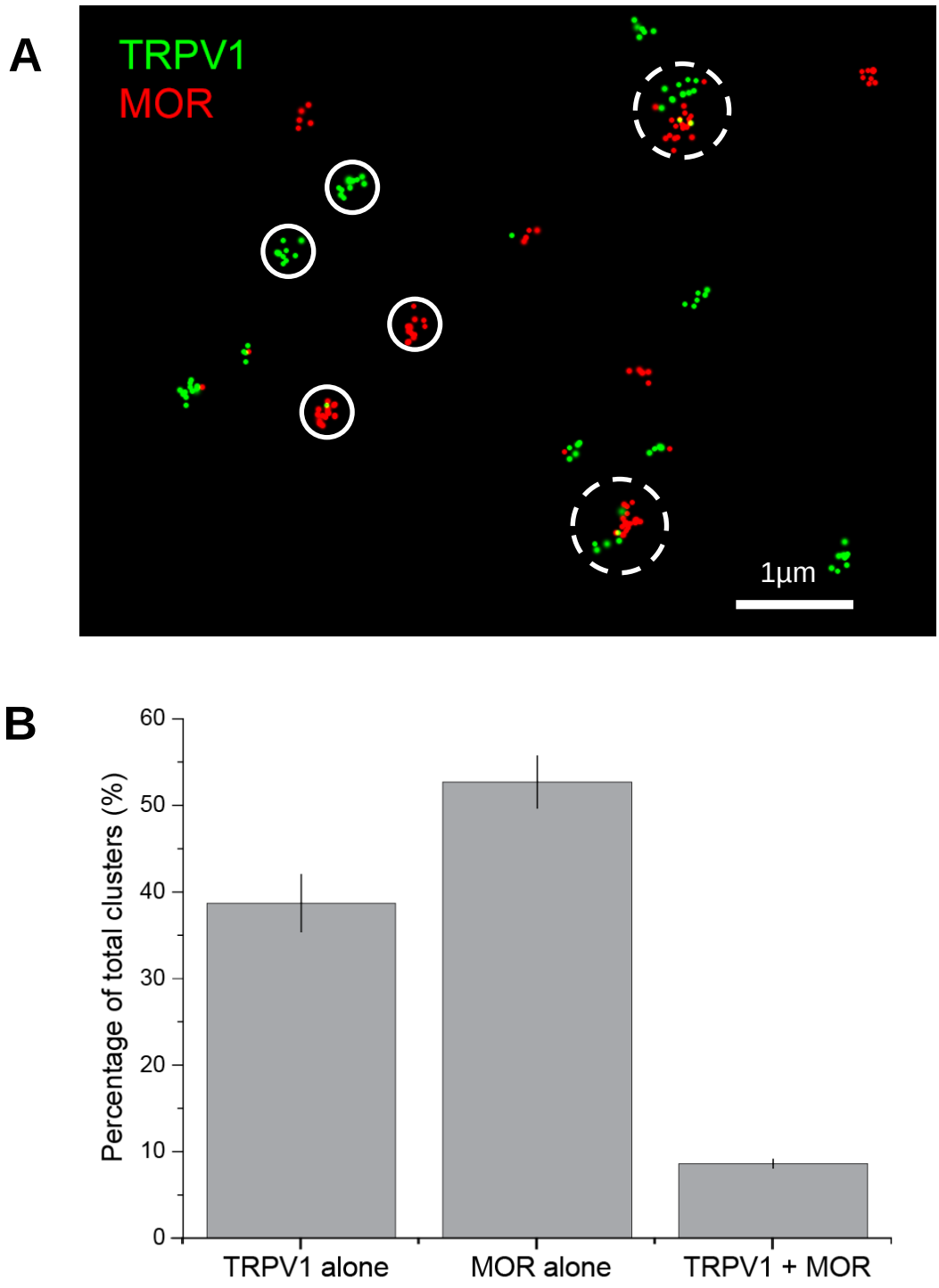

Figure 6.8: Multi-protein complexes in DRG neurons observed by STORM. (A) Representative images showing STORM between TRPV1 (Green) and MOR (Red). Solid white circles indicate individual clusters and dashed circles indicate potential complexes consisting of 2 proteins. (B) Cluster analysis between TRPV1 and MOR showing percentage of TRPV1 alone, MOR alone and both complexes together identified.

were designated as co-localised (345 clusters, 8.6 ± 3.2%, n=5). Yet, this was a minor fraction and, on a whole, both STORM and PLA report that there is no proximity between TRPV1 and MOR receptors in the majority of instances in DRG neurons.

STORM was then used to look at the potential interactions between ANO1 and TRPV1. Using PLA we have already shown that at least some of these proteins are in close proximity in DRGs (see above). Cultured DRG neurons were immunostained with ANO1 and TRPV1 primary antibodies and the same secondary dye-pairs were used as with TRPV1 and MOR STORM studies. Unlike the TRPV1-MOR STORM experiment, ANO1 and TRPV1 showed significantly more clustering (2314 clusters, 42.6 ± 4.1%, n=6) (Fig. 6.9A and B). 54.3 ± 4.2% of TRPV1 was found in TRPV1-only clusters (2919 clusters, n=6) (Fig. 6.9A and C). Interestingly, ANO1 was scarcely present on its own (164 clusters, 3.1 ± 0.33%, n=6) (Fig. 6.9C). Therefore, STORM demonstrates that most ANO1 molecules are found in close proximity or potentially in complexes with TRPV1, while this cannot be said about TRPV1, as more than half of TRPV1 clusters were without ANO1 (Fig. 6.9A and C).

We also tested TRPV1 and IP_3R1 interactions in DRG using STORM (Fig. 6.9B and C). As well as our PLA studies which show positive signals between these proteins, we were expecting proximity between TRPV1 and IP_3R1. The STORM analysis identified a smaller percentage of co-clustered TRPV1 and IP_3R1 proteins (735 clusters, 26.1% ± 3.0%, n=9) compared to ANO1 and TRPV1 (Fig. 6.9C). This was something that we also saw in our PLA, where the number of puncta between TRPV1 and IP_3R1 were less than those seen for ANO1 and TRPV1 (see above).

The next combination of proteins that we wanted to test using STORM were ANO1 and IP_3R1 to enable us to match all the PLA pairs with STORM analysis. Again, Gamper lab showed interactions between ANO1 and IP_3R1 in DRG neurons using co-immunoprecipitation studies and PLA (Jin et al., 2013). Similarly to TRPV1 and IP_3R1, we found that there was a smaller percentage of ANO1 and IP_3R1 clusters (355 clusters, 32.3 ± 6.1%, n=6) compared to ANO1 and TRPV1 clusters but the percentage was slightly higher than ANO1 and IP_3R1 clustering (Fig. 6.9C). Again,

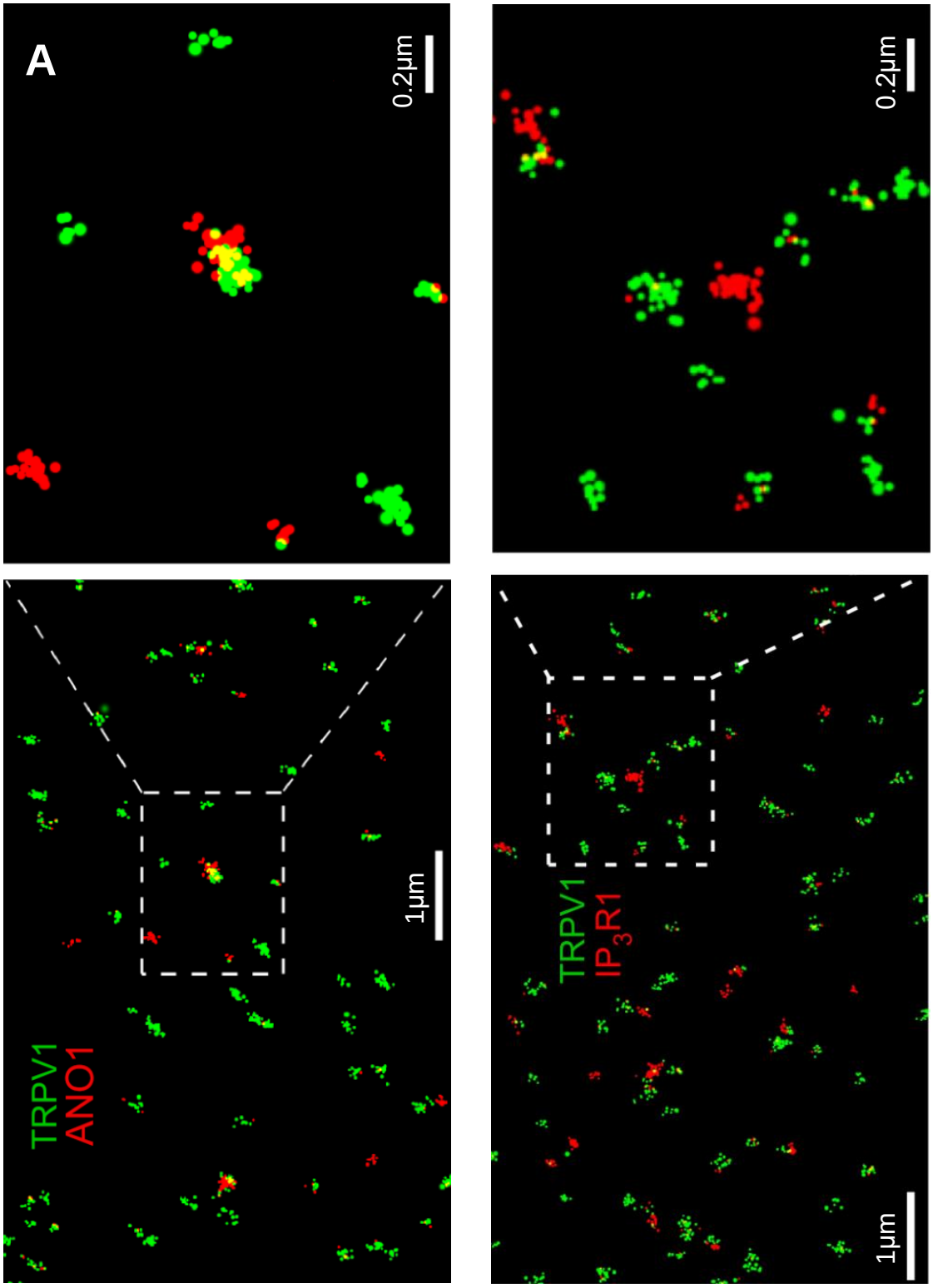
A
0.2µm
0.2µm
TRPV1
ANO1
1µm
TRPV1
IP3R1
1µm

B

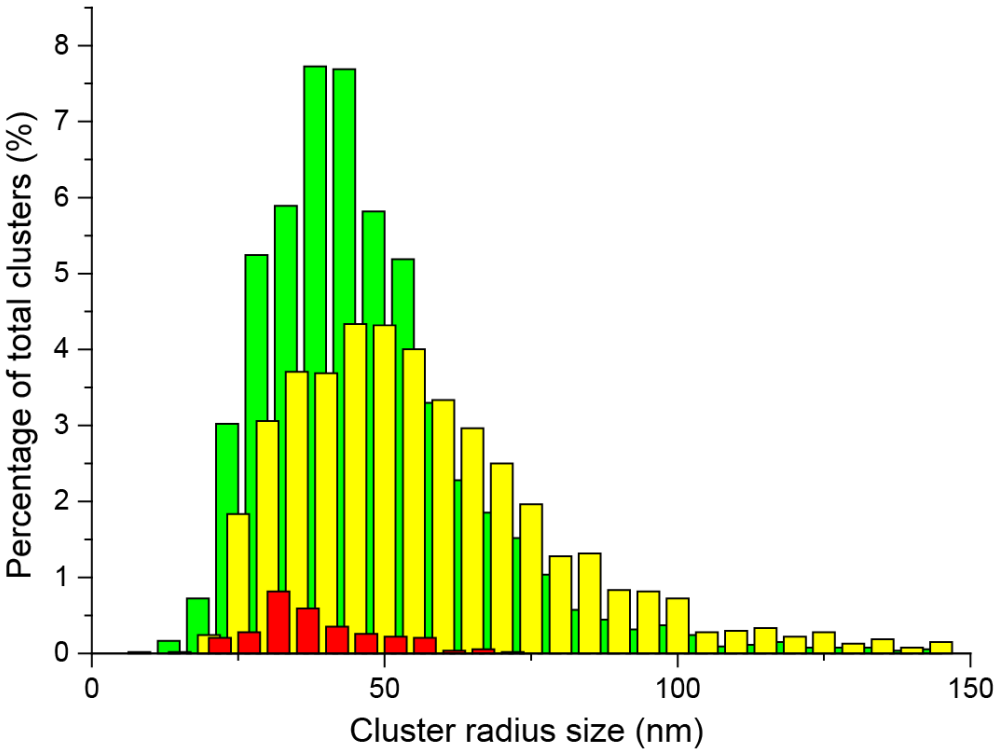
Percentage of total clusters (%)
0
1
2
3
4
5
6
7
8
0
50
100
150
Cluster radius size (nm)

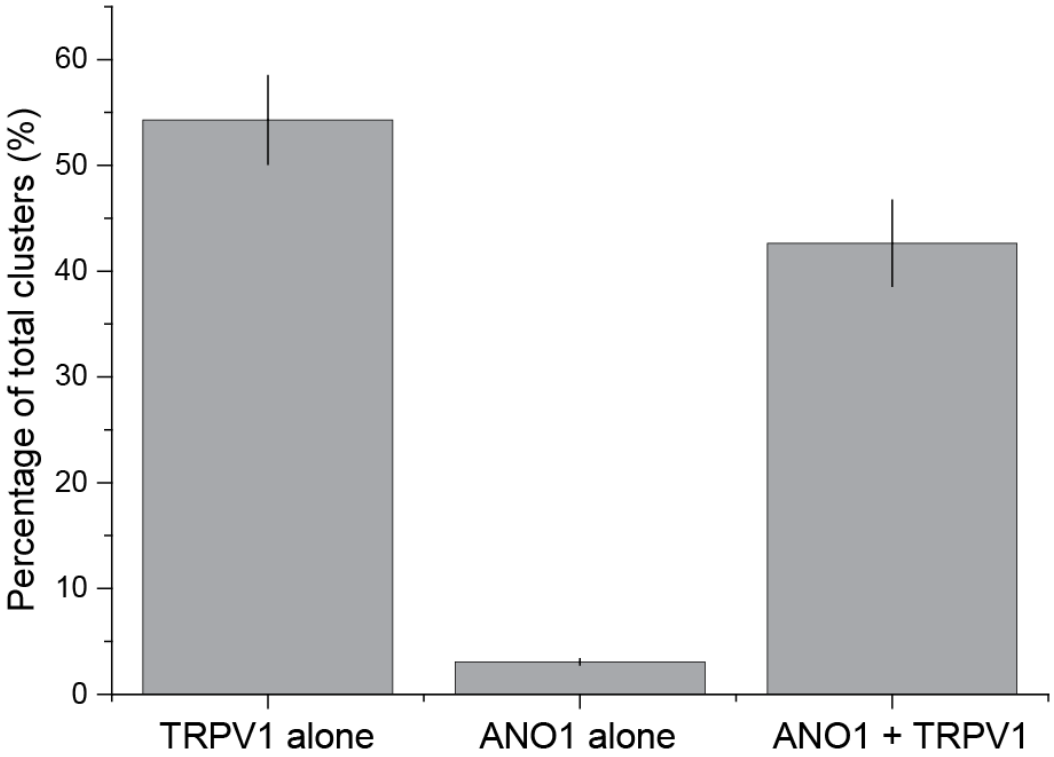
Percentage of total clusters (%)
0
10
20
30
40
50
60
TRPV1 alone
ANO1 alone
ANO1 + TRPV1

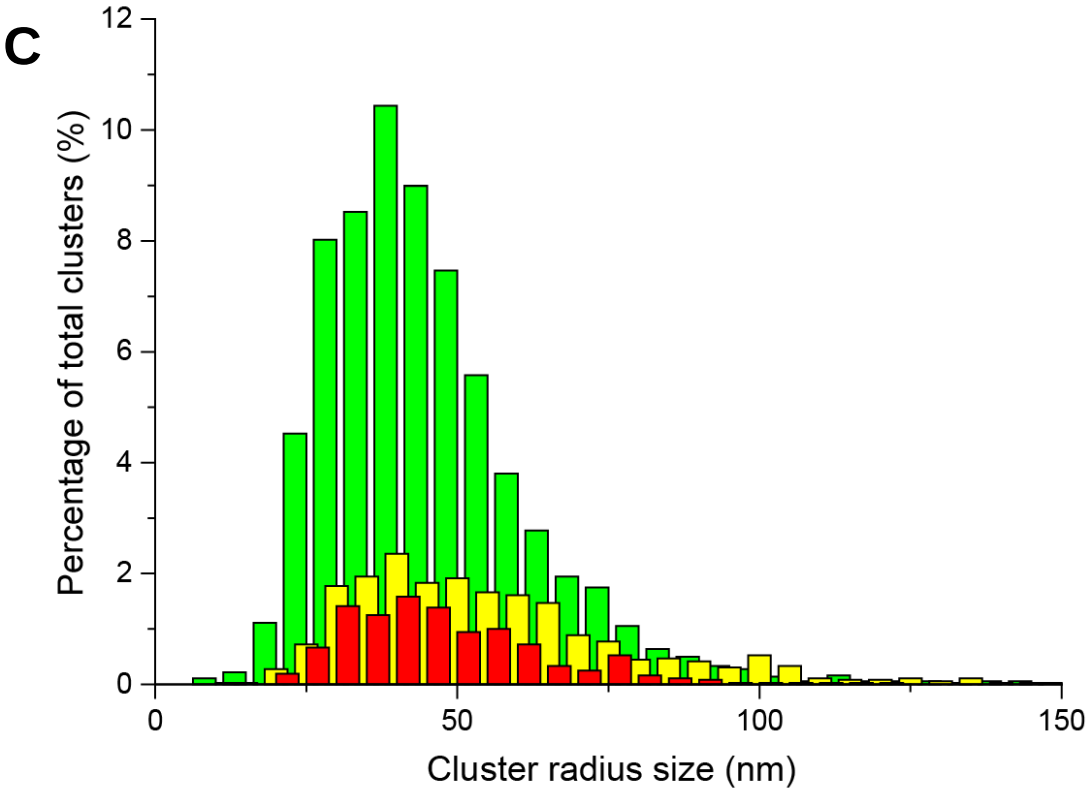
C
Percentage of total clusters (%)
Cluster radius size (nm)
0
2
4
6
8
10
12
0
50
100
150

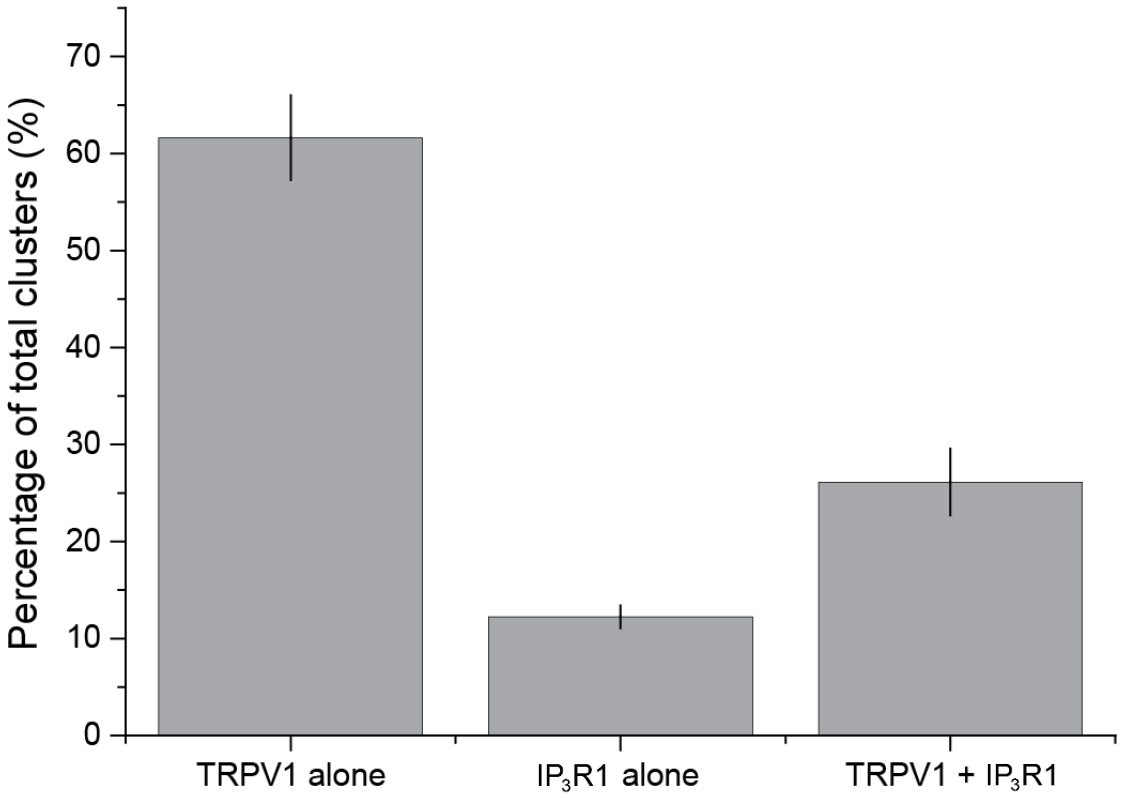
Percentage of total clusters (%)
0
10
20
30
40
50
60
70
TRPV1 alone
IP3R1 alone
TRPV1 + IP3R1

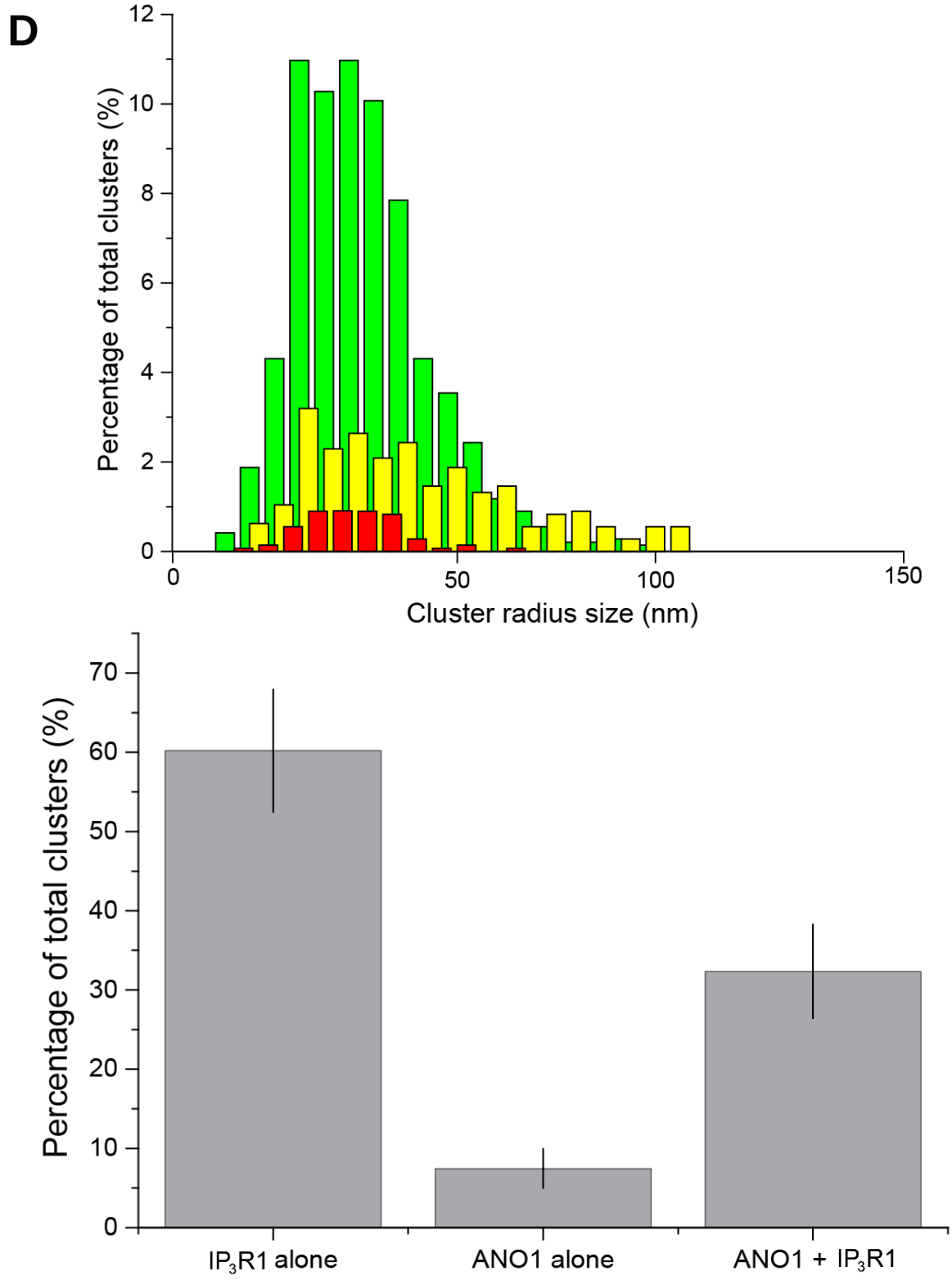

Figure 6.9: Investigating the presence of multi-protein complexes formed between ANO1, TRPV1 and IP₃R1 in DRG neurons. (A) Representative images showing STORM between; (upper panel) ANO1 (red) and TRPV1 (green) and (lower panel) TRPV1 (green) and IP₃R1 (red) (B) TRPV1 (green) and IP₃R1 (red). (C) Cluster analysis showing the percentage of clusters detected for ANO1 and TRPV1, (B) TRPV1 and IP₃R1 and (D) TRPV1 and IP₃R1.

the percentage of ANO1 alone has been found to be very small, suggesting in all of our STORM analysis that ANO1 is occupied or ‘bound up’- where it is in physical contact or in close proximity with another protein.

Finally, we performed preliminary 3-colour STORM experiments to investigate the presence of complexes that may include all 3 proteins. The protocol involved, triple co-immunostaining and the use of 3 dye-pairs with Alexa 405, Cy2 and Cy3 as the reporters for IP_3R1, ANO1 and TRPV1, respectively. Alexa 647 was used as the activator for all proteins. Running the 3-colour STORM revealed that there were some potential clusters which included all 3 proteins (352 clusters, 14.1 ± 0.8%, n=10) (Fig. 6.10A and B). In fact, this triple cluster was the largest population when looking at the co-clustering protein combinations (Fig. 6.10B and C). Yet, these experiments will need future confirmation.

A

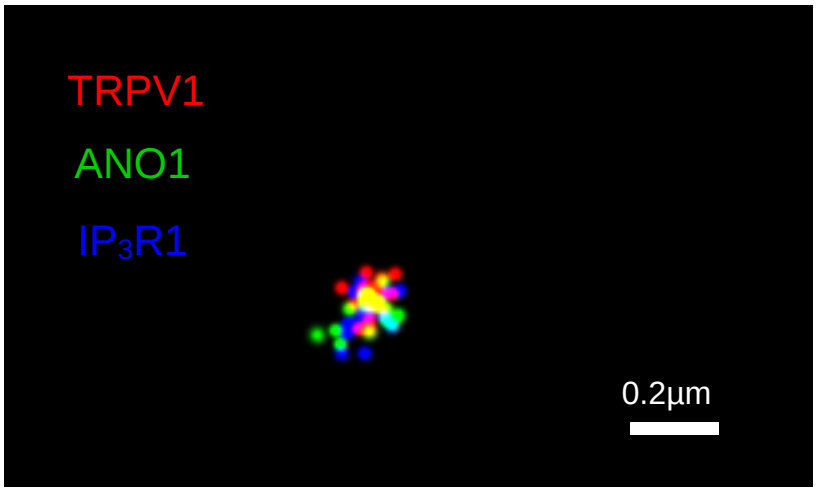
TRPV1
ANO1
IP3R1
0.2μm

B

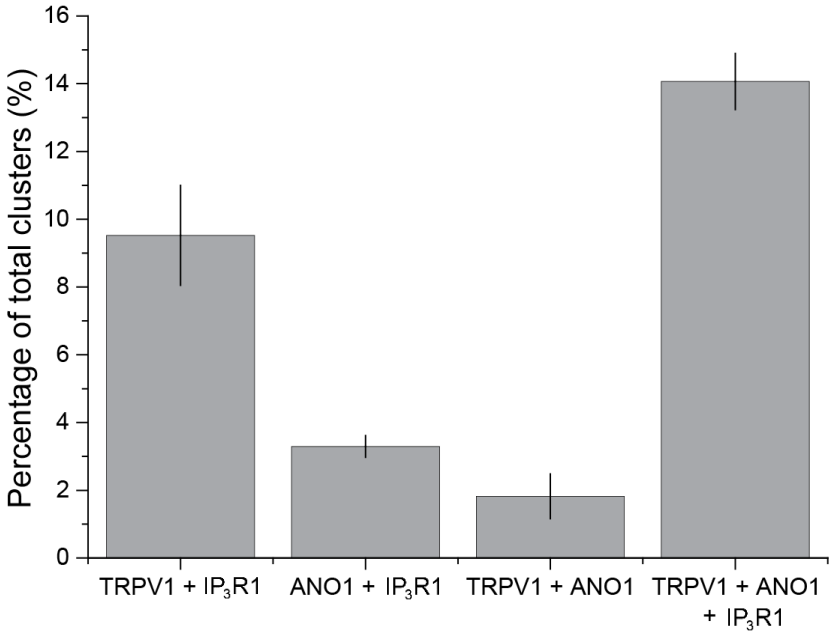
Percentage of total clusters (%)
0
2
4
6
8
10
12
14
16
TRPV1 + IP3R1
ANO1 + IP3R1
TRPV1 + ANO1
TRPV1 + ANO1 + IP3R1

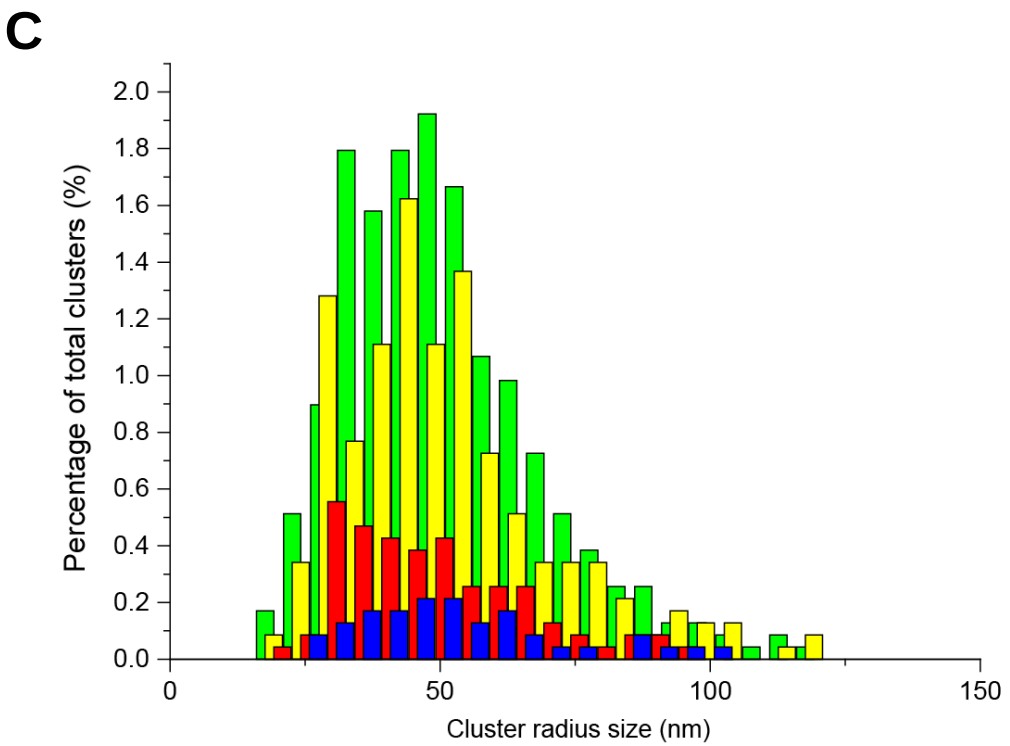

Figure 6.10: Three-color STORM in DRG neurons looking at ANO1, TRPV1 and IP_3R1. (A) Representative image showing an example of clustering between ANO1 (green) and TRPV1 (red) and IP_3R1 (blue). Scale= 0.2µm (B) Cluster analysis showing the percentage of clusters detected ANO1, TRPV1 and IP_3R1 and (C) spread of cluster radius size amongst these cluster percentages. Individual clusters of ANO1, TRPV1 and IP_3R1 removed for clarity.

6.3 Discussion

This chapter demonstrates the relationships between ANO1, TRPV1 and IP_3R1. Previous studies have been able to prove the physical interaction between ANO1 and TRPV1 in DRG neurons and in heterologous systems (Takayama et al., 2015). We have been able to reaffirm this finding and show in our experiments that ANO1 and TRPV1 are indeed in close contact with each other using both biochemical/ proteomics approaches and super-resolution microscopy (Fig. 6.7A, E and 6.8B). PLA works on the basis of 2 corresponding DNA probes that can ligate and produce fluorescence only if the 2 proteins of interest are within 40nm of each other. PLA has previously been used to successfully show the formation of STIM2 and Orai1 complexes in SOCE (Gruszczynska-Biegala and Kuznicki, 2013). Untreated cells show little signal however SOCE leads to greater proximity between the 2 proteins, causing the complex to form and become detectable with PLA (Gruszczynska-Biegala and Kuznicki, 2013). PLA was also used to show TRPV1 and TRPA1 co-localisation in mouse coronary artery endothelial cells (MCAECs) after propofol treatment, where these proteins contribute to the vasodilatory effect of propofol (Sinharoy et al., 2017). As mentioned earlier, IP_3R1 and ANO1 also show positive signals for PLA in DRG which demonstrates how ANO1 and IP_3R1 are positioned in a close arrangement so that Ca^{2+} release can overcome ANO1-activation restraints (Jin et al., 2013). In our hands, ANO1 and IP_3R1 also produced positive PLA signal (Fig. 6.7C and E), confirming previous findings (Jin et al., 2013; Cabrita et al., 2017). However, after obtaining evidence for TRPV1-evoked IP_3R1 activation in the previous chapter, we also considered the possibility of close proximity between these proteins. Interestingly there was positive PLA signal between TRPV1 and IP_3R1 indicating that at least some of these proteins are within 40nm of each other (Fig. 6.7B and E).

6.3.1 PLA and STORM demonstrate similar results for ANO1, TRPV1 and IP_3R1

These protein pairings were also investigated using a cutting-edge microscopy technique, STORM, which provides sub-diffraction limited resolution. Coupled with a newly developed cluster analysis paradigm, multi-colour STORM allows highly accurate localisation of proteins in relation to one another (Dani et al., 2010). Consistently, STORM results are very complementary to the PLA data (Fig. 6.7 and 6.8). ANO1 and TRPV1 showed the most co-clustering out of the 3 pairs, with ANO1

and TRPV1 showing less co-localisation with IP_3R1, however there are two scenarios which cannot be distinguished here: (i) ANO1-TRPV1 are in closer proximity or (ii) there are just numerically more ANO1-TRPV1 complexes.

6.3.2 Benefits provided by STORM over PLA

STORM has also revealed some further insights that were not possible to gain with PLA. Thus, it appears that ANO1 is mainly found clustered or in close proximity to one of the other proteins with only a small proportion on ANO1 channels found on their own (Fig. 6.8). This is logical as the low sensitivity of ANO1 would require close proximity to the Ca^{2+} source for efficient activity. Conversely, there is still a great deal of TRPV1 and IP_3R1 found alone presumably for interaction with other partners. PLA only allows visualisation of 2 proteins at a time however STORM can allow a greater number of proteins to be investigated. This enabled us to explore the potential for interactions between ANO1, TRPV1 and IP_3R1. In 3-colour STORM configuration, there are triple-clusters detected and interestingly these are the largest proportion of the multi-protein combinations being investigated. The other co-localised clusters are still present but less abundant which suggests that with ANO1 and TRPV1 co-localisation, there is a greater possibility that there is an IP_3R1 molecule in the local vicinity.

Taken together in the context of TRPV1-induced ANO1 activation, these results may indicate that at least in some DRG neurons there are multi-protein signalling complexes at ER-PM junctions containing ANO1 and TRPV1 at the plasma membrane and IP_3R1 in the juxtaposed ER membrane. This tri-protein arrangement may allow TRPV1 to feed into the already proposed mechanism of ANO1-IP_3R1 coupling in DRG neurons and activate ANO1. Ca^{2+} flooding into the cell via TRPV1 may reach a sufficient level of Ca^{2+} (at the mouth of the channel) to be able to activate ANO1 however this seems unlikely considering the results from our store-depletion experiments (see chapter 5). If the analysis from STORM revealed an overwhelming majority of clusters showing a single type of co-localisation (i.e. ANO1 and TRPV1) then one may be able to hypothesise that this co-localisation is the reason for a certain functional effect that has been identified. However, it seems as if both mechanisms of ANO1 activation may be occurring and this may serve to further strengthen ANO1's activity in terms of nociception. Both mechanisms would allow

ANO1 activation and, at the same time, allow TRPV1 to produce its interactions with other proteins i.e. with TRPA1 (see above). Even if TRPV1 is not physically coupled to ANO1, its ability to activate IP_3R1 via PLC may then be able to still provide activation of ANO1.

The benefits of STORM can be shown in the results obtained for ANO1 and TRPV1. For PLA the only information that we can obtain is that TRPV1 and ANO1 are within ~40nm of each other- we are unable to get an idea if this means the proteins are physically interacting, on the limit of 40nm from each other or anything in between. STORM provides an idea as to what the distribution of cluster size actually is and also the relative levels of non-interacting proteins present, again providing more information than just 2 proteins are close to each other. Furthermore, being able to visualise more than 2 proteins is also another major advantage of STORM.

There is a small percentage of clusters that were deemed to consist of TRPV1 and MOR co-localised together after being processed by the STORM clustering analysis, despite the majority of clusters being either only TRPV1 or only MOR positive. This could be due to the fact that STORM is a great deal more sensitive in judging the presence of co-localised proteins or the fact that the PLA analysis was unable to detect these due to biophysical constraints as part of the process (PLA probe interactions may not have occurred during the assays) which is still unlikely. Alternatively, Zhang and colleagues suggested that up to 10% clustering in STORM may be ‘false-positive’ in certain scenarios. This was derived from K_v7 homomer and multimer STORM experiments which revealed that $K_v7.1$ and 4 subunits (known to produce homomeric channels and don’t co-localise with each other) gave a 10% signal as multimers between the 2 subunits. Therefore, in this situation the clustering would be considered as false.

Chapter 7: ER movement to the PM upon ER activation monitored using TIRF

7.1 Introduction

ER-PM junctions are vital in controlling Ca^{2+}-dynamics in various cell types (Giordano et al., 2013). Due to the fact that our proteins of interest are found at these junctions and coupled with findings in previous chapters demonstrating the requirement of IP_3R1 for ANO1 activation and proximity of ER-PM proteins, some attention is required to show how these junctions are assembled and function in cells.

7.1.1 Junctophilin

In cardiac muscle, ER-PM junctions allow initiation of CICR as they enable the juxtaposition of VGCCs to RYR receptors. Therefore, as an action potential arrives, L-type VGCC activation is able to efficiently and reliably activate RYRs and allow excitation-contraction coupling due to the spatial arrangement between these two proteins (Beavers et al., 2014). A protein family known as the junctophilins has been found in cardiac cells; it was demonstrated that these proteins play a crucial role in tethering the ER/SR and the PM (Landstrom et al., 2014). The junctophilin family of proteins consists of 4 members; junctophilin 1-4, and structurally comprise of eight membrane-occupation and recognition nexus (MORN) motifs which tether to the PM, an α-helix, divergent region and a C-terminus transmembrane motif that anchors the protein into the ER/SR (Landstrom et al., 2011; Takeshima et al., 2015). In cardiac cells junctophilin 2 is the predominant isoform and has been shown to be important for this ER-PM association. In human cardiac tissue from patients who had died after hypertrophic cardiomyopathy (HCM), there was a reduction in junctophilin 2 (Landstrom et al., 2011) which has also been shown in rat models of HCM (Minamisawa et al., 2004). Partial silencing of junctophilin 2 in HL-1 cells displayed myocyte hypertrophy along with increased expression of markers for this process (Landstrom et al., 2011). Furthermore, Ca^{2+} dynamics in the cell (both L-type VGCC and RYR) were markedly reduced as there was a loss of the proximity between these proteins. SOCE is another process reliant on junctophilin proteins in skeletal muscle (Hirata et al., 2006). Silencing of both junctophilin 1 and 2 caused reduced SOCE as well as deformed triad junctions in these cells (Hirata et al., 2006). In other cell types such as T-cells, another isoform- junctophilin 4- has been found to play a role in SOCE (Woo et al., 2016). Jurkat cells have shown reduced levels of Ca^{2+} in

the ER stores when junctophilin 4 KO had occurred (Woo et al., 2016). Primary murine $CD4^+$ T-cells with junctophilin 4 KO also exhibited reduced ER Ca^{2+} content but interestingly, the occurrence of SOCE was also diminished. Junctophilin 4 co-localised with STIM1 and it was demonstrated that store-depletion promotes physical interaction between the two proteins. Loss of junctophilin 4, reduced the number of STIM1 clusters in these cells, thus implicating junctophilin 4 in recruiting STIM1 to ER-PM junctions (Woo et al., 2016). Recently, our lab has also shown the presence of junctophilin 1, 3 and 4 in DRG neurons where they seem to play a similar role as reported by Woo and colleagues (unpublished data).

7.1.2 Ist2

A protein known as Ist2 is involved in producing ER-PM junctions in the yeast saccharomyces cerevisiae (Pichler et al., 2001; Manford et al., 2012). Interestingly, Ist2 is the yeast orthologue of mammalian anoctamins which is localised to the ER and extends to the PM (Stefan et al., 2013). It has been demonstrated that loss of this junctional protein thorough gene deletion leads to loss of contacts between the ER and PM (Story et al., 2003; Manford et al., 2012; Wolf et al., 2012). A role for Ist2 involving the regulation of metabolic processes has been touted. Plasma membrane ATPase 1 (Pma1) induced H^+ efflux is thought to reduce pH in yeast cells and is governed by extracellular glucose (Morsomme and Boutry, 2000). Loss of Ist2 in yeast shows reduced H^+ efflux whereas overexpression of Ist2 results in a slightly faster rate of alkalisation of the cells (Wolf et al., 2012).

7.1.3 Dynamic ER activity

Although some ER-PM junctions are constitutive (Stefan et al., 2013; Okeke et al., 2016), the ongoing investigations of several groups suggest that in some instances, the ER is moving into closer proximity with the PM upon stimulation (e.g. store depletion) (Giordano et al., 2013; Courjaret and Machaca, 2014; Saheki et al., 2016). This could result in formation of de-novo junctions or rearrangement of existing junctions in a manner where the ER is closer to the PM. Such processes would be of high relevance to the functional activity of junctional ANO1-containing complexes in DRG neurons since shortening of the distance between ANO1 and IP_3R is expected to facilitate ANO1 activation.

One method thought to induce CaCC activity was SOCE as initially proposed by the Hartzell lab back in 1996 (Hartzell, 1996). It is reasonable to postulate that ANO1 activation through SOCE may well be possible, especially as replenishment of the ER is necessary to activate ANO1 through IP_3R. Recently, it has been demonstrated in oocytes that ANO1 activation requires SOCE however, this is not direct activation through Orai and STIM proteins (Courjaret and Machaca, 2014). It was proposed that Ca^{2+} entering the ER through SOCE is then delivered to ANO1 channels through the IP_3Rs. Furthermore, this process of SOCE involves regions of ER physically moving up to the PM when SOCE was initiated (Courjaret and Machaca, 2014).

A family of proteins called extended synaptotagmins (E-syts) are another example of tethering proteins which have been known to play a role in tethering ER to PM after stimulation of GPCRs (Saheki et al., 2016). This family consists of 3-members (E-syts 1-3); E-syts1 is of particular interest due to its Ca^{2+}-dependent nature (Min et al., 2007). Similarly to synaptotagmin, E-syts have five C2 domains, two of which are essential for the tethering to occur due to their Ca^{2+}-sensitive nature (Min et al., 2007; Malmersjo and Meyer, 2013) (Fig. 7.1). Ca^{2+} elevation causes the recruitment and tethering of the ER and PM thorough C2E and C2C domains at PIP_2 rich segments of the PM (Malmersjo and Meyer, 2013; Perez-Lara and Jahn, 2015) (Fig. 7.1). Mutants of E-syts1 have shown C2E to be vital for tethering and C2C vital in shortening of the distance between the ER and PM (Fernandez-Busnadiego et al., 2015). Ultimately, this close apposition between the ER-PM allows for processes such as DAG clearance through the synaptotagmin-like, mitochondrial-lipid binding protein (SMP) domain (Saheki et al., 2016). This was demonstrated in artificial liposomes using a FRET-based lipid-transfer assay where lipid transfer was visualised from a donor liposome to an acceptor liposome in the presence of E-syts1. Interestingly, E-syts are not required for SOCE, as E-syts 1-3 KO doesn't affect SOCE in HeLa cells (Giordano et al., 2013; Idevall-Hagren et al., 2015). Taken together, this shows that the ER is not a rigid organelle but rather dynamic in its ability to facilitate various cellular processes.

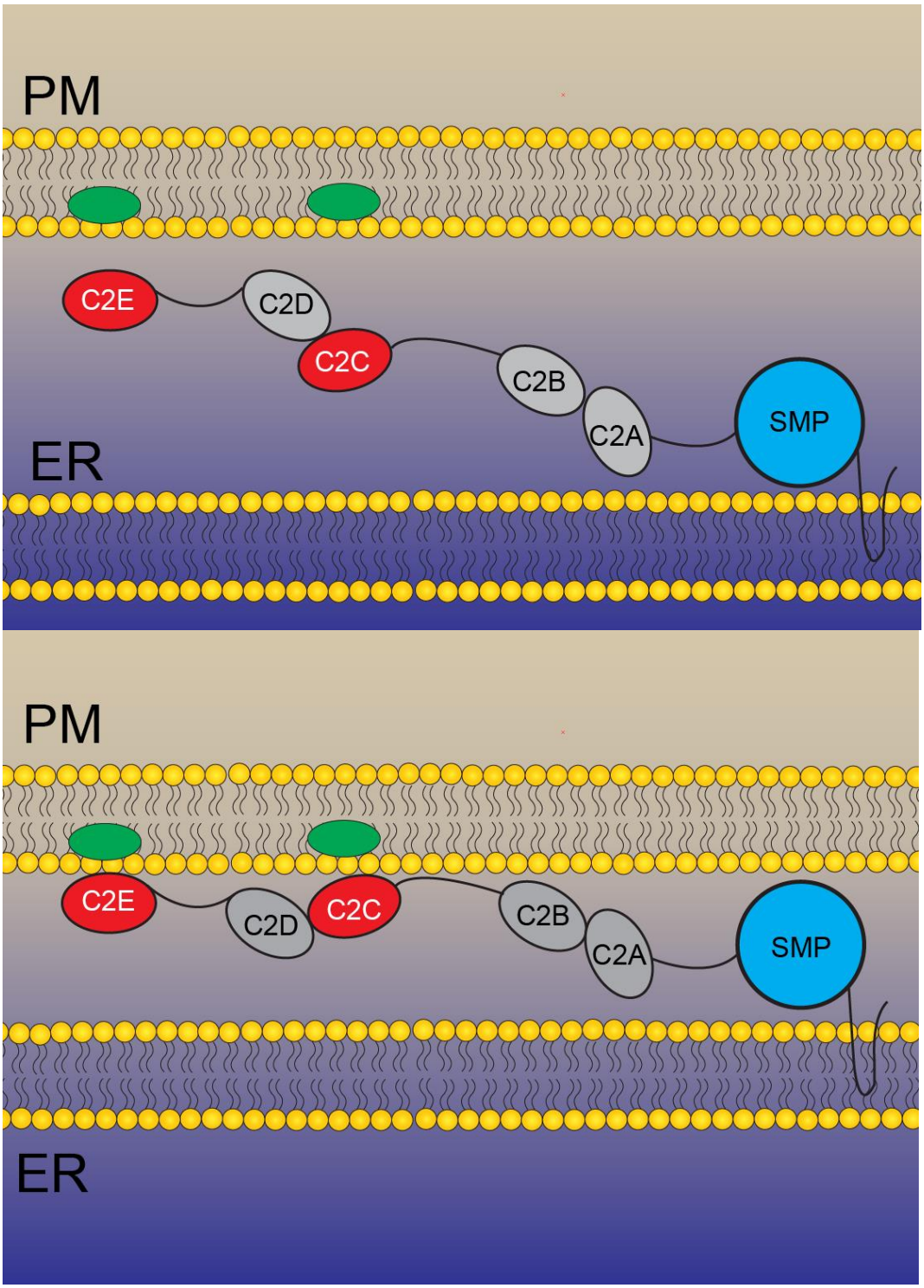

Figure 7.1: E-Syts1 in forming ER-PM junctions. Upper panel: In resting conditions, E-Syts1 is not tethered to the PM. Lower panel: Upon Ca^{2+} binding to the C2E and C2C domains, E-syts1 tethers to PIP_2 (green ovals) in the PM, allowing shortening of the distance between ER and PM. Figure based on (Krauss and Haucke, 2016).

7.2 Results

As part of their studies, two groups have recently used an interesting approach where they utilised a luminal ER marker, ER-oxGFP to monitor apposition between the ER and PM under TIRF (Giordano et al., 2013; Saheki et al., 2016). Under normal conditions in wild type cells, an elevation in Ca^{2+} in the cytoplasm led to the ER-oxGFP signal being increased which is thought to indicate greater areas of close proximity between the ER and the PM (Giordano et al., 2013; Saheki et al., 2016). Oxo-M (agonist of M_1R) stimulation of HeLa cells transfected with M_1R indeed induced an increase in TIRF signal for ER-oxGFP (Saheki et al., 2016).

To test whether there is any movement of the ER to the PM in DRG after engagement of the ER, we devised a TIRF-based imaging approach to visualise ER dynamics. An ER-specific tag was expressed in cells and monitored during application of several relevant agonists. By using TIRF, we are able to focus on the cell membrane at the specimen-glass coverslip interface and any increase in fluorescence of the ER marker will be indicative of the ER moving closer to the PM. DRG neurons were cultured and incubated with an ER-specific dye, ER-tracker Green (Thermofisher), 30 min before imaging. ER-tracker Green is conjugated to glibenclamide, a drug that binds to the sulphonyurea receptors of ATP-sensitive K^+ channels (Shen et al., 1992; Ripoll et al., 1993). As these receptors are highly localised to the ER, the tracker provides an ER-specific stain. To analyse our data, we devised a grid-based method using the Nikon Elements software to divide every cell footprint into a grid to allow us to be able to monitor both, the integral footprint fluorescence as well as the activity within specific regions within the cell (Fig. 7.2A). Performing TIRF on DRG stained with the ER tracker demonstrated that the ER is a dynamic organelle and its proximity to the PM is subject to fluctuations. As a control, we decided to apply no agonist (just standard bath solution) and monitor activity of the ER (Fig. 7.2B). We found that there was no increase in TIRF signal intensity but after 100 seconds there was a decrease in fluorescence (100 seconds: 0.95 ± 0.016 vs 132 seconds: 0.90 ± 0.016 n=5, 192 grids) however there was no increase in fluorescence during this application. This reduction in fluorescence may be due to bleaching or movement of the ER away from the PM as part of its dynamic activity.

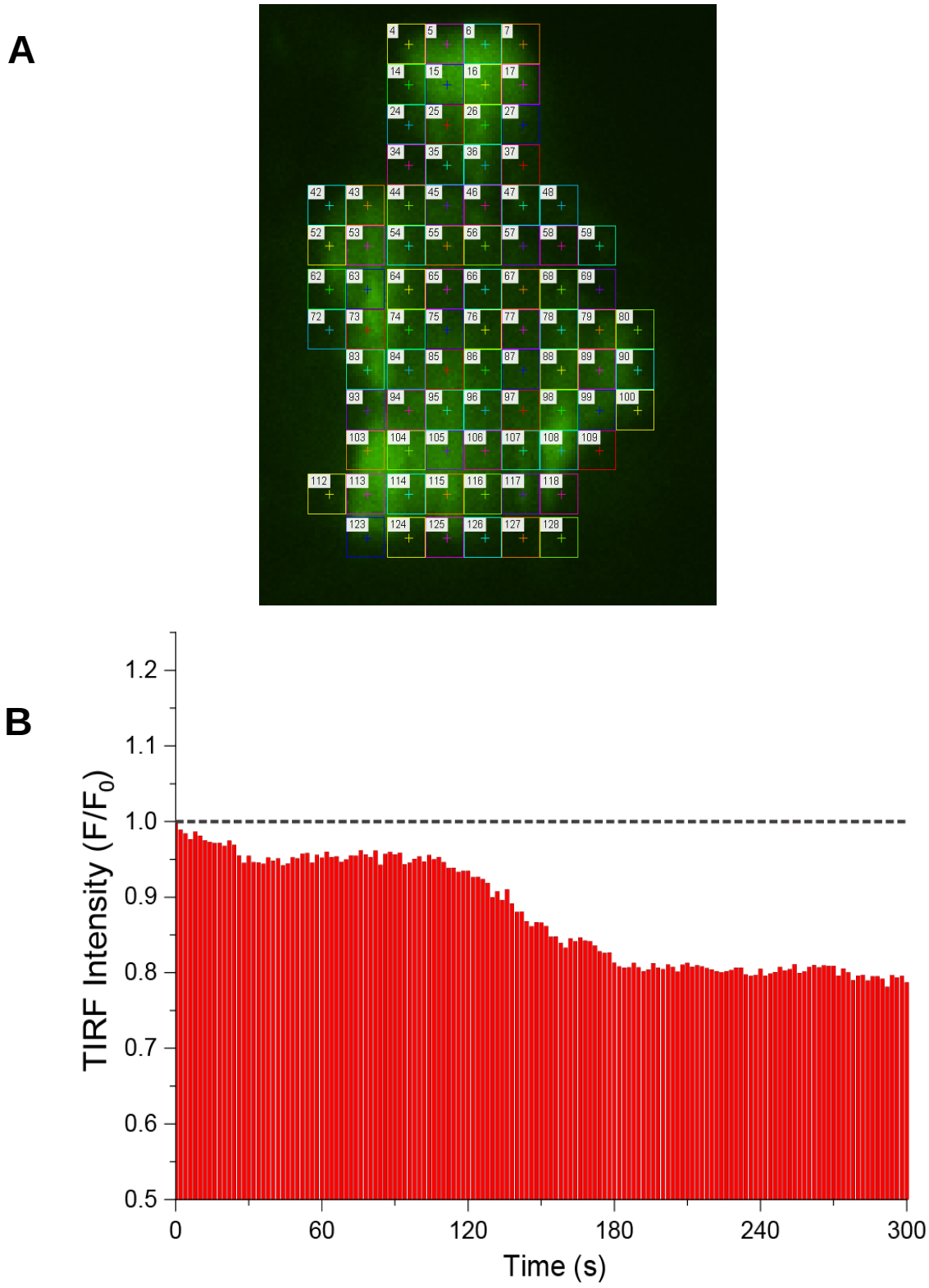

Figure 7.2: Motoring ER activity in DRG neurons. (A) Grid based analysis to take into account all areas of the each cell. (B) Control experiments where DRG loaded with ER-tracker Green and imaged (n=5) with no agonist application (just extracellular bath solution). All grids were averaged for each of cell and plotted as a histogram to monitor changes in TIRF intensity. No increase in fluorescence was seen during this period.

Upon bradykinin application, many areas didn't respond however, several areas responded with an increased intensity of ER-tracker signal (Fig. 7.3A, B and C). Comparing all cells imaged to each other showed that there were some cells which responded with a greater TIRF intensity compared to others ($p<0.05$, ANOVA, n=6). When taking all cells imaged into account, the signal decreases gradually (possibly photobleaching) but application of bradykinin leads to an increased level of fluorescence with respect to the pre-bradykinin signal intensity (Fig. 7.4D) (pre-bradykinin: 0.94± 0.00047 Vs peak bradykinin (250nM): 1.0009 ± 0.00036, $p<0.00001$ n=6, 429 grids). However, when comparing this to F/F_0 there is no significant difference.

Chapter 5 demonstrates that TRPV1 is able to engage IP_3R Ca^{2+} release. To test if TRPV1 also has a similar effect as B_2R activation, capsaicin was applied to DRG neurons stained with the ER tracker. Again there were some individual neurons that did show an increase of footprint fluorescence in certain grids images and also in the average TIRF intensity of single cells ($p<0.05$, ANOVA) (Fig 7.4A, B and C). The majority of neurons didn't show significant cell-wide with respect to F/F_0, however when comparing the pre-capsaicin application responses to post-capsaicin application responses, capsaicin application caused a significant increase in TIRF intensity (pre-capsaicin: 0.93 ± 0.0068 Vs peak capsaicin (1μM): 1.013 ± 0.029, $p<0.001$, n=5 cells, 305 grids). Comparing the peak TIRF intensity between bradykinin and capsaicin application showed no significant differences.

One significant issue which impeded TIRF imaging of DRG neurons was the fact that in culture conditions, neurons rarely reside on the glass as they prefer to position themselves on top of the glial cells. Therefore when on the glass, the neurons often have a limited footprint (as can be seen in Figs. 7.3B-4B) and make it difficult to obtain reliable TIRF recordings. As one moves away from the TIRF plane, the evanescent field depreciates exponentially so that the fluorophores that are located within the ER can no longer be excited and the signal is therefore lost. To circumvent this issue, we repeated these experiments using adherent HEK293 cells co-transfected with either B_2R or TRPV1 and another ER marker- viral-based ER-GFP (CellLight ER-GFP, BacMam 2.0). Once transfected, the construct enters cells and allows GFP to be expressed specifically in the ER.

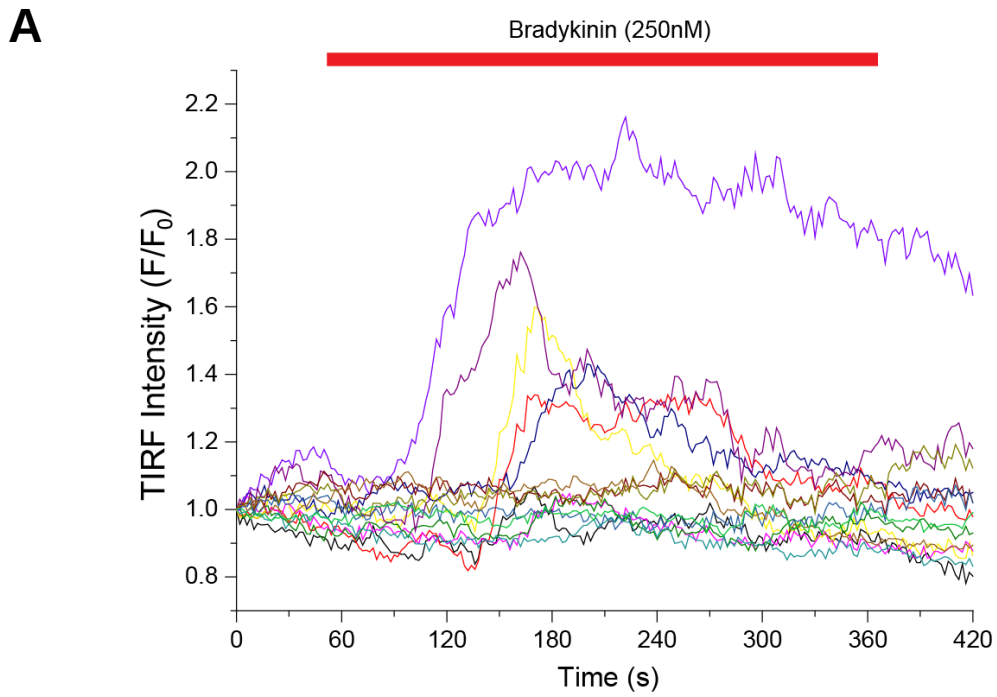
A
Bradykinin (250nM)
TIRF Intensity (F/F0)
2.2
2.0
1.8
1.6
1.4
1.2
1.0
0.8
0
60
120
180
240
300
360
420
Time (s)

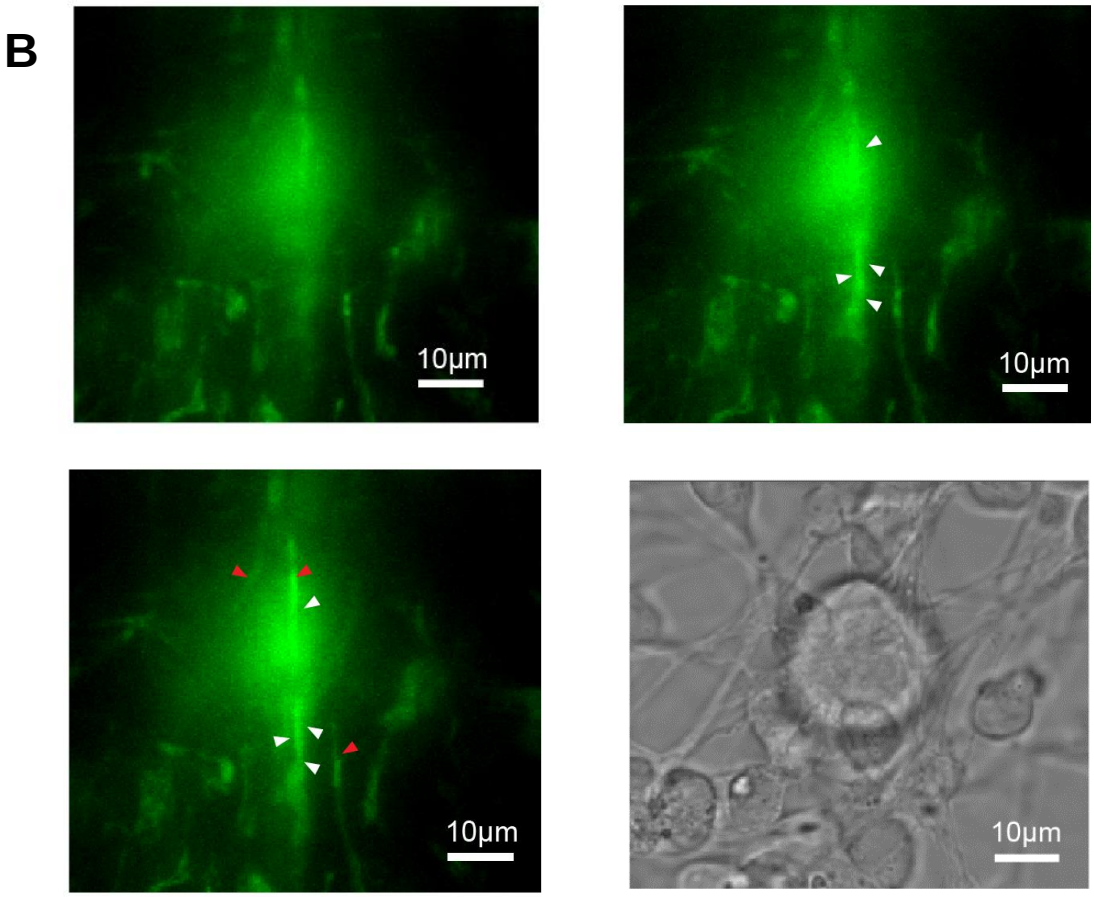
B
10μm
10μm
10μm
10μm

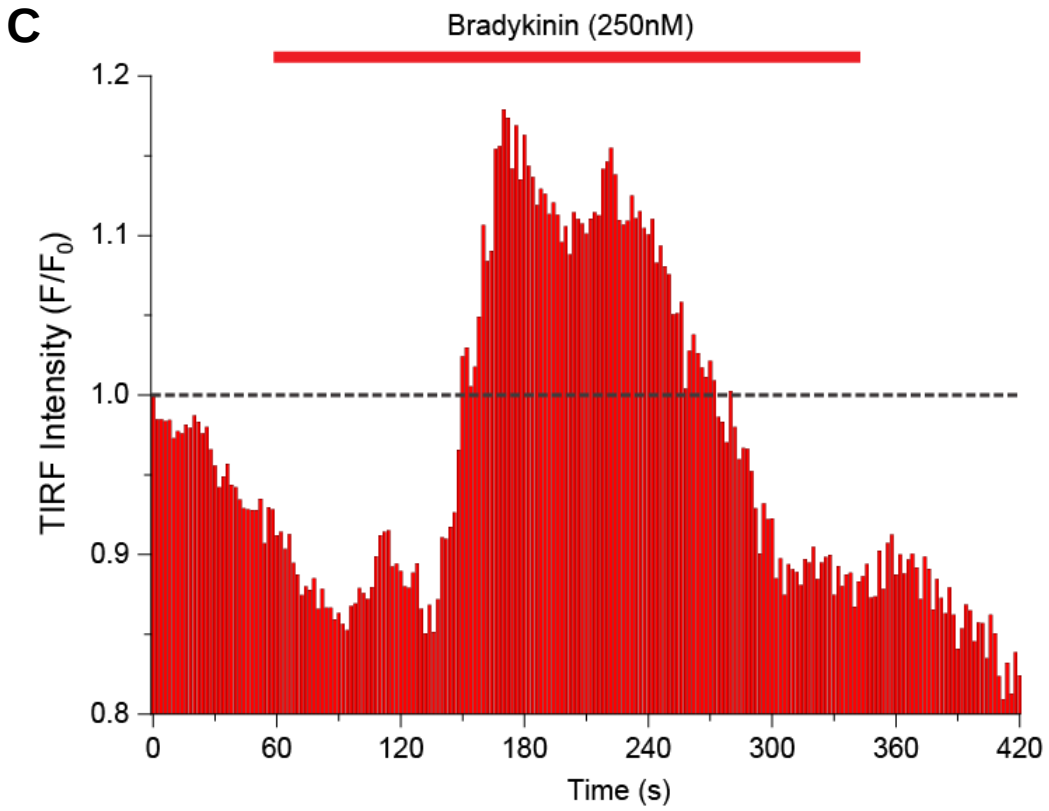
C
Bradykinin (250nM)
TIRF Intensity (F/F0)
1.2
1.1
1.0
0.9
0.8
0
60
120
180
240
300
360
420
Time (s)

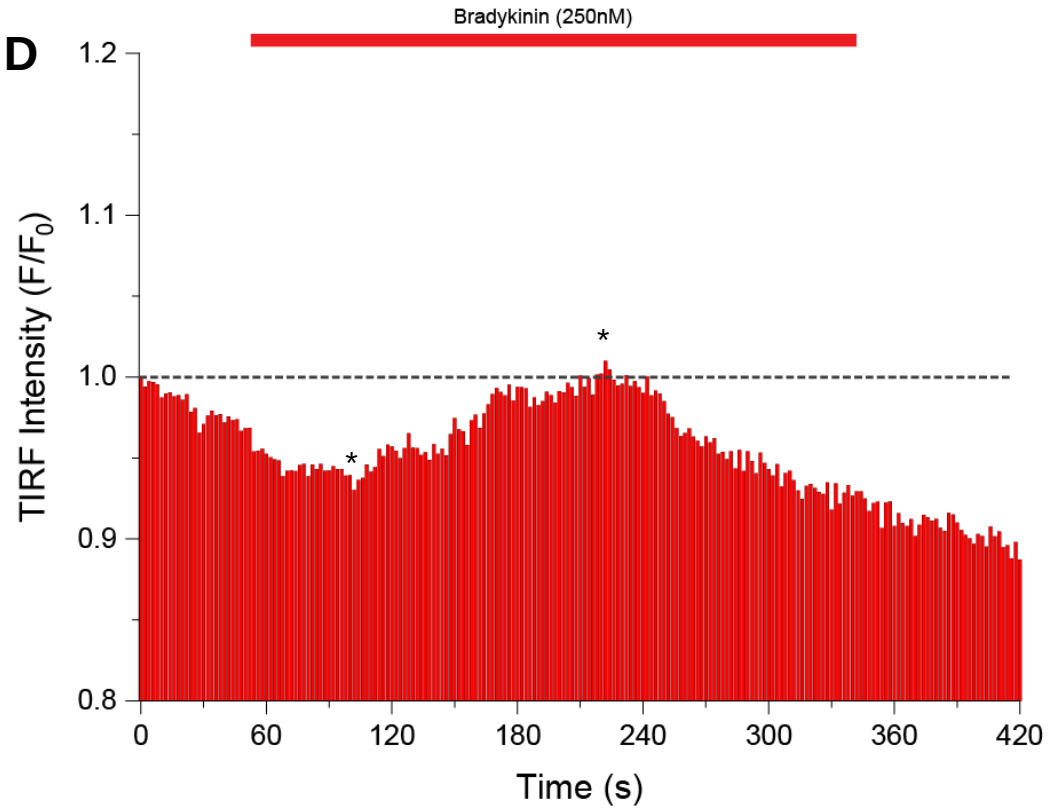
D
Bradykinin (250nM)
TIRF Intensity (F/F0)
1.2
1.1
1.0
0.9
0.8
*
*
0
60
120
180
240
300
360
420
Time (s)

Figure 7.3: ER movement in DRG cells loaded with ER-tracker Green under TIRF after bradykinin (250nM) application. (A) Representative traces showing 'responsive' and 'non-responsive' grids in response to bradykinin application. (B) Representative images of changes in TIRF signal intensity. Upper left panel: pre-bradykinin application TIRF signal (0 seconds), upper right panel: post bradykinin application (120 seconds), lower left panel: post bradykinin response (300 seconds). White arrows show changes after 120 seconds and red arrows show changes after 300 seconds post-bradykinin application, lower right panel: brightfield image of DRG being imaged. Images correspond to uppermost purple trace in (A) (C) Average changes (all grids) in TIRF intensity of one 'responsive' cell after bradykinin application. (D) Averages changes in TIRF intensity of all cells (n=6). SEM not shown for clarity. * denote comparison points for statistics.

A

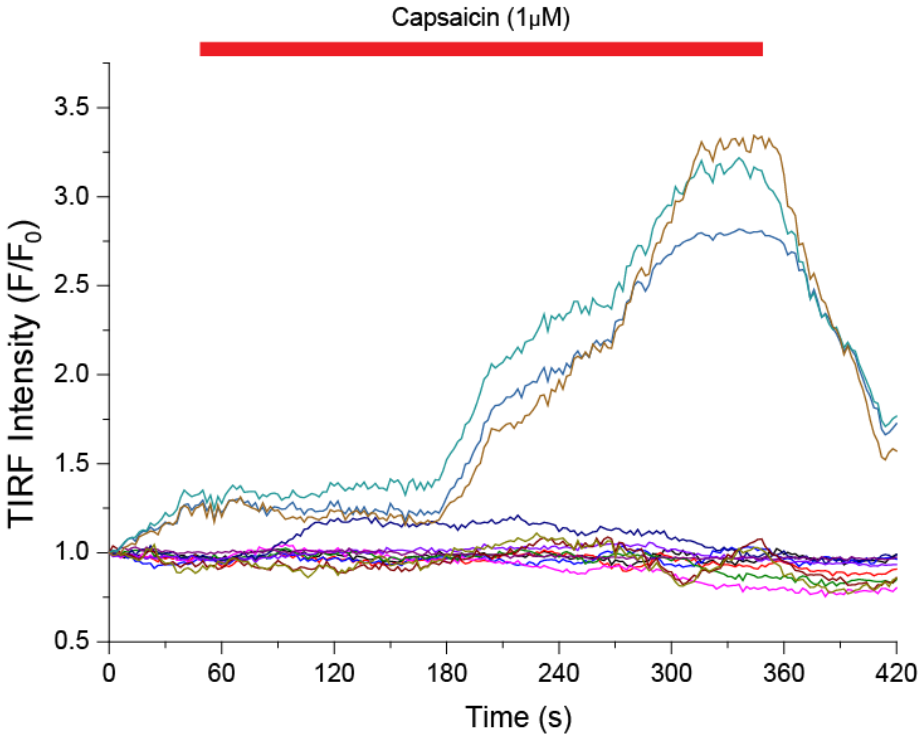
Capsaicin (1μM)
TIRF Intensity (F/F0)
3.5
3.0
2.5
2.0
1.5
1.0
0.5
0
60
120
180
240
300
360
420
Time (s)

B

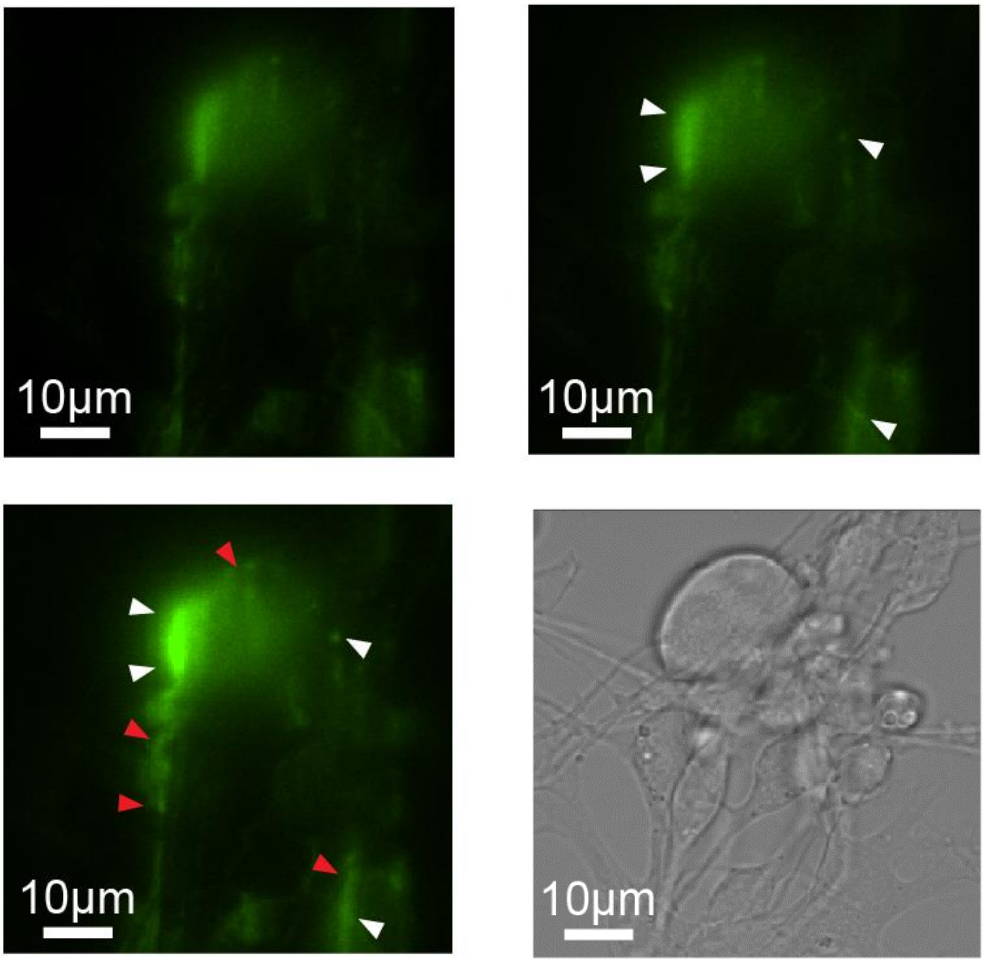
10μm
10μm
10μm
10μm

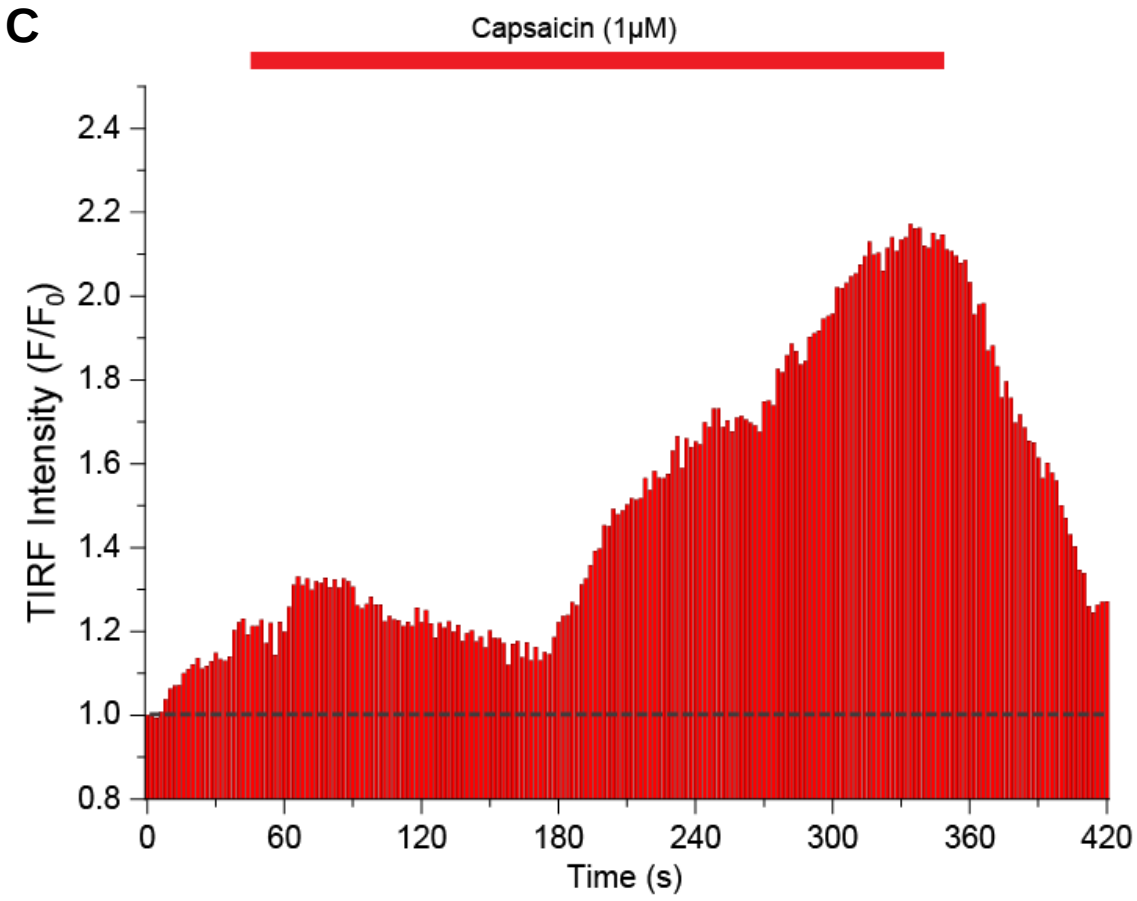
C
Capsaicin (1μM)
TIRF Intensity (F/F0)
2.4
2.2
2.0
1.8
1.6
1.4
1.2
1.0
0.8
0
60
120
180
240
300
360
420
Time (s)

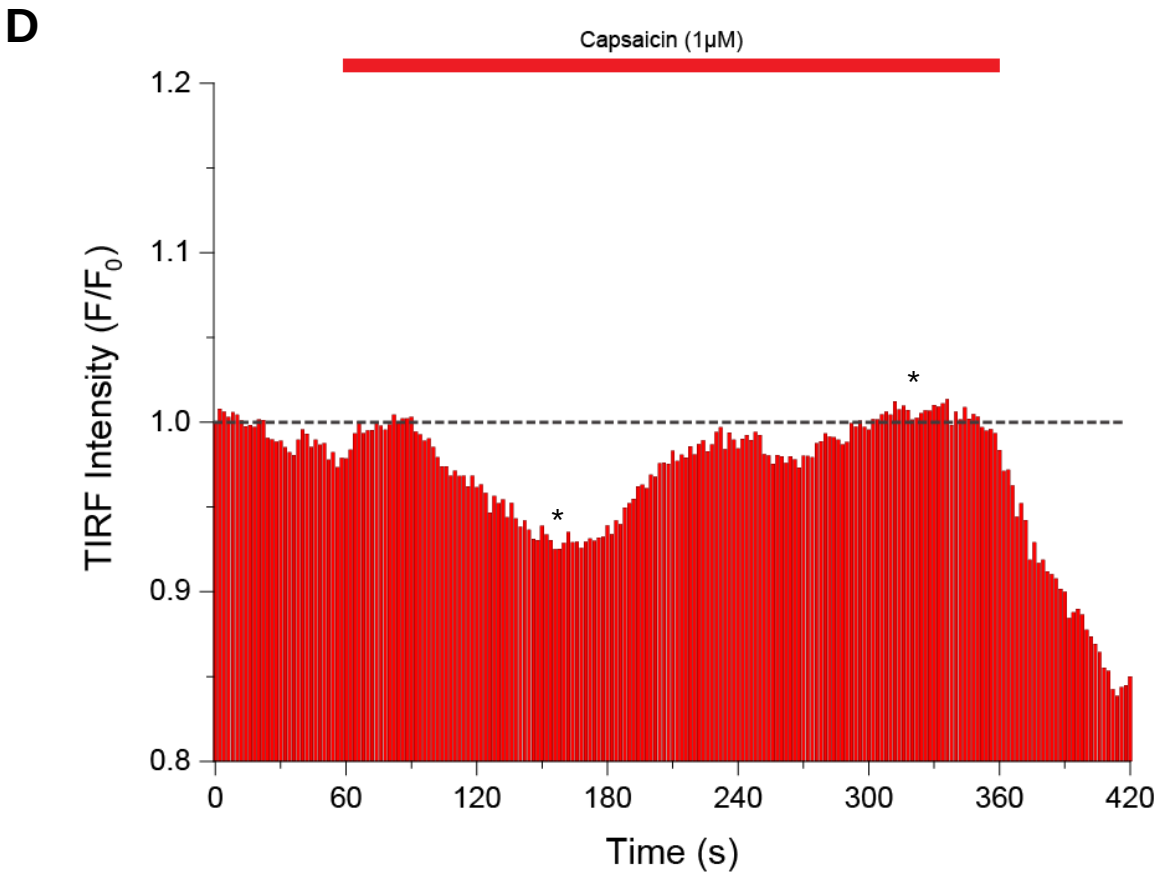
D
Capsaicin (1μM)
TIRF Intensity (F/F0)
1.2
1.1
1.0
0.9
0.8
*
*
0
60
120
180
240
300
360
420
Time (s)

Figure 7.4: ER movement in DRG cells loaded with ER-tracker Green under TIRF after capsaicin (1μM) application. (A) Representative traces showing 'responsive' and 'non-responsive' grids in response to capsaicin application. (B) Representative images of changes in TIRF signal intensity. Upper left panel: pre-capsaicin application TIRF signal (0 seconds), upper right panel: post capsaicin application (120 seconds), lower left panel: post capsaicin response (300 seconds). White arrows show changes after 120 seconds and red arrows show changes after 300 seconds post-capsaicin application, lower right panel: brightfield image of DRG being imaged. Images correspond to uppermost beige trace in (A). (C) Average changes (all grids) in TIRF intensity of one 'responsive' cell after capsaicin application. (D) Averages changes in TIRF intensity of all cells (n=6). SEM not shown for clarity. * denote comparison points for statistics.

We tested the effects of bradykinin and capsaicin using this new ER-marker. Application of bradykinin (250nM) again produced an increased TIRF signal which was significantly greater compared to F/F_0 (Fig. 7.5A, B and C) (1.05 ± 0.022, $p<0.01$, n=5, 164 grids).

Application of capsaicin on HEK293 cells transfected with TRPV1, gave an increase in TIRF intensity response, suggesting that indeed TRPV1 activation may induce an effect on the ER, which is similar to that of bradykinin (Fig. 7.6A, B and C). This is consistent with the Ca^{2+} imaging data presented in the Chapter 5, which demonstrated that capsaicin application induces robust Ca^{2+} release from the ER. Various areas of the cell show increased TIRF signal after capsaicin application (1.074 ± 0.028, $p<0.05$, n=6, 157 grids) (Fig. 7.6A, B, C and D). However, as with all cell responses, there were many areas where there was decreased or no increase in signal (Fig. 7.6D). Comparing peak TIRF intensity between the capsaicin and bradykinin application in HEK cells was not significantly different. In both conditions, there was no major decrease or fluctuations in TIRF intensity as was seen in DRG neurons (Fig. 7.3D and 4D). Therefore, HEK293 cells allow a more stable baseline and coupled with the less loss of signal, provide a potentially more efficient platform to perform these experiments on.

Another analysis approach for this TIRF data is to segment regions of interest (ROIs) using a cross correlated approach based on time courses (Fig. 7.7). Figure 7.7 has been produced by re-analysing the DRG data from figure 7.3 using this approach. The benefit of this analysis technique is the ROIs are segmented using software which is able to group/detect various aspects of the responses together according to their activity, which means that responses from different grids resulting from the same area of the DRG are not treated as 2 different responses. The benefit of this method compared to the grid approach used for analysis above is the fact that this is reproducible and removes any subjectivity. Furthermore, it provides a reproducible way of analysing this kind of data. Therefore, future experiments will be analysed using this technique.

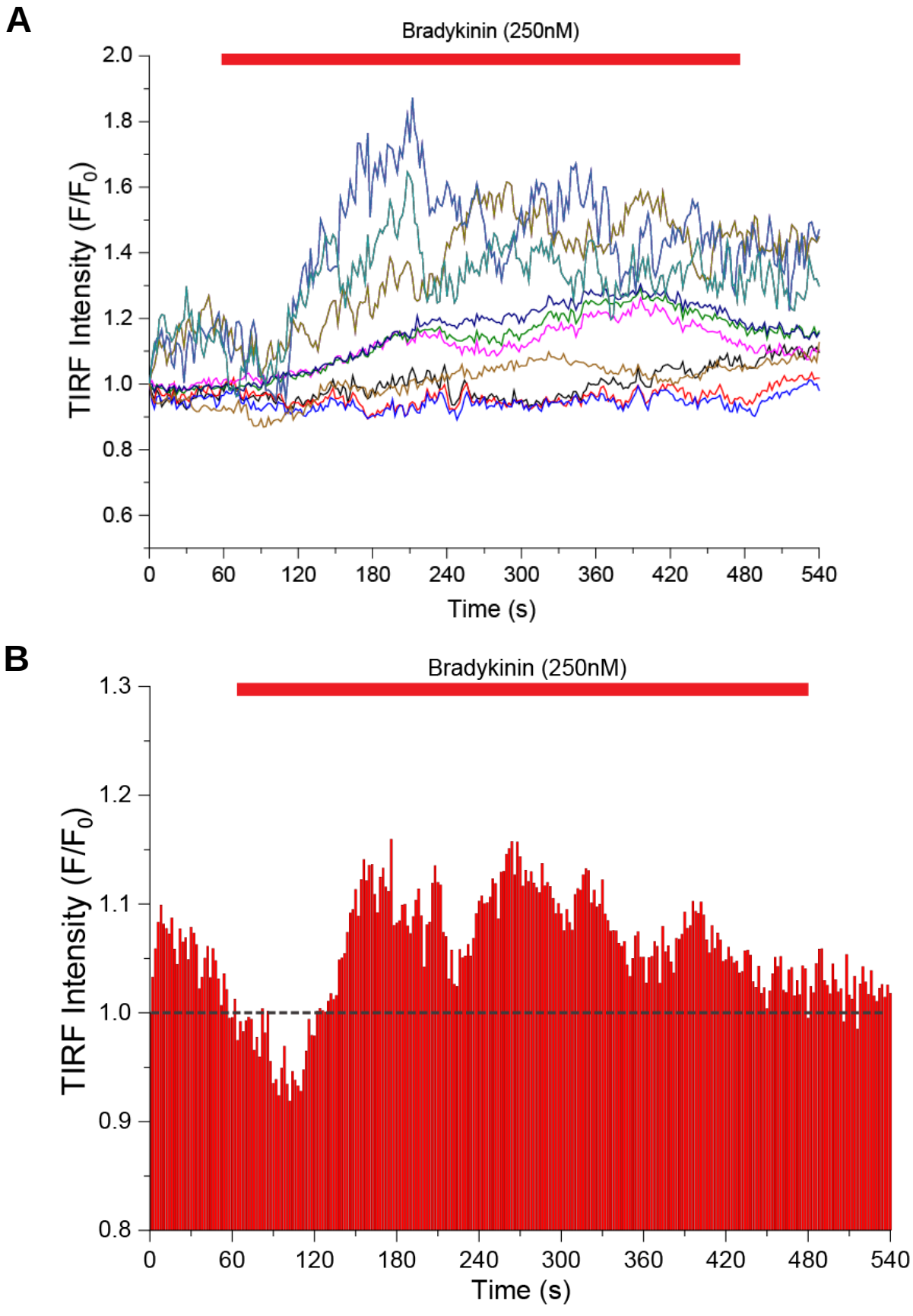
A
Bradykinin (250nM)
TIRF Intensity (F/F0)
2.0
1.8
1.6
1.4
1.2
1.0
0.8
0.6
0
60
120
180
240
300
360
420
480
540
Time (s)
B
Bradykinin (250nM)
TIRF Intensity (F/F0)
1.3
1.2
1.1
1.0
0.9
0.8
0
60
120
180
240
300
360
420
480
540
Time (s)

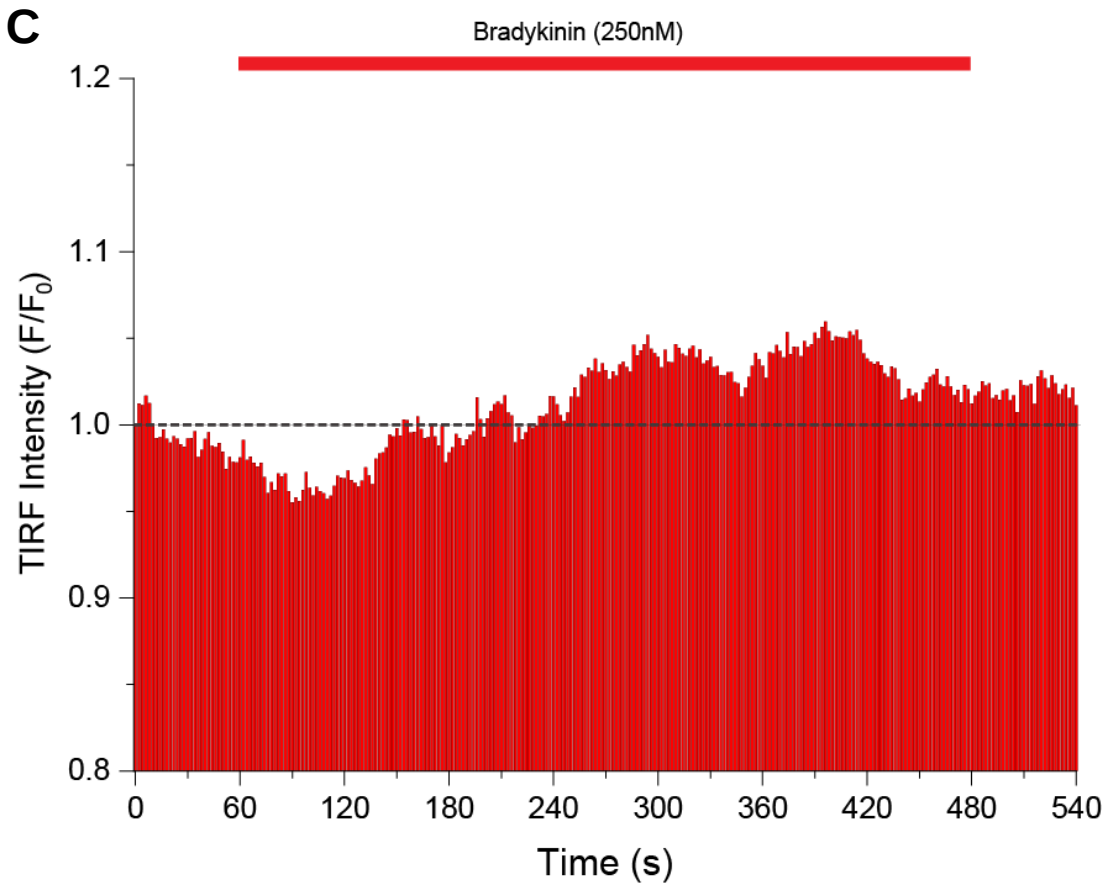

Figure 7.5: ER movement in HEK293 cells transfected with B_2R and CellLight ER-GFP under TIRF after bradykinin (250nM) application. (A) Representative traces showing 'responsive' and 'non-responsive' grids in response to bradykinin application. (B) Average changes (all grids) in TIRF intensity of one 'responsive' cell after bradykinin application. (C) Averages changes in TIRF intensity of all cells (n=6). SEM not shown for clarity.

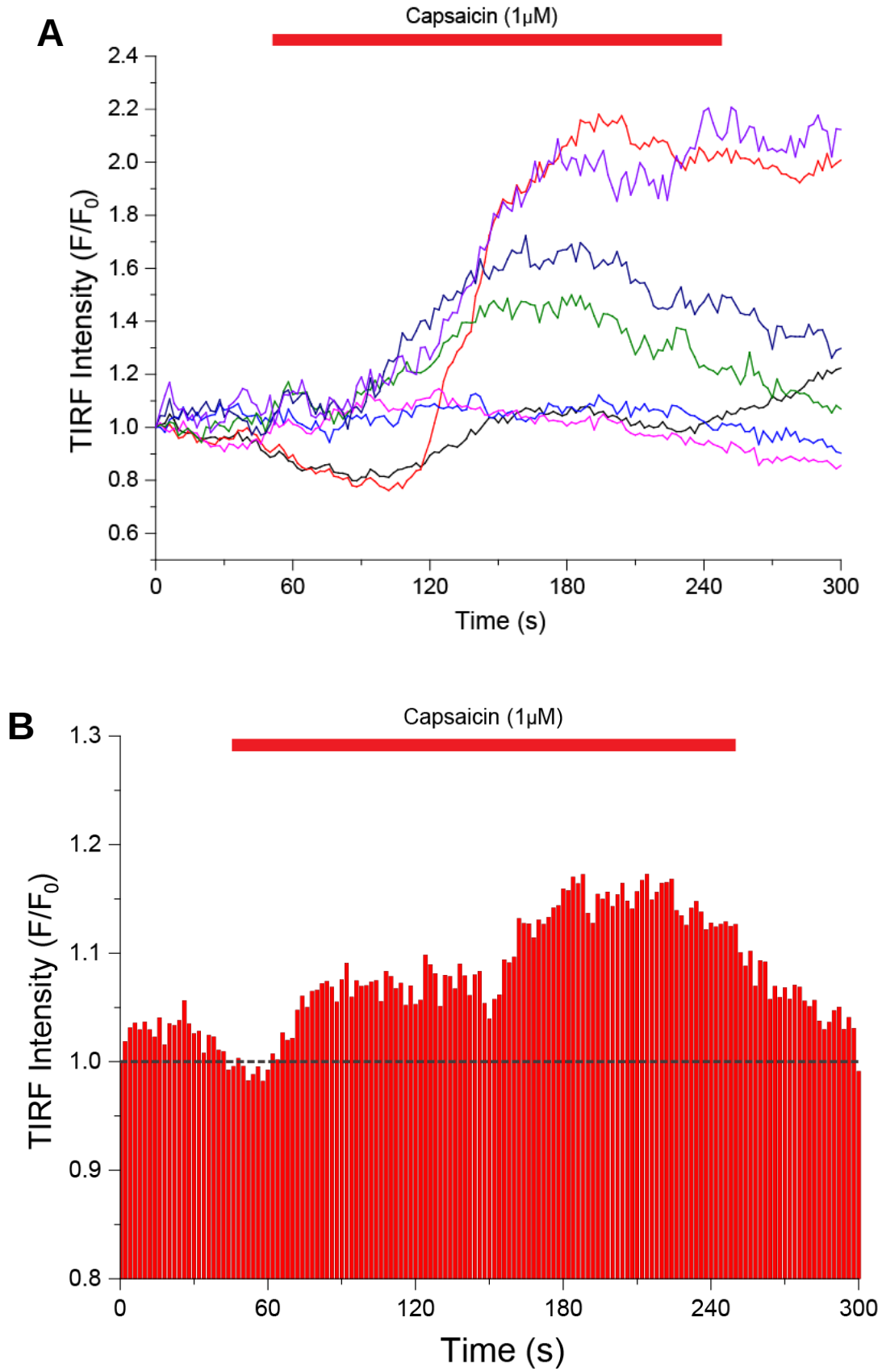
A
Capsaicin (1μM)
TIRF Intensity (F/F0)
2.4
2.2
2.0
1.8
1.6
1.4
1.2
1.0
0.8
0.6
0
60
120
180
240
300
Time (s)
B
Capsaicin (1μM)
TIRF Intensity (F/F0)
1.3
1.2
1.1
1.0
0.9
0.8
0
60
120
180
240
300
Time (s)

C

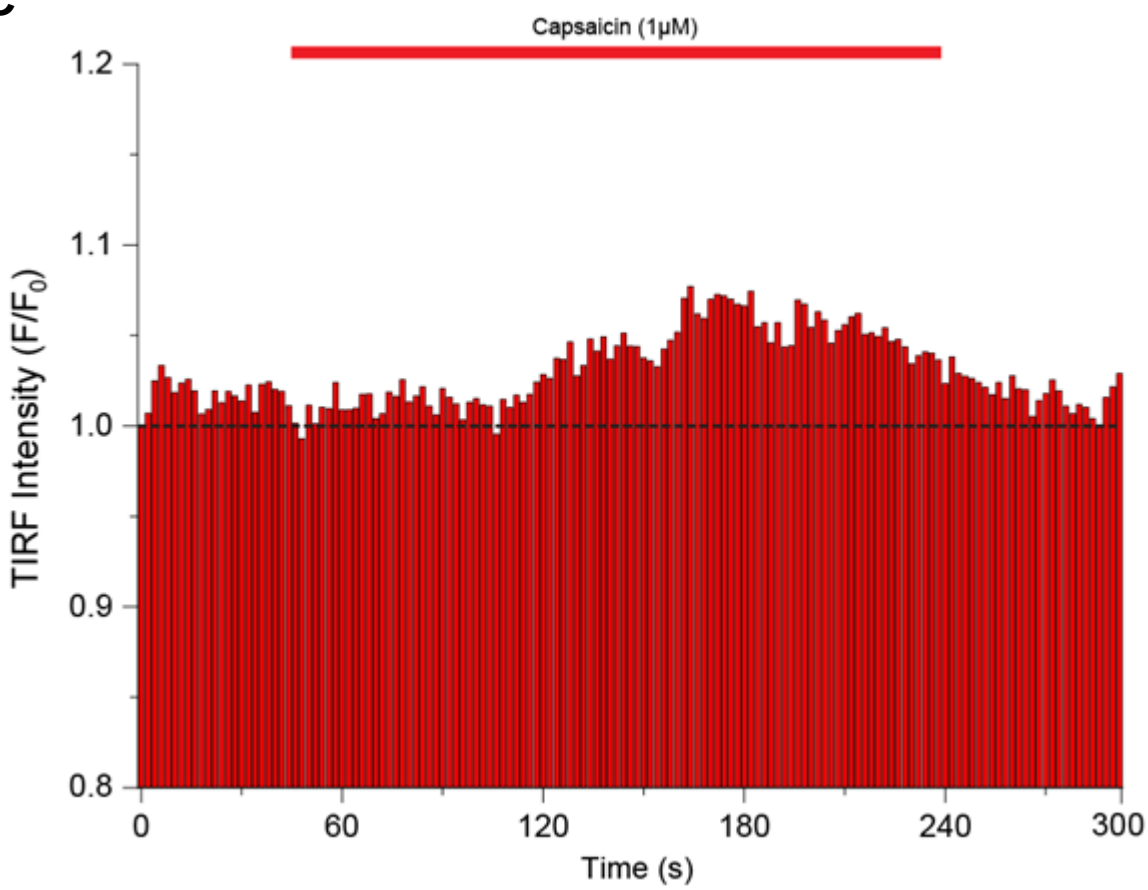
Capsaicin (1μM)
1.2
1.1
1.0
0.9
0.8
TIRF Intensity (F/F0)
0
60
120
180
240
300
Time (s)

D

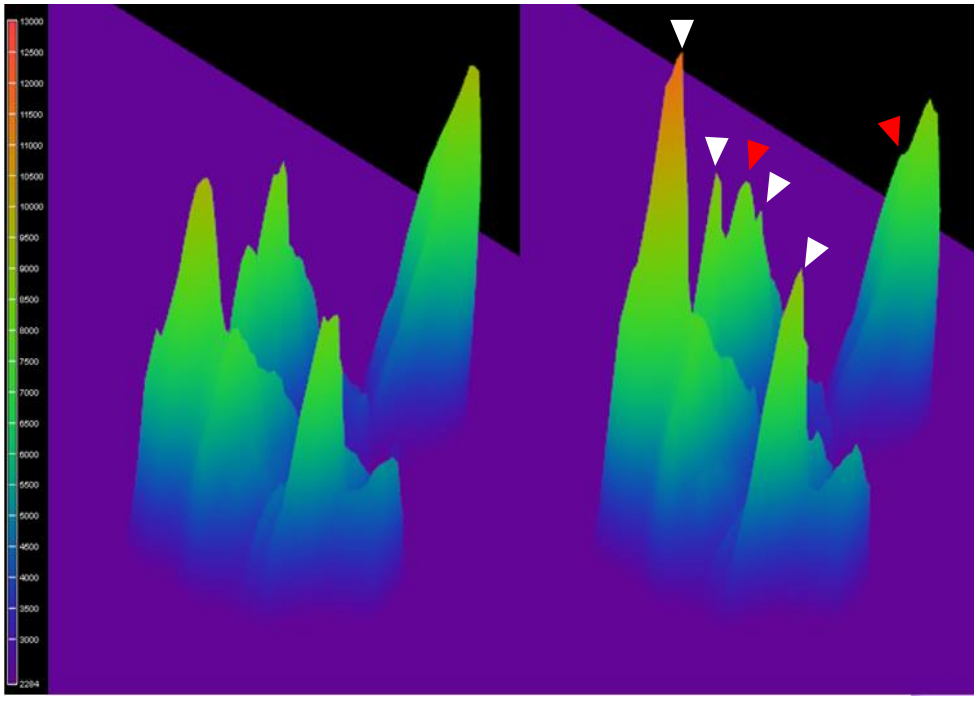

Figure 7.6: ER movement in HEK293 cells transfected with TRPV1 and CellLight ER-GFP under TIRF after capsaicin (1μM) application. (A) Representative traces showing 'responsive' and 'non-responsive' grids in response to capsaicin application. (B) Average changes (all grids) in TIRF intensity of one 'responsive' cell after capsaicin application. (C) Averages changes in TIRF intensity of all cells (n=6). SEM not shown for clarity. (D) Representative image showing intensity profile for application of capsaicin on a responsive HEK293 cell expressing TRPV1 and CellLight ER-GFP. Left panel: Pre-capsaicin application and right panel: Post-capsaicin application. White arrows show areas where there is increased ER-TIRF signal intensity after capsaicin application and red arrow shows area where there was a decreased signal.

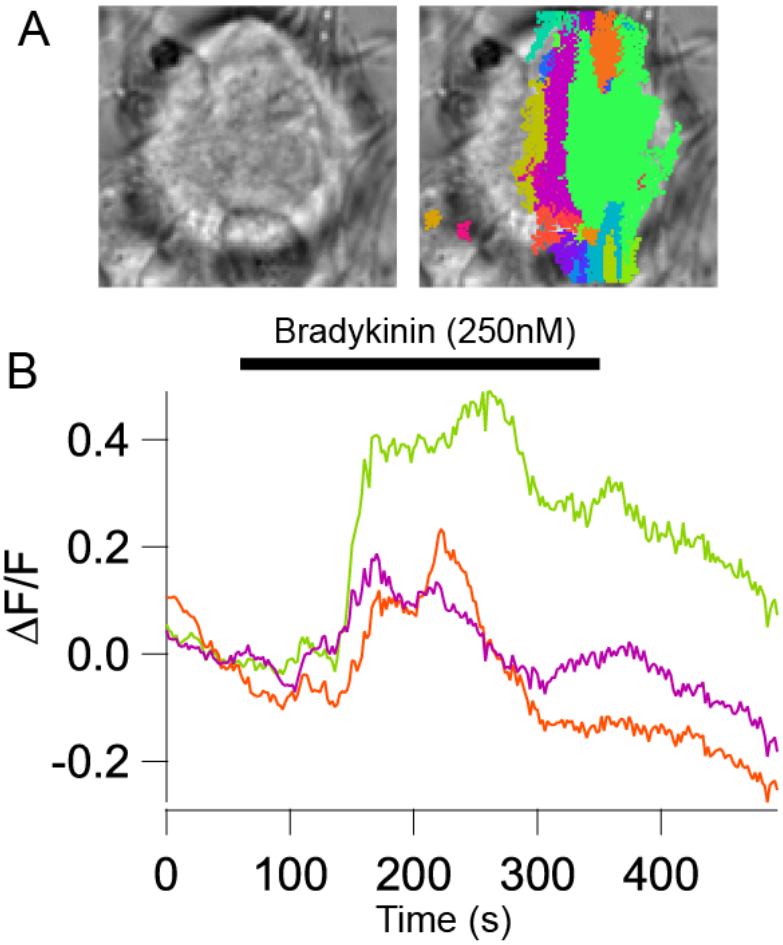
A
Bradykinin (250nM)
B
0.4
0.2
0.0
-0.2
ΔF/F
0
100
200
300
400
Time (s)

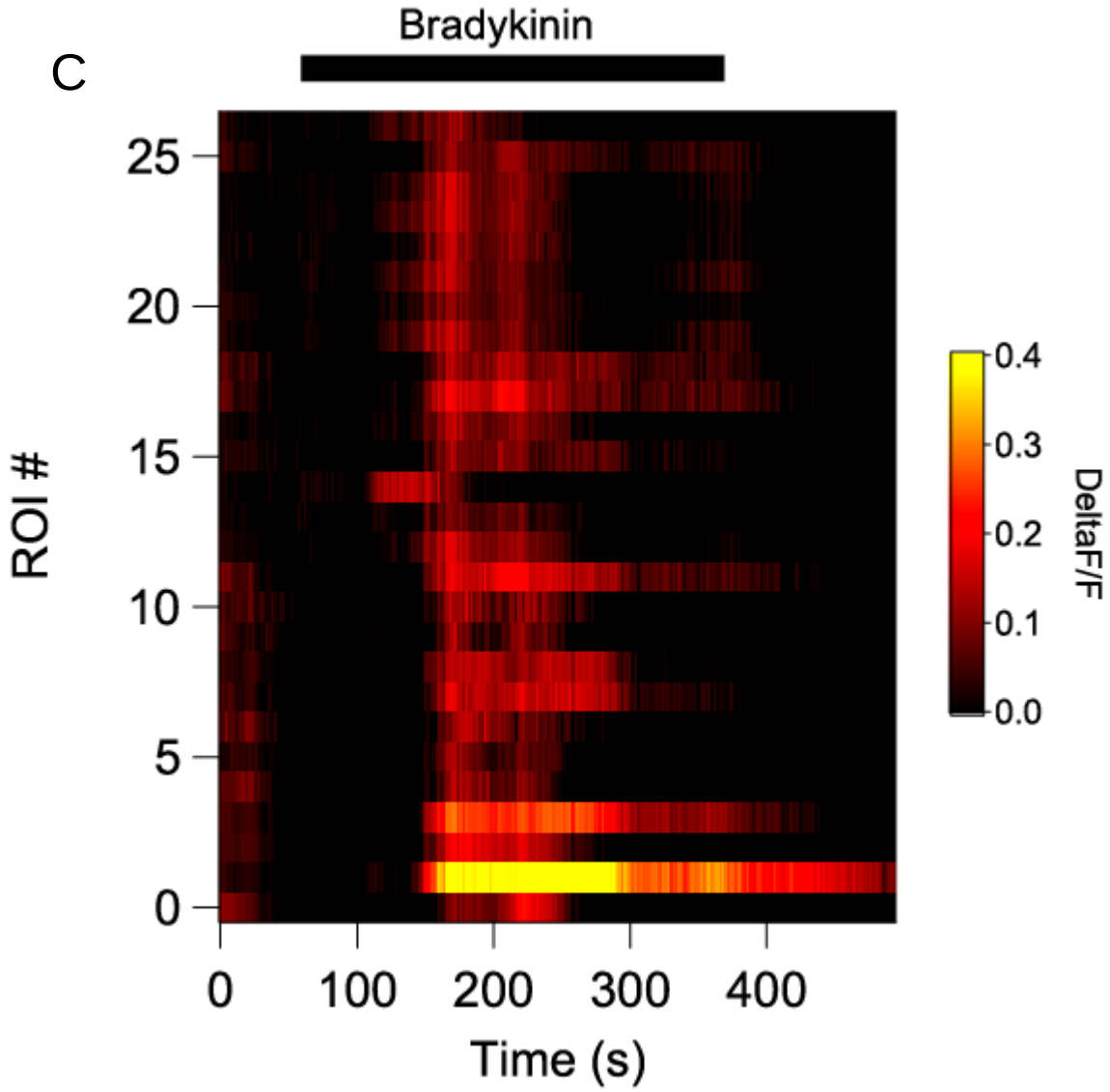

Figure 7.7: Cross correlation approach to analyse TIRF data. Software is able to detect ROIs by analysing the activity in different regions of the cell and combining areas of similar activity over time. (A) Image of DRG (left) and same DRG overlayed with ROIs detected by software (left). (B) Traces from respective colour-coded ROIs detected in (A) after bradykinin application. (C) Raster plot for all ROIs detected showing changes in activity over the duration of the experiment.

7.3 Discussion

Movement of the ER has been documented to occur upon stimulation of GPCRs such as M_1R and during SOCE (Courjaret and Machaca, 2014; Saheki et al., 2016). We decided to investigate this in our studies to understand whether there is any movement of the ER towards the membrane in DRG neurons upon IP_3R activation (after bradykinin or capsaicin application). The data suggest that in both DRG neurons and reconstituted expression systems (HEK293 cells transfected with B_2R or TRPV1), stimulation of ER Ca^{2+} release with either bradykinin or capsaicin did induce closer proximity between the ER and PM, as assessed by the increased ER TIRF signal. Some areas of the cell footprint showed a greater intensity in signal which we interpret as the ER moving closer to the glass-cell surface interface under TIRF (so moving to the PM). There may not be a requirement for all of the ER to move but small areas may translocate closer to the PM where for example, there are ANO1 and IP_3R receptors. The effects were more evident in HEK293 cells as compared to DRG (likely due to the better adherence of the former); capsaicin was found to be more effective in inducing ER-PM proximity as compared to DRG. Our results are also in good agreement with those reported by Courjaret and colleagues who reported that areas of the ER and PM move closer to each other during SOCE in oocytes (Courjaret and Machaca, 2014).

The data reported here are encouraging but should be treated as preliminary due to following facts: (i) it was difficult to image DRG neurons in TIRF mode (see above); (ii) ER-PM junctions in HEK293 cells may not necessarily be identical to these in DRG neurons; and (iii) due to 'patchy' responses within a footprint, these were difficult to analyse. Yet, these results are encouraging and warrant further investigation. Mechanistically, we suggest that both bradykinin (via G_q-PLCβ) and capsaicin (via Ca^{2+}-dependent PLCδ) induce ER Ca^{2+} release, which is associated with concurrent shortening of the ER-PM distance. At this point we cannot ascertain whether new ER-PM junctions are being induced or the process is restricted to the pre-existing junctions, but in either case, this tightening of the ER-PM proximity during the signal transduction may serve to enhance activation of ANO1 channels by the IP_3-mediated Ca^{2+} release from the ER.

These findings may cause one to speculate that ANO1 itself may also use such a mechanism to potentially tether PM-ER junctions. Ist2 consists of a polybasic C-

terminus domain which is rich in lysine and histidine residues and has been shown to be vital for Ist2 interactions with the PM (Juschke et al., 2005; Manford et al., 2012). Loss of this polybasic segment of Ist2 has been shown to abolish ER-PM contacts from forming and introducing a truncated Ist2 protein (consisting of 2 transmembrane domains and the C-terminus) into non-Ist2 expressing cells was sufficient to form ER-PM junctions again (Manford et al., 2012). Unfortunately, ANO1- a human orthologue of Ist2- does not possess this polybasic domain and even though they are related, ANO1 shares very little sequence similarity with Ist2 (Kunzelmann et al., 2016). Therefore, tethering of the ER to the PM has to be through another means. One protein discovered as part of the interactome for ANO1 was endoplasmic reticulum lipid raft-associated protein 1 (ERLIN1) (Perez-Cornejo et al., 2012), an IP_3R regulating protein which associates with IP_3R physically in an activity-dependent manner to facilitate processes such as ER-associated degradation of IP_3R (Pearce et al., 2009). Proteins such as these may therefore play a role in the tethering between ANO1 and TRPV1 which could be essential to identify to fully understand the mechanism in IP_3R-mediated ANO1 activation.

Chapter 8: General discussion

This thesis has focused on the activation of ANO1 by various pro-inflammatory mediators in the context of peripheral nociception. The discovery of ANO1 in 2008 reported expression in DRG neurons as well as many other tissues (Yang et al., 2008). Our lab was the first to characterise the activation of ANO1 in DRG neurons in 2010, which was mediated by bradykinin application (Liu et al., 2010). Pro-inflammatory mediators such as bradykinin are known to sensitise several sensory channels and enhance their activity in nociceptors as well as reduce inhibitory effects of other channels (Geppetti and Trevisani, 2004; Huang et al., 2006; Liu et al., 2010). Bradykinin application led to an excitatory Cl^--dependent inward current being elicited, which was also coupled to an inhibition of M-current (Liu et al., 2010). ANO1 activation in these cells was discovered to couple to the G_q pathway and ultimately IP_3R activation (Liu et al., 2010; Jin et al., 2013) and additionally this was facilitated through arrangement of the channels in functional ER-PM microdomains.

8.1 ANO1-IP_3R microdomains are essential for ANO1 activation

The results in this thesis confirm previous findings regarding coupling of ANO1 to IP_3R activation using a newly developed single cell imaging approach, combining both fura-2 Ca^{2+} imaging and a halide sensitive EYFP mutant to allow monitoring of concurrent Ca^{2+} dynamics and Cl^- channel activity, respectively. This is the first time both of these methods have been combined to simultaneously study CaCC activity. All previous studies to our knowledge have used a single method to record ANO1 activity, such as patch-clamp recordings (Yang et al., 2008; Xiao et al., 2011; Huang et al., 2012; Jin et al., 2013; Vocke et al., 2013) or imaging involving the halide sensitive approach when studying CaCC activity (de la Fuente et al., 2013; Bill et al., 2014; Bill et al., 2015; Seo et al., 2016). The advantage of the method developed herein is in that it allows us to directly correlate the dynamics and properties of intracellular Ca^{2+} signaling with ANO1 activation in live neurons. We successfully demonstrated this technique can be used to monitor CaCC activity and in terms of our study, activation is coupled to IP_3R. Furthermore, we were able to demonstrate that VGCC activation is poorly coupled to this CaCC activity, again highlighting the preference of ANO1 to local Ca^{2+} rises delivered through IP_3R activation. This was exemplified by the observation that EYFP (H148Q/I152L) mutant quenching was present during bradykinin application in extracellular Ca^{2+} free conditions but not

upon VGCC activation despite similar Ca^{2+} transients being observed in both cases. The low Ca^{2+} sensitivity of ANO1 dictates the requirement for high Ca^{2+} levels to induce activation which seemingly protects ANO1 activation from global Ca^{2+} rises (Yang et al., 2008; Liu et al., 2010; Jin et al., 2013). ANO1 activation through transient, highly localised Ca^{2+} elevation therefore provides selectivity in terms of activation. In a nociceptive context, one of the roles of ANO1 is its involvement in amplifying the effects of other stimuli thus providing increased pain sensation. If all Ca^{2+} signals were able to activate ANO1, then this amplification aspect would be lost therefore, only pro-nociceptive signals seem to activate ANO1 (see below).

The formation of Ca^{2+} microdomains allows the facilitation of ANO1 activation. ER-PM junctions provide the platform for microdomain formation between ANO1 and IP_3R, however the mechanism behind this junction formation is as of yet unknown. It may well be a protein that tethers the ER to the PM or ANO1 and IP_3R themselves that allow this to occur. A protein mentioned in the previous chapter, E-syt1 allows the ER and PM to come into close contact in a Ca^{2+} dependent manner (Min et al., 2007). Interestingly, there is high expression of this protein in DRG neurons as demonstrated by the Allen Brain Atlas. IP_3R activation causes Ca^{2+} release, which may cause E-syt1 to bring the ER and PM into closer proximity and therefore increase the localised Ca^{2+} concentration for ANO1 activation. However, this is somewhat unclear at the moment as studies have found that extracellular Ca^{2+} (through SOCE) is required for E-syt1 tethering but knocking out E-syt1 doesn't affect SOCE in HeLa cells (Giordano et al., 2013; Idevall-Hagren et al., 2015). Therefore, potential E-Syt1 studies in DRG neurons appear be an extremely enticing and intriguing prospect.

It has also been demonstrated using GST-pulldown assays that the intracellular loops between TM 2 and TM 3 and the C-terminus of ANO1 interact with IP_3R1 (Jin et al., 2013); this may tether both proteins and contribute to the formation of very tight ER-PM junctions and further enhance the effects of IP_3R localised Ca^{2+} increases, hence further facilitating ANO1 activation. As mentioned in the previous chapter, ERLIN1 is part of the ANO1 interactome (Perez-Cornejo et al., 2012) and is known to mediate IP_3R-related processes by physically interacting with IP_3R (Jin et al., 2014). Such a protein that interacts with both ANO1 and IP_3R may well be dependent on TM 2 and TM 3 and the C-terminus of ANO1 to form interactions

between the 2 proteins. Other scaffolding proteins such as Homer1b/c, are known to link IP_3Rs to PM-localised proteins (i.e. metabotropic glutamate receptors (Tu et al., 1998)), and has been found to interact with ANO1 and potentially play a role in the production of ER-PM junctions (unpublished data). Junctophilin proteins are expressed in DRG neurons and may also be involved in the formation of ER-PM junctions. Further research is required to elucidate such scenarios.

8.2 TRPV1 also activates ANO1 through ER Ca^{2+} mobilisation

TRPV1 is the prototypic noxious heat sensor of the body and is activated in a polymodal manner (Rohacs et al., 2008). Recent studies have been able to demonstrate coupling between ANO1 and TRPV1 in DRG neurons. ANO1 and TRPV1 were found to be physically coupled using biochemical approaches and Ca^{2+} buffering experiments (Takayama et al., 2015). It was proposed that the functional interaction between ANO1 and TRPV1 occurred through a local Ca^{2+} nanodomain (Takayama et al., 2015); this observation was made based on EGTA (slow Ca^{2+} buffer) and BAPTA (fast Ca^{2+} buffer) chelating experiments, where BAPTA and EGTA were both unable to inhibit ANO1 activity after TRPV1 activation hence the nanodomain idea was put forward. Yet, BAPTA has been known to inhibit Ca^{2+} nanodomains too (Eggermann et al., 2011; Arai and Jonas, 2014); an example of this has been demonstrated at synapses where neurotransmitter release occurs. Nanodomain coupling of presynaptic Ca^{2+} channels and Ca^{2+}-sensors (10-20nm) for neurotransmitter release has been established (Bucurenciu et al., 2008; Eggermann et al., 2011; Arai and Jonas, 2014). BAPTA has also been used successfully to inhibit such coupling in basket cells (Bucurenciu et al., 2008; Arai and Jonas, 2014). Therefore it is unclear as to the observations made by Takayama and colleagues.

Importantly, even if BAPTA inhibited ANO1 activity in these assays, it could still not distinguish between the direct effect of TRPV1 on ANO1 or ER-mobilising effects as BAPTA can also inhibit IP_3R-induced ANO1 activation (Jin et al., 2013). We used our dual imaging approach to show that TRPV1 was indeed able to induce an anionic flux in our setup; this was coupled to a rise in $[Ca^{2+}]_i$. Interestingly, we found that depletion of Ca^{2+} from internal stores significantly reduced both Ca^{2+} elevation and halide sensitive EYFP quenching induced in DRG after capsaicin application. Furthermore, capsaicin application to DRG in Ca^{2+}-free extracellular bath solution still evoked Ca^{2+} transients, suggesting that TRPV1 activation can induce

intracellular Ca^{2+} transients even in the absence of Ca^{2+} influx from the extracellular space.

TRPV1 has been found to activate PLC, which leads to subsequent IP_3 generation and hence IP_3R activation (Lukacs et al., 2007). Ca^{2+} independent PLCs may be present in DRG to facilitate this activity (Lukacs et al., 2007) or alternatively TRPV1 in the ER may induce this activity (Gallego-Sandin et al., 2009). Thus, the exact mechanism by which activation of TRPV1 causes ER Ca^{2+} release requires future investigation. To definitively show that the mobilisation of internal stores plays a role in TRPV1-induced ANO1 activation, we coupled our dual imaging approach to also monitor ER-Ca^{2+} dynamics using CEPIAs in CHO cells (Suzuki et al., 2014). Application of capsaicin produced Ca^{2+} elevation, EYFP quenching and a loss of ER Ca^{2+} in CHO cells transfected with ANO1 and TRPV1. This strengthened the notions regarding involvement of ER-Ca^{2+} release in TRPV1 activity and ANO1 activation. To further validate our findings and investigate the route by which Ca^{2+} is released, an IP_3R inhibitor, xestospongin C, was used to inhibit IP_3R in our triple imaging approach. Xestospongin C was able to reduce cytosolic Ca^{2+}, EYFP quenching and CEPIA-monitored ER Ca^{2+} release, which adds support to our conclusion that IP_3R is activated during TRPV1 activation. This is a logical means by which ANO1 is activated as (i) we have already established that activity of ANO1 requires IP_3R Ca^{2+} release, (ii) TRPV1 is able to activate PLCδ and produce IP_3 (Lukacs et al., 2007; Rohacs et al., 2008) and (iii) ER-localised TRPV1 activation has been found to induce cell death (Thomas et al., 2007) therefore would seem an unlikely mechanism for activity.

We have also demonstrated the proximity between ANO1 and TRPV1 using both PLA and STORM. Previously, it has been demonstrated that ANO1 and TRPV1 are found in complex with each other through biochemical studies (Takayama et al., 2015). We have been able to show that there is close proximity between these proteins in DRG neurons, however this doesn't necessarily mean a direct effect of TRPV1 on ANO1 as proposed by Takayama and colleagues. It could suggest localisation with ANO1 allows TRPV1 to influence ANO1 through already-coupled IP_3R. Furthermore, preliminary triple STORM indeed suggests the presence of complexes consisting of ANO1, TRPV1 and IP_3R1 in DRG.

Additional studies regarding the dynamics of the ER suggest that the distance between the ER and PM is reduced after stimulation of ER Ca^{2+} mobilising receptors. Bradykinin application to DRG transfected with an ER-specific marker demonstrated that certain areas of the ER respond with a greater intensity signal under TIRF, suggestive of closer proximity between the ER and PM. This was also the case after capsaicin application; whilst this does not definitively show the ER is mobilised by TRPV1 activation, the ER behaving in a manner similar to that after bradykinin application (which does induce ER-Ca^{2+} release) may be indicative of ER activation. Coupled to the findings of our PLA and STORM experiments, the ER may move to the PM to facilitate ANO1 activation by IP_3R. Further research is required to fully elucidate the mechanisms behind ER movement.

8.3 ANO1 in physiological pain

So where does this fit in with the process of pain transmission? ANO1 is also a heat sensor so activation under noxious temperatures contributes to heat pain signals (Cho et al., 2012) however it is in inflammatory pain where ANO1 activity is most likely to produce effects that contribute to pain. In nociceptors, the various pro-algesic effects happen at once, thus bradykinin release and TRPV1 activation could occur simultaneously along with other pro-inflammatory/algesic effects. In the context of inflammatory pain, tissue injury leads to release of pro-inflammatory mediators such as bradykinin and PAR-2 agonists and activation of ANO1 through the G_q-protein coupled signaling cascade (Linley et al., 2010). ANO1 is then able to produce a depolarising effect on the nociceptor, fitting in well with the depolarisation attributed to bradykinin-induced Ca^{2+} release (Linley et al., 2010). Simultaneously, activation of TRPV1 (i.e. proton release from injured tissue) leads to further depolarisation through its own cation influx and ANO1 activation- according to our results- via ER-induced Ca^{2+} release. In inflammatory conditions, it has been demonstrated that further Cl^- accumulation occurs in the cytosol; the concentration has been shown to elevate due to NKCC1 phosphorylation (Funk et al., 2008). These combined depolarisations will ultimately lead to Na_v activation and action potential firing. Moreover, depolarisation and $[Ca^{2+}]_i$ elevation through non-ANO1 activating means i.e. Na_v and VGCC activation, respectively, will subsequently affect ANO1 sensitivity meaning ANO1 will require lower $[Ca^{2+}]_i$ to be activated. In theory, this may allow other poorly-coupled Ca^{2+} sources to activate ANO1 however, this

may well be a factor contributing to or facilitating chronic pain conditions (see below). Additionally to the range of effects mentioned, other pro-algesic attributes of the inflammatory mediators (i.e. bradykinin causes TRPV1 sensitisation and M-current inhibition etc.), mean enhanced excitability of nociceptors and subsequently greater pain transmission. This demonstrates the complexity of nociception and how so many interconnecting aspects of this process occur, involving such a small number of proteins. Other, not yet resolved, aspects of ANO1 activation and nociception on a whole may well further connect into this paradigm.

8.4 Chronic pain involving ANO1: is there basis for this to occur?

When pain occurs without injury or persists after healing, it is referred to as chronic pain (Woolf and Mannion, 1999; Linley et al., 2010). One major reason for the onset of chronic pain conditions invovles the alteration in the excitability profile of nociceptors (Linley et al., 2010). A change in ion channel expression, whether this is an increase in excitatory or decrease in inhibitory channels, can lead to increased excitability of nociceptors- this also applies to ANO1 (Fig. 8.2). Firstly, ANO1 upregulation itself may underlie some aspects of chronic pain. If there are enhanced levels of ANO1 protein, activation of more channels will lead to an amplified ANO1-mediated Cl^- efflux, resulting in more microdomains being present through a greater number of ER-PM junctions (more ANO1 and IP_3R in closer proximity). Formation of de novo microdomains may lead to non ANO1-activating Ca^{2+} sources for example, VGCCs, which are known to be upregulated during chronic pain conditions (Perret and Luo, 2009), to gain proximity to ANO1 channels. In such a scenario VGCC activation could cause a positive feedback loop and overexcitability (see introduction). Lipid rafts maintain organisation of proteins in the plasma membrane and ANO1, TRPV1 and B_2R receptors are known to localise to these lipid-enriched areas of the membrane (Lamb et al., 2002; Sones et al., 2010; Szoke et al., 2010; Jin et al., 2013). Loss of lipid raft components such as cholesterol is known to alter ANO1 activation by reversing the coupling to VGCCs and uncoupling with IP_3R (Jin et al., 2013). This would also lead to over-activation of ANO1 through a positive-feedback loop by Ca^{2+} influx through VGCCs (Liu et al., 2010). Again this could be part of a chronic pain condition where standard coupling is lost and re-coupling to another non-ANO1 activating Ca^{2+} source occurs leading to overexcitability (i.e. VGCC) (Fig. 8.2).

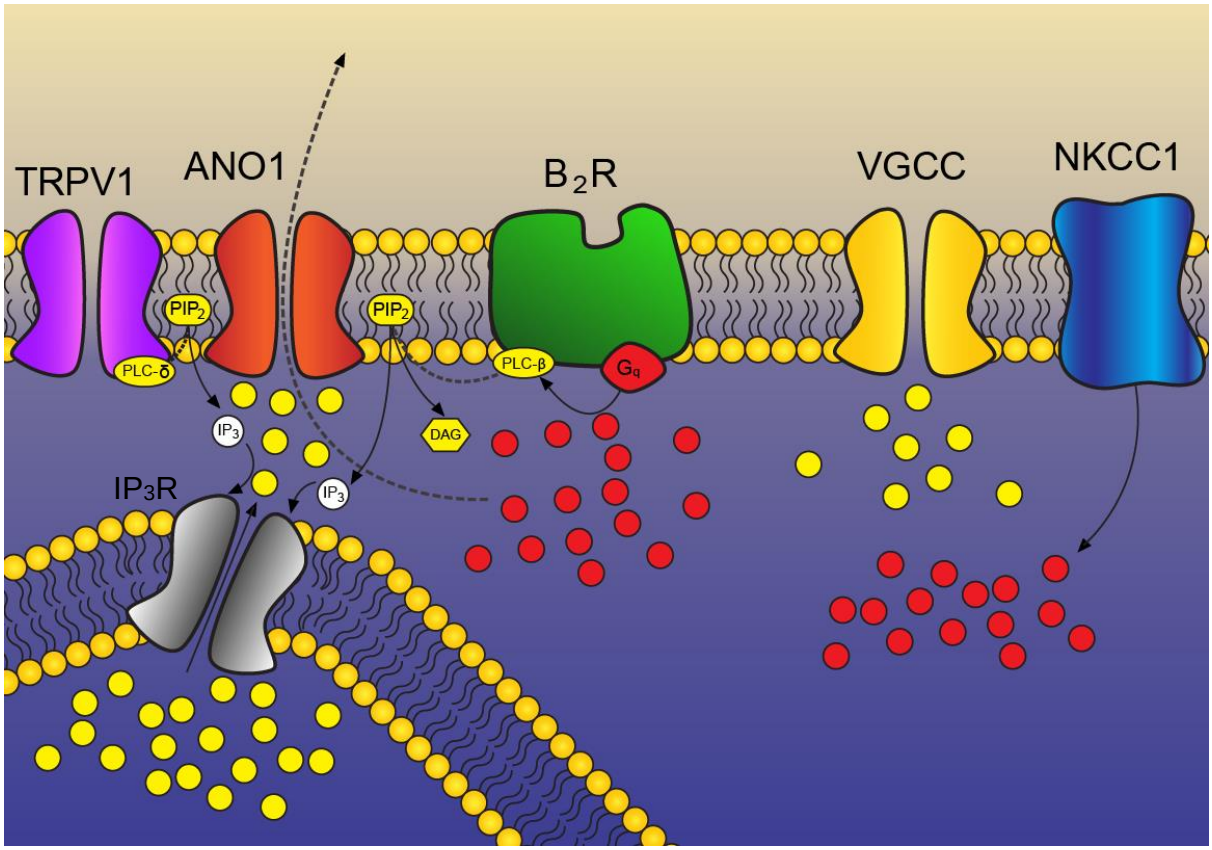

Figure 8.1: ANO1 in Inflammatory pain. Tissue damage leads to release of inflammatory mediators which activate receptors such as B_2R and TRPV1. Both are able to induce IP_3R activation and subsequent ANO1 activation through a local Ca^{2+} microdomain. NKCC1 accumulates Cl^- in the cytosol allowing the E_{cl} to be greater than resting membrane potential, hence inducing excitatory ANO1 activity. VGCCs on the other hand are not part of the microdomain, hence unable to activate ANO1 effectively. Other effects such as TRPV1 sensitisation by B_2R-activated PKC, M-current inhibition and increased $[Ca^{2+}]_i$ entry through IP_3R and TRPV1 (amongst other channels) depolarise nociceptive fibres and activate VGSCs, causing action potential firing. This further sensitises ANO1 leading to more activity and increased pain sensation.

NKCC1 expression is vital for accumulation of Cl^- in cells and DRG are known to express NKCC1 (Mao et al., 2012; Modol et al., 2014). Loss of NKCC1 through genetic ablation has been found to impair Cl^- accumulation in DRG and reduce thermal hyperalgesia in mice (Sung et al., 2000). Moreover, mechanical allodynia was also attenuated in mice with NKCC1-KO (Laird et al., 2004). This suggests a role for Cl^- accumulation, which ultimately results in excitatory activity of ANO1 (Liu et al., 2010). In inflammatory conditions, Cl^- accumulation is enhanced and serves to increase the driving force for Cl^- channel efflux (Funk et al., 2008). This isn't the only type of condition where Cl^- accumulation leads to alteration of normal neuronal activity. In epilepsy, hippocampal (Rivera et al., 1999; Palma et al., 2006) and cortical (Cohen et al., 2002; Jin et al., 2005) neurons show increased Cl^- accumulation causing GABAergic and glycinergic activation to become excitatory (Price et al., 2005). Neuropathic pain syndromes following spinal cord injury (SCI) also demonstrate Cl^- accumulation (from 31mM to 68mM), which was due to increased levels of NKCC1 protein as well as reduced KCC2 for Cl^- extrusion (Hasbargen et al., 2010). This imbalance in Cl^- regulatory proteins underlies neuropathic pain in SCI rat models and can be reduced by the NKCC1 blocker bumetanide (Hasbargen et al., 2010). Bumetanide also shows attenuation of pain responses in various pain models including TRPV1-dependent allodynia (Pitcher et al., 2007), histamine-induced itch and flare responses in skin (Willis et al., 2004) and formalin-induced nocifensive behavioural tests (Granados-Soto et al., 2005). This suggests increasing $[Cl^-]_i$ provides a greater means for ANO1 dependent excitatory activity, ultimately providing a platform by which ANO1 could be targeted for therapeutic intervention in pain syndromes.

8.5 Future research

All of the above mentioned points are fascinating aspects regarding putative roles ANO1 could play in chronic pain. Using this work as a basis for future studies may allow us to open new pathways for therapeutic intervention. In terms of the direction for future work, it may be worthwhile investigating the junctions that may be in place to allow ANO1 activation in DRG neurons. Some of these proteins have been suggested in chapter 7 and therefore it may be of interest to look at these in DRG neurons and if they are able to influence ANO1 activity. Gamper lab has already shown the presence of some junctophilin isoforms in DRG so it would be interesting

to demonstrate the effects of junctophilin KO on ANO1 activity- possibly utilising our halide-sensitive imaging approach developed in this thesis. Recently published material has suggested that E-syts proteins are able to play a role in trafficking of ANO1 proteins (Lerias et al., 2018). This may indicate a more complex role in not only trafficking but actual ANO1 activity given knockdown of E-syts family members reduces ANO1 current density (Lerias et al., 2018). Other investigations can include identifying various proteins that interact with ANO1 in DRG neurons so pulling down proteins using full-length ANO1 may be beneficial for this, hence providing a clearer picture of how these may lead to microdomain formation. As mentioned, if junctional proteins are indeed involved in aspects of ANO1 activity, they may also play a role in inflammatory or chronic pain by producing too many junctions, therefore generation of transgenic animals with DRG specific KO of potential microdomain proteins may allow us to find new ways to combat inflammatory pain. These are just some examples to pursue for further insight into the contribution of ANO1 to various types of pain.

To summarise, the various findings of this thesis provide greater insight into the mechanisms regarding ANO1 activation in DRG neurons, especially regarding TRPV1 activation. The activity of ANO1 leads to an excitatory effect and in the context of nociception, increased pain sensation. The methods used in this study will aid general studies into ANO1 and CaCCs in various tissues and allow greater understanding of mechanisms of Cl^- channel activity in general. However, further research is required to fully elucidate the implications of ANO1 in pain transmission.

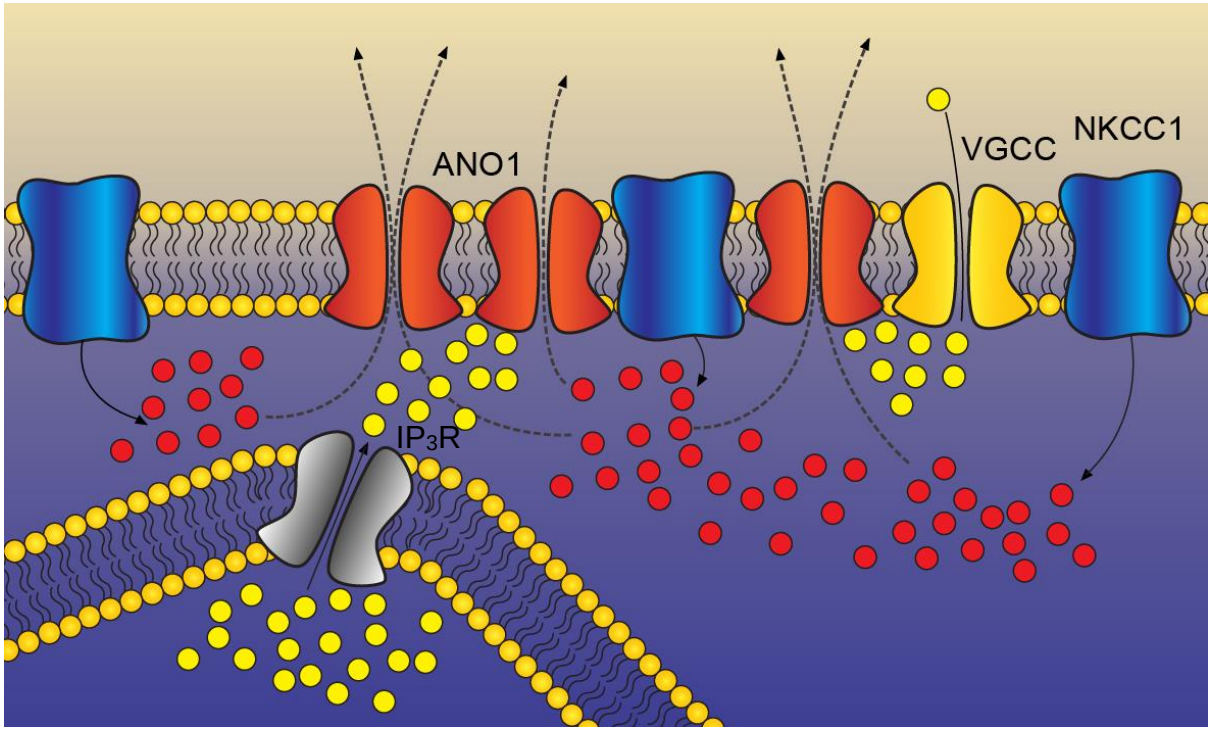

Figure 8.2: Potential ways by which ANO1 may contribute to chronic pain.
Increased ANO1 presence may lead to a greater number of ER-PM junctions hence greater coupling of IP_3R to ANO1 channels. Ca^{2+} release from the ER may result in a greater number of ANO1 channels being activated therefore, a greater excitatory effect. Loss of lipid rafts may result in loss of normal coupling and re-coupling to non-ANO1 activating Ca^{2+} sources, such as VGCCs. Positive feedback loops could form as ANO1-dependent excitation would activate more VGCC activation and result in action potential firing. Finally, upregulation of NKCC1 may lead to enhanced Cl^- accumulation, providing a greater driving force for ANO1 activity.

References

Abd El-Rahman RR, Harraz OF, Brett SE, Anfinogenova Y, Mufti RE, Goldman D, Welsh DG (2013) Identification of L- and T-type Ca2+ channels in rat cerebral arteries: role in myogenic tone development. American journal of physiology Heart and circulatory physiology 304:H58-71.

Accardi A, Pusch M (2003) Conformational changes in the pore of CLC-0. The Journal of general physiology 122:277-293.

Adomaviciene A, Smith KJ, Garnett H, Tammaro P (2013) Putative pore-loops of TMEM16/anoctamin channels affect channel density in cell membranes. The Journal of physiology 591:3487-3505.

Agarwal MK, Bhatia SJ, Desai SA, Bhure U, Melgiri S (2002) Effect of red chillies on small bowel and colonic transit and rectal sensitivity in men with irritable bowel syndrome. Indian journal of gastroenterology : official journal of the Indian Society of Gastroenterology 21:179-182.

Akagi H, Hirai K, Hishinuma F (1991) Cloning of a glycine receptor subtype expressed in rat brain and spinal cord during a specific period of neuronal development. FEBS letters 281:160-166.

Akbar A, Yiangou Y, Facer P, Walters JR, Anand P, Ghosh S (2008) Increased capsaicin receptor TRPV1-expressing sensory fibres in irritable bowel syndrome and their correlation with abdominal pain. Gut 57:923-929.

Akopian AN (2011) Regulation of nociceptive transmission at the periphery via TRPA1-TRPV1 interactions. Current pharmaceutical biotechnology 12:89-94.

Al-Jumaily M, Kozlenkov A, Mechaly I, Fichard A, Matha V, Scamps F, Valmier J, Carroll P (2007) Expression of three distinct families of calcium-activated chloride channel genes in the mouse dorsal root ganglion. Neuroscience bulletin 23:293-299.

Almaca J, Tian Y, Aldehni F, Ousingsawat J, Kongsuphol P, Rock JR, Harfe BD, Schreiber R, Kunzelmann K (2009) TMEM16 proteins produce volume-regulated chloride currents that are reduced in mice lacking TMEM16A. The Journal of biological chemistry 284:28571-28578.

Altier C, Dale CS, Kisilevsky AE, Chapman K, Castiglioni AJ, Matthews EA, Evans RM, Dickenson AH, Lipscombe D, Vergnolle N, Zamponi GW (2007) Differential role of N-type calcium channel splice isoforms in pain. The Journal of neuroscience : the official journal of the Society for Neuroscience 27:6363-6373.

Amadesi S, Cottrell GS, Divino L, Chapman K, Grady EF, Bautista F, Karanjia R, Barajas-Lopez C, Vanner S, Vergnolle N, Bunnett NW (2006) Protease-activated receptor 2 sensitizes TRPV1 by protein kinase Cepsilon- and A-dependent mechanisms in rats and mice. The Journal of physiology 575:555-571.

Ambudkar IS (2007) TRPC1: a core component of store-operated calcium channels. Biochemical Society transactions 35:96-100.

Amedee T, Despeyroux S (1995) ATP activates cationic and anionic conductances in Schwann cells cultured from dorsal root ganglia of the mouse. Proceedings Biological sciences 259:277-284.

Amir R, Michaelis M, Devor M (2002) Burst discharge in primary sensory neurons: triggered by subthreshold oscillations, maintained by depolarizing afterpotentials. The Journal of neuroscience : the official journal of the Society for Neuroscience 22:1187-1198.

Anand P, Bley K (2011) Topical capsaicin for pain management: therapeutic potential and mechanisms of action of the new high-concentration capsaicin 8% patch. British journal of anaesthesia 107:490-502.

Andre S, Boukhaddaoui H, Campo B, Al-Jumaily M, Mayeux V, Greuet D, Valmier J, Scamps F (2003) Axotomy-induced expression of calcium-activated chloride current in subpopulations of mouse dorsal root ganglion neurons. Journal of neurophysiology 90:3764-3773.

Andrei SR, Sinharoy P, Bratz IN, Damron DS (2016) TRPA1 is functionally co-expressed with TRPV1 in cardiac muscle: Co-localization at z-discs, costameres and intercalated discs. Channels (Austin) 10:395-409.

Aprison MH, Werman R (1965) The distribution of glycine in cat spinal cord and roots. Life sciences 4:2075-2083.

Arai I, Jonas P (2014) Nanodomain coupling explains Ca(2)(+) independence of transmitter release time course at a fast central synapse. eLife 3.

Arias-Calderón M, Almarza G, Díaz-Vegas A, Contreras-Ferrat A, Valladares D, Casas M, Toledo H, Jaimovich E, Buvinic S (2016) Characterization of a multiprotein complex involved in excitation-transcription coupling of skeletal muscle. Skeletal Muscle 6:15.

Arniges M, Vazquez E, Fernandez-Fernandez JM, Valverde MA (2004) Swelling-activated Ca2+ entry via TRPV4 channel is defective in cystic fibrosis airway epithelia. The Journal of biological chemistry 279:54062-54068.

Aronsen JM, Swift F, Sejersted OM (2013) Cardiac sodium transport and excitation-contraction coupling. J Mol Cell Cardiol 61:11-19.

Arora P, Ricks TK, Trejo J (2007) Protease-activated receptor signalling, endocytic sorting and dysregulation in cancer. Journal of cell science 120:921-928.

Arreola J, Melvin JE (2003) A novel chloride conductance activated by extracellular ATP in mouse parotid acinar cells. The Journal of physiology 547:197-208.

Avila-Medina J, Calderon-Sanchez E, Gonzalez-Rodriguez P, Monje-Quiroga F, Rosado JA, Castellano A, Ordonez A, Smani T (2016) Orai1 and TRPC1 Proteins Co-localize with CaV1.2 Channels to Form a Signal Complex in Vascular Smooth Muscle Cells. The Journal of biological chemistry 291:21148-21159.

Bader CR, Bertrand D, Schwartz EA (1982) Voltage-activated and calcium-activated currents studied in solitary rod inner segments from the salamander retina. The Journal of physiology 331:253-284.

Bader CR, Bertrand D, Schlichter R (1987) Calcium-activated chloride current in cultured sensory and parasympathetic quail neurones. The Journal of physiology 394:125-148.

Bagriantsev SN, Gracheva EO, Gallagher PG (2014) Piezo proteins: regulators of mechanosensation and other cellular processes. The Journal of biological chemistry 289:31673-31681.

Bannister RA, Pessah IN, Beam KG (2009) The skeletal L-type Ca(2+) current is a major contributor to excitation-coupled Ca(2+) entry. The Journal of general physiology 133:79-91.

Barbado M, Fablet K, Ronjat M, De Waard M (2009) Gene regulation by voltage-dependent calcium channels. Biochimica et biophysica acta 1793:1096-1104.

Barclay J, Patel S, Dorn G, Wotherspoon G, Moffatt S, Eunson L, Abdel'al S, Natt F, Hall J, Winter J, Bevan S, Wishart W, Fox A, Ganju P (2002) Functional downregulation of P2X3 receptor subunit in rat sensory neurons reveals a significant role in chronic neuropathic and inflammatory pain. The Journal of neuroscience : the official journal of the Society for Neuroscience 22:8139-8147.

Barnard EA, Skolnick P, Olsen RW, Mohler H, Sieghart W, Biggio G, Braestrup C, Bateson AN, Langer SZ (1998) International Union of Pharmacology. XV. Subtypes of gamma-aminobutyric acidA receptors: classification on the basis of subunit structure and receptor function. Pharmacological reviews 50:291-313.

Barnes S, Hille B (1989) Ionic channels of the inner segment of tiger salamander cone photoreceptors. The Journal of general physiology 94:719-743.

Barondeau DP, Putnam CD, Kassmann CJ, Tainer JA, Getzoff ED (2003) Mechanism and energetics of green fluorescent protein chromophore synthesis revealed by trapped intermediate structures. Proceedings of the National Academy of Sciences of the United States of America 100:12111-12116.

Barrera NP, Ormond SJ, Henderson RM, Murrell-Lagnado RD, Edwardson JM (2005) Atomic force microscopy imaging demonstrates that P2X2 receptors are trimers but that P2X6 receptor subunits do not oligomerize. The Journal of biological chemistry 280:10759-10765.

Barrett KE, Keely SJ (2000) Chloride secretion by the intestinal epithelium: molecular basis and regulatory aspects. Annual review of physiology 62:535-572.

Barro-Soria R, Schreiber R, Kunzelmann K (2008) Bestrophin 1 and 2 are components of the Ca(2+) activated Cl(-) conductance in mouse airways. Biochimica et biophysica acta 1783:1993-2000.

Barro-Soria R, Aldehni F, Almaca J, Witzgall R, Schreiber R, Kunzelmann K (2010) ER-localized bestrophin 1 activates Ca2+-dependent ion channels TMEM16A and SK4 possibly by acting as a counterion channel. Pflugers Archiv : European journal of physiology 459:485-497.

Barro Soria R, Spitzner M, Schreiber R, Kunzelmann K (2009) Bestrophin-1 enables Ca2+-activated Cl- conductance in epithelia. The Journal of biological chemistry 284:29405-29412.

Barton NJ, McQueen DS, Thomson D, Gauldie SD, Wilson AW, Salter DM, Chessell IP (2006) Attenuation of experimental arthritis in TRPV1R knockout mice. Experimental and molecular pathology 81:166-170.

Basbaum AI, Bautista DM, Scherrer G, Julius D (2009) Cellular and molecular mechanisms of pain. Cell 139:267-284.

Basilio D, Noack K, Picollo A, Accardi A (2014) Conformational changes required for H(+)/Cl(-) exchange mediated by a CLC transporter. Nature structural & molecular biology 21:456-463.

Bauer PJ (2001) The local Ca concentration profile in the vicinity of a Ca channel. Cell biochemistry and biophysics 35:49-61.

Baumann L, Gerstner A, Zong X, Biel M, Wahl-Schott C (2004) Functional characterization of the L-type Ca2+ channel Cav1.4alpha1 from mouse retina. Investigative ophthalmology & visual science 45:708-713.

Baumgarten CM, Fozzard HA (1981) Intracellular chloride activity in mammalian ventricular muscle. The American journal of physiology 241:C121-129.

Bautista DM, Sigal YM, Milstein AD, Garrison JL, Zorn JA, Tsuruda PR, Nicoll RA, Julius D (2008) Pungent agents from Szechuan peppers excite sensory neurons by inhibiting two-pore potassium channels. Nature neuroscience 11:772-779.

Beavers DL, Landstrom AP, Chiang DY, Wehrens XH (2014) Emerging roles of junctophilin-2 in the heart and implications for cardiac diseases. Cardiovascular research 103:198-205.

Becker CM, Hoch W, Betz H (1988) Glycine receptor heterogeneity in rat spinal cord during postnatal development. The EMBO journal 7:3717-3726.

Ben-Ari Y (2002) Excitatory actions of gaba during development: the nature of the nurture. Nat Rev Neurosci 3:728-739.

Ben-Ari Y, Cherubini E, Corradetti R, Gaiarsa JL (1989) Giant synaptic potentials in immature rat CA3 hippocampal neurones. The Journal of physiology 416:303-325.

Ben-Ari Y, Khazipov R, Leinekugel X, Caillard O, Gaiarsa JL (1997) GABAA, NMDA and AMPA receptors: a developmentally regulated 'menage a trois'. Trends in neurosciences 20:523-529.

Beneski DA, Catterall WA (1980) Covalent labeling of protein components of the sodium channel with a photoactivable derivative of scorpion toxin. Proceedings of the National Academy of Sciences of the United States of America 77:639-643.

Benitah JP, Kerfant BG, Vassort G, Richard S, Gomez AM (2002) Altered communication between L-type calcium channels and ryanodine receptors in heart failure. Frontiers in bioscience : a journal and virtual library 7:e263-275.

Berridge MJ (1993) Inositol trisphosphate and calcium signalling. Nature 361:315-325.

Berridge MJ (2006) Calcium microdomains: organization and function. Cell Calcium 40:405-412.

Bevers EM, Williamson PL (2010) Phospholipid scramblase: an update. FEBS letters 584:2724-2730.

Bhave G, Zhu W, Wang H, Brasier DJ, Oxford GS, Gereau RWt (2002) cAMP-dependent protein kinase regulates desensitization of the capsaicin receptor (VR1) by direct phosphorylation. Neuron 35:721-731.

Biggs JE, Yates JM, Loescher AR, Clayton NM, Boissonade FM, Robinson PP (2007) Changes in vanilloid receptor 1 (TRPV1) expression following lingual nerve injury. European journal of pain 11:192-201.

Bill A, Gutierrez A, Kulkarni S, Kemp C, Bonenfant D, Voshol H, Duvvuri U, Gaither LA (2015) ANO1/TMEM16A interacts with EGFR and correlates with sensitivity to EGFR-targeting therapy in head and neck cancer. Oncotarget 6:9173-9188.

Bill A, Hall ML, Borawski J, Hodgson C, Jenkins J, Piechon P, Popa O, Rothwell C, Tranter P, Tria S, Wagner T, Whitehead L, Gaither LA (2014) Small molecule-facilitated degradation of ANO1 protein: a new targeting approach for anticancer therapeutics. The Journal of biological chemistry 289:11029-11041.

Billig GM, Pal B, Fidzinski P, Jentsch TJ (2011) Ca2+-activated Cl- currents are dispensable for olfaction. Nature neuroscience 14:763-769.

Biro T, Bodo E, Telek A, Geczy T, Tychsen B, Kovacs L, Paus R (2006) Hair cycle control by vanilloid receptor-1 (TRPV1): evidence from TRPV1 knockout mice. The Journal of investigative dermatology 126:1909-1912.

Bito V, Heinzel FR, Biesmans L, Antoons G, Sipido KR (2008) Crosstalk between L-type Ca2+ channels and the sarcoplasmic reticulum: alterations during cardiac remodelling. Cardiovascular research 77:315-324.

Bizhanova A, Kopp P (2009) Minireview: The sodium-iodide symporter NIS and pendrin in iodide homeostasis of the thyroid. Endocrinology 150:1084-1090.

Black JA, Liu S, Tanaka M, Cummins TR, Waxman SG (2004) Changes in the expression of tetrodotoxin-sensitive sodium channels within dorsal root ganglia neurons in inflammatory pain. Pain 108:237-247.

Blais C, Marceau F, Rouleau JL, Adam A (2000) The kallikrein-kininogen-kinin system: lessons from the quantification of endogenous kinins. Peptides 21:1903-1940.

Bodi I, Mikala G, Koch SE, Akhter SA, Schwartz A (2005) The L-type calcium channel in the heart: the beat goes on. The Journal of clinical investigation 115:3306-3317.

Bodo E, Kovacs I, Telek A, Varga A, Paus R, Kovacs L, Biro T (2004) Vanilloid receptor-1 (VR1) is widely expressed on various epithelial and mesenchymal cell types of human skin. The Journal of investigative dermatology 123:410-413.

Bodo E, Biro T, Telek A, Czifra G, Griger Z, Toth BI, Mescalchin A, Ito T, Bettermann A, Kovacs L, Paus R (2005) A hot new twist to hair biology: involvement of vanilloid receptor-1 (VR1/TRPV1) signaling in human hair growth control. The American journal of pathology 166:985-998.

Boland B, Himpens B, Vincent MF, Gillis JM, Casteels R (1992) ATP activates P2x-contracting and P2y-relaxing purinoceptors in the smooth muscle of mouse vas deferens. British journal of pharmacology 107:1152-1158.

Boland B, Himpens B, Paques C, Casteels R, Gillis JM (1993) ATP induced-relaxation in the mouse bladder smooth muscle. British journal of pharmacology 108:749-753.

Bolduc V, Marlow G, Boycott KM, Saleki K, Inoue H, Kroon J, Itakura M, Robitaille Y, Parent L, Baas F, Mizuta K, Kamata N, Richard I, Linssen WH, Mahjneh I, de Visser M, Bashir R, Brais B (2010) Recessive mutations in the putative calcium-activated chloride channel Anoctamin 5 cause proximal LGMD2L and distal MMD3 muscular dystrophies. American journal of human genetics 86:213-221.

Bolotina VM (2012) Orai1, STIM1, and iPLA2beta determine arterial vasoconstriction. Arteriosclerosis, thrombosis, and vascular biology 32:1066-1067.

Bompadre SG, Ai T, Cho JH, Wang X, Sohma Y, Li M, Hwang TC (2005) CFTR gating I: Characterization of the ATP-dependent gating of a phosphorylation-independent CFTR channel (DeltaR-CFTR). The Journal of general physiology 125:361-375.

Bootman MD, Lipp P, Berridge MJ (2001) The organisation and functions of local Ca(2+) signals. Journal of cell science 114:2213-2222.

Borsani G, Rugarli EI, Taglialatela M, Wong C, Ballabio A (1995) Characterization of a human and murine gene (CLCN3) sharing similarities to voltage-gated chloride channels and to a yeast integral membrane protein. Genomics 27:131-141.

Boudes M, Sar C, Menigoz A, Hilaire C, Pequignot MO, Kozlenkov A, Marmorstein A, Carroll P, Valmier J, Scamps F (2009) Best1 is a gene regulated by nerve injury and required for Ca2+-activated Cl- current expression in axotomized sensory neurons. The Journal of neuroscience : the official journal of the Society for Neuroscience 29:10063-10071.

Bourinet E, Soong TW, Sutton K, Slaymaker S, Mathews E, Monteil A, Zamponi GW, Nargeot J, Snutch TP (1999) Splicing of alpha 1A subunit gene generates phenotypic variants of P- and Q-type calcium channels. Nature neuroscience 2:407-415.

Bourinet E, Alloui A, Monteil A, Barrere C, Couette B, Poirot O, Pages A, McRory J, Snutch TP, Eschalier A, Nargeot J (2005) Silencing of the Cav3.2 T-type calcium channel gene in sensory neurons demonstrates its major role in nociception. The EMBO journal 24:315-324.

Breese NM, George AC, Pauers LE, Stucky CL (2005) Peripheral inflammation selectively increases TRPV1 function in IB4-positive sensory neurons from adult mouse. Pain 115:37-49.

Bristow DR, Bowery NG, Woodruff GN (1986) Light microscopic autoradiographic localisation of [3H]glycine and [3H]strychnine binding sites in rat brain. European journal of pharmacology 126:303-307.

Britschgi A et al. (2013) Calcium-activated chloride channel ANO1 promotes breast cancer progression by activating EGFR and CAMK signaling. Proceedings of the National Academy of Sciences of the United States of America 110:E1026-1034.

Brofeldt BT, Cornwell P, Doherty D, Batra K, Gunther RA (1989) Topical lidocaine in the treatment of partial-thickness burns. The Journal of burn care & rehabilitation 10:63-68.

Bron R, Wood RJ, Brock JA, Ivanusic JJ (2014) Piezo2 expression in corneal afferent neurons. The Journal of comparative neurology 522:2967-2979.

Brooks PM, Day RO (1991) Nonsteroidal antiinflammatory drugs--differences and similarities. The New England journal of medicine 324:1716-1725.

Brozovich FV, Nicholson CJ, Degen CV, Gao YZ, Aggarwal M, Morgan KG (2016) Mechanisms of Vascular Smooth Muscle Contraction and the Basis for Pharmacologic Treatment of Smooth Muscle Disorders. Pharmacological reviews 68:476-532.

Brumback AC, Staley KJ (2008) Thermodynamic regulation of NKCC1-mediated Cl- cotransport underlies plasticity of GABA(A) signaling in neonatal neurons. Journal of Neuroscience 28:1301-1312.

Brunner JD, Lim NK, Schenck S, Duerst A, Dutzler R (2014) X-ray structure of a calcium-activated TMEM16 lipid scramblase. Nature 516:207-212.

Buchholz B, Faria D, Schley G, Schreiber R, Eckardt KU, Kunzelmann K (2014) Anoctamin 1 induces calcium-activated chloride secretion and proliferation of renal cyst-forming epithelial cells. Kidney international 85:1058-1067.

Bucurenciu I, Kulik A, Schwaller B, Frotscher M, Jonas P (2008) Nanodomain coupling between Ca2+ channels and Ca2+ sensors promotes fast and efficient transmitter release at a cortical GABAergic synapse. Neuron 57:536-545.

Bulley S, Neeb ZP, Burris SK, Bannister JP, Thomas-Gatewood CM, Jangsangthong W, Jaggar JH (2012) TMEM16A/ANO1 channels contribute to the myogenic response in cerebral arteries. Circ Res 111:1027-1036.

Burnstock G, Nistri A, Khakh BS, Giniatullin R (2014) ATP-gated P2X receptors in health and disease. Frontiers in cellular neuroscience 8:204.

Cabrita I, Benedetto R, Fonseca A, Wanitchakool P, Sirianant L, Skryabin BV, Schenk LK, Pavenstadt H, Schreiber R, Kunzelmann K (2017) Differential effects of anoctamins on intracellular calcium signals. FASEB journal : official publication of the Federation of American Societies for Experimental Biology 31:2123-2134.

Campiglio M, Flucher BE (2015) The role of auxiliary subunits for the functional diversity of voltage-gated calcium channels. Journal of cellular physiology 230:2019-2031.

Capes DL, Goldschen-Ohm MP, Arcisio-Miranda M, Bezanilla F, Chanda B (2013) Domain IV voltage-sensor movement is both sufficient and rate limiting for fast inactivation in sodium channels. The Journal of general physiology 142:101-112.

Caputo A, Piano I, Demontis GC, Bacchi N, Casarosa S, Della Santina L, Gargini C (2015) TMEM16A is associated with voltage-gated calcium channels in mouse retina and its function is disrupted upon mutation of the auxiliary alpha2delta4 subunit. Frontiers in cellular neuroscience 9:422.

Caputo A, Caci E, Ferrera L, Pedemonte N, Barsanti C, Sondo E, Pfeffer U, Ravazzolo R, Zegarra-Moran O, Galietta LJ (2008) TMEM16A, a membrane protein associated with calcium-dependent chloride channel activity. Science 322:590-594.

Carrasco S, Meyer T (2011) STIM proteins and the endoplasmic reticulum-plasma membrane junctions. Annual review of biochemistry 80:973-1000.

Cassell A, Grandis JR (2010) Investigational EGFR-targeted therapies in HNSCC. Expert opinion on investigational drugs 19:709-722.

Castellano LE, Trevino CL, Rodriguez D, Serrano CJ, Pacheco J, Tsutsumi V, Felix R, Darszon A (2003) Transient receptor potential (TRPC) channels in human sperm: expression, cellular localization and involvement in the regulation of flagellar motility. FEBS letters 541:69-74.

Castoldi E, Collins PW, Williamson PL, Bevers EM (2011) Compound heterozygosity for 2 novel TMEM16F mutations in a patient with Scott syndrome. Blood 117:4399-4400.

Caterina MJ, Julius D (2001) The vanilloid receptor: a molecular gateway to the pain pathway. Annual review of neuroscience 24:487-517.

Caterina MJ, Schumacher MA, Tominaga M, Rosen TA, Levine JD, Julius D (1997) The capsaicin receptor: a heat-activated ion channel in the pain pathway. Nature 389:816-824.

Caterina MJ, Leffler A, Malmberg AB, Martin WJ, Trafton J, Petersen-Zeitz KR, Koltzenburg M, Basbaum AI, Julius D (2000) Impaired nociception and pain sensation in mice lacking the capsaicin receptor. Science 288:306-313.

Catterall WA (1995) Structure and function of voltage-gated ion channels. Annual review of biochemistry 64:493-531.

Catterall WA (2000a) From ionic currents to molecular mechanisms: the structure and function of voltage-gated sodium channels. Neuron 26:13-25.

Catterall WA (2000b) Structure and regulation of voltage-gated Ca2+ channels. Annual review of cell and developmental biology 16:521-555.

Catterall WA (2012) Voltage-gated sodium channels at 60: structure, function and pathophysiology. The Journal of physiology 590:2577-2589.

Catterall WA, Few AP (2008) Calcium channel regulation and presynaptic plasticity. Neuron 59:882-901.

Catterall WA, Perez-Reyes E, Snutch TP, Striessnig J (2005) International Union of Pharmacology. XLVIII. Nomenclature and structure-function relationships of voltage-gated calcium channels. Pharmacological reviews 57:411-425.

Cavanaugh DJ, Chesler AT, Jackson AC, Sigal YM, Yamanaka H, Grant R, O'Donnell D, Nicoll RA, Shah NM, Julius D, Basbaum AI (2011) Trpv1 reporter mice reveal highly restricted brain distribution and functional

expression in arteriolar smooth muscle cells. The Journal of neuroscience : the official journal of the Society for Neuroscience 31:5067-5077.

Cereda V, Poole DJ, Palena C, Das S, Bera TK, Remondo C, Gulley JL, Arlen PM, Yokokawa J, Pastan I, Schlom J, Tsang KY (2010) New gene expressed in prostate: a potential target for T cell-mediated prostate cancer immunotherapy. Cancer immunology, immunotherapy : CII 59:63-71.

Chalfie M, Tu Y, Euskirchen G, Ward WW, Prasher DC (1994) Green fluorescent protein as a marker for gene expression. Science 263:802-805.

Chang G, Chen L, Mao J (2007) Opioid tolerance and hyperalgesia. The Medical clinics of North America 91:199-211.

Chen CC, Akopian AN, Sivilotti L, Colquhoun D, Burnstock G, Wood JN (1995) A P2X purinoceptor expressed by a subset of sensory neurons. Nature 377:428-431.

Cheng KT, Liu X, Ong HL, Swaim W, Ambudkar IS (2011) Local Ca(2)+ entry via Orai1 regulates plasma membrane recruitment of TRPC1 and controls cytosolic Ca(2)+ signals required for specific cell functions. PLoS biology 9:e1001025.

Cheng W, Yang F, Takanishi CL, Zheng J (2007) Thermosensitive TRPV channel subunits coassemble into heteromeric channels with intermediate conductance and gating properties. The Journal of general physiology 129:191-207.

Cheng W, Yang F, Liu S, Colton CK, Wang C, Cui Y, Cao X, Zhu MX, Sun C, Wang K, Zheng J (2012) Heteromeric heat-sensitive transient receptor potential channels exhibit distinct temperature and chemical response. The Journal of biological chemistry 287:7279-7288.

Chesnoy-Marchais D (1983) Characterization of a chloride conductance activated by hyperpolarization in Aplysia neurones. The Journal of physiology 342:277-308.

Chiono M, Mahey R, Tate G, Cooper DM (1995) Capacitative Ca2+ entry exclusively inhibits cAMP synthesis in C6-2B glioma cells. Evidence that physiologically evoked Ca2+ entry regulates Ca(2+)-inhibitable adenylyl cyclase in non-excitable cells. The Journal of biological chemistry 270:1149-1155.

Chizh BA, Illes P (2001) P2X receptors and nociception. Pharmacological reviews 53:553-568.

Cho H, Yang YD, Lee J, Lee B, Kim T, Jang Y, Back SK, Na HS, Harfe BD, Wang F, Raouf R, Wood JN, Oh U (2012) The calcium-activated chloride channel anoctamin 1 acts as a heat sensor in nociceptive neurons. Nature neuroscience 15:1015-1021.

Choi SI, Lim JY, Yoo S, Kim H, Hwang SW (2016) Emerging Role of Spinal Cord TRPV1 in Pain Exacerbation. Neural plasticity 2016:5954890.

Christoph T, Gillen C, Mika J, Grunweller A, Schafer MK, Schiene K, Frank R, Jostock R, Bahrenberg G, Weihe E, Erdmann VA, Kurreck J (2007) Antinociceptive effect of antisense oligonucleotides against the vanilloid receptor VR1/TRPV1. Neurochemistry international 50:281-290.

Chuang HH, Prescott ED, Kong H, Shields S, Jordt SE, Basbaum AI, Chao MV, Julius D (2001) Bradykinin and nerve growth factor release the capsaicin receptor from PtdIns(4,5)P2-mediated inhibition. Nature 411:957-962.

Cia D, Bordais A, Varela C, Forster V, Sahel JA, Rendon A, Picaud S (2005) Voltage-gated channels and calcium homeostasis in mammalian rod photoreceptors. Journal of neurophysiology 93:1468-1475.

Cibulsky SM, Sather WA (2003) Control of ion conduction in L-type Ca2+ channels by the concerted action of S5-6 regions. Biophysical journal 84:1709-1719.

Cizkova D, Marsala J, Lukacova N, Marsala M, Jergova S, Orendacova J, Yaksh TL (2002) Localization of N-type Ca2+ channels in the rat spinal cord following chronic constrictive nerve injury. Experimental brain research 147:456-463.

Clapham DE (2003) TRP channels as cellular sensors. Nature 426:517-524.

Cobine CA, Hannah EE, Zhu MH, Lyle HE, Rock JR, Sanders KM, Ward SM, Keef KD (2017) ANO1 in intramuscular interstitial cells of Cajal plays a key role in the generation of slow waves and tone in the internal anal sphincter. The Journal of physiology 595:2021-2041.

Cockayne DA, Dunn PM, Zhong Y, Rong W, Hamilton SG, Knight GE, Ruan HZ, Ma B, Yip P, Nunn P, McMahon SB, Burnstock G, Ford AP (2005) P2X2 knockout mice and P2X2/P2X3 double knockout mice reveal a role for the P2X2 receptor subunit in mediating multiple sensory effects of ATP. The Journal of physiology 567:621-639.

Coelho RR, Souza EP, Soares PM, Meireles AV, Santos GC, Scarparo HC, Assreuy AM, Criddle DN (2004) Effects of chloride channel blockers on hypotonicity-induced contractions of the rat trachea. British journal of pharmacology 141:367-373.

Cohen I, Navarro V, Clemenceau S, Baulac M, Miles R (2002) On the origin of interictal activity in human temporal lobe epilepsy in vitro. Science 298:1418-1421.

Colomar A, Amedee T (2001) ATP stimulation of P2X(7) receptors activates three different ionic conductances on cultured mouse Schwann cells. The European journal of neuroscience 14:927-936.

Corda D, Marcocci C, Kohn LD, Axelrod J, Luini A (1985) Association of the changes in cytosolic Ca2+ and iodide efflux induced by thyrotropin and by the stimulation of alpha 1-adrenergic receptors in cultured rat thyroid cells. The Journal of biological chemistry 260:9230-9236.

Costa MR, Catterall WA (1984) Phosphorylation of the alpha subunit of the sodium channel by protein kinase C. Cellular and molecular neurobiology 4:291-297.

Coste B, Mathur J, Schmidt M, Earley TJ, Ranade S, Petrus MJ, Dubin AE, Patapoutian A (2010) Piezo1 and Piezo2 are essential components of distinct mechanically activated cation channels. Science 330:55-60.

Coste B, Xiao B, Santos JS, Syeda R, Grandl J, Spencer KS, Kim SE, Schmidt M, Mathur J, Dubin AE, Montal M, Patapoutian A (2012) Piezo proteins are pore-forming subunits of mechanically activated channels. Nature 483:176-181.

Coughlin SR (2000) Thrombin signalling and protease-activated receptors. Nature 407:258-264.

Courjaret R, Machaca K (2014) Mid-range Ca2+ signalling mediated by functional coupling between store-operated Ca2+ entry and IP3-dependent Ca2+ release. Nature communications 5:3916.

Courjaret R, Hodeify R, Hubrack S, Ibrahim A, Dib M, Daas S, Machaca K (2016) The Ca2+-activated Cl- channel Ano1 controls microvilli length and membrane surface area in the oocyte. Journal of cell science 129:2548-2558.

Craggs TD (2009) Green fluorescent protein: structure, folding and chromophore maturation. Chemical Society reviews 38:2865-2875.

Criddle DN, de Moura RS, Greenwood IA, Large WA (1996) Effect of niflumic acid on noradrenaline-induced contractions of the rat aorta. British journal of pharmacology 118:1065-1071.

Criddle DN, Raraty MG, Neoptolemos JP, Tepikin AV, Petersen OH, Sutton R (2004) Ethanol toxicity in pancreatic acinar cells: mediation by nonoxidative fatty acid metabolites. Proceedings of the National Academy of Sciences of the United States of America 101:10738-10743.

Crutzen R, Virreira M, Markadieu N, Shlyonsky V, Sener A, Malaisse WJ, Beauwens R, Boom A, Golstein PE (2016) Anoctamin 1 (Ano1) is required for glucose-induced membrane potential oscillations and insulin secretion by murine beta-cells. Pflugers Archiv : European journal of physiology 468:573-591.

Csanady L, Nairn AC, Gadsby DC (2006) Thermodynamics of CFTR channel gating: a spreading conformational change initiates an irreversible gating cycle. The Journal of general physiology 128:523-533.

Cuffe JE, Bielfeld-Ackermann A, Thomas J, Leipziger J, Korbmacher C (2000) ATP stimulates Cl- secretion and reduces amiloride-sensitive Na+ absorption in M-1 mouse cortical collecting duct cells. The Journal of physiology 524 Pt 1:77-90.

Cummins TR, Howe JR, Waxman SG (1998) Slow closed-state inactivation: a novel mechanism underlying ramp currents in cells expressing the hNE/PN1 sodium channel. The Journal of neuroscience : the official journal of the Society for Neuroscience 18:9607-9619.

Cunningham SA, Awayda MS, Bubien JK, Ismailov, II, Arrate MP, Berdiev BK, Benos DJ, Fuller CM (1995) Cloning of an epithelial chloride channel from bovine trachea. The Journal of biological chemistry 270:31016-31026.

Curtis DR, Hosli L, Johnston GA (1967) Inhibition of spinal neurons by glycine. Nature 215:1502-1503.

Danahay H, Atherton H, Jones G, Bridges RJ, Poll CT (2002) Interleukin-13 induces a hypersecretory ion transport phenotype in human bronchial epithelial cells. American journal of physiology Lung cellular and molecular physiology 282:L226-236.

Dani A, Huang B, Bergan J, Dulac C, Zhuang X (2010) Superresolution imaging of chemical synapses in the brain. Neuron 68:843-856.

Das S, Hahn Y, Nagata S, Willingham MC, Bera TK, Lee B, Pastan I (2007) NGEP, a prostate-specific plasma membrane protein that promotes the association of LNCaP cells. Cancer research 67:1594-1601.

Dauner K, Mobus C, Frings S, Mohrlen F (2013) Targeted expression of anoctamin calcium-activated chloride channels in rod photoreceptor terminals of the rodent retina. Investigative ophthalmology & visual science 54:3126-3136.

Davies JC, Alton EW, Bush A (2007) Cystic fibrosis. Bmj 335:1255-1259.

Davis AJ, Shi J, Pritchard HA, Chadha PS, Leblanc N, Vasilikostas G, Yao Z, Verkman AS, Albert AP, Greenwood IA (2013) Potent vasorelaxant activity of the TMEM16A inhibitor T16A(inh) -A01. British journal of pharmacology 168:773-784.

Davis JB, Gray J, Gunthorpe MJ, Hatcher JP, Davey PT, Overend P, Harries MH, Latcham J, Clapham C, Atkinson K, Hughes SA, Rance K, Grau E, Harper AJ, Pugh PL, Rogers DC, Bingham S, Randall A, Sheardown SA (2000) Vanilloid receptor-1 is essential for inflammatory thermal hyperalgesia. Nature 405:183-187.

Day RN, Davidson MW (2009) The fluorescent protein palette: tools for cellular imaging. Chemical Society reviews 38:2887-2921.

Day RO, Graham GG (2013) Non-steroidal anti-inflammatory drugs (NSAIDs). Bmj 346:f3195.

de la Fuente S, Fonteriz RI, Montero M, Alvarez J (2013) Ca2+ homeostasis in the endoplasmic reticulum measured with a new low-Ca2+-affinity targeted aequorin. Cell Calcium 54:37-45.

Deba F, Bessac BF (2015) Anoctamin-1 Cl(-) channels in nociception: activation by an N-aroylaminothiazole and capsaicin and inhibition by T16A[inh]-A01. Molecular pain 11:55.

Delgado R, Mura CV, Bacigalupo J (2016) Single Ca(2+)-activated Cl(-) channel currents recorded from toad olfactory cilia. BMC neuroscience 17:17.

Delpire E (2000) Cation-Chloride Cotransporters in Neuronal Communication. News in physiological sciences : an international journal of physiology produced jointly by the International Union of Physiological Sciences and the American Physiological Society 15:309-312.

Dent MA, Raisman G, Lai FA (1996) Expression of type 1 inositol 1,4,5-trisphosphate receptor during axogenesis and synaptic contact in the central and peripheral nervous system of developing rat. Development 122:1029-1039.

Dib-Hajj SD, Cummins TR, Black JA, Waxman SG (2010) Sodium channels in normal and pathological pain. Annual review of neuroscience 33:325-347.

Dibattista M, Amjad A, Maurya DK, Sagheddu C, Montani G, Tirindelli R, Menini A (2012) Calcium-activated chloride channels in the apical region of mouse vomeronasal sensory neurons. The Journal of general physiology 140:3-15.

Dionisio N, Smani T, Woodard GE, Castellano A, Salido GM, Rosado JA (2015) Homer proteins mediate the interaction between STIM1 and Cav1.2 channels. Biochimica et biophysica acta 1853:1145-1153.

Djouhri L, Lawson SN (2004) Abeta-fiber nociceptive primary afferent neurons: a review of incidence and properties in relation to other afferent A-fiber neurons in mammals. Brain research Brain research reviews 46:131-145.

Djouhri L, Newton R, Levinson SR, Berry CM, Carruthers B, Lawson SN (2003) Sensory and electrophysiological properties of guinea-pig sensory neurones expressing Nav 1.7 (PN1) Na+ channel alpha subunit protein. The Journal of physiology 546:565-576.

Docherty RJ, Yeats JC, Bevan S, Boddeke HW (1996) Inhibition of calcineurin inhibits the desensitization of capsaicin-evoked currents in cultured dorsal root ganglion neurones from adult rats. Pflugers Archiv : European journal of physiology 431:828-837.

Dohan O, De la Vieja A, Paroder V, Riedel C, Artani M, Reed M, Ginter CS, Carrasco N (2003) The sodium/iodide Symporter (NIS): characterization, regulation, and medical significance. Endocrine reviews 24:48-77.

Dolphin AC (2012) Calcium channel auxiliary alpha2delta and beta subunits: trafficking and one step beyond. Nat Rev Neurosci 13:542-555.

Dong X, Han S, Zylka MJ, Simon MI, Anderson DJ (2001) A diverse family of GPCRs expressed in specific subsets of nociceptive sensory neurons. Cell 106:619-632.

Du X, Gamper N (2013) Potassium Channels in Peripheral Pain Pathways: Expression, Function and Therapeutic Potential. Current neuropharmacology 11:621-640.

Du X, Gao H, Jaffe D, Zhang H, Gamper N (2017a) M-type K+ channels in peripheral nociceptive pathways. British journal of pharmacology.

Du X, Hao H, Yang Y, Huang S, Wang C, Gigout S, Ramli R, Li X, Jaworska E, Edwards I, Deuchars J, Yanagawa Y, Qi J, Guan B, Jaffe DB, Zhang H, Gamper N (2017b) Local GABAergic signaling within sensory ganglia controls peripheral nociceptive transmission. The Journal of clinical investigation 127:1741-1756.

Dubin AE, Patapoutian A (2010) Nociceptors: the sensors of the pain pathway. The Journal of clinical investigation 120:3760-3772.

Dubin AE, Schmidt M, Mathur J, Petrus MJ, Xiao B, Coste B, Patapoutian A (2012) Inflammatory signals enhance piezo2-mediated mechanosensitive currents. Cell reports 2:511-517.

Dudok B et al. (2015) Cell-specific STORM super-resolution imaging reveals nanoscale organization of cannabinoid signaling. Nature neuroscience 18:75-86.

Duffieux F, Annereau JP, Boucher J, Miclet E, Pamlard O, Schneider M, Stoven V, Lallemand JY (2000) Nucleotide-binding domain 1 of cystic fibrosis transmembrane conductance regulator production of a suitable protein for structural studies. Eur J Biochem 267:5306-5312.

Duran C, Qu Z, Osunkoya AO, Cui Y, Hartzell HC (2012) ANOs 3-7 in the anoctamin/Tmem16 Cl- channel family are intracellular proteins. American journal of physiology Cell physiology 302:C482-493.

Dutertre S, Drwal M, Laube B, Betz H (2012) Probing the pharmacological properties of distinct subunit interfaces within heteromeric glycine receptors reveals a functional betabeta agonist-binding site. Journal of neurochemistry 122:38-47.

Dutzler R, Campbell EB, MacKinnon R (2003) Gating the selectivity filter in ClC chloride channels. Science 300:108-112.

Dutzler R, Campbell EB, Cadene M, Chait BT, MacKinnon R (2002) X-ray structure of a ClC chloride channel at 3.0 A reveals the molecular basis of anion selectivity. Nature 415:287-294.

Eggermann E, Bucurenciu I, Goswami SP, Jonas P (2011) Nanodomain coupling between Ca(2)(+) channels and sensors of exocytosis at fast mammalian synapses. Nat Rev Neurosci 13:7-21.

El Chemaly A, Norez C, Magaud C, Bescond J, Chatelier A, Fares N, Findlay I, Jayle C, Becq F, Faivre JF, Bois P (2014) ANO1 contributes to angiotensin-II-activated Ca2+-dependent Cl- current in human atrial fibroblasts. J Mol Cell Cardiol 68:12-19.

Eliasson E, Golubinskaya V, Nilsson H (2014) Bestrophin-3 is expressed in the mouse intestine (1122.1). The FASEB Journal 28.

Elsliger MA, Wachter RM, Hanson GT, Kallio K, Remington SJ (1999) Structural and spectral response of green fluorescent protein variants to changes in pH. Biochemistry 38:5296-5301.

Endo M (2009) Calcium-induced calcium release in skeletal muscle. Physiological reviews 89:1153-1176.

Endres-Becker J, Heppenstall PA, Mousa SA, Labuz D, Oksche A, Schafer M, Stein C, Zollner C (2007) Mu-opioid receptor activation modulates transient receptor potential vanilloid 1 (TRPV1) currents in sensory neurons in a model of inflammatory pain. Molecular pharmacology 71:12-18.

Eslamian L, Borzabadi-Farahani A, Edini HZ, Badiee MR, Lynch E, Mortazavi A (2013) The analgesic effect of benzocaine mucoadhesive patches on orthodontic pain caused by elastomeric separators, a preliminary study. Acta odontologica Scandinavica 71:1168-1173.

Ester M, Kriegel H-P, Sander J, Xu X (1996) A density-based algorithm for discovering clusters a density-based algorithm for discovering clusters in large spatial databases with noise. In: Proceedings of the Second International Conference on Knowledge Discovery and Data Mining, pp 226-231. Portland, Oregon: AAAI Press.

Ettinger A, Wittmann T (2014) Fluorescence live cell imaging. Methods in cell biology 123:77-94.

Fagan KA, Mahey R, Cooper DM (1996) Functional co-localization of transfected Ca(2+)-stimulable adenylyl cyclases with capacitative Ca2+ entry sites. The Journal of biological chemistry 271:12438-12444.

Fagan KA, Mons N, Cooper DM (1998) Dependence of the Ca2+-inhibitable adenylyl cyclase of C6-2B glioma cells on capacitative Ca2+ entry. The Journal of biological chemistry 273:9297-9305.

Fanger CM, Ghanshani S, Logsdon NJ, Rauer H, Kalman K, Zhou J, Beckingham K, Chandy KG, Cahalan MD, Aiyar J (1999) Calmodulin mediates calcium-dependent activation of the intermediate conductance KCa channel, IKCa1. The Journal of biological chemistry 274:5746-5754.

Faria D, Rock JR, Romao AM, Schweda F, Bandulik S, Witzgall R, Schlatter E, Heitzmann D, Pavenstadt H, Herrmann E, Kunzelmann K, Schreiber R (2014) The calcium-activated chloride channel Anoctamin 1 contributes to the regulation of renal function. Kidney international 85:1369-1381.

Faucherre A, Kissa K, Nargeot J, Mangoni ME, Jopling C (2014) Piezo1 plays a role in erythrocyte volume homeostasis. Haematologica 99:70-75.

Fehon RG, McClatchey AI, Bretscher A (2010) Organizing the cell cortex: the role of ERM proteins. Nature reviews Molecular cell biology 11:276-287.

Feigenspan A, Bormann J (1998) GABA-gated Cl- channels in the rat retina. Progress in retinal and eye research 17:99-126.

Fernandez-Busnadiego R, Saheki Y, De Camilli P (2015) Three-dimensional architecture of extended synaptotagmin-mediated endoplasmic reticulum-plasma membrane contact sites. Proceedings of the National Academy of Sciences of the United States of America 112:E2004-2013.

Fernihough J, Gentry C, Bevan S, Winter J (2005) Regulation of calcitonin gene-related peptide and TRPV1 in a rat model of osteoarthritis. Neuroscience letters 388:75-80.

Ferrera L, Caputo A, Ubby I, Bussani E, Zegarra-Moran O, Ravazzolo R, Pagani F, Galietta LJ (2009) Regulation of TMEM16A chloride channel properties by alternative splicing. The Journal of biological chemistry 284:33360-33368.

Fields HL, Emson PC, Leigh BK, Gilbert RF, Iversen LL (1980) Multiple opiate receptor sites on primary afferent fibres. Nature 284:351-353.

Finch EA, Turner TJ, Goldin SM (1991) Calcium as a coagonist of inositol 1,4,5-trisphosphate-induced calcium release. Science 252:443-446.

Fischer M, Mak S, McNaughton P (2010) Sensitisation of Nociceptors – What are Ion Channels Doing?

Fischer MJ, Balasuriya D, Jeggle P, Goetze TA, McNaughton PA, Reeh PW, Edwardson JM (2014) Direct evidence for functional TRPV1/TRPA1 heteromers. Pflugers Archiv : European journal of physiology 466:2229-2241.

Fish KN (2009) Total internal reflection fluorescence (TIRF) microscopy. Current protocols in cytometry Chapter 12:Unit12 18.

Fisher SI, Hartzell HC (2017) Poring over furrows. eLife 6.

Fiumelli H, Cancedda L, Poo MM (2005) Modulation of GABAergic transmission by activity via postsynaptic Ca2+-dependent regulation of KCC2 function. Neuron 48:773-786.

Flis K, Hinzpeter A, Edelman A, Kurlandzka A (2005) The functioning of mammalian ClC-2 chloride channel in Saccharomyces cerevisiae cells requires an increased level of Kha1p. The Biochemical journal 390:655-664.

Flor H, Elbert T, Knecht S, Wienbruch C, Pantev C, Birbaumer N, Larbig W, Taub E (1995) Phantom-limb pain as a perceptual correlate of cortical reorganization following arm amputation. Nature 375:482-484.

Foskett JK, White C, Cheung KH, Mak DO (2007) Inositol trisphosphate receptor Ca2+ release channels. Physiological reviews 87:593-658.

Fossat P, Dobremez E, Bouali-Benazzouz R, Favereaux A, Bertrand SS, Kilk K, Leger C, Cazalets JR, Langel U, Landry M, Nagy F (2010) Knockdown of L calcium channel subtypes: differential effects in neuropathic pain. The Journal of neuroscience : the official journal of the Society for Neuroscience 30:1073-1085.

Fredriksson S, Gullberg M, Jarvius J, Olsson C, Pietras K, Gustafsdottir SM, Ostman A, Landegren U (2002) Protein detection using proximity-dependent DNA ligation assays. Nature biotechnology 20:473-477.

Frizzell RA, Hanrahan JW (2012) Physiology of epithelial chloride and fluid secretion. Cold Spring Harbor perspectives in medicine 2:a009563.

Froh M, Thurman RG, Wheeler MD (2002) Molecular evidence for a glycine-gated chloride channel in macrophages and leukocytes. American journal of physiology Gastrointestinal and liver physiology 283:G856-863.

Fry CH, Sui G, Wu C (2006) T-type Ca2+ channels in non-vascular smooth muscles. Cell Calcium 40:231-239.

Fugazzola L, Cerutti N, Mannavola D, Vannucchi G, Beck-Peccoz P (2001) The role of pendrin in iodide regulation. Experimental and clinical endocrinology & diabetes : official journal, German Society of Endocrinology [and] German Diabetes Association 109:18-22.

Fukuda A, Tanaka M, Yamada Y, Muramatsu K, Shimano Y, Nishino H (1998a) Simultaneous optical imaging of intracellular Cl- in neurons in different layers of rat neocortical slices: advantages and limitations. Neuroscience research 32:363-371.

Fukuda A, Muramatsu K, Okabe A, Shimano Y, Hida H, Fujimoto I, Nishino H (1998b) Changes in intracellular Ca2+ induced by GABAA receptor activation and reduction in Cl- gradient in neonatal rat neocortex. Journal of neurophysiology 79:439-446.

Fukuoka T, Tokunaga A, Tachibana T, Dai Y, Yamanaka H, Noguchi K (2002) VR1, but not P2X(3), increases in the spared L4 DRG in rats with L5 spinal nerve ligation. Pain 99:111-120.

Funk K, Woitecki A, Franjic-Wurtz C, Gensch T, Mohrlen F, Frings S (2008) Modulation of chloride homeostasis by inflammatory mediators in dorsal root ganglion neurons. Molecular pain 4:32.

Gadsby DC (2009) Ion channels versus ion pumps: the principal difference, in principle. Nature reviews Molecular cell biology 10:344-352.

Gadsby DC, Vergani P, Csanady L (2006) The ABC protein turned chloride channel whose failure causes cystic fibrosis. Nature 440:477-483.

Gailly P, Boland B, Paques C, Himpens B, Casteels R, Gillis JM (1993) Post-receptor pathway of the ATP-induced relaxation in smooth muscle of the mouse vas deferens. British journal of pharmacology 110:326-330.

Galietta LJ, Haggie PM, Verkman AS (2001a) Green fluorescent protein-based halide indicators with improved chloride and iodide affinities. FEBS letters 499:220-224.

Galietta LV, Jayaraman S, Verkman AS (2001b) Cell-based assay for high-throughput quantitative screening of CFTR chloride transport agonists. American journal of physiology Cell physiology 281:C1734-1742.

Gallego-Sandin S, Rodriguez-Garcia A, Alonso MT, Garcia-Sancho J (2009) The endoplasmic reticulum of dorsal root ganglion neurons contains functional TRPV1 channels. The Journal of biological chemistry 284:32591-32601.

Gallos G, Remy KE, Danielsson J, Funayama H, Fu XW, Chang HY, Yim P, Xu D, Emala CW, Sr. (2013) Functional expression of the TMEM16 family of calcium-activated chloride channels in airway smooth muscle. American journal of physiology Lung cellular and molecular physiology 305:L625-634.

Ganguly K, Schinder AF, Wong ST, Poo M (2001) GABA itself promotes the developmental switch of neuronal GABAergic responses from excitation to inhibition. Cell 105:521-532.

Gao DY, Zhang BL, Leung MCT, Au SCL, Wong PYD, Shum WWC (2016) Coupling of TRPV6 and TMEM16A in epithelial principal cells of the rat epididymis. The Journal of general physiology 148:161-182.

Garcia-Alcocer G, Mejia C, Berumen LC, Miledi R, Martinez-Torres A (2008) Developmental expression of glycine receptor subunits in rat cerebellum. International journal of developmental neuroscience : the official journal of the International Society for Developmental Neuroscience 26:319-322.

Garcia-Sanz N, Fernandez-Carvajal A, Morenilla-Palao C, Planells-Cases R, Fajardo-Sanchez E, Fernandez-Ballester G, Ferrer-Montiel A (2004) Identification of a tetramerization domain in the C terminus of the vanilloid receptor. The Journal of neuroscience : the official journal of the Society for Neuroscience 24:5307-5314.

García G, Martínez-Rojas VA, Rocha-González HI, Granados-Soto V, Murbartián J (2014) Evidence for the participation of Ca2+-activated chloride channels in formalin-induced acute and chronic nociception. Brain research 1579:35-44.

Garcia MA, Yang N, Quinton PM (2009) Normal mouse intestinal mucus release requires cystic fibrosis transmembrane regulator-dependent bicarbonate secretion. The Journal of clinical investigation 119:2613-2622.

Ge J, Li W, Zhao Q, Li N, Chen M, Zhi P, Li R, Gao N, Xiao B, Yang M (2015) Architecture of the mammalian mechanosensitive Piezo1 channel. Nature 527:64-69.

Geppetti P, Trevisani M (2004) Activation and sensitisation of the vanilloid receptor: role in gastrointestinal inflammation and function. British journal of pharmacology 141:1313-1320.

Geyer M, Huang F, Sun Y, Vogel SM, Malik AB, Taylor CW, Komarova YA (2015) Microtubule-Associated Protein EB3 Regulates IP3 Receptor Clustering and Ca(2+) Signaling in Endothelial Cells. Cell reports 12:79-89.

Giordano F, Saheki Y, Idevall-Hagren O, Colombo SF, Pirruccello M, Milosevic I, Gracheva EO, Bagriantsev SN, Borgese N, De Camilli P (2013) PI(4,5)P(2)-dependent and Ca(2+)-regulated ER-PM interactions mediated by the extended synaptotagmins. Cell 153:1494-1509.

Golias C, Charalabopoulos A, Stagikas D, Charalabopoulos K, Batistatou A (2007) The kinin system--bradykinin: biological effects and clinical implications. Multiple role of the kinin system--bradykinin. Hippokratia 11:124-128.

Gomez-Pinilla PJ, Gibbons SJ, Bardsley MR, Lorincz A, Pozo MJ, Pasricha PJ, Van de Rijn M, West RB, Sarr MG, Kendrick ML, Cima RR, Dozois EJ, Larson DW, Ordog T, Farrugia G (2009) Ano1 is a selective marker of interstitial cells of Cajal in the human and mouse gastrointestinal tract. American journal of physiology Gastrointestinal and liver physiology 296:G1370-1381.

Gomez NM, Tamm ER, Straubeta O (2013) Role of bestrophin-1 in store-operated calcium entry in retinal pigment epithelium. Pflugers Archiv : European journal of physiology 465:481-495.

Granados-Soto V, Arguelles CF, Alvarez-Leefmans FJ (2005) Peripheral and central antinociceptive action of Na+-K+-2Cl- cotransporter blockers on formalin-induced nociception in rats. Pain 114:231-238.

Grenningloh G, Schmieden V, Schofield PR, Seeburg PH, Siddique T, Mohandas TK, Becker CM, Betz H (1990) Alpha subunit variants of the human glycine receptor: primary structures, functional expression and chromosomal localization of the corresponding genes. The EMBO journal 9:771-776.

Grizel AV, Glukhov GS, Sokolova OS (2014) Mechanisms of activation of voltage-gated potassium channels. Acta naturae 6:10-26.

Gruszczynska-Biegala J, Kuznicki J (2013) Native STIM2 and ORAI1 proteins form a calcium-sensitive and thapsigargin-insensitive complex in cortical neurons. Journal of neurochemistry 126:727-738.

Guilbaud G, Benoist JM, Levante A, Gautron M, Willer JC (1992) Primary somatosensory cortex in rats with pain-related behaviours due to a peripheral mononeuropathy after moderate ligation of one sciatic nerve: neuronal responsivity to somatic stimulation. Experimental brain research 92:227-245.

Gunther W, Piwon N, Jentsch TJ (2003) The ClC-5 chloride channel knock-out mouse - an animal model for Dent's disease. Pflugers Archiv : European journal of physiology 445:456-462.

Guo A, Vulchanova L, Wang J, Li X, Elde R (1999) Immunocytochemical localization of the vanilloid receptor 1 (VR1): relationship to neuropeptides, the P2X3 purinoceptor and IB4 binding sites. The European journal of neuroscience 11:946-958.

Gurkoff G, Shahlaie K, Lyeth B, Berman R (2013) Voltage-gated calcium channel antagonists and traumatic brain injury. Pharmaceuticals 6:788-812.

Gutman GA, Chandy KG, Grissmer S, Lazdunski M, McKinnon D, Pardo LA, Robertson GA, Rudy B, Sanguinetti MC, Stuhmer W, Wang X (2005) International Union of Pharmacology. LIII. Nomenclature and molecular relationships of voltage-gated potassium channels. Pharmacological reviews 57:473-508.

Ha GE, Cheong E (2017) Spike Frequency Adaptation in Neurons of the Central Nervous System. Experimental neurobiology 26:179-185.

Hains BC, Saab CY, Lo AC, Waxman SG (2004a) Sodium channel blockade with phenytoin protects spinal cord axons, enhances axonal conduction, and improves functional motor recovery after contusion SCI. Experimental neurology 188:365-377.

Hains BC, Saab CY, Klein JP, Craner MJ, Waxman SG (2004b) Altered sodium channel expression in second-order spinal sensory neurons contributes to pain after peripheral nerve injury. The Journal of neuroscience : the official journal of the Society for Neuroscience 24:4832-4839.

Hakamata Y, Nakai J, Takeshima H, Imoto K (1992) Primary structure and distribution of a novel ryanodine receptor/calcium release channel from rabbit brain. FEBS letters 312:229-235.

Hanukoglu I, Boggula VR, Vaknine H, Sharma S, Kleyman T, Hanukoglu A (2017) Expression of epithelial sodium channel (ENaC) and CFTR in the human epidermis and epidermal appendages. Histochemistry and cell biology 147:733-748.

Harhun MI, Sukhanova K, Gordienko D, Dyskina Y (2015) Molecular identification of P2X receptors in vascular smooth muscle cells from rat anterior, posterior, and basilar arteries. Pharmacological reports : PR 67:1055-1060.

Harraz OF, Brett SE, Zechariah A, Romero M, Puglisi JL, Wilson SM, Welsh DG (2015) Genetic ablation of CaV3.2 channels enhances the arterial myogenic response by modulating the RyR-BKCa axis. Arteriosclerosis, thrombosis, and vascular biology 35:1843-1851.

Harraz OF, Abd El-Rahman RR, Bigdely-Shamloo K, Wilson SM, Brett SE, Romero M, Gonzales AL, Earley S, Vigmond EJ, Nygren A, Menon BK, Mufti RE, Watson T, Starreveld Y, Furstenhaupt T, Muellerleile PR, Kurjiaka DT, Kyle BD, Braun AP, Welsh DG (2014) Ca(V)3.2 channels and the induction of negative feedback in cerebral arteries. Circ Res 115:650-661.

Hartzell C, Putzier I, Arreola J (2005) Calcium-activated chloride channels. Annual review of physiology 67:719-758.

Hartzell HC (1996) Activation of different Cl currents in Xenopus oocytes by Ca liberated from stores and by capacitative Ca influx. The Journal of general physiology 108:157-175.

Hasbargen T, Ahmed MM, Miranpuri G, Li L, Kahle KT, Resnick D, Sun D (2010) Role of NKCC1 and KCC2 in the development of chronic neuropathic pain following spinal cord injury. Annals of the New York Academy of Sciences 1198:168-172.

Hattori M, Gouaux E (2012) Molecular mechanism of ATP binding and ion channel activation in P2X receptors. Nature 485:207-212.

Haverkamp S, Muller U, Harvey K, Harvey RJ, Betz H, Wassle H (2003) Diversity of glycine receptors in the mouse retina: localization of the alpha3 subunit. The Journal of comparative neurology 465:524-539.

Heim R, Prasher DC, Tsien RY (1994) Wavelength mutations and posttranslational autoxidation of green fluorescent protein. Proceedings of the National Academy of Sciences of the United States of America 91:12501-12504.

Heim R, Cubitt AB, Tsien RY (1995) Improved green fluorescence. Nature 373:663-664.

Heinke B, Balzer E, Sandkuhler J (2004) Pre- and postsynaptic contributions of voltage-dependent Ca2+ channels to nociceptive transmission in rat spinal lamina I neurons. The European journal of neuroscience 19:103-111.

Heinze C, Seniuk A, Sokolov MV, Huebner AK, Klementowicz AE, Szijarto IA, Schleifenbaum J, Vitzthum H, Gollasch M, Ehmke H, Schroeder BC, Hubner CA (2014) Disruption of vascular Ca2+-activated chloride currents lowers blood pressure. The Journal of clinical investigation 124:675-686.

Hell JW, Westenbroek RE, Warner C, Ahlijanian MK, Prystay W, Gilbert MM, Snutch TP, Catterall WA (1993) Identification and differential subcellular localization of the neuronal class C and class D L-type calcium channel alpha 1 subunits. The Journal of cell biology 123:949-962.

Helton TD, Xu W, Lipscombe D (2005) Neuronal L-type calcium channels open quickly and are inhibited slowly. The Journal of neuroscience : the official journal of the Society for Neuroscience 25:10247-10251.

Henriques R, Griffiths C, Hesper Rego E, Mhlanga MM (2011) PALM and STORM: unlocking live-cell super-resolution. Biopolymers 95:322-331.

Hicks D et al. (2011) A founder mutation in Anoctamin 5 is a major cause of limb-girdle muscular dystrophy. Brain : a journal of neurology 134:171-182.

Hidalgo C, Gonzalez ME, Garcia AM (1986) Calcium transport in transverse tubules isolated from rabbit skeletal muscle. Biochimica et biophysica acta 854.

Hirata Y, Brotto M, Weisleder N, Chu Y, Lin P, Zhao X, Thornton A, Komazaki S, Takeshima H, Ma J, Pan Z (2006) Uncoupling store-operated Ca2+ entry and altered Ca2+ release from sarcoplasmic reticulum through silencing of junctophilin genes. Biophysical journal 90:4418-4427.

Holland IB (2011) ABC transporters, mechanisms and biology: an overview. Essays in biochemistry 50:1-17.

Hollenhorst MI, Richter K, Fronius M (2011) Ion transport by pulmonary epithelia. Journal of biomedicine & biotechnology 2011:174306.

Horiuchi K, Le Gall S, Schulte M, Yamaguchi T, Reiss K, Murphy G, Toyama Y, Hartmann D, Saftig P, Blobel CP (2007) Substrate Selectivity of Epidermal Growth Factor-Receptor Ligand Sheddases and their Regulation by Phorbol Esters and Calcium Influx. Molecular Biology of the Cell 18:176-188.

Horvath B, Vaczi K, Hegyi B, Gonczi M, Dienes B, Kistamas K, Banyasz T, Magyar J, Baczko I, Varro A, Seprenyi G, Csernoch L, Nanasi PP, Szentandrassy N (2016) Sarcolemmal Ca(2+)-entry through L-type Ca(2+) channels controls

the profile of Ca(2+)-activated Cl(-) current in canine ventricular myocytes. J Mol Cell Cardiol 97:125-139.

Hoshi N, Zhang JS, Omaki M, Takeuchi T, Yokoyama S, Wanaverbecq N, Langeberg LK, Yoneda Y, Scott JD, Brown DA, Higashida H (2003) AKAP150 signaling complex promotes suppression of the M-current by muscarinic agonists. Nature neuroscience 6:564-571.

Huang D, Liang C, Zhang F, Men H, Du X, Gamper N, Zhang H (2016) Inflammatory mediator bradykinin increases population of sensory neurons expressing functional T-type Ca(2+) channels. Biochemical and biophysical research communications 473:396-402.

Huang F, Rock JR, Harfe BD, Cheng T, Huang X, Jan YN, Jan LY (2009a) Studies on expression and function of the TMEM16A calcium-activated chloride channel. Proceedings of the National Academy of Sciences of the United States of America 106:21413-21418.

Huang F, Wang X, Ostertag EM, Nuwal T, Huang B, Jan YN, Basbaum AI, Jan LY (2013) TMEM16C facilitates Na(+)-activated K+ currents in rat sensory neurons and regulates pain processing. Nature neuroscience 16:1284-1290.

Huang J, Zhang X, McNaughton PA (2006) Inflammatory pain: the cellular basis of heat hyperalgesia. Current neuropharmacology 4:197-206.

Huang P, Liu J, Di A, Robinson NC, Musch MW, Kaetzel MA, Nelson DJ (2001) Regulation of human CLC-3 channels by multifunctional Ca2+/calmodulin-dependent protein kinase. The Journal of biological chemistry 276:20093-20100.

Huang SY, Bolser D, Liu HY, Hwang TC, Zou X (2009b) Molecular modeling of the heterodimer of human CFTR's nucleotide-binding domains using a protein-protein docking approach. Journal of molecular graphics & modelling 27:822-828.

Huang WC, Xiao S, Huang F, Harfe BD, Jan YN, Jan LY (2012) Calcium-activated chloride channels (CaCCs) regulate action potential and synaptic response in hippocampal neurons. Neuron 74:179-192.

Hudson LJ, Bevan S, Wotherspoon G, Gentry C, Fox A, Winter J (2001) VR1 protein expression increases in undamaged DRG neurons after partial nerve injury. The European journal of neuroscience 13:2105-2114.

Huguenard JR (1996) Low-threshold calcium currents in central nervous system neurons. Annual review of physiology 58:329-348.

Hwang SJ, Blair PJ, Britton FC, O'Driscoll KE, Hennig G, Bayguinov YR, Rock JR, Harfe BD, Sanders KM, Ward SM (2009) Expression of anoctamin 1/TMEM16A by interstitial cells of Cajal is fundamental for slow wave activity in gastrointestinal muscles. The Journal of physiology 587:4887-4904.

Hyde K, Reid CJ, Tebbutt SJ, Weide L, Hollingsworth MA, Harris A (1997) The cystic fibrosis transmembrane conductance regulator as a marker of human pancreatic duct development. Gastroenterology 113:914-919.

Idevall-Hagren O, Lu A, Xie B, De Camilli P (2015) Triggered Ca2+ influx is required for extended synaptotagmin 1-induced ER-plasma membrane tethering. The EMBO journal 34:2291-2305.

Iino M (1990) Biphasic Ca2+ dependence of inositol 1,4,5-trisphosphate-induced Ca release in smooth muscle cells of the guinea pig taenia caeci. The Journal of general physiology 95:1103-1122.

Ikeda R, Gu JG (2014) Piezo2 channel conductance and localization domains in Merkel cells of rat whisker hair follicles. Neuroscience letters 583:210-215.

Ikejima K, Qu W, Stachlewitz RF, Thurman RG (1997) Kupffer cells contain a glycine-gated chloride channel. The American journal of physiology 272:G1581-1586.

Imler E, Zinsmaier KE (2014) TRPV1 channels: not so inactive on the ER. Neuron 84:659-661.

Inoue K, Koizumi S, Fuziwara S, Denda S, Inoue K, Denda M (2002) Functional vanilloid receptors in cultured normal human epidermal keratinocytes. Biochemical and biophysical research communications 291:124-129.

Iosco C, Cosentino C, Sirna L, Romano R, Cursano S, Mongia A, Pompeo G, di Bernardo J, Ceccarelli C, Tallini G, Rhoden KJ (2014) Anoctamin 1 is apically expressed on thyroid follicular cells and contributes to ATP- and calcium-activated iodide efflux. Cellular physiology and biochemistry : international journal of experimental cellular physiology, biochemistry, and pharmacology 34:966-980.

Ishimaru Y, Matsunami H (2009) Transient receptor potential (TRP) channels and taste sensation. Journal of dental research 88:212-218.

Ito G, Okamoto R, Murano T, Shimizu H, Fujii S, Nakata T, Mizutani T, Yui S, Akiyama-Morio J, Nemoto Y, Okada E, Araki A, Ohtsuka K, Tsuchiya K, Nakamura T, Watanabe M (2013) Lineage-specific expression of bestrophin-2 and bestrophin-4 in human intestinal epithelial cells. PloS one 8:e79693.

Jaffe DB, Wang B, Brenner R (2011) Shaping of action potentials by type I and type II large-conductance Ca(2)+-activated K+ channels. Neuroscience 192:205-218.

Jarvis MF et al. (2002) A-317491, a novel potent and selective non-nucleotide antagonist of P2X3 and P2X2/3 receptors, reduces chronic inflammatory and neuropathic pain in the rat. Proceedings of the National Academy of Sciences of the United States of America 99:17179-17184.

Jayaraman S, Verkman AS (2000) Quenching mechanism of quinolinium-type chloride-sensitive fluorescent indicators. Biophysical chemistry 85:49-57.

Jentsch TJ, Steinmeyer K, Schwarz G (1990) Primary structure of Torpedo marmorata chloride channel isolated by expression cloning in Xenopus oocytes. Nature 348:510-514.

Jentsch TJ, Friedrich T, Schriever A, Yamada H (1999) The CLC chloride channel family. Pflugers Archiv : European journal of physiology 437:783-795.

Jeske NA, Berg KA, Cousins JC, Ferro ES, Clarke WP, Glucksman MJ, Roberts JL (2006) Modulation of bradykinin signaling by EP24.15 and EP24.16 in cultured trigeminal ganglia. Journal of neurochemistry 97:13-21.

Jia L, Liu W, Guan L, Lu M, Wang K (2015) Inhibition of Calcium-Activated Chloride Channel ANO1/TMEM16A Suppresses Tumor Growth and Invasion in Human Lung Cancer. PloS one 10:e0136584.

Jin X, Huguenard JR, Prince DA (2005) Impaired Cl- extrusion in layer V pyramidal neurons of chronically injured epileptogenic neocortex. Journal of neurophysiology 93:2117-2126.

Jin X, Shah S, Du X, Zhang H, Gamper N (2014) Activation of Ca -activated Cl channel ANO1 by localized Ca signals. The Journal of physiology.

Jin X, Morsy N, Winston J, Pasricha PJ, Garrett K, Akbarali HI (2004) Modulation of TRPV1 by nonreceptor tyrosine kinase, c-Src kinase. American journal of physiology Cell physiology 287:C558-563.

Jin X, Shah S, Liu Y, Zhang H, Lees M, Fu Z, Lippiat JD, Beech DJ, Sivaprasadarao A, Baldwin SA, Zhang H, Gamper N (2013) Activation of the Cl- channel ANO1 by localized calcium signals in nociceptive sensory neurons requires coupling with the IP3 receptor. Science signaling 6:ra73.

Johansson T, Norris T, Peilot-Sjogren H (2013) Yellow fluorescent protein-based assay to measure GABA(A) channel activation and allosteric modulation in CHO-K1 cells. PloS one 8:e59429.

Johnston GA (2005) GABA(A) receptor channel pharmacology. Current pharmaceutical design 11:1867-1885.

Joo NS, Krouse ME, Wu JV, Saenz Y, Jayaraman S, Verkman AS, Wine JJ (2001) HCO3- transport in relation to mucus secretion from submucosal glands. JOP : Journal of the pancreas 2:280-284.

Jukema BN, de Maat S, Maas C (2016) Processing of Factor XII during Inflammatory Reactions. Front Med 3.

Jung J, Nam JH, Park HW, Oh U, Yoon JH, Lee MG (2013) Dynamic modulation of ANO1/TMEM16A HCO3(-) permeability by Ca2+/calmodulin. Proceedings of the National Academy of Sciences of the United States of America 110:360-365.

Jung J, Shin JS, Lee SY, Hwang SW, Koo J, Cho H, Oh U (2004) Phosphorylation of vanilloid receptor 1 by Ca2+/calmodulin-dependent kinase II regulates its vanilloid binding. The Journal of biological chemistry 279:7048-7054.

Juschke C, Wachter A, Schwappach B, Seedorf M (2005) SEC18/NSF-independent, protein-sorting pathway from the yeast cortical ER to the plasma membrane. The Journal of cell biology 169:613-622.

Kaeser PS, Deng L, Wang Y, Dulubova I, Liu X, Rizo J, Sudhof TC (2011) RIM proteins tether Ca2+ channels to presynaptic active zones via a direct PDZ-domain interaction. Cell 144:282-295.

Kanai Y, Nakazato E, Fujiuchi A, Hara T, Imai A (2005) Involvement of an increased spinal TRPV1 sensitization through its up-regulation in mechanical allodynia of CCI rats. Neuropharmacology 49:977-984.

Kanazawa T, Matsumoto S (2014) Expression of transient receptor potential vanilloid 1 and anoctamin 1 in rat trigeminal ganglion neurons innervating the tongue. Brain research bulletin 106:17-20.

Kane Dickson V, Pedi L, Long SB (2014) Structure and insights into the function of a Ca(2+)-activated Cl(-) channel. Nature 516:213-218.

Kaneda M, Farrant M, Cull-Candy SG (1995) Whole-cell and single-channel currents activated by GABA and glycine in granule cells of the rat cerebellum. The Journal of physiology 485 (Pt 2):419-435.

Kaneko H, Mohrlen F, Frings S (2006) Calmodulin contributes to gating control in olfactory calcium-activated chloride channels. The Journal of general physiology 127:737-748.

Kang D, Kim D (2006) TREK-2 (K2P10.1) and TRESK (K2P18.1) are major background K+ channels in dorsal root ganglion neurons. American journal of physiology Cell physiology 291:C138-146.

Kang D, Choe C, Kim D (2005) Thermosensitivity of the two-pore domain K+ channels TREK-2 and TRAAK. The Journal of physiology 564:103-116.

Kaplan AP, Ghebrehiwet B (2010) The plasma bradykinin-forming pathways and its interrelationships with complement. Mol Immunol 47:2161-2169.

Kaupp UB (2010) Olfactory signalling in vertebrates and insects: differences and commonalities. Nat Rev Neurosci 11:188-200.

Kim BJ, Nam JH, Kim KH, Joo M, Ha TS, Weon KY, Choi S, Jun JY, Park EJ, Wie J, So I, Nah SY (2014) Characteristics of gintonin-mediated membrane depolarization of pacemaker activity in cultured interstitial cells of Cajal. Cellular physiology and biochemistry : international journal of experimental cellular physiology, biochemistry, and pharmacology 34:873-890.

Kim DS, Yoon CH, Lee SJ, Park SY, Yoo HJ, Cho HJ (2001) Changes in voltage-gated calcium channel alpha(1) gene expression in rat dorsal root ganglia following peripheral nerve injury. Brain research Molecular brain research 96:151-156.

Kim H (2008) Cerulein pancreatitis: oxidative stress, inflammation, and apoptosis. Gut and liver 2:74-80.

Kim HY, Park CK, Cho IH, Jung SJ, Kim JS, Oh SB (2008) Differential Changes in TRPV1 expression after trigeminal sensory nerve injury. The journal of pain : official journal of the American Pain Society 9:280-288.

Kinnman N, Lindblad A, Housset C, Buentke E, Scheynius A, Strandvik B, Hultcrantz R (2000) Expression of cystic fibrosis transmembrane conductance regulator in liver tissue from patients with cystic fibrosis. Hepatology 32:334-340.

Kirton HM, Pettinger L, Gamper N (2013) Transient overexpression of genes in neurons using nucleofection. Methods in molecular biology 998:55-64.

Kitamura K, Yamazaki J (2001) Chloride channels and their functional roles in smooth muscle tone in the vasculature. Japanese journal of pharmacology 85:351-357.

Kleene SJ, Gesteland RC (1991) Calcium-activated chloride conductance in frog olfactory cilia. The Journal of neuroscience : the official journal of the Society for Neuroscience 11:3624-3629.

Kondo M, Tsuji M, Hara K, Arimura K, Yagi O, Tagaya E, Takeyama K, Tamaoki J (2017) Chloride ion transport and overexpression of TMEM16A in a guinea-pig asthma model. Clinical and experimental allergy : journal of the British Society for Allergy and Clinical Immunology 47:795-804.

Koplas PA, Rosenberg RL, Oxford GS (1997) The role of calcium in the desensitization of capsaicin responses in rat dorsal root ganglion neurons. The Journal of neuroscience : the official journal of the Society for Neuroscience 17:3525-3537.

Korade Z, Kenworthy AK (2008) Lipid rafts, cholesterol, and the brain. Neuropharmacology 55:1265-1273.

Koschak A, Reimer D, Huber I, Grabner M, Glossmann H, Engel J, Striessnig J (2001) alpha 1D (Cav1.3) subunits can form l-type Ca2+ channels activating at negative voltages. The Journal of biological chemistry 276:22100-22106.

Kosten TR, George TP (2002) The neurobiology of opioid dependence: implications for treatment. Science & practice perspectives 1:13-20.

Krauss M, Haucke V (2016) Directing lipid transport at membrane contact sites. Nature cell biology 18:461-463.

Kubo T, Taguchi K, Ueda M (1998) L-type calcium channels in vascular smooth muscle cells from spontaneously hypertensive rats: effects of calcium agonist and antagonist. Hypertension research : official journal of the Japanese Society of Hypertension 21:33-37.

Kunzelmann K (2001) CFTR: interacting with everything? News in physiological sciences : an international journal of physiology produced jointly by the International Union of Physiological Sciences and the American Physiological Society 16:167-170.

Kunzelmann K, Cabrita I, Wanitchakool P, Ousingsawat J, Sirianant L, Benedetto R, Schreiber R (2016) Modulating Ca(2)(+) signals: a common theme for TMEM16, Ist2, and TMC. Pflugers Archiv : European journal of physiology 468:475-490.

Kunzelmann K, Tian Y, Martins JR, Faria D, Kongsuphol P, Ousingsawat J, Thevenod F, Roussa E, Rock J, Schreiber R (2011) Anoctamins. Pflugers Archiv : European journal of physiology 462:195-208.

Kuruma A, Hartzell HC (1999) Dynamics of calcium regulation of chloride currents in Xenopus oocytes. The American journal of physiology 276:C161-175.

Kwak J, Wang MH, Hwang SW, Kim TY, Lee SY, Oh U (2000) Intracellular ATP increases capsaicin-activated channel activity by interacting with nucleotide-binding domains. The Journal of neuroscience : the official journal of the Society for Neuroscience 20:8298-8304.

Kwan KY, Allchorne AJ, Vollrath MA, Christensen AP, Zhang DS, Woolf CJ, Corey DP (2006) TRPA1 contributes to cold, mechanical, and chemical nociception but is not essential for hair-cell transduction. Neuron 50:277-289.

Laird JM, Garcia-Nicas E, Delpire EJ, Cervero F (2004) Presynaptic inhibition and spinal pain processing in mice: a possible role of the NKCC1 cation-chloride co-transporter in hyperalgesia. Neuroscience letters 361:200-203.

Lamb ME, Zhang C, Shea T, Kyle DJ, Leeb-Lundberg LM (2002) Human B1 and B2 bradykinin receptors and their agonists target caveolae-related lipid rafts to different degrees in HEK293 cells. Biochemistry 41:14340-14347.

Lambert RC, Maulet Y, Mouton J, Beattie R, Volsen S, De Waard M, Feltz A (1997) T-type Ca2+ current properties are not modified by Ca2+ channel beta subunit depletion in nodosus ganglion neurons. The Journal of neuroscience : the official journal of the Society for Neuroscience 17:6621-6628.

Landstrom AP, Beavers DL, Wehrens XH (2014) The junctophilin family of proteins: from bench to bedside. Trends in molecular medicine 20:353-362.

Landstrom AP, Kellen CA, Dixit SS, van Oort RJ, Garbino A, Weisleder N, Ma J, Wehrens XH, Ackerman MJ (2011) Junctophilin-2 expression silencing causes cardiocyte hypertrophy and abnormal intracellular calcium-handling. Circulation Heart failure 4:214-223.

Lang F, Foller M, Lang K, Lang P, Ritter M, Vereninov A, Szabo I, Huber SM, Gulbins E (2007) Cell volume regulatory ion channels in cell proliferation and cell death. Methods in enzymology 428:209-225.

Lanner JT, Georgiou DK, Joshi AD, Hamilton SL (2010) Ryanodine receptors: structure, expression, molecular details, and function in calcium release. Cold Spring Harbor perspectives in biology 2:a003996.

Latremoliere A, Woolf CJ (2009) Central sensitization: a generator of pain hypersensitivity by central neural plasticity. The journal of pain : official journal of the American Pain Society 10:895-926.

Launikonis BS, Rios E (2007) Store-operated Ca2+ entry during intracellular Ca2+ release in mammalian skeletal muscle. The Journal of physiology 583:81-97.

Leblanc N, Ledoux J, Saleh S, Sanguinetti A, Angermann J, O'Driscoll K, Britton F, Perrino BA, Greenwood IA (2005) Regulation of calcium-activated chloride channels in smooth muscle cells: a complex picture is emerging. Canadian journal of physiology and pharmacology 83:541-556.

Leblanc N, Forrest AS, Ayon RJ, Wiwchar M, Angermann JE, Pritchard HA, Singer CA, Valencik ML, Britton F, Greenwood IA (2015) Molecular and functional significance of Ca(2+)-activated Cl(-) channels in pulmonary arterial smooth muscle. Pulmonary circulation 5:244-268.

Lee B, Cho H, Jung J, Yang YD, Yang DJ, Oh U (2014) Anoctamin 1 contributes to inflammatory and nerve-injury induced hypersensitivity. Molecular pain 10:5.

Lee J, Cha SK, Sun TJ, Huang CL (2005) PIP2 activates TRPV5 and releases its inhibition by intracellular Mg2+. The Journal of general physiology 126:439-451.

Lee S (2013) Pharmacological Inhibition of Voltage-gated Ca(2+) Channels for Chronic Pain Relief. Current neuropharmacology 11:606-620.

Lerias JR, Pinto MC, Botelho HM, Awatade NT, Quaresma MC, Silva IAL, Wanitchakool P, Schreiber R, Pepperkok R, Kunzelmann K, Amaral MD

(2018) A novel microscopy-based assay identifies extended synaptotagmin-1 (ESYT1) as a positive regulator of anoctamin 1 traffic. Biochimica et biophysica acta 1865:421-431.

Lewis C, Neidhart S, Holy C, North RA, Buell G, Surprenant A (1995) Coexpression of P2X2 and P2X3 receptor subunits can account for ATP-gated currents in sensory neurons. Nature 377:432-435.

Li CL, Li KC, Wu D, Chen Y, Luo H, Zhao JR, Wang SS, Sun MM, Lu YJ, Zhong YQ, Hu XY, Hou R, Zhou BB, Bao L, Xiao HS, Zhang X (2016) Somatosensory neuron types identified by high-coverage single-cell RNA-sequencing and functional heterogeneity. Cell research 26:967.

Li Y, Um SY, McDonald TV (2006) Voltage-gated potassium channels: regulation by accessory subunits. The Neuroscientist : a review journal bringing neurobiology, neurology and psychiatry 12:199-210.

Liao M, Cao E, Julius D, Cheng Y (2013) Structure of the TRPV1 ion channel determined by electron cryo-microscopy. Nature 504:107-112.

Liddle RA, Nathan JD (2004) Neurogenic inflammation and pancreatitis. Pancreatology : official journal of the International Association of Pancreatology 4:551-559; discussion 559-560.

Lindia JA, Kohler MG, Martin WJ, Abbadie C (2005) Relationship between sodium channel NaV1.3 expression and neuropathic pain behavior in rats. Pain 117:145-153.

Linley JE, Rose K, Ooi L, Gamper N (2010) Understanding inflammatory pain: ion channels contributing to acute and chronic nociception. Pflugers Archiv : European journal of physiology 459:657-669.

Lishko PV, Procko E, Jin X, Phelps CB, Gaudet R (2007) The ankyrin repeats of TRPV1 bind multiple ligands and modulate channel sensitivity. Neuron 54:905-918.

Liu B, Zhang C, Qin F (2005) Functional recovery from desensitization of vanilloid receptor TRPV1 requires resynthesis of phosphatidylinositol 4,5-bisphosphate. The Journal of neuroscience : the official journal of the Society for Neuroscience 25:4835-4843.

Liu B, Linley JE, Du X, Zhang X, Ooi L, Zhang H, Gamper N (2010) The acute nociceptive signals induced by bradykinin in rat sensory neurons are mediated by inhibition of M-type K+ channels and activation of Ca2+-activated Cl- channels. The Journal of clinical investigation 120:1240-1252.

Liu S, Feng J, Luo J, Yang P, Brett TJ, Hu H (2016) Eact, a small molecule activator of TMEM16A, activates TRPV1 and elicits pain- and itch-related behaviours. British journal of pharmacology 173:1208-1218.

Liu X, Singh BB, Ambudkar IS (2003) TRPC1 is required for functional store-operated Ca2+ channels. Role of acidic amino acid residues in the S5-S6 region. The Journal of biological chemistry 278:11337-11343.

Liu X, Cheng KT, Bandyopadhyay BC, Pani B, Dietrich A, Paria BC, Swaim WD, Beech D, Yildrim E, Singh BB, Birnbaumer L, Ambudkar IS (2007) Attenuation of store-operated Ca2+ current impairs salivary gland fluid secretion in

TRPC1(-/-) mice. Proceedings of the National Academy of Sciences of the United States of America 104:17542-17547.

Liu YN, Zhang HR, Huang DY, Qi JL, Xu JX, Gao HX, Du XN, Gamper N, Zhang HL (2015) Characterization of the effects of Cl- channel modulators on TMEM16A and bestrophin-1 Ca2+ activated Cl- channels. Pflug Arch Eur J Phy 467:1417-1430.

Lolignier S, Eijkelkamp N, Wood JN (2015) Mechanical allodynia. Pflugers Archiv : European journal of physiology 467:133-139.

Lu L, Zhang Q, Timofeyev V, Zhang Z, Young JN, Shin HS, Knowlton AA, Chiamvimonvat N (2007) Molecular coupling of a Ca2+-activated K+ channel to L-type Ca2+ channels via alpha-actinin2. Circ Res 100:112-120.

Lu L, Sirish P, Zhang Z, Woltz RL, Li N, Timofeyev V, Knowlton AA, Zhang XD, Yamoah EN, Chiamvimonvat N (2015) Regulation of gene transcription by voltage-gated L-type calcium channel, Cav1.3. The Journal of biological chemistry 290:4663-4676.

Ludwig A, Flockerzi V, Hofmann F (1997) Regional expression and cellular localization of the alpha1 and beta subunit of high voltage-activated calcium channels in rat brain. The Journal of neuroscience : the official journal of the Society for Neuroscience 17:1339-1349.

Lukacs V, Thyagarajan B, Varnai P, Balla A, Balla T, Rohacs T (2007) Dual regulation of TRPV1 by phosphoinositides. The Journal of neuroscience : the official journal of the Society for Neuroscience 27:7070-7080.

Lundberg JM, Martling CR, Saria A (1983a) Substance P and capsaicin-induced contraction of human bronchi. Acta physiologica Scandinavica 119:49-53.

Lundberg JM, Brodin E, Saria A (1983b) Effects and distribution of vagal capsaicin-sensitive substance P neurons with special reference to the trachea and lungs. Acta physiologica Scandinavica 119:243-252.

Lynch JW (2004) Molecular structure and function of the glycine receptor chloride channel. Physiological reviews 84:1051-1095.

Ma L, Zhang X, Zhou M, Chen H (2012) Acid-sensitive TWIK and TASK two-pore domain potassium channels change ion selectivity and become permeable to sodium in extracellular acidification. The Journal of biological chemistry 287:37145-37153.

Mackenzie L, Bootman MD, Berridge MJ, Lipp P (2001) Predetermined recruitment of calcium release sites underlies excitation-contraction coupling in rat atrial myocytes. The Journal of physiology 530:417-429.

Maddox FN, Valeyev AY, Poth K, Holohean AM, Wood PM, Davidoff RA, Hackman JC, Luetje CW (2004) GABAA receptor subunit mRNA expression in cultured embryonic and adult human dorsal root ganglion neurons. Brain research Developmental brain research 149:143-151.

Maduke M, Miller C, Mindell JA (2000) A decade of CLC chloride channels: structure, mechanism, and many unsettled questions. Annual review of biophysics and biomolecular structure 29:411-438.

Maingret F, Patel AJ, Lesage F, Lazdunski M, Honore E (1999) Mechano- or acid stimulation, two interactive modes of activation of the TREK-1 potassium channel. The Journal of biological chemistry 274:26691-26696.

Maingret F, Lauritzen I, Patel AJ, Heurteaux C, Reyes R, Lesage F, Lazdunski M, Honore E (2000) TREK-1 is a heat-activated background K+ channel. Embo Journal 19:2483-2491.

Maksimovic S, Nakatani M, Baba Y, Nelson AM, Marshall KL, Wellnitz SA, Firozi P, Woo SH, Ranade S, Patapoutian A, Lumpkin EA (2014) Epidermal Merkel cells are mechanosensory cells that tune mammalian touch receptors. Nature 509:617-621.

Malmersjo S, Meyer T (2013) Inside-out connections: the ER meets the plasma membrane. Cell 153:1423-1424.

Malvezzi M, Chalat M, Janjusevic R, Picollo A, Terashima H, Menon AK, Accardi A (2013) Ca2+-dependent phospholipid scrambling by a reconstituted TMEM16 ion channel. Nature communications 4:2367.

Mandle RJ, Colman RW, Kaplan AP (1976) Identification of Prekallikrein and High-Molecular-Weight Kininogen as a Complex in Human-Plasma. Proceedings of the National Academy of Sciences of the United States of America 73:4179-4183.

Manford AG, Stefan CJ, Yuan HL, Macgurn JA, Emr SD (2012) ER-to-plasma membrane tethering proteins regulate cell signaling and ER morphology. Developmental cell 23:1129-1140.

Mangoni ME, Couette B, Bourinet E, Platzer J, Reimer D, Striessnig J, Nargeot J (2003) Functional role of L-type Cav1.3 Ca2+ channels in cardiac pacemaker activity. Proceedings of the National Academy of Sciences of the United States of America 100:5543-5548.

Manoury B, Tamuleviciute A, Tammaro P (2010) TMEM16A/anoctamin 1 protein mediates calcium-activated chloride currents in pulmonary arterial smooth muscle cells. The Journal of physiology 588:2305-2314.

Mantegazza M, Catterall WA (2012) Voltage-Gated Na+ Channels: Structure, Function, and Pathophysiology. In: Jasper's Basic Mechanisms of the Epilepsies, 4th Edition (Noebels JL, Avoli M, Rogawski MA, Olsen RW, Delgado-Escueta AV, eds). Bethesda (MD).

Mao S, Garzon-Muvdi T, Di Fulvio M, Chen Y, Delpire E, Alvarez FJ, Alvarez-Leefmans FJ (2012) Molecular and functional expression of cation-chloride cotransporters in dorsal root ganglion neurons during postnatal maturation. Journal of neurophysiology 108:834-852.

Marchant JS, Chang YT, Chung SK, Irvine RF, Taylor CW (1997) Rapid kinetic measurements of 45Ca2+ mobilization reveal that Ins(2,4,5)P3 is a partial agonist at hepatic InsP3 receptors. The Biochemical journal 321 (Pt 3):573-576.

Markadieu N, Delpire E (2014) Physiology and pathophysiology of SLC12A1/2 transporters. Pflugers Archiv : European journal of physiology 466:91-105.

Marks AR (1997) Intracellular calcium-release channels: regulators of cell life and death. The American journal of physiology 272:H597-605.

Marmorstein AD, Marmorstein LY, Rayborn M, Wang X, Hollyfield JG, Petrukhin K (2000) Bestrophin, the product of the Best vitelliform macular dystrophy gene (VMD2), localizes to the basolateral plasma membrane of the retinal pigment epithelium. Proceedings of the National Academy of Sciences of the United States of America 97:12758-12763.

Marsh B, Acosta C, Djouhri L, Lawson SN (2012) Leak K+ channel mRNAs in dorsal root ganglia: Relation to inflammation and spontaneous pain behaviour. Molecular and Cellular Neuroscience 49:375-386.

Marsh JA, Teichmann SA (2015) Structure, dynamics, assembly, and evolution of protein complexes. Annual review of biochemistry 84:551-575.

Marshall IC, Taylor CW (1993) Biphasic effects of cytosolic Ca2+ on Ins(1,4,5)P3-stimulated Ca2+ mobilization in hepatocytes. Journal of Biological Chemistry 268:13214-13220.

Martin AC, Willoughby D, Ciruela A, Ayling LJ, Pagano M, Wachten S, Tengholm A, Cooper DM (2009) Capacitative Ca2+ entry via Orai1 and stromal interacting molecule 1 (STIM1) regulates adenylyl cyclase type 8. Molecular pharmacology 75:830-842.

Martin SC (1992) ATP activates a Ca(2+)-dependent Cl- current in the rat thyroid cell line, FRTL-5. The Journal of membrane biology 125:243-253.

Matchkov VV, Aalkjaer C, Nilsson H (2004) A cyclic GMP-dependent calcium-activated chloride current in smooth-muscle cells from rat mesenteric resistance arteries. The Journal of general physiology 123:121-134.

Mathie A, Veale EL (2015) Two-pore domain potassium channels: potential therapeutic targets for the treatment of pain. Pflugers Archiv : European journal of physiology 467:931-943.

McClatchey AI (2012) ERM proteins. Current biology : CB 22:R784-785.

McClatchey AI, Fehon RG (2009) Merlin and the ERM proteins--regulators of receptor distribution and signaling at the cell cortex. Trends in cell biology 19:198-206.

Mehta G, Sims EJ, Culross F, McCormick JD, Mehta A (2004) Potential benefits of the UK Cystic Fibrosis Database. Journal of the Royal Society of Medicine 97 Suppl 44:60-71.

Middleton RE, Pheasant DJ, Miller C (1996) Homodimeric architecture of a ClC-type chloride ion channel. Nature 383:337-340.

Miledi R (1982) A calcium-dependent transient outward current in Xenopus laevis oocytes. Proceedings of the Royal Society of London Series B, Biological sciences 215:491-497.

Miller C, White MM (1984) Dimeric structure of single chloride channels from Torpedo electroplax. Proceedings of the National Academy of Sciences of the United States of America 81:2772-2775.

Min SW, Chang WP, Sudhof TC (2007) E-Syts, a family of membranous Ca2+-sensor proteins with multiple C2 domains. Proceedings of the National Academy of Sciences of the United States of America 104:3823-3828.

Minamisawa S, Oshikawa J, Takeshima H, Hoshijima M, Wang Y, Chien KR, Ishikawa Y, Matsuoka R (2004) Junctophilin type 2 is associated with caveolin-3 and is down-regulated in the hypertrophic and dilated cardiomyopathies. Biochemical and biophysical research communications 325:852-856.

Miranda A, Nordstrom E, Mannem A, Smith C, Banerjee B, Sengupta JN (2007) The role of transient receptor potential vanilloid 1 in mechanical and chemical visceral hyperalgesia following experimental colitis. Neuroscience 148:1021-1032.

Mitrirattanakul S, Ramakul N, Guerrero AV, Matsuka Y, Ono T, Iwase H, Mackie K, Faull KF, Spigelman I (2006) Site-specific increases in peripheral cannabinoid receptors and their endogenous ligands in a model of neuropathic pain. Pain 126:102-114.

Mizumura K, Sugiura T, Katanosaka K, Banik RK, Kozaki Y (2009) Excitation and sensitization of nociceptors by bradykinin: what do we know? Experimental brain research 196:53-65.

Mizuta K, Tsutsumi S, Inoue H, Sakamoto Y, Miyatake K, Miyawaki K, Noji S, Kamata N, Itakura M (2007) Molecular characterization of GDD1/TMEM16E, the gene product responsible for autosomal dominant gnathodiaphyseal dysplasia. Biochemical and biophysical research communications 357:126-132.

Modol L, Cobianchi S, Navarro X (2014) Prevention of NKCC1 phosphorylation avoids downregulation of KCC2 in central sensory pathways and reduces neuropathic pain after peripheral nerve injury. Pain 155:1577-1590.

Mohammad-Panah R, Harrison R, Dhani S, Ackerley C, Huan L-J, Wang Y, Bear CE (2003) The Chloride Channel ClC-4 Contributes to Endosomal Acidification and Trafficking. Journal of Biological Chemistry 278:29267-29277.

Mohapatra DP, Nau C (2005) Regulation of Ca2+-dependent desensitization in the vanilloid receptor TRPV1 by calcineurin and cAMP-dependent protein kinase. The Journal of biological chemistry 280:13424-13432.

Moiseenkova-Bell VY, Stanciu LA, Serysheva, II, Tobe BJ, Wensel TG (2008) Structure of TRPV1 channel revealed by electron cryomicroscopy. Proceedings of the National Academy of Sciences of the United States of America 105:7451-7455.

Molineux ML, McRory JE, McKay BE, Hamid J, Mehaffey WH, Rehak R, Snutch TP, Zamponi GW, Turner RW (2006) Specific T-type calcium channel isoforms are associated with distinct burst phenotypes in deep cerebellar nuclear neurons. Proceedings of the National Academy of Sciences of the United States of America 103:5555-5560.

Montell C (2005) The TRP superfamily of cation channels. Science's STKE : signal transduction knowledge environment 2005:re3.

Morales-Lazaro SL, Serrano-Flores B, Llorente I, Hernandez-Garcia E, Gonzalez-Ramirez R, Banerjee S, Miller D, Gududuru V, Fells J, Norman D, Tigyi G, Escalante-Alcalde D, Rosenbaum T (2014) Structural determinants of the transient receptor potential 1 (TRPV1) channel activation by phospholipid analogs. The Journal of biological chemistry 289:24079-24090.

Mori M, Heuss C, Gahwiler BH, Gerber U (2001) Fast synaptic transmission mediated by P2X receptors in CA3 pyramidal cells of rat hippocampal slice cultures. The Journal of physiology 535:115-123.

Morita K, David G, Barrett JN, Barrett EF (1993) Posttetanic hyperpolarization produced by electrogenic Na(+)-K+ pump in lizard axons impaled near their motor terminals. Journal of neurophysiology 70:1874-1884.

Moriyama T, Higashi T, Togashi K, Iida T, Segi E, Sugimoto Y, Tominaga T, Narumiya S, Tominaga M (2005) Sensitization of TRPV1 by EP1 and IP reveals peripheral nociceptive mechanism of prostaglandins. Molecular pain 1:3.

Morsomme P, Boutry M (2000) The plant plasma membrane H(+)-ATPase: structure, function and regulation. Biochimica et biophysica acta 1465:1-16.

Morton RA, Norlin MS, Vollmer CC, Valenzuela CF (2013) Characterization of L-type voltage-gated Ca(2+) channel expression and function in developing CA3 pyramidal neurons. Neuroscience 238:59-70.

Nakai J, Imagawa T, Hakamat Y, Shigekawa M, Takeshima H, Numa S (1990) Primary structure and functional expression from cDNA of the cardiac ryanodine receptor/calcium release channel. FEBS letters 271:169-177.

Namadurai S, Yereddi NR, Cusdin FS, Huang CL, Chirgadze DY, Jackson AP (2015) A new look at sodium channel beta subunits. Open biology 5:140192.

Namkung W, Phuan PW, Verkman AS (2011) TMEM16A inhibitors reveal TMEM16A as a minor component of calcium-activated chloride channel conductance in airway and intestinal epithelial cells. The Journal of biological chemistry 286:2365-2374.

Naraghi M, Neher E (1997) Linearized buffered Ca2+ diffusion in microdomains and its implications for calculation of [Ca2+] at the mouth of a calcium channel. The Journal of neuroscience : the official journal of the Society for Neuroscience 17:6961-6973.

Nassar MA, Baker MD, Levato A, Ingram R, Mallucci G, McMahon SB, Wood JN (2006) Nerve injury induces robust allodynia and ectopic discharges in Nav1.3 null mutant mice. Molecular pain 2:33.

Nathan JD, Peng RY, Wang Y, McVey DC, Vigna SR, Liddle RA (2002) Primary sensory neurons: a common final pathway for inflammation in experimental pancreatitis in rats. American journal of physiology Gastrointestinal and liver physiology 283:G938-946.

Nathan JD, Patel AA, McVey DC, Thomas JE, Prpic V, Vigna SR, Liddle RA (2001) Capsaicin vanilloid receptor-1 mediates substance P release in experimental pancreatitis. American journal of physiology Gastrointestinal and liver physiology 281:G1322-1328.

Neher E (1998) Usefulness and limitations of linear approximations to the understanding of Ca++ signals. Cell Calcium 24:345-357.

Neussert R, Muller C, Milenkovic VM, Strauss O (2010) The presence of bestrophin-1 modulates the Ca2+ recruitment from Ca2+ stores in the ER. Pflugers Archiv : European journal of physiology 460:163-175.

Nguyen L, Malgrange B, Belachew S, Rogister B, Rocher V, Moonen G, Rigo JM (2002) Functional glycine receptors are expressed by postnatal nestin-positive neural stem/progenitor cells. The European journal of neuroscience 15:1299-1305.

Ni AG, Agata J, Yang Z, Chao R, Chao J (2003) Overexpression of kinin B-1 receptors induces hypertensive response to Des-Arg(9)-bradykinin and susceptibility to inflammation. Journal of Biological Chemistry 278:219-225.

Nicke A, Baumert HG, Rettinger J, Eichele A, Lambrecht G, Mutschler E, Schmalzing G (1998) P2X1 and P2X3 receptors form stable trimers: a novel structural motif of ligand-gated ion channels. The EMBO journal 17:3016-3028.

Nilius B (2007) TRP channels in disease. Biochimica et biophysica acta 1772:805-812.

Nilius B, Mahieu F, Prenen J, Janssens A, Owsianik G, Vennekens R, Voets T (2006) The Ca2+-activated cation channel TRPM4 is regulated by phosphatidylinositol 4,5-biphosphate. The EMBO journal 25:467-478.

Noble D, Borysova L, Wray S, Burdyga T (2014) Store-operated Ca(2)(+) entry and depolarization explain the anomalous behaviour of myometrial SR: effects of SERCA inhibition on electrical activity, Ca(2)(+) and force. Cell Calcium 56:188-194.

North RA (2002) Molecular physiology of P2X receptors. Physiological reviews 82:1013-1067.

Numazaki M, Tominaga T, Takeuchi K, Murayama N, Toyooka H, Tominaga M (2003) Structural determinant of TRPV1 desensitization interacts with calmodulin. Proceedings of the National Academy of Sciences of the United States of America 100:8002-8006.

Nymann-Andersen J, Wang H, Chen L, Kittler JT, Moss SJ, Olsen RW (2002) Subunit specificity and interaction domain between GABA(A) receptor-associated protein (GABARAP) and GABA(A) receptors. Journal of neurochemistry 80:815-823.

O'Connell AD, Morton MJ, Hunter M (2002) Two-pore domain K+ channels—molecular sensors. Biochimica et Biophysica Acta (BBA) - Biomembranes 1566:152-161.

O'Driscoll KE, Leblanc N, Hatton WJ, Britton FC (2009) Functional properties of murine bestrophin 1 channel. Biochemical and biophysical research communications 384:476-481.

O'Driscoll KE, Hatton WJ, Burkin HR, Leblanc N, Britton FC (2008) Expression, localization, and functional properties of Bestrophin 3 channel isolated from

mouse heart. American journal of physiology Cell physiology 295:C1610-1624.

Obata K, Oide M, Tanaka H (1978) Excitatory and inhibitory actions of GABA and glycine on embryonic chick spinal neurons in culture. Brain research 144:179-184.

Obata K, Katsura H, Mizushima T, Yamanaka H, Kobayashi K, Dai Y, Fukuoka T, Tokunaga A, Tominaga M, Noguchi K (2005) TRPA1 induced in sensory neurons contributes to cold hyperalgesia after inflammation and nerve injury. The Journal of clinical investigation 115:2393-2401.

Obradovic A, Hwang SM, Scarpa J, Hong SJ, Todorovic SM, Jevtovic-Todorovic V (2014) CaV3.2 T-type calcium channels in peripheral sensory neurons are important for mibefradil-induced reversal of hyperalgesia and allodynia in rats with painful diabetic neuropathy. PloS one 9:e91467.

Ohsawa M, Miyabe Y, Katsu H, Yamamoto S, Ono H (2013) Identification of the sensory nerve fiber responsible for lysophosphatidic acid-induced allodynia in mice. Neuroscience 247:65-74.

Okeke E, Dingsdale H, Parker T, Voronina S, Tepikin AV (2016) Endoplasmic reticulum-plasma membrane junctions: structure, function and dynamics. The Journal of physiology 594:2837-2847.

Oliveira MC, Pelegrini-da-Silva A, Tambeli CH, Parada CA (2009) Peripheral mechanisms underlying the essential role of P2X3,2/3 receptors in the development of inflammatory hyperalgesia. Pain 141:127-134.

Olson PA, Tkatch T, Hernandez-Lopez S, Ulrich S, Ilijic E, Mugnaini E, Zhang H, Bezprozvanny I, Surmeier DJ (2005) G-protein-coupled receptor modulation of striatal CaV1.3 L-type Ca2+ channels is dependent on a Shank-binding domain. The Journal of neuroscience : the official journal of the Society for Neuroscience 25:1050-1062.

Ong HL, Cheng KT, Liu X, Bandyopadhyay BC, Paria BC, Soboloff J, Pani B, Gwack Y, Srikanth S, Singh BB, Gill D, Ambudkar IS (2007) Dynamic Assembly of TRPC1-STIM1-Orai1 Ternary Complex Is Involved in Store-operated Calcium Influx: Evidence for Similarities in Store-Operated and Calcium Release-Activated Calcium Channel components(). The Journal of biological chemistry 282:9105-9116.

Ono K, Iijima T (2010) Cardiac T-type Ca2+ channels in the heart. Journal of Molecular and Cellular Cardiology 48:65-70.

Ormo M, Cubitt AB, Kallio K, Gross LA, Tsien RY, Remington SJ (1996) Crystal structure of the Aequorea victoria green fluorescent protein. Science 273:1392-1395.

Otsu K, Willard HF, Khanna VK, Zorzato F, Green NM, MacLennan DH (1990) Molecular cloning of cDNA encoding the Ca2+ release channel (ryanodine receptor) of rabbit cardiac muscle sarcoplasmic reticulum. The Journal of biological chemistry 265:13472-13483.

Pakhomov AA, Martynov VI (2008) GFP family: structural insights into spectral tuning. Chemistry & biology 15:755-764.

Palma E, Amici M, Sobrero F, Spinelli G, Di Angelantonio S, Ragozzino D, Mascia A, Scoppetta C, Esposito V, Miledi R, Eusebi F (2006) Anomalous levels of Cl- transporters in the hippocampal subiculum from temporal lobe epilepsy patients make GABA excitatory. Proceedings of the National Academy of Sciences of the United States of America 103:8465-8468.

Pankratov Y, Lalo U, Krishtal O, Verkhratsky A (2002) Ionotropic P2X purinoreceptors mediate synaptic transmission in rat pyramidal neurones of layer II/III of somato-sensory cortex. The Journal of physiology 542:529-536.

Pankratov Y, Lalo U, Krishtal O, Verkhratsky A (2003) P2X receptor-mediated excitatory synaptic currents in somatosensory cortex. Molecular and cellular neurosciences 24:842-849.

Pankratov Y, Lalo U, Castro E, Miras-Portugal MT, Krishtal O (1999) ATP receptor-mediated component of the excitatory synaptic transmission in the hippocampus. Progress in brain research 120:237-249.

Parekh AB (2008) Ca2+ microdomains near plasma membrane Ca2+ channels: impact on cell function. The Journal of physiology 586:3043-3054.

Parekh AB, Putney JW, Jr. (2005) Store-operated calcium channels. Physiological reviews 85:757-810.

Park E, Campbell EB, MacKinnon R (2017) Structure of a CLC chloride ion channel by cryo-electron microscopy. Nature 541:500-505.

Park JF, Luo ZD (2010) Calcium channel functions in pain processing. Channels 4:510-517.

Parker D, Hill R, Grillner S (1996) Electrogenic pump and a Ca(2+)- dependent K+ conductance contribute to a posttetanic hyperpolarization in lamprey sensory neurons. Journal of neurophysiology 76:540-553.

Patel AJ, Lesage F, Maingret F, Fink M, Duprat F, Lazdunski M, Honore EL (1999) A mammalian two pore domain mechano-gated S-like K+ channel. Biophysical journal 76:A202-A202.

Patrick AE, Thomas PJ (2012) Development of CFTR Structure. Frontiers in pharmacology 3:162.

Paulino C, Neldner Y, Lam AK, Kalienkova V, Brunner JD, Schenck S, Dutzler R (2017) Structural basis for anion conduction in the calcium-activated chloride channel TMEM16A. eLife 6.

Pawlowski K, Lepisto M, Meinander N, Sivars U, Varga M, Wieslander E (2006) Novel conserved hydrolase domain in the CLCA family of alleged calcium-activated chloride channels. Proteins 63:424-439.

Pearce MM, Wormer DB, Wilkens S, Wojcikiewicz RJ (2009) An endoplasmic reticulum (ER) membrane complex composed of SPFH1 and SPFH2 mediates the ER-associated degradation of inositol 1,4,5-trisphosphate receptors. The Journal of biological chemistry 284:10433-10445.

Peddareddygari LR, Oberoi K, Grewal RP (2014) Congenital insensitivity to pain: a case report and review of the literature. Case reports in neurological medicine 2014:141953.

Pedemonte N, Galietta LJ (2014) Structure and function of TMEM16 proteins (anoctamins). Physiological reviews 94:419-459.

Perez-Alvarez A, Hernandez-Vivanco A, Caba-Gonzalez JC, Albillos A (2011) Different roles attributed to Cav1 channel subtypes in spontaneous action potential firing and fine tuning of exocytosis in mouse chromaffin cells. Journal of neurochemistry 116:105-121.

Perez-Cornejo P, Gokhale A, Duran C, Cui Y, Xiao Q, Hartzell HC, Faundez V (2012) Anoctamin 1 (Tmem16A) Ca2+-activated chloride channel stoichiometrically interacts with an ezrin-radixin-moesin network. Proceedings of the National Academy of Sciences of the United States of America 109:10376-10381.

Perez-Lara A, Jahn R (2015) Extended synaptotagmins (E-Syts): Architecture and dynamics of membrane contact sites revealed. Proceedings of the National Academy of Sciences of the United States of America 112:4837-4838.

Perez-Reyes E (2003) Molecular Physiology of Low-Voltage-Activated T-type Calcium Channels. Physiological reviews 83:117-161.

Perret D, Luo ZD (2009) Targeting voltage-gated calcium channels for neuropathic pain management. Neurotherapeutics : the journal of the American Society for Experimental NeuroTherapeutics 6:679-692.

Peters CJ, Yu H, Tien J, Jan YN, Li M, Jan LY (2015) Four basic residues critical for the ion selectivity and pore blocker sensitivity of TMEM16A calcium-activated chloride channels. Proceedings of the National Academy of Sciences of the United States of America 112:3547-3552.

Petrukhin K, Koisti MJ, Bakall B, Li W, Xie G, Marknell T, Sandgren O, Forsman K, Holmgren G, Andreasson S, Vujic M, Bergen AA, McGarty-Dugan V, Figueroa D, Austin CP, Metzker ML, Caskey CT, Wadelius C (1998) Identification of the gene responsible for Best macular dystrophy. Nature genetics 19:241-247.

Peyronnet R, Martins JR, Duprat F, Demolombe S, Arhatte M, Jodar M, Tauc M, Duranton C, Paulais M, Teulon J, Honore E, Patel A (2013) Piezo1-dependent stretch-activated channels are inhibited by Polycystin-2 in renal tubular epithelial cells. EMBO reports 14:1143-1148.

Pfeiffer F, Graham D, Betz H (1982) Purification by affinity chromatography of the glycine receptor of rat spinal cord. The Journal of biological chemistry 257:9389-9393.

Pichler H, Gaigg B, Hrastnik C, Achleitner G, Kohlwein SD, Zellnig G, Perktold A, Daum G (2001) A subfraction of the yeast endoplasmic reticulum associates with the plasma membrane and has a high capacity to synthesize lipids. Eur J Biochem 268:2351-2361.

Piechotta K, Weth F, Harvey RJ, Friauf E (2001) Localization of rat glycine receptor alpha1 and alpha2 subunit transcripts in the developing auditory brainstem. The Journal of comparative neurology 438:336-352.

Piechotta PL, Rapedius M, Stansfeld PJ, Bollepalli MK, Ehrlich G, Andres-Enguix I, Fritzenschaft H, Decher N, Sansom MS, Tucker SJ, Baukrowitz T (2011) The pore structure and gating mechanism of K2P channels. The EMBO journal 30:3607-3619.

Pietra G, Dibattista M, Menini A, Reisert J, Boccaccio A (2016) The Ca2+-activated Cl- channel TMEM16B regulates action potential firing and axonal targeting in olfactory sensory neurons. The Journal of general physiology 148:293-311.

Pifferi S, Cenedese V, Menini A (2012) Anoctamin 2/TMEM16B: a calcium-activated chloride channel in olfactory transduction. Exp Physiol 97:193-199.

Pifferi S, Pascarella G, Boccaccio A, Mazzatenta A, Gustincich S, Menini A, Zucchelli S (2006) Bestrophin-2 is a candidate calcium-activated chloride channel involved in olfactory transduction. Proceedings of the National Academy of Sciences of the United States of America 103:12929-12934.

Pineda-Farias JB, Barragan-Iglesias P, Loeza-Alcocer E, Torres-Lopez JE, Rocha-Gonzalez HI, Perez-Severiano F, Delgado-Lezama R, Granados-Soto V (2015) Role of anoctamin-1 and bestrophin-1 in spinal nerve ligation-induced neuropathic pain in rats. Molecular pain 11:41.

Pinho-Ribeiro FA, Verri WA, Jr., Chiu IM (2017) Nociceptor Sensory Neuron-Immune Interactions in Pain and Inflammation. Trends in immunology 38:5-19.

Piper AS, Large WA (2003) Multiple conductance states of single Ca2+-activated Cl- channels in rabbit pulmonary artery smooth muscle cells. The Journal of physiology 547:181-196.

Pitcher MH, Price TJ, Entrena JM, Cervero F (2007) Spinal NKCC1 blockade inhibits TRPV1-dependent referred allodynia. Molecular pain 3:17.

Plant LD (2012) A Role for K2P Channels in the Operation of Somatosensory Nociceptors. Frontiers in molecular neuroscience 5:21.

Pleger B, Tegenthoff M, Schwenkreis P, Janssen F, Ragert P, Dinse HR, Volker B, Zenz M, Maier C (2004) Mean sustained pain levels are linked to hemispherical side-to-side differences of primary somatosensory cortex in the complex regional pain syndrome I. Experimental brain research 155:115-119.

Prakriya M, Lewis RS (2015) Store-Operated Calcium Channels. Physiological reviews 95:1383-1436.

Prescott ED, Julius D (2003) A modular PIP2 binding site as a determinant of capsaicin receptor sensitivity. Science 300:1284-1288.

Price TJ, Cervero F, de Koninck Y (2005) Role of cation-chloride-cotransporters (CCC) in pain and hyperalgesia. Current topics in medicinal chemistry 5:547-555.

Pritchard HA, Leblanc N, Albert AP, Greenwood IA (2014) Inhibitory role of phosphatidylinositol 4,5-bisphosphate on TMEM16A-encoded calcium-activated chloride channels in rat pulmonary artery. British journal of pharmacology 171:4311-4321.

Qu Z, Wei RW, Hartzell HC (2003) Characterization of Ca2+-activated Cl- currents in mouse kidney inner medullary collecting duct cells. American journal of physiology Renal physiology 285:F326-335.

Qu Z, Fischmeister R, Hartzell C (2004) Mouse bestrophin-2 is a bona fide Cl(-) channel: identification of a residue important in anion binding and conduction. The Journal of general physiology 123:327-340.

Qu Z, Yao W, Yao R, Liu X, Yu K, Hartzell C (2014) The Ca(2+) -activated Cl(-) channel, ANO1 (TMEM16A), is a double-edged sword in cell proliferation and tumorigenesis. Cancer medicine 3:453-461.

Qu Z, Wang B, Zhang Z, Ma L, Li D, Zhuang L, Chi J, Liu J (2016) Functions of ANO1/TMEM16A, Ca2+-activated Cl- channels in Regulation of Blood Pressure and Vascular Remodeling: Qu Z et al . Roles of ANO1 in vascular contractility and remodeling.

Rajagopal M, Kathpalia PP, Thomas SV, Pao AC (2011) Activation of P2Y1 and P2Y2 receptors induces chloride secretion via calcium-activated chloride channels in kidney inner medullary collecting duct cells. American journal of physiology Renal physiology 301:F544-553.

Rajagopal M, Kathpalia PP, Widdicombe JH, Pao AC (2012) Differential effects of extracellular ATP on chloride transport in cortical collecting duct cells. American journal of physiology Renal physiology 303:F483-491.

Ranade SS, Qiu Z, Woo SH, Hur SS, Murthy SE, Cahalan SM, Xu J, Mathur J, Bandell M, Coste B, Li YS, Chien S, Patapoutian A (2014a) Piezo1, a mechanically activated ion channel, is required for vascular development in mice. Proceedings of the National Academy of Sciences of the United States of America 111:10347-10352.

Ranade SS, Woo S-H, Dubin AE, Moshourab RA, Wetzel C, Petrus M, Mathur J, Bégay V, Coste B, Mainquist J, Wilson AJ, Francisco AG, Reddy K, Qiu Z, Wood JN, Lewin GR, Patapoutian A (2014b) Piezo2 is the major transducer of mechanical forces for touch sensation in mice. Nature 516:121-125.

Ranade SS, Woo SH, Dubin AE, Moshourab RA, Wetzel C, Petrus M, Mathur J, Begay V, Coste B, Mainquist J, Wilson AJ, Francisco AG, Reddy K, Qiu Z, Wood JN, Lewin GR, Patapoutian A (2014c) Piezo2 is the major transducer of mechanical forces for touch sensation in mice. Nature 516:121-125.

Rasband MN, Park EW, Vanderah TW, Lai J, Porreca F, Trimmer JS (2001) Distinct potassium channels on pain-sensing neurons. Proceedings of the National Academy of Sciences of the United States of America 98:13373-13378.

Rasche S, Toetter B, Adler J, Tschapek A, Doerner JF, Kurtenbach S, Hatt H, Meyer H, Warscheid B, Neuhaus EM (2010) Tmem16b is specifically expressed in the cilia of olfactory sensory neurons. Chemical senses 35:239-245.

Rashid MH, Inoue M, Bakoshi S, Ueda H (2003) Increased expression of vanilloid receptor 1 on myelinated primary afferent neurons contributes to the antihyperalgesic effect of capsaicin cream in diabetic neuropathic pain in mice. The Journal of pharmacology and experimental therapeutics 306:709-717.

Reddy G, Liu Z, Thirumalai D (2012) Denaturant-dependent folding of GFP. Proceedings of the National Academy of Sciences of the United States of America 109:17832-17838.

Reddy MM, Light MJ, Quinton PM (1999) Activation of the epithelial Na+ channel (ENaC) requires CFTR Cl- channel function. Nature 402:301-304.

Reisert J, Bauer PJ, Yau KW, Frings S (2003) The Ca-activated Cl channel and its control in rat olfactory receptor neurons. The Journal of general physiology 122:349-363.

Remington SJ (2006) Fluorescent proteins: maturation, photochemistry and photophysics. Current opinion in structural biology 16:714-721.

Restrepo D (2005) The ins and outs of intracellular chloride in olfactory receptor neurons. Neuron 45:481-482.

Reuter D, Zierold K, Schroder WH, Frings S (1998) A depolarizing chloride current contributes to chemoelectrical transduction in olfactory sensory neurons in situ. The Journal of neuroscience : the official journal of the Society for Neuroscience 18:6623-6630.

Ribelayga C (2010) Vertebrate vision: TRP channels in the spotlight. Current biology : CB 20:R278-280.

Riordan JR, Rommens JM, Kerem B, Alon N, Rozmahel R, Grzelczak Z, Zielenski J, Lok S, Plavsic N, Chou JL, et al. (1989) Identification of the cystic fibrosis gene: cloning and characterization of complementary DNA. Science 245:1066-1073.

Ripoll C, Lederer WJ, Nichols CG (1993) On the mechanism of inhibition of KATP channels by glibenclamide in rat ventricular myocytes. Journal of cardiovascular electrophysiology 4:38-47.

Rivera C, Voipio J, Payne JA, Ruusuvuori E, Lahtinen H, Lamsa K, Pirvola U, Saarma M, Kaila K (1999) The K+/Cl- co-transporter KCC2 renders GABA hyperpolarizing during neuronal maturation. Nature 397:251-255.

Rizzuto R, Pozzan T (2006) Microdomains of intracellular Ca2+: molecular determinants and functional consequences. Physiological reviews 86:369-408.

Robertson B (1989) Characteristics of GABA-activated chloride channels in mammalian dorsal root ganglion neurones. The Journal of physiology 411:285-300.

Robinson NC, Huang P, Kaetzel MA, Lamb FS, Nelson DJ (2004) Identification of an N-terminal amino acid of the CLC-3 chloride channel critical in phosphorylation-dependent activation of a CaMKII-activated chloride current. The Journal of physiology 556:353-368.

Rocha-Gonzalez HI, Mao S, Alvarez-Leefmans FJ (2008) Na+,K+,2Cl- cotransport and intracellular chloride regulation in rat primary sensory neurons: thermodynamic and kinetic aspects. Journal of neurophysiology 100:169-184.

Rock JR, O'Neal WK, Gabriel SE, Randell SH, Harfe BD, Boucher RC, Grubb BR (2009) Transmembrane protein 16A (TMEM16A) is a Ca2+-regulated Cl- secretory channel in mouse airways. The Journal of biological chemistry 284:14875-14880.

Rohacs T, Thyagarajan B, Lukacs V (2008) Phospholipase C mediated modulation of TRPV1 channels. Molecular neurobiology 37:153-163.

Rohacs T, Lopes CM, Michailidis I, Logothetis DE (2005) PI(4,5)P2 regulates the activation and desensitization of TRPM8 channels through the TRP domain. Nature neuroscience 8:626-634.

Romanenko VG, Catalan MA, Brown DA, Putzier I, Hartzell HC, Marmorstein AD, Gonzalez-Begne M, Rock JR, Harfe BD, Melvin JE (2010) Tmem16A encodes the Ca2+-activated Cl- channel in mouse submandibular salivary gland acinar cells. The Journal of biological chemistry 285:12990-13001.

Rose KE, Lunardi N, Boscolo A, Dong X, Erisir A, Jevtovic-Todorovic V, Todorovic SM (2013) Immunohistological demonstration of CaV3.2 T-type voltage-gated calcium channel expression in soma of dorsal root ganglion neurons and peripheral axons of rat and mouse. Neuroscience 250:263-274.

Rosenbaum T, Gordon-Shaag A, Munari M, Gordon SE (2004) Ca2+/calmodulin modulates TRPV1 activation by capsaicin. The Journal of general physiology 123:53-62.

Ru F, Sun H, Jurcakova D, Herbstsomer RA, Meixong J, Dong X, Undem BJ (2017) Mechanisms of pruritogen-induced activation of itch nerves in isolated mouse skin. The Journal of physiology 595:3651-3666.

Runft LL, Watras J, Jaffe LA (1999) Calcium release at fertilization of Xenopus eggs requires type I IP(3) receptors, but not SH2 domain-mediated activation of PLCgamma or G(q)-mediated activation of PLCbeta. Developmental biology 214:399-411.

Rush AM, Dib-Hajj SD, Liu S, Cummins TR, Black JA, Waxman SG (2006) A single sodium channel mutation produces hyper- or hypoexcitability in different types of neurons. Proceedings of the National Academy of Sciences of the United States of America 103:8245-8250.

Russell JA, Lai-Fook SJ (1979) Reflex bronchoconstriction induced by capsaicin in the dog. Journal of applied physiology: respiratory, environmental and exercise physiology 47:961-967.

Rust MJ, Bates M, Zhuang X (2006) Sub-diffraction-limit imaging by stochastic optical reconstruction microscopy (STORM). Nature methods 3:793-795.

Saheki Y, Bian X, Schauder CM, Sawaki Y, Surma MA, Klose C, Pincet F, Reinisch KM, De Camilli P (2016) Control of plasma membrane lipid homeostasis by the extended synaptotagmins. Nature cell biology 18:504-515.

Samways DS, Egan TM (2011) Calcium-dependent decrease in the single-channel conductance of TRPV1. Pflugers Archiv : European journal of physiology 462:681-691.

Samways DS, Khakh BS, Egan TM (2008) Tunable calcium current through TRPV1 receptor channels. The Journal of biological chemistry 283:31274-31278.

Sanchez-Alonso JL, Bhargava A, O'Hara T, Glukhov AV, Schobesberger S, Bhogal N, Sikkel MB, Mansfield C, Korchev YE, Lyon AR, Punjabi PP, Nikolaev VO, Trayanova NA, Gorelik J (2016) Microdomain-Specific Modulation of L-Type Calcium Channels Leads to Triggered Ventricular Arrhythmia in Heart Failure. Circ Res 119:944-955.

Sancho M, Garcia-Pascual A, Triguero D (2012) Presence of the Ca2+-activated chloride channel anoctamin 1 in the urethra and its role in excitatory neurotransmission. American journal of physiology Renal physiology 302:F390-400.

Santicioli P, Del Bianco E, Tramontana M, Geppetti P, Maggi CA (1992) Release of calcitonin gene-related peptide like-immunoreactivity induced by electrical field stimulation from rat spinal afferents is mediated by conotoxin-sensitive calcium channels. Neuroscience letters 136:161-164.

Santulli G, Marks AR (2015) Essential Roles of Intracellular Calcium Release Channels in Muscle, Brain, Metabolism, and Aging. Current molecular pharmacology 8:206-222.

Sardini A, Amey JS, Weylandt KH, Nobles M, Valverde MA, Higgins CF (2003) Cell volume regulation and swelling-activated chloride channels. Biochimica et biophysica acta 1618:153-162.

Sather WA, McCleskey EW (2003) Permeation and selectivity in calcium channels. Annual review of physiology 65:133-159.

Schachter JB, Sromek SM, Nicholas RA, Harden TK (1997) HEK293 human embryonic kidney cells endogenously express the P2Y1 and P2Y2 receptors. Neuropharmacology 36:1181-1187.

Schmulson MJ, Valdovinos MA, Milke P (2003) Chili pepper and rectal hyperalgesia in irritable bowel syndrome. The American journal of gastroenterology 98:1214-1215.

Schreiber R, Uliyakina I, Kongsuphol P, Warth R, Mirza M, Martins JR, Kunzelmann K (2010) Expression and function of epithelial anoctamins. The Journal of biological chemistry 285:7838-7845.

Schroeder BC, Cheng T, Jan YN, Jan LY (2008) Expression cloning of TMEM16A as a calcium-activated chloride channel subunit. Cell 134:1019-1029.

Scriven DR, Asghari P, Schulson MN, Moore ED (2010) Analysis of Cav1.2 and ryanodine receptor clusters in rat ventricular myocytes. Biophysical journal 99:3923-3929.

Scudieri P, Sondo E, Caci E, Ravazzolo R, Galietta LJ (2013) TMEM16A-TMEM16B chimaeras to investigate the structure-function relationship of calcium-activated chloride channels. The Biochemical journal 452:443-455.

Scudieri P, Caci E, Venturini A, Sondo E, Pianigiani G, Marchetti C, Ravazzolo R, Pagani F, Galietta LJ (2015) Ion channel and lipid scramblase activity associated with expression of TMEM16F/ANO6 isoforms. The Journal of physiology 593:3829-3848.

Scudieri P, Caci E, Bruno S, Ferrera L, Schiavon M, Sondo E, Tomati V, Gianotti A, Zegarra-Moran O, Pedemonte N, Rea F, Ravazzolo R, Galietta LJ (2012) Association of TMEM16A chloride channel overexpression with airway goblet cell metaplasia. The Journal of physiology 590:6141-6155.

Seo Y, Lee HK, Park J, Jeon DK, Jo S, Jo M, Namkung W (2016) Ani9, A Novel Potent Small-Molecule ANO1 Inhibitor with Negligible Effect on ANO2. PloS one 11:e0155771.

Shah BS, Rush AM, Liu S, Tyrrell L, Black JA, Dib-Hajj SD, Waxman SG (2004) Contactin associates with sodium channel Nav1.3 in native tissues and increases channel density at the cell surface. The Journal of neuroscience : the official journal of the Society for Neuroscience 24:7387-7399.

Shah SK, Abraham P, Mistry FP (2000) Effect of cold pressor test and a high-chilli diet on rectosigmoid motility in irritable bowel syndrome. Indian journal of gastroenterology : official journal of the Indian Society of Gastroenterology 19:161-164.

Shaner NC, Patterson GH, Davidson MW (2007) Advances in fluorescent protein technology. Journal of cell science 120:4247-4260.

Shen WK, Tung RT, Kurachi Y (1992) Activation of the cardiac ATP-sensitive K+ channel by ER-001533, a newly synthesized vasorelaxant. Circ Res 70:1054-1061.

Sheppard DN, Welsh MJ (1999) Structure and function of the CFTR chloride channel. Physiological reviews 79:S23-45.

Sheridan JT, Worthington EN, Yu K, Gabriel SE, Hartzell HC, Tarran R (2011) Characterization of the oligomeric structure of the Ca(2+)-activated Cl- channel Ano1/TMEM16A. The Journal of biological chemistry 286:1381-1388.

Shimomura O (2005) The discovery of aequorin and green fluorescent protein. J Microsc 217:1-15.

Shimomura O, Johnson FH, Saiga Y (1962) Extraction, purification and properties of aequorin, a bioluminescent protein from the luminous hydromedusan, Aequorea. Journal of cellular and comparative physiology 59:223-239.

Shin YH, Lee SW, Kim M, Choi SY, Cong X, Yu GY, Park K (2016) Epigenetic regulation of CFTR in salivary gland. Biochemical and biophysical research communications 481:31-37.

Shorer Z, Wajsbrot E, Liran TH, Levy J, Parvari R (2014) A novel mutation in SCN9A in a child with congenital insensitivity to pain. Pediatric neurology 50:73-76.

Sidi S, Friedrich RW, Nicolson T (2003) NompC TRP channel required for vertebrate sensory hair cell mechanotransduction. Science 301:96-99.

Sieghart W (1995) Structure and pharmacology of gamma-aminobutyric acidA receptor subtypes. Pharmacological reviews 47:181-234.

Siegmund SV, Uchinami H, Osawa Y, Brenner DA, Schwabe RF (2005) Anandamide induces necrosis in primary hepatic stellate cells. Hepatology 41:1085-1095.

Sigel E, Steinmann ME (2012) Structure, function, and modulation of GABA(A) receptors. The Journal of biological chemistry 287:40224-40231.

Singh RD, Gibbons SJ, Saravanaperumal SA, Du P, Hennig GW, Eisenman ST, Mazzone A, Hayashi Y, Cao C, Stoltz GJ, Ordog T, Rock JR, Harfe BD, Szurszewski JH, Farrugia G (2014) Ano1, a Ca2+-activated Cl- channel, coordinates contractility in mouse intestine by Ca2+ transient coordination between interstitial cells of Cajal. The Journal of physiology 592:4051-4068.

Sinharoy P, Bratz IN, Sinha S, Showalter LE, Andrei SR, Damron DS (2017) TRPA1 and TRPV1 contribute to propofol-mediated antagonism of U46619-induced constriction in murine coronary arteries. PloS one 12:e0180106.

Smyth JT, Dehaven WI, Jones BF, Mercer JC, Trebak M, Vazquez G, Putney JW, Jr. (2006) Emerging perspectives in store-operated Ca2+ entry: roles of Orai, Stim and TRP. Biochimica et biophysica acta 1763:1147-1160.

Snapp E (2005) Design and use of fluorescent fusion proteins in cell biology. Current protocols in cell biology Chapter 21:Unit 21 24.

Snider WD, McMahon SB (1998) Tackling pain at the source: new ideas about nociceptors. Neuron 20:629-632.

Solinas S, Masoli S, Subramaniyam S (2013) High-Voltage-Activated Calcium Channels. In: Encyclopedia of Computational Neuroscience (Jaeger D, Jung R, eds), pp 1-7. New York, NY: Springer New York.

Solinet S, Mahmud K, Stewman SF, Ben El Kadhi K, Decelle B, Talje L, Ma A, Kwok BH, Carreno S (2013) The actin-binding ERM protein Moesin binds to and stabilizes microtubules at the cell cortex. The Journal of cell biology 202:251-260.

Sones WR, Davis AJ, Leblanc N, Greenwood IA (2010) Cholesterol depletion alters amplitude and pharmacology of vascular calcium-activated chloride channels. Cardiovascular research 87:476-484.

Sood R, Bear C, Auerbach W, Reyes E, Jensen T, Kartner N, Riordan JR, Buchwald M (1992) Regulation of CFTR expression and function during differentiation of intestinal epithelial cells. The EMBO journal 11:2487-2494.

Staley K, Smith R, Schaack J, Wilcox C, Jentsch TJ (1996) Alteration of GABAA receptor function following gene transfer of the CLC-2 chloride channel. Neuron 17:543-551.

Stander S, Moormann C, Schumacher M, Buddenkotte J, Artuc M, Shpacovitch V, Brzoska T, Lippert U, Henz BM, Luger TA, Metze D, Steinhoff M (2004) Expression of vanilloid receptor subtype 1 in cutaneous sensory nerve fibers, mast cells, and epithelial cells of appendage structures. Experimental dermatology 13:129-139.

Staruschenko A, Jeske NA, Akopian AN (2010) Contribution of TRPV1-TRPA1 interaction to the single channel properties of the TRPA1 channel. The Journal of biological chemistry 285:15167-15177.

Stefan CJ, Manford AG, Emr SD (2013) ER-PM connections: sites of information transfer and inter-organelle communication. Current opinion in cell biology 25:434-442.

Stein AT, Ufret-Vincenty CA, Hua L, Santana LF, Gordon SE (2006) Phosphoinositide 3-kinase binds to TRPV1 and mediates NGF-stimulated TRPV1 trafficking to the plasma membrane. The Journal of general physiology 128:509-522.

Stephan AB, Shum EY, Hirsh S, Cygnar KD, Reisert J, Zhao H (2009) ANO2 is the cilial calcium-activated chloride channel that may mediate olfactory amplification. Proceedings of the National Academy of Sciences of the United States of America 106:11776-11781.

Stiber J, Hawkins A, Zhang ZS, Wang S, Burch J, Graham V, Ward CC, Seth M, Finch E, Malouf N, Williams RS, Eu JP, Rosenberg P (2008) STIM1 signalling

controls store-operated calcium entry required for development and contractile function in skeletal muscle. Nature cell biology 10:688-697.

Stobrawa SM, Breiderhoff T, Takamori S, Engel D, Schweizer M, Zdebik AA, Bosl MR, Ruether K, Jahn H, Draguhn A, Jahn R, Jentsch TJ (2001) Disruption of ClC-3, a chloride channel expressed on synaptic vesicles, leads to a loss of the hippocampus. Neuron 29:185-196.

Stohr H, Heisig JB, Benz PM, Schoberl S, Milenkovic VM, Strauss O, Aartsen WM, Wijnholds J, Weber BH, Schulz HL (2009) TMEM16B, a novel protein with calcium-dependent chloride channel activity, associates with a presynaptic protein complex in photoreceptor terminals. The Journal of neuroscience : the official journal of the Society for Neuroscience 29:6809-6818.

Stolz M, Klapperstuck M, Kendzierski T, Detro-Dassen S, Panning A, Schmalzing G, Markwardt F (2015) Homodimeric anoctamin-1, but not homodimeric anoctamin-6, is activated by calcium increases mediated by the P2Y1 and P2X7 receptors. Pflugers Archiv : European journal of physiology 467:2121-2140.

Story GM, Peier AM, Reeve AJ, Eid SR, Mosbacher J, Hricik TR, Earley TJ, Hergarden AC, Andersson DA, Hwang SW, McIntyre P, Jegla T, Bevan S, Patapoutian A (2003) ANKTM1, a TRP-like channel expressed in nociceptive neurons, is activated by cold temperatures. Cell 112:819-829.

Strong TV, Boehm K, Collins FS (1994) Localization of cystic fibrosis transmembrane conductance regulator mRNA in the human gastrointestinal tract by in situ hybridization. The Journal of clinical investigation 93:347-354.

Sugiura T, Tominaga M, Katsuya H, Mizumura K (2002) Bradykinin lowers the threshold temperature for heat activation of vanilloid receptor 1. Journal of neurophysiology 88:544-548.

Sui J, Cotard S, Andersen J, Zhu P, Staunton J, Lee M, Lin S (2010) Optimization of a Yellow fluorescent protein-based iodide influx high-throughput screening assay for cystic fibrosis transmembrane conductance regulator (CFTR) modulators. Assay and drug development technologies 8:656-668.

Sun H, Tsunenari T, Yau KW, Nathans J (2002) The vitelliform macular dystrophy protein defines a new family of chloride channels. Proceedings of the National Academy of Sciences of the United States of America 99:4008-4013.

Sun H, Xia Y, Paudel O, Yang XR, Sham JS (2012) Chronic hypoxia-induced upregulation of Ca2+-activated Cl- channel in pulmonary arterial myocytes: a mechanism contributing to enhanced vasoreactivity. The Journal of physiology 590:3507-3521.

Sun RQ, Lawand NB, Lin Q, Willis WD (2004a) Role of calcitonin gene-related peptide in the sensitization of dorsal horn neurons to mechanical stimulation after intradermal injection of capsaicin. Journal of neurophysiology 92:320-326.

Sun RQ, Tu YJ, Lawand NB, Yan JY, Lin Q, Willis WD (2004b) Calcitonin gene-related peptide receptor activation produces PKA- and PKC-dependent mechanical hyperalgesia and central sensitization. Journal of neurophysiology 92:2859-2866.

Sung KW, Kirby M, McDonald MP, Lovinger DM, Delpire E (2000) Abnormal GABAA receptor-mediated currents in dorsal root ganglion neurons isolated from Na-K-2Cl cotransporter null mice. The Journal of neuroscience : the official journal of the Society for Neuroscience 20:7531-7538.

Suzuki A, Shinoda M, Honda K, Shirakawa T, Iwata K (2016) Regulation of transient receptor potential vanilloid 1 expression in trigeminal ganglion neurons via methyl-CpG binding protein 2 signaling contributes tongue heat sensitivity and inflammatory hyperalgesia in mice. Molecular pain 12:1744806916633206.

Suzuki J, Umeda M, Sims PJ, Nagata S (2010) Calcium-dependent phospholipid scrambling by TMEM16F. Nature 468:834-838.

Suzuki J, Kanemaru K, Ishii K, Ohkura M, Okubo Y, Iino M (2014) Imaging intraorganellar Ca2+ at subcellular resolution using CEPIA. Nature communications 5:4153.

Szabo A, Helyes Z, Sandor K, Bite A, Pinter E, Nemeth J, Banvolgyi A, Bolcskei K, Elekes K, Szolcsanyi J (2005) Role of transient receptor potential vanilloid 1 receptors in adjuvant-induced chronic arthritis: in vivo study using gene-deficient mice. The Journal of pharmacology and experimental therapeutics 314:111-119.

Szallasi A, Conte B, Goso C, Blumberg PM, Manzini S (1993a) Characterization of a peripheral vanilloid (capsaicin) receptor in the urinary bladder of the rat. Life sciences 52:PL221-226.

Szallasi A, Conte B, Goso C, Blumberg PM, Manzini S (1993b) Vanilloid receptors in the urinary bladder: regional distribution, localization on sensory nerves, and species-related differences. Naunyn-Schmiedeberg's archives of pharmacology 347:624-629.

Szoke E, Borzsei R, Toth DM, Lengl O, Helyes Z, Sandor Z, Szolcsanyi J (2010) Effect of lipid raft disruption on TRPV1 receptor activation of trigeminal sensory neurons and transfected cell line. European journal of pharmacology 628:67-74.

Ta CM, Acheson KE, Rorsman NJG, Jongkind RC, Tammaro P (2017) Contrasting effects of phosphatidylinositol 4,5-bisphosphate on cloned TMEM16A and TMEM16B channels. British journal of pharmacology 174:2984-2999.

Takaki M (2003) Gut pacemaker cells: the interstitial cells of Cajal (ICC). Journal of smooth muscle research = Nihon Heikatsukin Gakkai kikanshi 39:137-161.

Takayama Y, Uta D, Furue H, Tominaga M (2015) Pain-enhancing mechanism through interaction between TRPV1 and anoctamin 1 in sensory neurons. Proceedings of the National Academy of Sciences of the United States of America 112:5213-5218.

Takayama Y, Shibasaki K, Suzuki Y, Yamanaka A, Tominaga M (2014) Modulation of water efflux through functional interaction between TRPV4 and TMEM16A/anoctamin 1. The FASEB Journal 28:2238-2248.

Takeshima H, Hoshijima M, Song LS (2015) Ca(2)(+) microdomains organized by junctophilins. Cell Calcium 58:349-356.

Takeshima H, Nishimura S, Matsumoto T, Ishida H, Kangawa K, Minamino N, Matsuo H, Ueda M, Hanaoka M, Hirose T, et al. (1989) Primary structure and expression from complementary DNA of skeletal muscle ryanodine receptor. Nature 339:439-445.

Tal M, Bennett GJ (1994) Extra-territorial pain in rats with a peripheral mononeuropathy: mechano-hyperalgesia and mechano-allodynia in the territory of an uninjured nerve. Pain 57:375-382.

Talley EM, Solorzano G, Lei QB, Kim D, Bayliss DA (2001) CNS distribution of members of the two-pore-domain (KCNK) potassium channel family. Journal of Neuroscience 21:7491-7505.

Tanaka T, Nangaku M (2014) ANO1: an additional key player in cyst growth. Kidney international 85:1007-1009.

Tantama M, Hung YP, Yellen G (2012) Optogenetic reporters: Fluorescent protein-based genetically encoded indicators of signaling and metabolism in the brain. Progress in brain research 196:235-263.

Taylor CW, Tovey SC (2010) IP(3) receptors: toward understanding their activation. Cold Spring Harbor perspectives in biology 2:a004010.

Taylor R, Roper S (1994) Ca(2+)-dependent Cl- conductance in taste cells from Necturus. Journal of neurophysiology 72:475-478.

Terashima H, Picollo A, Accardi A (2013) Purified TMEM16A is sufficient to form Ca2+-activated Cl- channels. Proceedings of the National Academy of Sciences of the United States of America 110:19354-19359.

Theriault E, Otsuka M, Jessell T (1979) Capsaicin-evoked release of substance P from primary sensory neurons. Brain research 170:209-213.

Thomas KC, Sabnis AS, Johansen ME, Lanza DL, Moos PJ, Yost GS, Reilly CA (2007) Transient receptor potential vanilloid 1 agonists cause endoplasmic reticulum stress and cell death in human lung cells. The Journal of pharmacology and experimental therapeutics 321:830-838.

Thoreson WB, Rabl K, Townes-Anderson E, Heidelberger R (2004) A highly Ca2+-sensitive pool of vesicles contributes to linearity at the rod photoreceptor ribbon synapse. Neuron 42:595-605.

Thoreson WB, Stella SL, Jr., Bryson EI, Clements J, Witkovsky P (2002) D2-like dopamine receptors promote interactions between calcium and chloride channels that diminish rod synaptic transfer in the salamander retina. Visual neuroscience 19:235-247.

Tian Y, Kongsuphol P, Hug M, Ousingsawat J, Witzgall R, Schreiber R, Kunzelmann K (2011) Calmodulin-dependent activation of the epithelial calcium-dependent chloride channel TMEM16A. FASEB journal : official publication of the Federation of American Societies for Experimental Biology 25:1058-1068.

Tien J, Lee HY, Minor DL, Jr., Jan YN, Jan LY (2013) Identification of a dimerization domain in the TMEM16A calcium-activated chloride channel (CaCC). Proceedings of the National Academy of Sciences of the United States of America 110:6352-6357.

Tien J, Peters CJ, Wong XM, Cheng T, Jan YN, Jan LY, Yang H (2014) A comprehensive search for calcium binding sites critical for TMEM16A calcium-activated chloride channel activity. eLife 3.

Todorovic SM, Jevtovic-Todorovic V (2006) The role of T-type calcium channels in peripheral and central pain processing. CNS & neurological disorders drug targets 5:639-653.

Torres GE, Egan TM, Voigt MM (1998) Topological analysis of the ATP-gated ionotropic [correction of ionotrophic] P2X2 receptor subunit. FEBS letters 425:19-23.

Tottene A, Moretti A, Pietrobon D (1996) Functional diversity of P-type and R-type calcium channels in rat cerebellar neurons. The Journal of neuroscience : the official journal of the Society for Neuroscience 16:6353-6363.

Touska F, Marsakova L, Teisinger J, Vlachova V (2011) A "cute" desensitization of TRPV1. Current pharmaceutical biotechnology 12:122-129.

Trescot AM, Datta S, Lee M, Hansen H (2008) Opioid pharmacology. Pain physician 11:S133-153.

Trevisani M, Smart D, Gunthorpe MJ, Tognetto M, Barbieri M, Campi B, Amadesi S, Gray J, Jerman JC, Brough SJ, Owen D, Smith GD, Randall AD, Harrison S, Bianchi A, Davis JB, Geppetti P (2002) Ethanol elicits and potentiates nociceptor responses via the vanilloid receptor-1. Nature neuroscience 5:546-551.

Tricoire L, Tsuzuki K, Courjean O, Gibelin N, Bourout G, Rossier J, Lambolez B (2006) Calcium dependence of aequorin bioluminescence dissected by random mutagenesis. Proceedings of the National Academy of Sciences of the United States of America 103:9500-9505.

Tsunemi T, Saegusa H, Ishikawa K, Nagayama S, Murakoshi T, Mizusawa H, Tanabe T (2002) Novel Cav2.1 splice variants isolated from Purkinje cells do not generate P-type Ca2+ current. The Journal of biological chemistry 277:7214-7221.

Tsunenari T, Nathans J, Yau KW (2006) Ca2+-activated Cl- current from human bestrophin-4 in excised membrane patches. The Journal of general physiology 127:749-754.

Tsunenari T, Sun H, Williams J, Cahill H, Smallwood P, Yau KW, Nathans J (2003) Structure-function analysis of the bestrophin family of anion channels. The Journal of biological chemistry 278:41114-41125.

Tsutsumi S, Kamata N, Vokes TJ, Maruoka Y, Nakakuki K, Enomoto S, Omura K, Amagasa T, Nagayama M, Saito-Ohara F, Inazawa J, Moritani M, Yamaoka T, Inoue H, Itakura M (2004) The novel gene encoding a putative transmembrane protein is mutated in gnathodiaphyseal dysplasia (GDD). American journal of human genetics 74:1255-1261.

Tu JC, Xiao B, Yuan JP, Lanahan AA, Leoffert K, Li M, Linden DJ, Worley PF (1998) Homer binds a novel proline-rich motif and links group 1 metabotropic glutamate receptors with IP3 receptors. Neuron 21:717-726.

Tuteja N (2009) Signaling through G protein coupled receptors. Plant signaling & behavior 4:942-947.

Twyffels L, Strickaert A, Virreira M, Massart C, Van Sande J, Wauquier C, Beauwens R, Dumont JE, Galietta LJ, Boom A, Kruys V (2014) Anoctamin-1/TMEM16A is the major apical iodide channel of the thyrocyte. American journal of physiology Cell physiology 307:C1102-1112.

Tympanidis P, Casula MA, Yiangou Y, Terenghi G, Dowd P, Anand P (2004) Increased vanilloid receptor VR1 innervation in vulvodynia. European journal of pain 8:129-133.

Usoskin D, Furlan A, Islam S, Abdo H, Lonnerberg P, Lou D, Hjerling-Leffler J, Haeggstrom J, Kharchenko O, Kharchenko PV, Linnarsson S, Ernfors P (2015) Unbiased classification of sensory neuron types by large-scale single-cell RNA sequencing. Nature neuroscience 18:145-153.

Valtschanoff JG, Rustioni A, Guo A, Hwang SJ (2001) Vanilloid receptor VR1 is both presynaptic and postsynaptic in the superficial laminae of the rat dorsal horn. The Journal of comparative neurology 436:225-235.

Van Buren JJ, Bhat S, Rotello R, Pauza ME, Premkumar LS (2005) Sensitization and translocation of TRPV1 by insulin and IGF-I. Molecular pain 1:17.

Vaughan-Jones RD (1979) Non-passive chloride distribution in mammalian heart muscle: micro-electrode measurement of the intracellular chloride activity. The Journal of physiology 295:83-109.

Verkman AS, Galietta LJ (2009) Chloride channels as drug targets. Nature reviews Drug discovery 8:153-171.

Vermeer S et al. (2010) Targeted next-generation sequencing of a 12.5 Mb homozygous region reveals ANO10 mutations in patients with autosomal-recessive cerebellar ataxia. American journal of human genetics 87:813-819.

Viitanen TM, Sukumaran P, Lof C, Tornquist K (2013) Functional coupling of TRPC2 cation channels and the calcium-activated anion channels in rat thyroid cells: implications for iodide homeostasis. Journal of cellular physiology 228:814-823.

Vilceanu D, Honore P, Hogan QH, Stucky CL (2010) Spinal nerve ligation in mouse upregulates TRPV1 heat function in injured IB4-positive nociceptors. The journal of pain : official journal of the American Pain Society 11:588-599.

Vocke K, Dauner K, Hahn A, Ulbrich A, Broecker J, Keller S, Frings S, Mohrlen F (2013) Calmodulin-dependent activation and inactivation of anoctamin calcium-gated chloride channels. The Journal of general physiology 142:381-404.

Vydyanathan A, Wu ZZ, Chen SR, Pan HL (2005) A-type voltage-gated K+ currents influence firing properties of isolectin B4-positive but not isolectin B4-negative primary sensory neurons. Journal of neurophysiology 93:3401-3409.

Waldron JB, Sawynok J (2004) Peripheral P2X receptors and nociception: interactions with biogenic amine systems. Pain 110:79-89.

Walker RG, Willingham AT, Zuker CS (2000) A Drosophila mechanosensory transduction channel. Science 287:2229-2234.

Wang B, Li C, Huai R, Qu Z (2015) Overexpression of ANO1/TMEM16A, an arterial Ca2+-activated Cl- channel, contributes to spontaneous hypertension. J Mol Cell Cardiol 82:22-32.

Wang H, Olsen RW (2000) Binding of the GABA(A) receptor-associated protein (GABARAP) to microtubules and microfilaments suggests involvement of the cytoskeleton in GABARAPGABA(A) receptor interaction. Journal of neurochemistry 75:644-655.

Wang H, Bedford FK, Brandon NJ, Moss SJ, Olsen RW (1999) GABA(A)-receptor-associated protein links GABA(A) receptors and the cytoskeleton. Nature 397:69-72.

Wang Q, Leo MD, Narayanan D, Kuruvilla KP, Jaggar JH (2016) Local coupling of TRPC6 to ANO1/TMEM16A channels in smooth muscle cells amplifies vasoconstriction in cerebral arteries. American journal of physiology Cell physiology 310:C1001-1009.

Wang SQ, Song LS, Lakatta EG, Cheng H (2001) Ca2+ signalling between single L-type Ca2+ channels and ryanodine receptors in heart cells. Nature 410:592-596.

Watanabe E, Akagi H (1995) Distribution patterns of mRNAs encoding glycine receptor channels in the developing rat spinal cord. Neuroscience research 23:377-382.

Waxman SG, Kocsis JD, Black JA (1994) Type III sodium channel mRNA is expressed in embryonic but not adult spinal sensory neurons, and is reexpressed following axotomy. Journal of neurophysiology 72:466-470.

Weaver CD, Partridge JG, Yao TL, Moates JM, Magnuson MA, Verdoorn TA (1998) Activation of glycine and glutamate receptors increases intracellular calcium in cells derived from the endocrine pancreas. Molecular pharmacology 54:639-646.

Weiss SJ, Philp NJ, Grollman EF (1984) Effect of thyrotropin on iodide efflux in FRTL-5 cells mediated by Ca2+. Endocrinology 114:1108-1113.

Weng HJ, Patel KN, Jeske NA, Bierbower SM, Zou W, Tiwari V, Zheng Q, Tang Z, Mo GC, Wang Y, Geng Y, Zhang J, Guan Y, Akopian AN, Dong X (2015) Tmem100 Is a Regulator of TRPA1-TRPV1 Complex and Contributes to Persistent Pain. Neuron 85:833-846.

Werman R, Davidoff RA, Aprison MH (1967) Inhibition of motoneurones by iontophoresis of glycine. Nature 214:681-683.

Wes PD, Chevesich J, Jeromin A, Rosenberg C, Stetten G, Montell C (1995) TRPC1, a human homolog of a Drosophila store-operated channel. Proceedings of the National Academy of Sciences of the United States of America 92:9652-9656.

Westenbroek RE, Hoskins L, Catterall WA (1998) Localization of Ca2+ channel subtypes on rat spinal motor neurons, interneurons, and nerve terminals. The Journal of neuroscience : the official journal of the Society for Neuroscience 18:6319-6330.

Westenbroek RE, Hell JW, Warner C, Dubel SJ, Snutch TP, Catterall WA (1992) Biochemical properties and subcellular distribution of an N-type calcium channel alpha 1 subunit. Neuron 9:1099-1115.

Wick EC, Pikios S, Grady EF, Kirkwood KS (2006a) Calcitonin gene-related peptide partially mediates nociception in acute experimental pancreatitis. Surgery 139:197-201.

Wick EC, Hoge SG, Grahn SW, Kim E, Divino LA, Grady EF, Bunnett NW, Kirkwood KS (2006b) Transient receptor potential vanilloid 1, calcitonin gene-related peptide, and substance P mediate nociception in acute pancreatitis. American journal of physiology Gastrointestinal and liver physiology 290:G959-969.

Wieseler-Frank J, Maier SF, Watkins LR (2004) Glial activation and pathological pain. Neurochemistry international 45:389-395.

Willis EF, Clough GF, Church MK (2004) Investigation into the mechanisms by which nedocromil sodium, frusemide and bumetanide inhibit the histamine-induced itch and flare response in human skin in vivo. Clinical and experimental allergy : journal of the British Society for Allergy and Clinical Immunology 34:450-455.

Willoughby D, Cooper DM (2007) Organization and Ca2+ regulation of adenylyl cyclases in cAMP microdomains. Physiological reviews 87:965-1010.

Wilschanski M, Novak I (2013) The cystic fibrosis of exocrine pancreas. Cold Spring Harbor perspectives in medicine 3:a009746.

Wolf W, Kilic A, Schrul B, Lorenz H, Schwappach B, Seedorf M (2012) Yeast Ist2 recruits the endoplasmic reticulum to the plasma membrane and creates a ribosome-free membrane microcompartment. PloS one 7:e39703.

Woo JS, Srikanth S, Nishi M, Ping P, Takeshima H, Gwack Y (2016) Junctophilin-4, a component of the endoplasmic reticulum-plasma membrane junctions, regulates Ca2+ dynamics in T cells. Proceedings of the National Academy of Sciences of the United States of America 113:2762-2767.

Woo SH, Ranade S, Weyer AD, Dubin AE, Baba Y, Qiu Z, Petrus M, Miyamoto T, Reddy K, Lumpkin EA, Stucky CL, Patapoutian A (2014) Piezo2 is required for Merkel-cell mechanotransduction. Nature 509:622-626.

Woodin MA, Ganguly K, Poo MM (2003) Coincident pre- and postsynaptic activity modifies GABAergic synapses by postsynaptic changes in Cl- transporter activity. Neuron 39:807-820.

Woolf CJ (2010) What is this thing called pain? The Journal of clinical investigation 120:3742-3744.

Woolf CJ (2011) Central sensitization: implications for the diagnosis and treatment of pain. Pain 152:S2-15.

Woolf CJ, Mannion RJ (1999) Neuropathic pain: aetiology, symptoms, mechanisms, and management. Lancet 353:1959-1964.

Xiao Q, Yu K, Perez-Cornejo P, Cui Y, Arreola J, Hartzell HC (2011) Voltage- and calcium-dependent gating of TMEM16A/Ano1 chloride channels are physically coupled by the first intracellular loop. Proceedings of the National Academy of Sciences of the United States of America 108:8891-8896.

Xu K, Babcock HP, Zhuang X (2012) Dual-objective STORM reveals three-dimensional filament organization in the actin cytoskeleton. Nature methods 9:185-188.

Yadid G, Youdim MB, Zinder O (1990) High-affinity strychnine binding to adrenal medulla chromaffin cell membranes. European journal of pharmacology 175:365-366.

Yamada J, Okabe A, Toyoda H, Kilb W, Luhmann HJ, Fukuda A (2004) Cl- uptake promoting depolarizing GABA actions in immature rat neocortical neurones is mediated by NKCC1. The Journal of physiology 557:829-841.

Yang EK, Takimoto K, Hayashi Y, de Groat WC, Yoshimura N (2004) Altered expression of potassium channel subunit mRNA and α-dendrotoxin sensitivity of potassium currents in rat dorsal root ganglion neurons after axotomy. Neuroscience 123:867-874.

Yang SN, Berggren PO (2006) The role of voltage-gated calcium channels in pancreatic beta-cell physiology and pathophysiology. Endocrine reviews 27:621-676.

Yang T, Liu Q, Kloss B, Bruni R, Kalathur RC, Guo Y, Kloppmann E, Rost B, Colecraft HM, Hendrickson WA (2014) Structure and selectivity in bestrophin ion channels. Science 346:355-359.

Yang TT, Cheng L, Kain SR (1996) Optimized codon usage and chromophore mutations provide enhanced sensitivity with the green fluorescent protein. Nucleic Acids Res 24:4592-4593.

Yang YD, Cho H, Koo JY, Tak MH, Cho Y, Shim WS, Park SP, Lee J, Lee B, Kim BM, Raouf R, Shin YK, Oh U (2008) TMEM16A confers receptor-activated calcium-dependent chloride conductance. Nature 455:1210-1215.

Yarden Y (2001) The EGFR family and its ligands in human cancer. signalling mechanisms and therapeutic opportunities. European journal of cancer 37 Suppl 4:S3-8.

Yiangou Y, Facer P, Ford A, Brady C, Wiseman O, Fowler CJ, Anand P (2001) Capsaicin receptor VR1 and ATP-gated ion channel P2X3 in human urinary bladder. BJU international 87:774-779.

Young AB, Snyder SH (1973) Strychnine binding associated with glycine receptors of the central nervous system. Proceedings of the National Academy of Sciences of the United States of America 70:2832-2836.

Yu K, Duran C, Qu Z, Cui YY, Hartzell HC (2012) Explaining calcium-dependent gating of anoctamin-1 chloride channels requires a revised topology. Circ Res 110:990-999.

Yu K, Zhu J, Qu Z, Cui YY, Hartzell HC (2014) Activation of the Ano1 (TMEM16A) chloride channel by calcium is not mediated by calmodulin. The Journal of general physiology 143:253-267.

Yudin Y, Lukacs V, Cao C, Rohacs T (2011) Decrease in phosphatidylinositol 4,5-bisphosphate levels mediates desensitization of the cold sensor TRPM8 channels. The Journal of physiology 589:6007-6027.

Zamponi GW, Snutch TP (2013) Advances in voltage-gated calcium channel structure, function and physiology. Biochimica et biophysica acta 1828:1521.

Zhang CH, Wang P, Liu DH, Chen CP, Zhao W, Chen X, Chen C, He WQ, Qiao YN, Tao T, Sun J, Peng YJ, Lu P, Zheng K, Craige SM, Lifshitz LM, Keaney JF, Jr., Fogarty KE, ZhuGe R, Zhu MS (2016a) The molecular basis of the genesis of basal tone in internal anal sphincter. Nature communications 7:11358.

Zhang J, Carver CM, Choveau FS, Shapiro MS (2016b) Clustering and Functional Coupling of Diverse Ion Channels and Signaling Proteins Revealed by Super-resolution STORM Microscopy in Neurons. Neuron 92:461-478.

Zhang J, Bal M, Bierbower S, Zaika O, Shapiro MS (2011a) AKAP79/150 signal complexes in G-protein modulation of neuronal ion channels. The Journal of neuroscience : the official journal of the Society for Neuroscience 31:7199-7211.

Zhang X, Huang J, McNaughton PA (2005) NGF rapidly increases membrane expression of TRPV1 heat-gated ion channels. The EMBO journal 24:4211-4223.

Zhang XF, Han P, Neelands TR, McGaraughty S, Honore P, Surowy CS, Zhang D (2011b) Coexpression and activation of TRPV1 suppress the activity of the KCNQ2/3 channel. The Journal of general physiology 138:341-352.

Zhang Y, Stanton JB, Wu J, Yu K, Hartzell HC, Peachey NS, Marmorstein LY, Marmorstein AD (2010) Suppression of Ca2+ signaling in a mouse model of Best disease. Human molecular genetics 19:1108-1118.

Zheng J (2013) Molecular Mechanism of TRP Channels. Comprehensive Physiology 3:221-242.

Zhou Y, Greka A (2016) Calcium-permeable ion channels in the kidney. American journal of physiology Renal physiology 310:F1157-1167.

Zhuang X (2009) Nano-imaging with Storm. Nature photonics 3:365-367.

Zhuang ZY, Xu H, Clapham DE, Ji RR (2004) Phosphatidylinositol 3-kinase activates ERK in primary sensory neurons and mediates inflammatory heat hyperalgesia through TRPV1 sensitization. The Journal of neuroscience : the official journal of the Society for Neuroscience 24:8300-8309.

Zimmermann K, Leffler A, Fischer MM, Messlinger K, Nau C, Reeh PW (2005) The TRPV1/2/3 activator 2-aminoethoxydiphenyl borate sensitizes native nociceptive neurons to heat in wildtype but not TRPV1 deficient mice. Neuroscience 135:1277-1284.

Zimmermann MB, Jooste PL, Pandav CS (2008) Iodine-deficiency disorders. Lancet 372:1251-1262.

Zuber B, Nikonenko I, Klauser P, Muller D, Dubochet J (2005) The mammalian central nervous synaptic cleft contains a high density of periodically organized complexes. Proceedings of the National Academy of Sciences of the United States of America 102:19192-19197.